



THE UNIVERSITY OF  
**WAIKATO**  
*Te Whare Wānanga o Waikato*

Research Commons

<http://waikato.researchgateway.ac.nz/>

## Research Commons at the University of Waikato

### Copyright Statement:

The digital copy of this thesis is protected by the Copyright Act 1994 (New Zealand).

The thesis may be consulted by you, provided you comply with the provisions of the Act and the following conditions of use:

- Any use you make of these documents or images must be for research or private study purposes only, and you may not make them available to any other person.
- Authors control the copyright of their thesis. You will recognise the author's right to be identified as the author of the thesis, and due acknowledgement will be made to the author where appropriate.
- You will obtain the author's permission before publishing any material from the thesis.

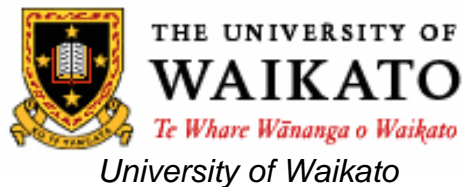
# Morphodynamics of the Whitianga Tidal Inlet, Buffalo Bay, New Zealand

A thesis submitted in partial fulfillment  
of the requirements for the degree of

*Master of Science*

in Earth and Ocean Sciences  
at the University of Waikato by

*Lauren Steeghs*



2007

## ***Abstract***

---

The primary aim of this study was to investigate the sedimentation processes within Buffalo Bay, particularly within and adjacent to the Whitianga tidal inlet, in order to ascertain reasons for the shoaling at both the inlet, and the identified shallow zone around Pandora Rock.

Comparison of historic bathymetries suggests the ebb delta and ebb discharge channel of the Whitianga tidal inlet are rapidly accreting and the ebb tidal discharge channel is gradually migrating northeast towards Whakapenui Point. Accretion rates of up to  $25 \text{ cm y}^{-1}$  were calculated in the ebb delta and inlet discharge channel area between 1979 and 1995 and aerial photo comparisons suggest the ebb delta area had increased by 400 % between 1990 and 2002. Results of the hydrodynamic and sediment transport modelling suggest the rapid accretion in the ebb delta vicinity is likely to be caused by a combination of catchment estuary inputs, which are deposited on the ebb tide as the ebb flow decelerates over the ebb delta, and inputs that have been moved south along Buffalo Beach by flood currents and an eddy that forms landward of the ebb tidal discharge. Residual tidal velocities further suggest a deposition zone in the ebb delta vicinity resulting from opposing currents and the deceleration of currents.

Hydrodynamic modelling results indicate the isolated shallow zone around Pandora rock appears to be caused by a transient eddy in the southern section of Buffalo Bay. The eddy is formed by the ebb tidal discharge from the inlet. Accretion probably occurs in the centre of the eddy which moves north as the ebb tide progresses.

Results obtained from a current meter and sediment trap deployed in northern Buffalo Bay suggest suspended sediment transport is minimal in northern Buffalo Bay, only occurring with large wave activity. Results of the hydrodynamic and sediment transport modelling further demonstrate that this area experiences low flow velocities, and has little interaction with the rest of Buffalo Bay. The minimal sediment input to this area, combined with the occasional erosion of the seafloor, primarily by wave activity, is thought to have resulted in long term erosion of northwestern Buffalo Bay between 1938 and 1979. Although the beach and nearshore is eroding, it is likely the addition of sediment would act to stabilise this section of eroding beach. Renourishment material could be provided by the ebb delta, the southern tip of Buffalo Bay or the isolated sandbar northeast of the inlet entrance.

## **Acknowledgements**

---

Firstly I would like to thank Environment Waikato, the Mercury Bay Community Council, Whitianga Waterways, the Whitianga Marina society and Alistair Simms for their financial support which enabled this research to take place. I would also like to thank Environment Waikato for supplying data and information and especially Vernon Pickett for his help and interest with the topic

To my chief supervisor Prof. Terry Healy, thank you for the open door, your guidance and encouragement. The time and effort you put into the study and your patience is much appreciated. Thanks also to my secondary supervisor, Dr Willem de Lange, for your large 'data-base' of knowledge and guidance with this research project.

A special thanks to Kyle Spiers and my 'unofficial supervisor' Gegar Prasetya for all their modelling help, general guidance, curries and discussions of many topics. Dirk Immenga, thank you for the field help and much appreciated input into this study. Also thanks to Ross Marsden at MetService for supplying weather data and helpful advice, and Carol Kohl of LINZ for the collection of hydrographic charts and maps.

Thanks to all the other students who helped me out, particularly in times of high stress! Thanks Greg for all the help with GIS, Kate and Nigel, my office buddies, for conversation and encouragement and all the other cool cats undertaking MSc research this year.

A big thank you goes to my family for every type of support, and providing lots of fun times. A special thanks to Mum for the long morning teas eating chocolate muffins, and the pep talks, and to Jo for your support, advice and jovial outlook. Thanks Lynn for the late-night and last-minute editing and proof-reading! And finally, a big thanks to Hayden, for listening to my ramblings, cooking me dinner and making me laugh as much as possible over the last 5 years.

# **Table of Contents**

---

<b>Chapter One – Introduction</b> .....	1
1.1 The problem.....	1
1.2 Objectives .....	5
1.3 Thesis structure .....	6
<b>Chapter Two – Description of Buffalo and Mercury Bays</b> .....	7
2.1 Introduction .....	7
2.2 Physical setting.....	8
2.2.1 Tectonic setting and geology .....	9
2.2.3 Sediment characteristics .....	10
2.3 Weather and Climate .....	18
2.4 Oceanographic Setting.....	18
2.4.1 Waves.....	19
2.4.2 Tides and currents.....	25
2.4.3 Sediment transport .....	26
2.5 Conclusion .....	28
<b>Chapter Three – Tidal Inlet Configuration</b> .....	30
3.1 Primary elements of a tidal inlet.....	30
3.1.1 Ebb tidal deltas.....	33
3.1.2 Flood tidal deltas .....	35
3.1.3 Inlet stability .....	35
3.2 Morphology of the Whitianga tidal inlet.....	36
3.3 Comparison of aerial photos to identify shoreline change adjacent to the inlet.....	41
3.4 Bathymetry comparisons .....	50
3.5 Conclusions .....	57
<b>Chapter Four – Data Analysis</b> .....	59
4.1 Field deployments .....	59
4.1.1 S4 current metres .....	60
4.1.2 DOBIE.....	61
4.1.3 Sediment traps .....	62
4.1.4 Limitations .....	63
4.2 Results and discussion of instrument data .....	64
4.2.1 Analysis of data.....	64
4.2.2 S4 tidal data.....	65

4.2.3 Currents .....	69
4.2.4 Wave data .....	76
4.2.5 Sediment .....	80
4.3 Conclusion .....	83
<b>Chapter Five – Hydrodynamic Model Results .....</b>	<b>84</b>
5.1 Tidal Model setup .....	85
5.1.1 General model inputs .....	85
5.1.2 Bathymetry .....	88
5.1.3 Boundary conditions .....	89
5.2 Tidal Model calibration .....	92
5.2.1 Elevation .....	92
5.2.2 Current speed and direction .....	95
5.3 Tidal Model validation .....	99
5.4 Experimental design .....	102
5.5 Model results of tidal flow .....	104
5.5.1 Mercury Bay .....	104
5.5.2 Buffalo Bay and Whitianga tidal inlet .....	106
5.6 Discussion and implications of Results .....	116
5.7 Wave model inputs .....	121
5.8 Wave model output .....	122
5.8.1 Boat loading facility .....	131
5.9 Discussion and implications of results .....	133
5.10 Conclusions .....	136
<b>Chapter Six – Modelling of Sediment Transport .....</b>	<b>138</b>
6.1 Sediment transport Model .....	138
6.1.1 Model setup .....	138
6.1.2 Model output – Bed level change .....	140
6.2 particle tracking Model .....	145
6.2.1 Model setup .....	145
6.2.2 Model-output – Particle tracks .....	146
6.2.3 Model-output – sediment dispersal .....	151
6.3 Discussion and Implications or results .....	155
6.3.1 Bed level change .....	155
6.3.2 Sediment transport .....	156
6.3.3 Sediment concentration .....	170
6.4 Conclusion .....	171

<b>Chapter 7 – Conclusions</b> .....	173
7.1 Physical setting .....	173
7.2 Morphological change .....	174
7.3 Buffalo Hay hydrodynamic monitoring .....	175
7.4 Model results .....	175
7.4.1 Wave behaviour .....	176
7.4.2 Boat ramp location .....	176
7.4.3 Sediment transport .....	177
7.4.4 Isolated shallow zone .....	177
7.4.5 Renourishment .....	178
7.5 Future Morphology .....	178
7.6 Suggestions for future research .....	179
 <b>Reference List</b> .....	 180

# List of Figures

---

## Chapter One:

- Figure 1.1 Location of the Whitianga inlet within Mercury Bay, situated on the North East coast of the North Island New Zealand. Dotted ellipse indicates shallow zone identified in the Notice to Mariners, 2005. Source: LINZ, 2005a. **2**
- Figure 1.2 The primary study location, the Whitianga inlet, including Buffalo Beach. The Whitianga Wharf and Marina are shown by red arrows. Source: LINZ, 2005a. **3**

## Chapter Two:

- Figure 2.1 Geology of Mercury Bay (adapted from Skinner, 1995). **10**
- Figure 2.2 The textural distribution of the sediment within Mercury Bay as given by Smith (1980) through surficial sediment sampling, showing zones of sediment and their relative size class. The pyramid shows the frequency distribution of sediment classes within Mercury Bay. A tendency towards sand is obvious. **14**
- Figure 2.3 Zones of wave convergence and divergence within mercury Bay ( $H=1.93$  m,  $T=5.48$  s). (i) Shows patterns form a northeast wave approach angle ( $45^\circ$ ). (ii) Shows waves approaching from the east. (iii) Shows a southeast wave approach. From Paton (1993). **21**
- Figure 2.4 The wave refraction patterns in Buffalo Bay looking north (top) and looking south (bottom). The dotted line illustrates the curvature of the wave line along Buffalo Beach. Photos taken in 1962. Source: Environment Waikato. **23**
- Figure 2.5 The inferred current cell sizes and directions within inner Mercury Bay as given by Cooper (2003) using current velocity data form S4 deployments. **26**

## Chapter Three:

- Figure 3.1 The principal morphological components of a tidal inlet on a sandy coast. Source: Hume and Herdendorf (1985). **32**
- Figure 3.2 The digitised bathymetry and primary elements of the Whitianga tidal inlet system constructed using soundings taken in 1995. Datum: Mean Sea Level (MSL). **37**
- Figure 3.3 Logarithmic plot of the tidal prism versus cross sectional area (morphological stability) of selected tidal inlets in New Zealand as given by Heath (1975) and other named works. Source: Hume and Herdendorf, 1988b. The rectangle indicates Whitianga inlet stability as calculated by the author. Whitianga 1 refers to the stability using data from Hume and Herdendorf (1992,1993) and Whitianga 2 refers to stability approximated using the area calculated by author and approximate estimated decrease in tidal prism. **40**
- Figure 3.4 Whitianga township 1944. Note the extensive dune ridges. Source: Environment Waikato, 2006 **42**
- Figure 3.5 The Whitianga township, inlet and southern Buffalo Beach in 1990. The dotted line area represents the beach area in 1944 and the solid line area is the beach area in 1990. Source: Environment Waikato, 2006 **43**
- Figure 3.6 Whitianga township, Inlet and Buffalo Bay 1995. Source: Environment Waikato, 2006 **44**
- Figure 3.7 Mercury Bay 2002 showing the large plume of sediment exiting the Whitianga Harbour. The green area shows the beach area in 1995 and the outlined area shows the each area for 2002. Source: LINZ, 2006 **45**

Figure 3.8 The beach area change from 1995 to 2002 for the southern section of Buffalo Beach. The dark green area shows the beach area for 1995 and the aqua area shows the beach area for 2002. Photo A has the 2002 area over top of the 1995 area, and photo B shows the 1995 area on top of the 2002 area. The white line indicates the approximate position of the ebb delta. Source: LINZ, 2005 **47**

Figure 3.9 The beach area change from 1995 to 2002 for the northern section of Buffalo Beach. The dark green area shows the beach area for 1995 and the aqua area shows the beach area for 2002. Photo A has the 2002 area over top of the 1995 area, and photo B shows the 1995 area on top of the 2002 area. Source: LINZ, 2005 **48**

Figure 3.10 The shoreline change at Buffalo Beach between 1944 and 1978 attained through non-rectified aerial photo comparisons. Healy et. al. (1981). **49**

Figure 3.11 The digitised bathymetry of Buffalo Bay in 1938 and 1979 based upon soundings undertaken by the RNZN. Datum converted to MSL. **51**

Figure 3.12 The residual map of Buffalo Bay showing areas of accretion and erosion between 1938 and 1979. White areas represent minimal or no change in depth. The two integers represent accretion and scour. Arrow indicates the Taputapuatea Stream entry. **53**

Figure 3.13 Residual map of the Whitianga inlet showing areas of accretion and erosion between 1979 and 1995. White areas represent minimal or no change in depth. The two integers represent accretion and scour **56**

## **Chapter Four:**

Figure 4.1 Map of Mercury Bay showing the instrument locations for the first deployment (22<sup>nd</sup> November to 30<sup>th</sup> of December 2005) indicated by white circles with solid centres, and second deployment (21<sup>st</sup> March to 5<sup>th</sup> May 2006) indicated by solid circles. Circles with rings around them indicate where sediment traps were attached to the instrument frame. Map adapted from LINZ (2005a). **60**

Figure 4.2 The S4 current meter with its frame. Sediment traps were fastened to the sides, as seen to the left of the photo. Photo taken by author. **61**

Figure 4.3 The DOBIE water level gauge in an ocean frame. Photo taken by author. **62**

Figure 4.4 An example of the type of sediment traps used, seen attached to the S4 frame. The cap on top of the trap is removed after they are deployed. Photo taken by author. **63**

Figure 4.5 The lag times of the M2 tidal wave constituent between instrument sites within Mercury Bay using data from both deployments, 22<sup>nd</sup> November to 30<sup>th</sup> December 2005 and 21<sup>st</sup> March to 2<sup>nd</sup> May 2006. Note arrows do not necessarily indicate flow paths. Map adapted from LINZ (2005a). **66**

Figure 4.6 The total, tidal and non-tidal sea level elevation at Buffalo Bay for the second deployment (21<sup>st</sup> March to 2<sup>nd</sup> May 2006). The total elevation is relative to the depth the instrument was deployed at (4 m) and the tidal elevation is relative to the mean sea level of the data set. **67**

Figure 4.7 The non-tidal water level elevation at Buffalo Bay relative to the depth of the instrument (~4 m) and the inverse atmospheric pressure recorded at the Whitianga aerodrome for the duration of the second deployment 21<sup>st</sup> March to 2<sup>nd</sup> May 2006. **68**

Figure 4.8 The total, tidal and non-tidal water level elevation at the wharf for the second deployment 21<sup>st</sup> March to 2<sup>nd</sup> May 2006. Some data was removed due to errors. The total elevation is relative to the depth the instrument was deployed at (~8.5 m) and the tidal elevation is relative to the mean sea level of the data set. **69**

Figure 4.9 The current direction (degrees) (given as the direction the current is traveling towards) and speed ( $\text{m s}^{-1}$ ) at a) Whitianga wharf and b) Buffalo Bay sites between the 21<sup>st</sup> March and 2<sup>nd</sup> May 2006. **70**

Figure 4.10 The non-tidal current speed and direction at the Buffalo Bay site. Directions are derived from U and V vectors which are positive or negative according to their direction relative to compass direction (0-360°). Positive values represent north and east current components and negative values represent south and west current components. **72**

Figure 4.11 The a) non-tidal current speed at Buffalo Bay; b) the wind speed recorded at Slipper Island; and c) the wave height at Buffalo Bay for the second deployment, 21<sup>st</sup> March to 2<sup>nd</sup> May 2006. **75**

Figure 4.12 A) The significant wave heights; and B, the wave periods recorded at Buffalo Bay and the wharf monitoring site during the second deployment from 21<sup>st</sup> of March to the 2<sup>nd</sup> of May 2006. **77**

Figure 4.13 The wave height (top) and wave period (bottom) recorded at the Buffalo Bay site over the second deployment from 21<sup>st</sup> of March to the 5<sup>th</sup> of May 2006. The dashed line represents a 9 second wave period and dashed ellipse indicates the rapid drop in wave period. **78**

Figure 4.14 The recorded wave directions at the Buffalo Bay (top) and wharf sites (bottom) for the second deployment, 21<sup>st</sup> March to 2<sup>nd</sup> May 2006. Lines on the top graph indicate the location of the majority of wave approach directions from 60-80°. **79**

Figure 4.15 The sediment accumulation rate for each sediment trap site for the second deployment, 21<sup>st</sup> March to 5<sup>th</sup> May 2006. **81**

## **Chapter Five:**

Figure 5.1 The Bathymetry used to model Mercury Bay and Buffalo Bay. Dotted line indicates the initial open boundary placement for Buffalo Bay. **91**

Figure 5.2 The model predicted and measured tidal water level elevation at a) Buffalo Bay, b) the entrance, and c) the wharf over the 10 day calibration period, 8<sup>th</sup> -18<sup>th</sup> April 2006. Measurements are plotted hourly for the model-simulated elevation and for the elevation at the wharf and Buffalo Bay sites. The measured elevation at the entrance site is plotted at 10 minute intervals. The Mean Absolute Error (MAE) is given also. **94**

Figure 5.3 An example of the time series of measured current speed 1 m off the bed at a) the wharf and b) Buffalo Bay sites, and depth averaged speed (derived from the measured current speed recorded by an S4 current metre 1 m off the bed), at a) the wharf, and b) Buffalo Bay. **96**

Figure 5.4 The model-simulated and measured current speed at a) the wharf site and b) the Buffalo Bay site for the 8<sup>th</sup>- 18<sup>th</sup> April 2006. The model-predicted speed is depth averaged and the measured depth averaged speed is derived from the measured current speed recorded by an S4 current metre 1 m off the bed at the Buffalo Bay site. Measured and simulated speeds are plotted hourly. **97**

Figure 5.5 Rose plots of the model simulated and measured current speeds and direction (moving to) at a) Buffalo Bay, and b) the wharf over the calibration period. The model simulated plots have been rotated 82.5 degrees clockwise. Calm is defined as the percentage of the speed below 0.1 m/s for Buffalo Bay and below 0.36 m/s for the wharf site. 10 % represents the percentage of currents at each speed. The palette for each site is given in ms<sup>-1</sup>. **99**

Figure 5.6 The model simulated and measured elevation at a) Buffalo Bay, b) the entrance and c) the wharf site over the spring and neap cycles. Measurements are plotted hourly for the model-simulated elevation and for the elevation at the wharf and Buffalo Bay sites. The measured elevation at the entrance site is plotted at 10 minute intervals. **101**

Figure 5.7 Rose plots of the model simulated and measured current speeds and direction at a) Buffalo Bay, and b) the wharf over the validation period. The model simulated plots have been rotated 82.5 degrees clockwise. Calm is defined as the percentage of the speed below

0.16 m/s for Buffalo Bay and below 0.36 m/s for the wharf site. 10 % represents the percentage of currents at each speed. The palette for each site is given in  $\text{ms}^{-1}$ . **102**

Figure 5.8 Comparison of the measured current speed at the wharf and model simulated current speeds with no wind and with a westerly wind of 12 m/s. The model-simulated speed is depth averaged and the depth averaged speed is derived from the measured current speed recorded by an S4 current metre 1 m off the bed at the wharf site. **103**

Figure 5.9 Frames of the hydrodynamic model output for Mercury Bay on the ebb tide, illustrating the eddy on either side of the ebb jet as well as behind the Wharekaho headland **105**

Figure 5.10 Sequence of snapshots of the hydrodynamic model output for Buffalo Bay over an ebb tide and part of the flood tide. **110**

Figure 5.11 Sequence of snapshots of the speed and direction of currents at the Whitianga inlet over an ebb tidal cycle. Numbers correspond to minutes since ebb tide commenced. **112**

Figure 5.12 The residual circulation within a) Buffalo Bay and b) the tidal inlet over an average tidal cycle. Dashed line indicates likely areas of scour and dotted line indicates likely areas of deposition. **113**

Figure 5.13 Sequence of snapshots of the hydrodynamic model output for Buffalo Bay over an ebb tide for 1938 bathymetry. **115**

Figure 5.14 the path of the two eddy formations during the ebb tidal cycle at Buffalo Bay. The path of each eddy was determined by mapping the pathway of the centre of the eddy formation. The dashed line shows the path of the ebb jet and main tidal discharge from the inlet. The model-simulated pathways are compared with the 2002 aerial photo of Buffalo Bay. **116**

Figure 5.15 the path of the two eddy formations during the ebb tidal cycle at Buffalo Bay using 1995 and 1938 bathymetry. The path of each eddy was determined by mapping the pathway of the centre of the eddy formation. The dashed line shows the path of the ebb tidal discharge from the inlet. **120**

Figure 5.16 The wave behaviour within Mercury Bay with approach angles ranging from true north ( $0^\circ$ ) to true south ( $160^\circ$ ) using a wave height of 3 m and wave period of 9 seconds on the open boundary. **125**

Figure 5.17 The elevation of Buffalo Bay with a wave height of 3 m, wave period of 9 seconds and approach from  $90^\circ$  at the entrance to Mercury Bay. Arrows indicate wave propagation direction and ovals indicate areas of wave energy convergence. **126**

Figure 5.18 The elevation within Buffalo Bay with a 3 m wave height and 11 and 9 second wave period at the open boundary propagating from  $90^\circ$ . **127**

Figure 5.19 Sequence of snapshots of the wave height distribution within Buffalo Bay with approach directions of 10 – 150 degrees. A wave height of 3 m and period of 9 seconds were used at the open boundary. Note the reflection effect of the Wharekaho headland which causes larger wave heights at the southern end of Buffalo Beach. Dotted line indicates the potential breaking wave zone. **129**

Figure 5.20 The wave energy convergence within Buffalo Bay. Oblique aerial photos taken in 1962 looking a) north and b) south. Arrows show direction of wave propagation and ovals show areas of wave energy convergence. Source: Environment Waikato **130**

Figure 5.21 The 3 breakwater designs trailed at Ohuka Beach and the wave height distribution and elevation within Buffalo Bay due to the three hypothetical breakwater designs at Ohuka. **132**

Figure 5.22 The areas of high and low wave energy (H and L) and the resultant long shore current directions along Buffalo Beach for a) a 3 m and 9 second wave at the entrance to Mercury Bay and b) a 3 m and 11 second wave at the entrance to Mercury Bay. **135**

Figure 5.23 The wave propagation direction at Ohuka beach for a 3 m 9 s wave, and the ideal location for the boat loading ramp (indicated by the dotted square). **136**

## **Chapter Six:**

Figure 6.1 The simulated average bed level change and direction of total sediment transport drawn by mean tidal flows over a 10 day period within the Whitianga inlet using a  $d_{50}$  of 0.15 mm. The speed and direction of each arrow is taken at the base or origin of the arrow. **141**

Figure 6.2 A. The simulated bed level change averaged drawn by mean tidal flows over a 10 day tidal cycle within the inlet using a  $d_{50}$  of 0.15 mm. The thick dotted line indicates the approximate flood delta position and the oval indicates possible sandwave bedforms. B. The residual tidal cycle velocity vector pattern within the Whitianga Inlet. **143**

Figure 6.3 The simulated tidally induced bed level change drawn by mean tidal flows averaged over a 10 day period within the Whitianga inlet using a sand diameter ( $d_{50}$ ) of 0.1, 0.15 0.2 and 1.0 mm. All plots relative to same scale. **144**

Figure 6.4 The suspended particulate matter particle tracks along Buffalo Beach and across the inlet gorge over a 10 day mean tidal flow period. Solid circles indicate the starting position of each particle. White squares indicate final position of particle. **147**

Figure 6.5 Simulated zones of suspended particle ebb tidal transport pathways in the inlet entrance vicinity. **148**

Figure 6.6 Simulated tidally derived suspended particulate matter particle tracks within the Whitianga inlet over a 10 day mean tidal flow period. Solid circles indicate the starting position of each particle. Arrows indicate direction of particle track where two tracks are overlaid. **151**

Figure 6.7 Snapshots of the suspended total sediment transport pathways at different stages of the tide within Buffalo Bay, as simulated in the PAP model. **154**

Figure 6.8 The relationship between a) velocity and b) areas of deposition from a wall jet-plume. Source: Hoyal et. al., 2003. **156**

Figure 6.9 The maximum speed and subsequent direction of flow within the Whitianga estuary for the flood and ebb tide. Solid circles indicate position of particles released in the PAP model. **158**

Figure 6.10 The probable progression of a) the ebb delta shape and size and b) the tidal channel orientation. A. (--) indicates the approximate current ebb delta location, based on 2002 and 2005 aerial photos. (●●) indicates the approximate 1995 ebb delta position based on 1990 and 1995 aerial photos and 1995 hydrographic soundings. (-●) indicates the approximate ebb delta position in 1938 based on the 1944 aerial photos and 1938 hydrographic soundings. The solid line indicates the approximate future shape of the ebb delta in 10 years if left to evolve naturally. The arrow shows direction of sediment transport in this section of Buffalo Bay. B. (-●) indicates the tidal channel position in 1938 based on hydrographic soundings. (●●) indicates the approximate orientation of the tidal channel in 1995 based on the 1995 and 1979 hydrographic surveys. The solid line indicates the approximate future tidal channel realignment if ebb delta growth continues **160**

Figure 6.11 The two possible groin shape options (1 and 2), which were modelled to establish their effect on Buffalo Bay hydrodynamics. **162**

Figure 6.12 The current speed and direction around groin option 1 at the Whitianga inlet. **163**

Figure 6.13 The current speed and direction around groin option 2 at the Whitianga inlet. **164**

Figure 6.14 Snapshots of the suspended sediment transport pathways at different stages of the tide within Buffalo Bay using groin option 1, as calculated in the PAP model. Dashed oval on snapshot 6 shows the area of highest sediment concentration on the landward side of the groin. **165**

Figure 6.15 Snapshots of the suspended sediment transport pathways at different stages of the tide within Buffalo Bay using groin option 2, as calculated in the PAP model. Dashed oval on snapshot 6 shows the area of highest sediment concentration on the landward side of the groin. **166**

Figure 6.16 Snapshots of the particle tracks with sediment released within the inlet gorge and along Buffalo Beach for groin options 1 and 2. **167**

Figure 6.17 An example of an artificial headland from the Kashima Coast Japan (from Committee of coastal engineering and Japan Society civil engineering, 1994). **169**

Figure 6.18 The mapped pathway of the model-simulated sediment dispersal over an ebb tidal cycle matched with the 2002 aerial photo. The more solid the line, the more time in the ebb tidal cycle has elapsed. **171**

## List of Tables

---

### Chapter Two:

Table 2.1. The wave conditions for Mercury Bay using data from; Harris (1985) who used wave statistics from wave recorders at Hicks Bay, Bream Bay and Great Barrier Island, and Harris et.al. (1983) and Pickrell and Mitchell (1979), who used data provided by a wave recorder off Hicks Bay on the east coast of the North Island to interpolate swell directions. Swell waves are waves generated offshore and typically have larger periods. Sea waves are locally generated waves that have much smaller periods and are typically generated by the prevailing wind. **19**

### Chapter Three:

Table 3.1. Characteristics of selected tidal inlets on the north east coast of the North Island. Inlet types after Hume and Herdendorf (1988b) are: 4 = single spit; 5 = tombolo; 6 = barrier island. Sediment sizes after (Hume and Herdendorf, 1992) are fs = fine sand; ms = medium sand; lag or shell or gravel lag. Ebb delta shape type: 2 = Constricted ebb delta, 3 = high angle half delta, 4 = low angle half delta. Data taken from Hicks and Hume (1996) and Hume and Herdendorf (1992 and 1993). Some data for Whangapoua and Whangamata are missing. Whitianga 2 refers to statistics calculated by the author for this study. **38**

### Chapter Four:

Table 4.1 The Instruments used in the first field deployment, 22<sup>nd</sup> November to 30<sup>th</sup> December 2005 and the second deployment 21<sup>st</sup> March to 2<sup>nd</sup> May 2006. **59**

Table 4.2 The phase and amplitude and the calculated phase lag of the M<sub>2</sub> tidal constituent at each instrument site. **65**

Table 4.3 The wave statistics for Buffalo Bay and Whitianga wharf sites over the second (21<sup>st</sup> March to 2<sup>nd</sup> May 2006) deployment. **76**

### Chapter Five:

Table 5.1 The input variables for the hydrodynamic model calibration. **92**

Table 5.2 The input variables used for the PMS model **122**

Table 5.3 The wave statistics used to generate wave behaviour models **123**

### Chapter Six:

Table 6.1 The input variables for the MIKE 21 ST model **139**

Table 6.2 The input variables for the MIKE 21/3 PAP model **145**

## ***Chapter One - Introduction***

---

### ***1.1 The problem: Rapid Inlet Shoaling Coincident with Increasing Inlet Utilisation***

Mercury Bay is a large semi-enclosed embayment situated on the eastern Coromandel Peninsula of New Zealand (Figure 1.1). Within Mercury Bay lie Buffalo Bay and the township of Whitianga (Figure 1.2) which has a resident population of approximately 4000 but can swell to around 34,000 in the summer period of December to January (Neumann and Orams, 2005).

Many holiday makers are attracted to Whitianga due to the good facilities for recreational boating. The sheltered harbour of Whitianga estuary is ideal for vessel moorings and there is a great demand for these, both within the estuary channel and a 187 berth marina (V. Pickett, pers. comm., 2006). Further up the estuary, Whitianga Waterways, a canal subdivision connected to the Whitianga estuary, has been developed. When complete, this will provide 1600 sections, with many having private boat access to the Whitianga estuary (Neumann and Orams, 2005). In addition, a number of commercial vessels use the Whitianga wharf (Figure 1.2) as a port for unloading and loading seafood (scallops, tuna and squid) collected by commercial fishing boat operations within the greater Mercury Bay or eastern Coromandel area (Department of Conservation, 1990; Neumann and Orams, 2005). The wharf also serves as a departure point for passengers taking part in tours and local scenic adventures. Due to these factors, recreational and commercial boat traffic is substantial in and out of the inlet and within the greater Mercury Bay.

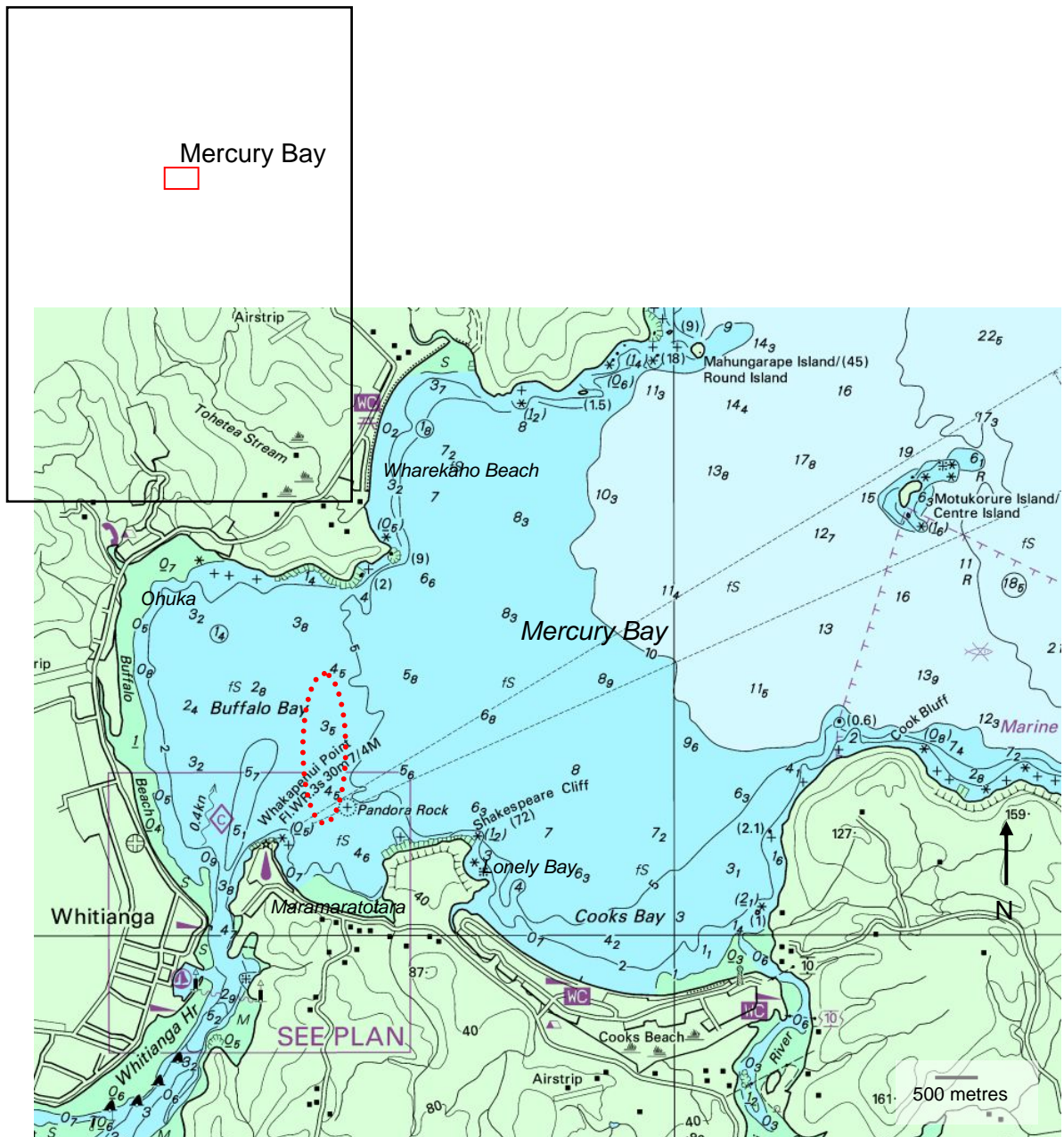


Figure 1.1 Location of the Whitianga inlet within Mercury Bay, situated on the North East coast of the North Island New Zealand. Dotted ellipse indicates shallow zone identified in the Notice to Mariners, 2005. Source: LINZ, 2005a.

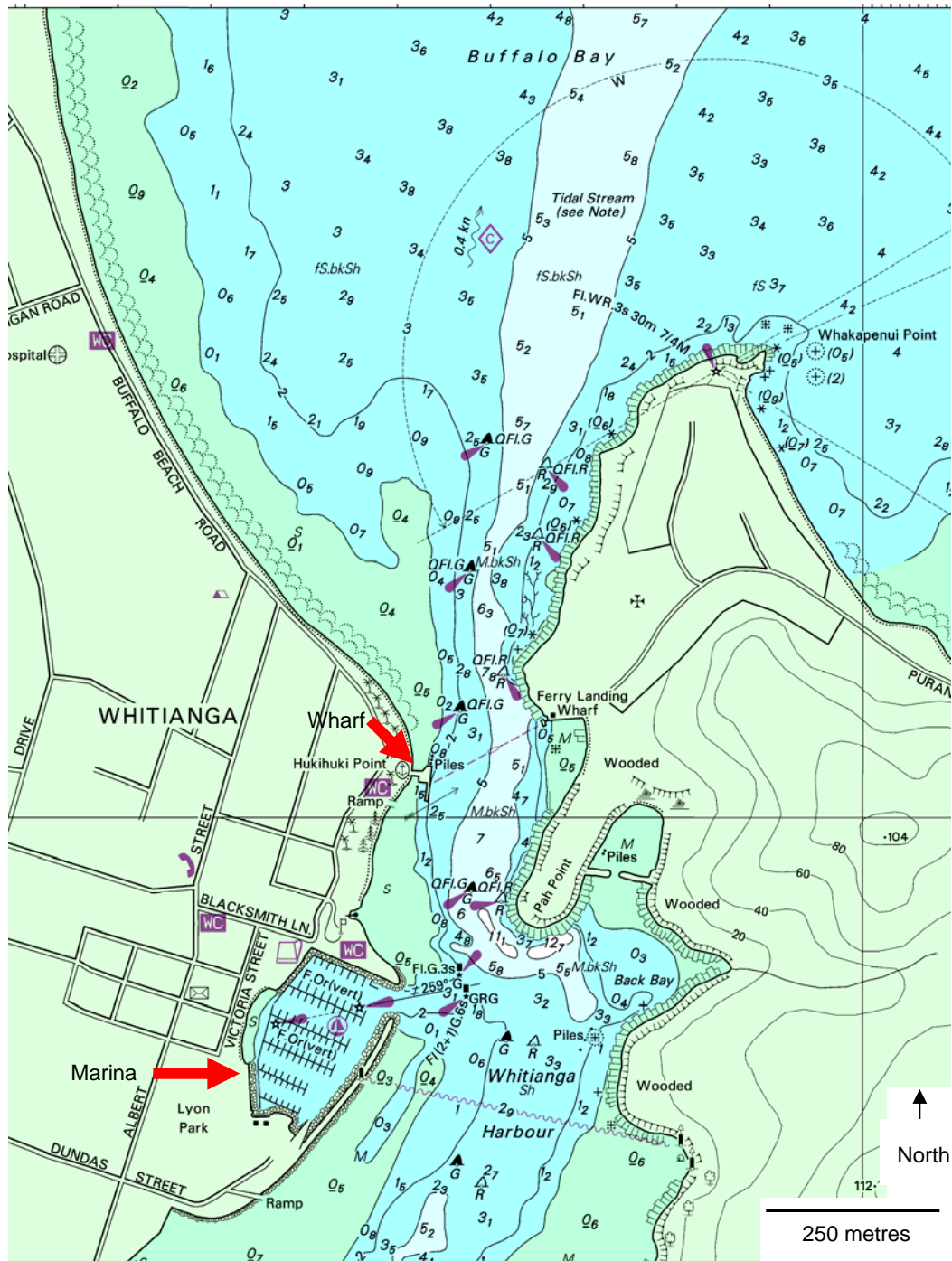


Figure 1.2 The primary study location, the Whitianga tidal inlet. The Whitianga wharf and marina are shown by large arrows. Source: LINZ, 2005a.

In September 2005, the Whitianga Harbourmaster issued a temporary “Notice to Mariners” pertaining to the shallow nature of the Whitianga Harbour entrance with depths of only 1 m relative to Chart Datum (CD) recorded in an isolated shallow zone, situated at the entrance to Buffalo Bay around Pandora Rock. The official

notice is still valid (December 2006) and can be viewed in appendix 1. The notice identifies the following problems:

1. *A sandbar has developed in the approaches to Whitianga extending from Pandora Rock (36° 49'.5S., 175° 43'.3E.) to a position one mile northwards.*
2. *Depths as shallow as one metre have been recorded in position 36° 49'.27S., 175° 43'.14E.*
3. *Vessels may encounter steep, breaking waves when onshore swell opposes the outgoing tide.*
4. *Mariners are cautioned to exercise care when navigating in the vicinity. (LINZ, 2005b)*

Recent anecdotal evidence from local users of the Harbour (G Vincent, pers. comm., 2006) suggests that presently at low tide, the inlet is so shallow in places that larger vessels (~ 8 m length and ~1.5 m draught) cannot exit the harbour. This shoaling creates a navigation problem for the many commercial and recreational vessels that use the harbour. Local users of the inlet and members of the Buffalo Bay community are becoming increasingly concerned about the shoaling at the inlet, and indeed, the long term future of the inlet.

Boat traffic is likely to increase further with substantial commercial and residential developments planned for the Whitianga township (Neumann and Orams, 2005) and land development likely at surrounding beach settlements such as Cooks Beach and Maramaratotara Bay. It is self-evident that such developments and the subsequent pressure on the inlet and adjacent harbour facilities require an increasingly sophisticated knowledge and understanding of the fundamental sedimentation processes effecting shoaling within the inlet itself, and also the adjacent Buffalo Bay sediment transport patterns. This is the main focus of the research in this thesis.

## **1.2 Objectives**

The overall aim of this study is to investigate the sedimentation processes within Buffalo Bay, particularly within and adjacent to the Whitianga inlet, primarily to ascertain reasons for the shoaling of the Whitianga tidal inlet and the cause of the shallow zone around Pandora Rock.

To investigate these issues, a major component of the research is to calibrate and apply the MIKE 21 DHI numerical model, which can be used to simulate most hydrodynamic processes, including wave simulations, tides, general current systems and sediment transport within Buffalo and Mercury Bays. In order to have confidence in the model simulations, the other key aspect of the study is the collection of high quality data for calibration and validation of the model. Once the validity of the model predictions has been established, it can be used to predict scenarios such as sediment transport and wave patterns under changing conditions.

Accordingly, the specific objectives of the study are:

1. To identify the extent of morphological change around the Whitianga inlet leading to the condition of shoaling including:
  - Establishing changes in the Whitianga inlet configuration and nearshore bathymetry using historical hydrographic charts and sounding sheets.
2. To establish the strength and patterns of tidal currents within inner Mercury Bay and entering and exiting the tidal inlet comprising Whitianga Harbour from 2-dimensional hydrodynamic modelling for the purpose of identifying present sediment transport pathways to investigate:
  - The cause of inlet shallowing;
  - The cause of the isolated shallow zone within Buffalo Bay;
  - The ultimate fate of the sediment emplaced on the beach for re-nourishment at Ohuka Beach to establish if it contributes to shallowing of the inlet;
3. To investigate wave propagation behaviour within Buffalo Bay to assess:

- Refraction patterns and energy concentration patterns in the Bay and their role in sediment transport and shoaling on the inlet;
- Optimal location for a new boat ramp within Buffalo Bay based upon wave energy concentration patterns.

4. Predict future morphology and extent of shoaling intensity on the tidal inlet

### **1.3 Thesis Structure**

Chapter 2: Gives a detailed background description of the study area for the purposes of understanding the infilling occurring in the inlet and to identify all factors contributing to the current sedimentation patterns and processes.

Chapter 3: Provides a background of tidal inlets and associated characteristics. The morphology of the Whitianga inlet is detailed and past and current trends in the morphology of the inlet and Buffalo Beach are identified by comparing aerial photos and digitised historic bathymetric charts

Chapter 4: Outlines the data collection and analysis phase. Results of the tidal, current, sediment and wave data are given.

Chapter 5: Provides a description of hydrodynamic (tidal and wave) model inputs and the application of the calibration and validation data is given. Model outputs for the tidal and wave behaviour are discussed.

Chapter 6: Addresses the inputs and results obtained from the sediment transport models. Conclusions and implications relating to the sediment transport in Buffalo Bay and on the Whitianga tidal inlet are made from the combined results of chapters 5 and 6.

Chapter 7: Provides an overview of the research and conclusions concerning the key hydrodynamic and sedimentation processes, and suggestions for future work.

## ***Chapter Two – Environmental Background Impacting on Shoaling at the Whitianga Inlet and Buffalo Bay***

---

The sedimentation problem at the Whitianga tidal inlet and within Buffalo Bay is closely related to sedimentary processes within the Whitianga estuary catchment. This chapter reviews the morphological setting in Buffalo Bay and the greater Mercury Bay, in so far as it provides understanding for physical aspects such as geology, tectonic setting, sediments, weather, tidal currents, and wave climate. Understanding of the physical background is necessary in order to fully understand the contributing factors to present hydrodynamic and sedimentation processes within Buffalo Bay and at the Whitianga tidal inlet.

### ***2.1 Introduction***

The beaches within Mercury Bay are headland controlled and have formed predominantly due to wave refraction patterns (Paton, 1993). Whitianga is the most extensive prograded barrier system on the east Coromandel coast (Abrahamson, 1987) with Buffalo Beach fronting over 30 Holocene dune ridges covering 5-6 kilometres (Healy et al, 1981). Whitianga estuary is difficult to classify as it is not a typical barrier enclosed or headland enclosed estuary, rather it is an intergrade between the two.

Mercury Bay has a history of sediment-related issues associated with a long record of coastal development dating back to the late 1800's (Loomb, 2006). The level of development on the east Coromandel coast has been significant since the mid 1960's (Healy et al., 1981). Most of the development took place on sandy foreshores or bay barriers (Healy et al., 1981). The concentrated subdivision developments coupled with the sensitivity of the environment in which they are located, have contributed to a high susceptibility to erosion and storm damage on many beaches on the east Coromandel coast.

The central section of Buffalo Beach is exposed to greater wave energy compared to the northern and southern ends of the beach, which are both sheltered by headlands (Cooper, 2003). Due to this, the central section of the beach, possibly eroded between 10 to 20 metres between the 1970's and 1980's (Healy et al., 1981). Much of the coastline here is backed by reserve so the erosion presents minimal risk to private property but does reduce the size of the reserve which is used by the whole community and is a significant tourist attraction and asset. Many protection methods such as seawalls, groins and renourishment, have been implemented over the past 50 years (Cooper, 2003) to combat the erosion along various sections of Buffalo Beach.

The most detailed and relevant investigations of coastal environmental processes in Mercury Bay are contained in 5 previous theses:

- Smith (1980) investigated the sea level oscillations, hydrology and sedimentology of Mercury Bay,
- Abrahamson (1987) developed an understanding of late Quaternary stratigraphy and evolution of coastal embayments on the east Coromandel Peninsula,
- Bradshaw (1991) examined the nearshore and inner shelf sedimentation on the east Coromandel coast,
- Paton (1993) made a study of the hydrodynamics and morphodynamics of selected cusped beaches on the Eastern Coromandel Peninsula; and,
- Cooper (2003) undertook a study of the coastal hydrodynamics and shoreline change at Buffalo Beach.

## **2.2 Physical Setting**

The essential physiographic setting of the east Coromandel Coast is described by Abrahamson (1978) as comprising:

- A coast aligned along an active plate margin;
- Volcanic activity along the eastern coast during the Pleistocene and Holocene periods which produced widespread tephras; and,

- a physiography distinguished by high terrain with small catchments, which typically experience a moderately wet climate.

These factors combine to form a coastline dissected by numerous streams and rivers which supply sediment to the nearshore (Abrahamson, 1978). The tectonic setting, geology, and sediment characteristics are discussed in the following sections.

### *2.2.1 Tectonic setting and geology of the Whitianga estuary catchment*

The tectonic setting of Mercury Bay produces the steep erodible catchments that contribute to high sediment runoff rates and the geology of the area dictates the sediment characteristics within the Whitianga estuary catchment. The east Coromandel coastline lies within the Coromandel Volcanic Zone (CVZ) which is part of the Hauraki Volcanic Region, comprising the largest area of andesite-dacite volcanoes in New Zealand (Skinner, 1986, 1995). The steep sided Coromandel Range runs through the centre of the Coromandel Peninsula. To the western side of the range lies the Hauraki depression, a down faulted graben (Thompson, 1966).

Coromandel Peninsula lies adjacent to the active margin of the Australian and Pacific tectonic plates which has resulted in an uplifted horst block, down-tilted to the east on the peninsula (Schoefield, 1967). The active plate setting has also caused faulting on the Coromandel Peninsula resulting in the gradual downwarping of some coastal sediments and also the formation of deep basins within which shelf and coastal sedimentation can occur (Bradshaw, 1991).

The Peninsula's position astride this active plate margin dominates the region's geology of predominantly tertiary volcanic rocks (Bradshaw, 1991). From Whitianga to Hot Water Beach the geology consists predominantly of rhyolite and andesite (Figure 2.1) (Skinner, 1995; Cooper, 2003). A thin layer of Quaternary tephra deposits overlies some areas and the weathering of these deposits has caused a deep regolith (Skinner, 1995). Hydrothermal alteration has facilitated erosion of this regolith which has been further destabilised by anthropogenic influences such as the

removal of forest (Bradshaw, 1991). Therefore the naturally high sediment load is exacerbated by land use changes in the Whitianga catchment.

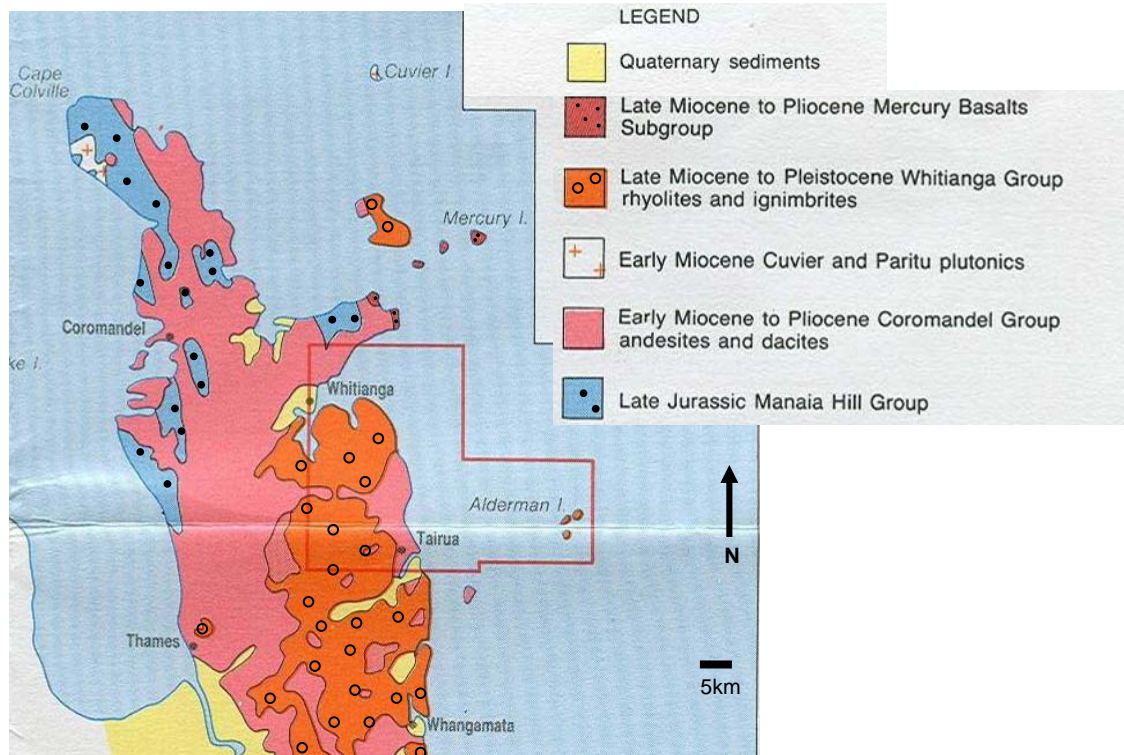


Figure 2.1 Geology of Mercury Bay (adapted from Skinner, 1995).

### 2.2.3 Sediment characteristics of Buffalo and Mercury Bays

The sediment characteristics within Mercury Bay, Buffalo Bay and at the Whitianga inlet provide an insight into the source and transport pathways of sediment. Due to its shape, Mercury Bay is a self-contained sediment system (Raudkivi, 1981; Abrahamson, 1987; Bradshaw 1991). The Whitianga estuary provides the primary source of sediment to Mercury Bay (Cooper, 2003; Mead and Moores, 2004) and has a total catchment area of 441 km<sup>2</sup>, receiving flow from 4 main rivers. The Waiwawa is the longest of these rivers draining a catchment of 190 km<sup>2</sup>, accounting for over 40 % of the Whitianga estuary catchment. The Whenuakite, Whangamaroro and Ounuora Rivers contribute catchments of 90 km<sup>2</sup>, 77 km<sup>2</sup> and 25 km<sup>2</sup> respectively (Cooper, 2003).

The Purangi estuary to the southern end of Cooks Bay also contributes to sediment input to Mercury Bay but the extent is unknown. Comparison of 1971 and 2002

aerial photos show a sand spit is growing across the mouth of the Purangi estuary, and anecdotal evidence from local residents suggests the estuary is becoming shallower every year. The estuary catchment is small, covering only 0.45 km<sup>2</sup> (McClay, 1976), and presently there are no sedimentation records or hydrodynamic data available for the estuary.

It is highly probable that there are increased amounts of sediment exiting the Whitianga estuary due to land changes. Healy and Dell (1987) noted that many eastern Coromandel harbours had rapidly infilled in the decades preceding their study. However, estuary infilling is a natural process and eventually, if left to evolve naturally, all estuaries will eventually fill with sediment. The upper reaches will become pasture, swamp or even housing developments while the lower reaches become choked with marine deposits causing them to only flow in times of high rainfall or at high tide (Hume and Swales, 2003). New Zealand has many 'dead' or infilled estuaries, particularly on the northeast coast. Examples on the Coromandel Peninsula include Hot Water Beach, Otama, and Waikawau (Hume and Swales, 2003).

Healy and Dell (1987) attribute the rapid infilling in many Coromandel Peninsula estuarine catchments to increased sedimentation rates, coinciding with felling of dense native bush and aided by an increased sediment yield from pasture land. Kauri logging was a big industry in many Coromandel estuary catchments, beginning in the 1800's. Milling in the Whitianga catchment ceased in the 1930's (McGlone, 1988) but an exotic (*pinus radiata*) forestry sector is now operating within the catchment. Steeper portions of the catchment have been allowed to regenerate back to native bush but flat to rolling areas have been cultivated for forestry, agriculture and horticulture. In recent decades, intensification of subdivision has occurred within the catchment also. Thus although kauri milling is no longer contributing to sediment runoff in the catchment, the exotic forestry industry, dairy operations and subdivision all contribute to the current high sedimentation rates within the Whitianga estuary

It is estimated that Polynesians settled the Coromandel Peninsula in c. 700 BP (Hume and Dahm, 1991). Europeans settled the Peninsula around 1830 and according to Sale (1978) both Maori and European settlers caused accidental and controlled burn off and felling of previously densely forested areas. This clearing resulted in accelerated levels of fine, muddy sediment runoff into estuarine areas. Hume and Dahm (1991) investigated the effects of settlement on the Coromandel Peninsula on sedimentation rates. Core stratigraphy was investigated using pollen and radiocarbon dating in the Firth of Thames, and Coromandel and Whangapoua harbours, to identify pre-Polynesian horizons. They ascertained that prior to any settlement, sedimentation rates in most Coromandel harbours were in the order of 0.1-0.2  $\text{mmy}^{-1}$ . However post-European settlement rates ranged from 0.3-2.8  $\text{mmy}^{-1}$  (Hume and Dahm, 1991).

Sedimentation rates have been calculated for the Tairua estuary, which is similar to the Whitianga estuary; comprising a catchment draining 280  $\text{km}^2$  of steep and erodible, weathered andesite, dacite and rhyolite. Hume and Gibb (1987) identified a wood debris layer within shallow inter-tidal sediments in the Tairua estuary. The layer was attributed to waste products produced by kauri log mills operating on the estuary coast between 1864 and 1909. This layer provides a datum to establish historical sedimentation rates within the estuary and compare them to present rates. Hume and Gibb (1987) were able to estimate a sedimentation rate for the middle of Tairua Harbour between 1933 and 1944 of 6  $\text{mmy}^{-1}$  which, if continued would rapidly infill the estuary. Below the marker of debris, there was a layer of shell accumulation. This suggests that prior to the logging operations, which saw large scale deforestation within the Tairua catchment, conditions within the estuary must have been favourable to shellfish and molluscs which do not normally tolerate high suspended sediment load in the water. This evidence proposes that the sedimentation rate increased due to deforestation. However, Hume and Gibb (1987) hypothesise that sedimentation rates may have started to decelerate recently due to reforestation in some of the catchment.

Similarly, Sheffield (1991) established pre- and post-European sedimentation rates within the Whangamata Estuary, situated south of Whitianga on the Coromandel Peninsula. She found rates of up to  $11 \text{ mmy}^{-1}$  in parts of the harbour between 1940-1990. From 1140-1940 AD the rate was estimated to be only  $0.28 \text{ mmy}^{-1}$ , highlighting a massive increase in sedimentation post-1940 when mining and land developments intensified in the catchment (Sheffield et al., 1995). The examples of Tairua and Whangamata can not be directly applied to the Whitianga sedimentation situation as the catchments are not exactly the same, but they offer an insight into the relationship between sedimentation rates and anthropogenic influences in Coromandel Peninsula estuary catchments.

McGlone (1988) undertook a pollen analysis of 2 cores within the Whitianga Harbour to attain records of changes in the catchment. Through dating of pollen horizons, he established sedimentation rates within the harbour during the Polynesian era, prior to mass land clearing, ranged from  $0.6$  to  $1.1 \text{ mm year}^{-1}$ . For the period between 1970-1988 McGlone (1988) estimated sedimentation rates between  $9.11$ - to  $12.0 \text{ mm year}^{-1}$  within the Whitianga estuary, suggesting sedimentation rates remained high after kauri logging ceased.

The earliest sampling of surficial sediments within Mercury Bay was undertaken by Smith (1980) who undertook a survey of the general sedimentology of Mercury Bay (Figure 2.2). He suggested very fine, well sorted sand was the dominant textural class in Mercury Bay. A patch of sandy mud was identified at the northern side of Buffalo Bay, followed by prominent muddy sand facies running seaward. The highest mud concentrations in Mercury Bay were found in the sheltered areas which receive lower wave energies, particularly the northern side of Buffalo Bay. This corresponded to an area noted by Smith (1980) as occupied by an ebb tidal plume from the Whitianga estuary over a flood tide. Seaward of this area the mud forms a corridor along the northern side of Mercury Bay (Figure 2.2) (Smith, 1980). The nearshore of the southern half of Buffalo Bay is however mud free.

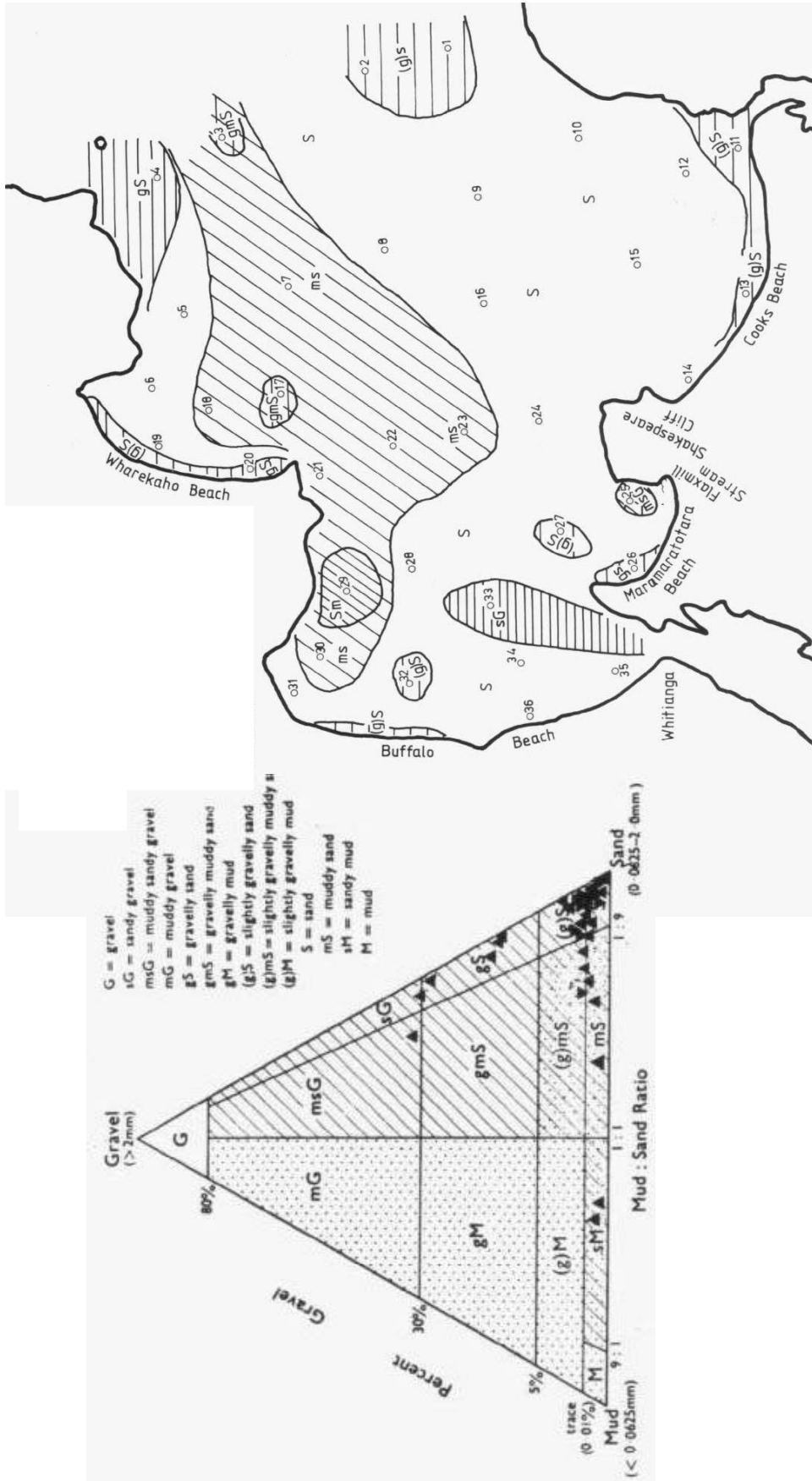


Figure 2.2 The textural distribution of the sediment within Mercury Bay as given by Smith (1980) through surficial sediment sampling, showing zones of sediment and their relative size class. The pyramid shows the frequency distribution of sediment classes within Mercury Bay. A tendency towards sand is obvious.

Smith (1980) hypothesised that the absence of the mud on the actual beach at the northern end of Buffalo Bay was suggestive of a low localised mud supply from the nearby streams. He suggested the mud was prevented from accumulating on the nearby beach due to local wind generated wave activity, which caused winnowing of these fine sediments. Smith (1980) interpreted from the mud distribution (Figure 2.2) that there was seaward suspended sediment dispersal from the northern end of Buffalo Bay, at Ohuka Beach, and was the first to point out that the beach and nearshore processes of Buffalo Beach are related to the sediment processes occurring on the Whitianga ebb tidal delta.

Gravels were found within the flood and ebb channels of the Whitianga estuary ebb tidal delta. High carbonate concentrations (shell material) were found at Maramaratotara, Cooks and particularly Lonely Bay Beaches, which is indicative of a local input of biogenic material. Local processes such as cliff erosion, reef and boulder attrition and abrasion within higher wave energy areas do produce coarser sand/gravel pockets (Smith, 1980).

A study conducted by Healy et al., (1981) surveyed 27 east Coromandel Peninsula beaches to provide baseline data of beach sediments. The study also inferred local sediment sources were dominant within Mercury Bay. Of the sediment systems studied from Port Jackson to Waihi Beach, no dominant littoral drift systems were identified; rather, most east Coromandel beaches were identified as closed systems (Healy et al., 1981). However, some east Coromandel beaches would have had significant interaction with the continental shelf, receiving sediment from offshore, imperative in their formation. This theory was investigated in relation to Whitianga by Abrahamson (1987).

The dune ridges and coastal plain lowlands of Whitianga were classified by Abrahamson (1987) as a prograded barrier, indicative of an abundance of sand. The Whitianga lowland consists of over 30 low relief sand ridges and she assumed an approximate rate of progradation to be close to 0.5 m a year over the last 1800 years. She suggested through dune and shelf sediment samples, that interaction between the shelf and local embayments such as Mercury Bay via diabathic systems

were very important in barrier formation in the late Quaternary times and could still be responsible for phases of local barrier progradation or erosion.

Bradshaw (1991) concurred with this view and proposed that local shelf sedimentation patterns were caused by processes occurring during the last sea level stabilisation, approximately 6500 years BP. He suggested that shelf sediments were reworked into equilibrium with the regional conditions on the eastern Coromandel. Fine sands were winnowed from coarser material during storms and were then transported onshore by wave-induced currents during calm conditions. Each embayment then became either a closed system unaffected by shelf sedimentation or an integral part of shelf transport with finer sands moving onshore to form barrier spits (Bradshaw et al., 1991). He further suggested that in earlier Holocene times the continental shelf was a dominant source of sediment for barrier spit deposits, as stated by Abrahamson (1987), but that presently the shelf is a temporary store of sediment for eroded beach sands during storms.

The abundant fine sediments identified by Smith (1980) and Bradshaw (1991) within Mercury Bay are suggestive that energy conditions are low or that supply of fine sediment is high. Bradshaw (1991) attributes the extensive occurrence of very fine grained shelf sands within Mercury Bay to the high terrestrial sediment inputs and suggests the most likely source of this sediment is the Whitianga harbour catchment. This is indicated by the high traces of biotite and abundant lithic fragments in the Buffalo Beach deposits which are typical of river supplied sediment (Bradshaw 1991).

Side scan sonar surveys presented by Bradshaw (1991) identified fine textured sediment to be dominant within Buffalo Bay. He established that mud content ranges from less than 5 % over the southern part of the inner Bay to up to 50% at the northern end of Buffalo Beach. This agrees with Smith's (1980) representation of sediment distribution (Figure 2.2). Bradshaw (1991) carried out seismic sub-bottom stratigraphy for the Mercury Bay which indicated a thick (15 m) nearshore wedge of sand just offshore from the Whitianga Harbour and a thinner (6 m) surficial covering of sediment on the inner shelf within Mercury Bay. These patterns were

interpreted as depicting an accreting shoreface within Mercury Bay (Bradshaw 1991).

Storm wave action was interpreted as an important process for reworking sediment nearshore and on the inner shelf (Bradshaw, 1991). The shape of the grains found within Mercury Bay provided evidence of terrestrial sands being reworked offshore from inner Mercury Bay (<10 m water depth) surface as grains within inner Mercury Bay were angular to very angular whereas they were increasingly rounder offshore in the outer Mercury Bay (> 10 m water depth). Further, the high degree of sorting in the Mercury Bay sediments is consistent with significant reworking of sediments (Bradshaw, 1991).

The most extensive sampling survey along Buffalo Beach was undertaken by Cooper (2003) who also sampled within Buffalo and Mercury Bays. From his study, Buffalo Beach sediments overall were found to be fine to medium sand with finer sediment found at the southern and northern ends of Buffalo Beach, whereas the central section of the beach contained more coarse material. Based on the sediment sampling and a side scan sonar survey, Cooper (2003) reported Buffalo Bay sediments were fine and noted a fining of sediment in the offshore direction. Northern Buffalo Bay showed the best sorting. Sediment within Mercury Bay was predominantly fine to very fine sand which agrees with previous sediment surveys (Smith, 1980; Healy and Dell, 1982).

The most recent and specific descriptions of sediment in the Whitianga inlet are given by Cooper (2003) based on side scan sonar interpretations. Only a section of the inlet gorge was mapped and this was described as consisting of shallow bedrock with a thin covering of coarse sand and gravel deposits. A shell lag was identified protruding well past the ebb delta and into Buffalo Bay, following the path of the ebb tidal discharge channel.

### **2.3 Weather and Climate**

Climate data provides information associated with the origin, intensity and frequency of weather systems in the Mercury Bay catchment. The eastern Coromandel experiences a temperate climate which is predominantly warm and humid (Maunder, 1974). Average rainfall is between 1800 and 2000 mm per year (NIWA, 2006). Occluded mid-latitude cyclones, sub-tropical Tasman depressions and decaying tropical cyclones can result in intense, particularly orographic, rainfall (Harris et al., 1983). In 1981 over 300 mm of rain was recorded at Whitianga over a 24 hour rainfall period (Hume and Dahm, 1991) and in 1996, 426 mm over 24 hours were recorded in Tairua (Environment Waikato, 2006). The rainfall provides a mechanism for sediment to be transported from the catchment into the harbour and inlet vicinity. Increased rainfall within the catchment creates higher levels of sediment runoff and freshwater input.

Wind is capable of creating surface currents, down and up welling currents and locally generated wind waves which affect the oceanographic setting of Buffalo Bay. The wind direction and speed at Buffalo Bay are significantly controlled by the steep surrounding topography. MetService wind data for 1972-1980 show the dominant wind direction is from the west (offshore directed) but also indicates a strong easterly and north-easterly component (Smith, 1980; Abrahamson, 1987). Cooper (2003) deployed an Automatic Weather Station for 240 days along Buffalo Beach to record wind data. He found the dominant wind direction was from the west (270 degrees) with fastest recorded velocities of  $\sim 12 \text{ ms}^{-1}$ . The only other wind direction recorded was from the southwest.

### **2.4 Oceanographic Setting**

The oceanographic setting relates to hydrodynamic systems within the study site such as the wave climate and current speed and direction. Wave and current systems both have implications for sediment transport and therefore morphology and shoaling activity.

### 2.4.1 Waves

Wave climate on the eastern Coromandel coast is extremely variable (Pickrell and Mitchell, 1979). Mercury Bay has a mixed wave climate which experiences both wind forced sea and swell waves (Table 2.1). Swell waves are waves generated offshore and typically have larger periods. Sea waves are locally generated waves that have much smaller periods and are typically generated by the prevailing wind. Storm waves typically occur due to low pressure systems moving over the Coromandel Peninsula. The dominant approach angle of waves to Mercury Bay is 45° (northeast) but the swell approach angle ranges from 0-135° (north to southeast) (Pickrell and Mitchell, 1979).

Waves in Mercury Bay (Table 2.1) are highest during storm conditions, but the average period is low so large waves arrive frequently, bringing more energy to the nearshore region. Pickrell and Mitchell (1979) noted a slight winter increase in wave height and wave period within Mercury Bay which they associated with an increase in the frequency of locally generated northerly winds and a decrease in the frequency of southerly winds in summer.

*Table 2.1. The wave conditions for Mercury Bay using data from; Harris (1985) who used wave statistics from wave recorders at Hicks Bay, Bream Bay and Great Barrier Island, and Harris et al. (1983) and Pickrell and Mitchell (1979), who used data provided by a wave recorder off Hicks Bay on the east coast of the North Island to interpolate swell directions. Swell waves are waves generated offshore and typically have larger periods. Sea waves are locally generated waves that have much smaller periods and are typically generated by the prevailing wind.*

Condition	Wave Type	Average significant wave height, $H_s$ in m	Average Period, $T$ in seconds
Fair-weather	Swell waves	0.91-1.73	8.3-13
	Sea waves	1-1.5	4-9
Storm	Swell waves	1-5	4-10

Smith (1980) constructed wave refraction diagrams using the graphical method outlined in the Shore Protection Manual (1977) combining idealised wave heights of 1 m, wave periods of 7 and 10 seconds and wave approach directions of 85 and 65°. This enabled wave energy concentration and dissipation within Mercury Bay to be modelled. He suggested that the height of swell and sea waves entering the bay are decreased due to refraction, diffraction and shoaling of the seabed. He identified two obvious features of the wave orthogonals entering Mercury Bay. Firstly, Motukorure (Centre) Island acted as a 'refractive lens' causing a wave shadow zone particularly noticed at Buffalo Beach, with higher energies reaching Cooks and Wharekaho Beaches. Secondly, Smith (1980) realised significant diffraction occurs within Mercury Bay and causes lateral dispersion of wave energy (Smith, 1980).

Paton (1993) also undertook a wave refraction analysis in Mercury Bay using the University of Waikato wave refraction programme called 'Refraction' which computes wave heights, maximum orbital velocities and maximum grain size moved based on the orthogonal spacing indicating wave energy. She noted the importance of wave refraction and diffraction in influencing the alongshore wave energy distribution within the nearshore zone of Mercury Bay beaches depending on wave approach direction (Figure 2.3).

Her diagrams show that waves travelling from the northeast (Figure 2.3 (i)) result in higher wave energies spread over the beaches within Mercury Bay, and cause considerable focusing along Buffalo Beach and around the Whitianga inlet. Waves from the east (Figure 2.3 (ii)) show marked focusing, more than (i), along Buffalo Beach but the inlet is relatively sheltered due to Cooks Bluff. In comparison a southeast wave approach results in minimal focusing on Buffalo Beach or the inlet, with little or no wave energy reaching either. All three diagrams show Motukorure Island causing a wave shadow zone, with wave energy low or non-existent in the lee of the Island. These diagrams used a particularly low period swell wave, atypical to average conditions within Mercury Bay. Longer period swell waves would result in increased refraction as they are more able to 'bend'. Paton (1993) states that although Maramaratotara and Buffalo Beaches have similar aspects to Wharekaho, Maramaratotara is sheltered by a broad headland (Shakespeare Cliff) and wave energy is even less along Buffalo Beach due to both refraction and diffraction.

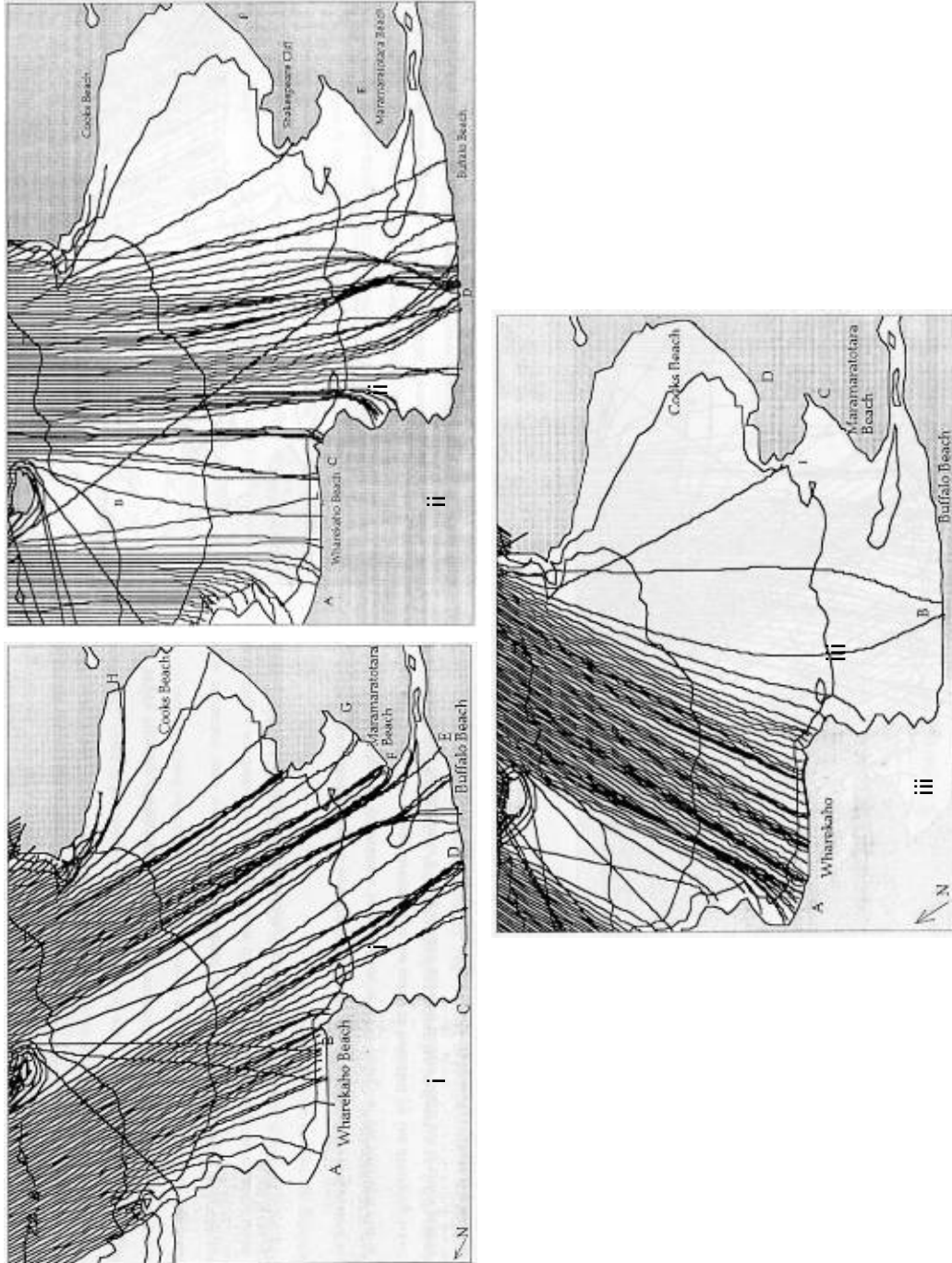


Figure 2.3 Zones of wave convergence and divergence within mercury Bay ( $H=1.93$  m,  $T=5.48$  s). (i) Shows patterns form a northeast wave approach angle ( $45^\circ$ ). (ii) Shows waves approaching from the east. (iii) Shows a southeast wave approach. From Paton (1993).

Cooper (2003) analysed wave climate of Buffalo Bay using 2 deployments of 3 S4ADW instruments. The approach angle of the waves within nearshore Buffalo Bay during his deployments was predominantly from the east with little variation apparent except near Ohuka (northern Buffalo Beach) where wave refraction around the Wharekaho headland altered the wave direction. Cooper (2003) found that wave heights varied considerably along Buffalo Beach. The headland at the northern end of the beach produced increased refraction activity which resulted in significant wave heights recorded here being half that of those recorded at central Buffalo beach areas. Cooper (2003) further suggested wave measurements indicated that the central section of Buffalo Beach actually received twice the energy of the northern end (Ohuka) over this deployment and is therefore directly exposed to waves generated from the east.

The mean recorded wave heights at each site ranged from 0.14 m offshore from Ohuka Beach to 0.55 m further offshore of the Wharekaho headland in Buffalo Bay. The minimum and maximum wave heights over both deployments were recorded at Ohuka and the offshore Wharekaho headland S4 sites respectively. This supports the theory that wave refraction diverges the wave energy reaching Ohuka Beach.

Aerial photos of Buffalo Bay often show waves refracting and converging at certain parts of Buffalo Beach. Figure 2.4 displays obvious deviations of wave lines running along the length of Buffalo Beach. The top photo illustrates the refraction of waves around Whakapenui Point and into the Whitianga inlet. The photo also indicates the concentration of wave energy on the mid to southern section of Buffalo Beach which is presently very narrow and now has a seawall in place to prevent further shoreline retreat. The bottom photo shows the concentration of wave energy on the centre section of Buffalo Beach with only smaller waves evident at Ohuka Beach.



Figure 2.4 The wave refraction patterns in Buffalo Bay looking north (top) and looking south (bottom). The dotted line illustrates the curvature of the wave line along Buffalo Beach. Photos taken in 1962. Source: Environment Waikato.

*Long period waves*

Seiching within Mercury Bay was first discussed by Smith (1980). He studied the tidal record at the Whitianga wharf between 1972-1974 and established the abundance of high frequency oscillations or seiches at the Whitianga wharf which were superimposed on the tidal wave for 10% of the 24 month record. Seiching was also identified by Goring (1999) in the Whitianga wharf tidal records for the period between July and November 1999. The seiche wave had an approximate period of one hour with varying phases and amplitudes. This seiching illustrates the vulnerability of Mercury Bay to tsunami waves which would be amplified by 10- or even 100-fold in size. This is because the shape of Mercury Bay evidently causes infragravity and tsunami waves to excite the natural resonance period of the Bay, causing an amplified tsunami effect and making Mercury Bay, and especially Whitianga inlet, highly vulnerable to tsunami hazard (Bell et al, 2004). Mercury Bay has experienced a number of recorded tsunami events in the last century, dating back to 1840. The largest of these recorded events was in 1960 as a result of an earthquake in Chile which exposed the wreck of the HMS Buffalo and resulted in run-up levels of ~2.5 m along Buffalo Beach (Bell et al, 2004). The tsunami may have contributed to sedimentation within Buffalo Bay and altered the configuration of the inlet by bringing sediment from the shelf into Buffalo Bay or by depositing Buffalo Beach sediments within Buffalo Bay.

The beaches within Mercury Bay exhibit well developed cusps some or all of the time. Smith (1980) associated these cusps with resonant edge waves within the Bay. The edge waves are trapped between the headlands which act as reflectors for maintaining edge wave harmonics (Smith, 1980). Paton (1993) used a time series of velocity and depth data obtained from a four hour S4 deployment to illustrate the occurrence of wave groupiness. Wave groupiness is a combination of two long period swell waves which causes a series of higher waves, followed by a series of lower waves and can influence and create edge waves. Paton (1993) suggested that edge waves existed at Buffalo Beach due to the groupiness of the waves that were recorded.

### 2.4.2 Tides and currents

The tidal wave within Mercury Bay is dominated by the  $M_2$  lunar semidiurnal tide (Goring, 1997, 1999). Other major constituents include the  $N_2$  semi-diurnal elliptical tide, the  $S_2$  semidiurnal solar tide and the  $K_1$  diurnal lunar tide. The mean sea level (MSL) is 1.30 m (Goring, 2003) and spring and neap tides are 1.62 m and 1.28 m respectively (Smith, 1980).

Smith (1980) studied the 2 year tidal record at the Whitianga wharf and collected seston, salinity and temperature samples to derive a conceptual model for tidal behaviour within Mercury Bay. He suggested a clockwise mean circulation pattern in Mercury Bay caused by the weak northward moving coastal current that passes the entrance to Mercury Bay, and tidal flows, particularly the ebb tide. Prior to Smith's investigation of the Bay, information was limited to minimal tidal data taken by the Royal New Zealand Navy. This tidal data taken in 1938 established a clockwise moving incoming tide which supports the theories of Smith (1980). He used salinity and temperature profiles of the Bay to attain a mean velocity of the circulation cell of  $0.04-0.06 \text{ m s}^{-1}$ , with inflow to the southern side of the Bay by Cooks Bluff and outflow occurring on the northern half of the Bay from Wharekaho Beach. The ebb tidal jet exiting the Whitianga Harbour was thought to cause forcing across and along the northern side of Buffalo Bay. The forcing was inferred as the cause of the clockwise circulation pattern, drawing water in the southern side with ebb flows leaving along the northern side of Mercury Bay (Smith, 1980).

In Cooper's (2003) hydrodynamic analysis (Figure 2.5) based on S4 current metre data, a similar clockwise rotating cell was identified within the greater Mercury Bay and a second, smaller ( $\sim 0.0012 \text{ m s}^{-1}$ ) circulation cell was inferred from current metre data in the nearshore zone of Buffalo Beach, moving anti-clockwise. Both of the cells (Figure 2.5) were assumed to be a result of the asymmetrical tidal flows characteristic of Mercury and Buffalo Bays, but the smaller cell in Buffalo Bay was assumed to be driven by the rotation of the larger cell in Mercury Bay.

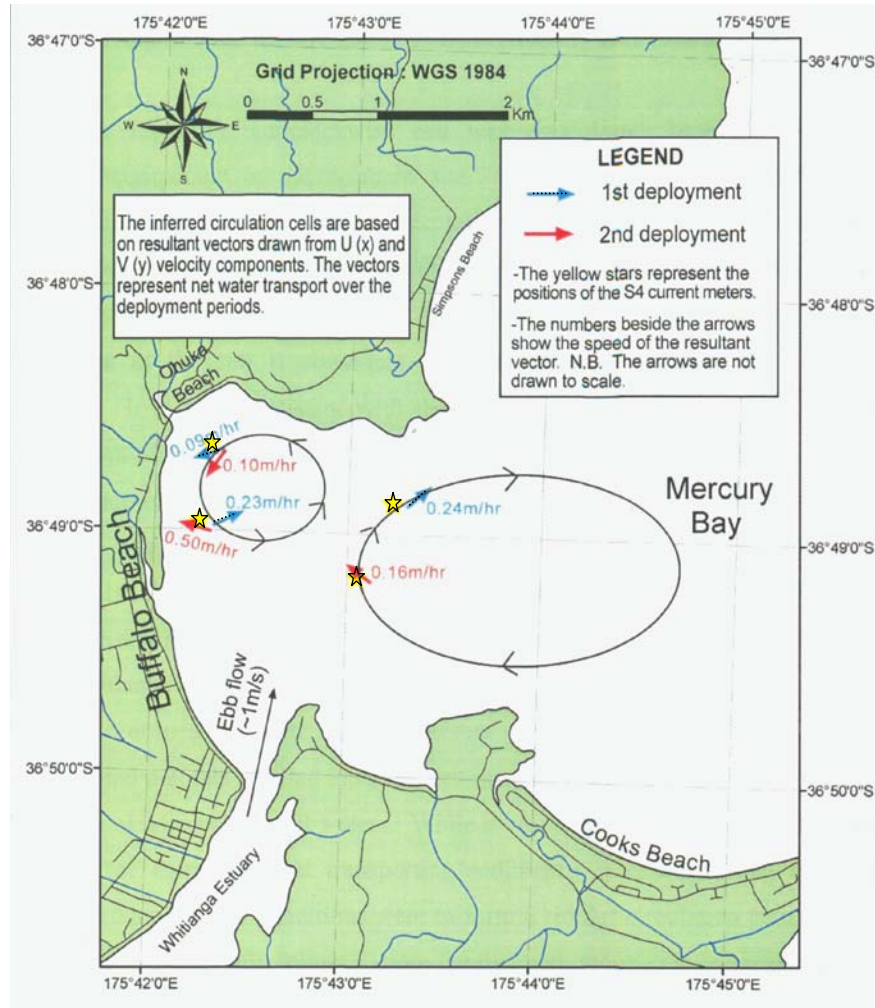


Figure 2.5 The inferred current cell sizes and directions within inner Mercury Bay as given by Cooper (2003) using current velocity data from S4 deployments.

### 2.4.3 Sediment transport

Using the method given by Komar and Miller (1975), Smith (1980) calculated wave orbital velocities and sediment entrainment thresholds. He suggested for sediment to be entrained over Mercury Bay, waves of  $H_s=0.6$  m are needed. He postulated that within the Mercury Bay, optimum sediment transport conditions occur during storm periods which produce elevated water levels and increased wave energy. These combined factors then erode and suspend beach sediment, which is then moved offshore by tides and storm-driven circulation (Smith, 1980).

The Coromandel shelf is storm-dominated whereby down-welling and up-welling events are common due to storm related wind directions (Bradshaw, 1991). This

typically means sediment transport is controlled by surface gravity waves and wind induced flows and entrainment events are episodic (Bradshaw, 1991). Bradshaw (1991) demonstrated that on the Coromandel coast, during onshore wind conditions typical of storms, currents form and flow offshore moving sediment towards the shelf. It is likely Mercury Bay receives some sediment reworked from the shelf in up-welling conditions, and could loose sediment to the shelf in down-welling conditions.

Cooper (2003) reported that increased current speeds correspond well to an increase in wave activity in Buffalo Bay, suggesting they may be important in sediment transport. He proposed that the headlands on either side of Buffalo Beach restrict sediment from the Harbour and beach face moving beyond Buffalo Bay with the predominant longshore transport taking sediment from the harbour to Buffalo Beach. However, he noted that suspended fine material could be carried out of Buffalo Bay and into the greater Mercury Bay.

Parabathic transport is weak along Buffalo Beach due to wave refraction patterns which do not allow for oblique wave approach, necessary for littoral drift initiation. Cooper (2003) used visual observation and comparisons of sand within the harbour to sand at the southern end of Buffalo Bay to suggest that the net littoral drift direction is south along Buffalo Beach, so sediment is transported down the beach and is then deposited around and within the inlet entrance where it maybe reworked onshore by wave activity.

Corroboration with the southward direction of net littoral drift direction is given by Healy (2003) who conducted a report for the Thames Coromandel District Council regarding remediation options for the eroding northern section of Buffalo Beach (Ohuka). Ohuka characteristically has no berm or offshore bar which suggests a low energy, dissipative wave environment. Evidence such as the frequent lag deposits of iron sand and the lack of frontal dunes, suggests the beach has a low sediment budget and is in an erosive state. In this report, Healy (2003) noted the tendency for stream mouths along Buffalo Beach to migrate south and that Ohuka beach conditions were characteristic of those observed at a beach updrift of a net littoral drift system. Moving south along Buffalo Beach, the frontal dune increases in size,

the mean grain size coarsens, beach berms become more developed and the beach face widens (Healy 2003). Healy (2003) suggested that these factors provided verification of a net littoral drift direction in the southwards direction, but the dominance or importance of this in relation to diabathic processes is still unknown.

## **2.5 Conclusion**

The factors significant in understanding the sediment transport in Buffalo Bay are:

1. The Mercury Bay catchment is very steep due to its tectonic setting astride a plate boundary which dominates the geology, primarily comprised of weathered and erodible rhyolite and andesite.
2. The primary source of sediment to the Whitianga inlet, Buffalo Bay and the greater Mercury Bay is the Whitianga estuary catchment which covers 441 km<sup>2</sup>. Sedimentation rates post the kauri milling era are still high which suggests present landuse within the catchment has significant influences. Sediment on the seafloor of Mercury Bay is generally very fine sand with some mud and coarse deposits. Buffalo Beach has predominantly fine sand with variations alongshore in grain size possibly due to supply from local streams. Mud deposits are found within Buffalo Bay in the northern end whereas the southern section has no mud deposits. Buffalo Bay has finer sediment than found on Buffalo Beach. The Whitianga tidal inlet gorge consists of predominantly coarse grained sediments with a lag of shells apparent in the channel seaward of the ebb delta.
3. Mercury Bay has a temperate climate with intense rainfall events common. The prevailing wind is derived from a westerly direction but southwesterlies, northeasterlies and easterlies also occur.
4. The wave climate in Mercury Bay is variable. Swell direction ranges from north to southeast and wave heights range from 0.9 metres in fair weather conditions to 5 metres in storm conditions. Wave refraction and diffraction behaviour is important within the whole Mercury Bay area.

5. The tidal signal primarily derives from the M2 constituent with a mean sea level of 1.3 m. Net currents move in a large clockwise cell around Mercury Bay with a second anticlockwise cell suggested within Buffalo Bay.
6. Sediment transport optimally occurs during storm conditions as waves have more ability to erode and suspend sediment. The Coromandel is a storm-dominated shelf and thus, down welling currents are common. Sediment transport within Buffalo Bay is dictated by the ebb tidal discharge from the inlet, and the net littoral drift direction south along Buffalo Beach.

## ***Chapter Three – Tidal inlet Configuration***

---

The key focus of this research is to understand the processes forcing morphological change at the Whitianga tidal inlet. In order to understand the existing and future form, the evolution of the inlet must be investigated.

This chapter presents a brief background on the general theory of tidal inlets and a description of the Whitianga tidal inlet. Comparisons of aerial photos and previous hydrographic charts and sounding sheets are used to show historical changes in bathymetry, and the morphological change of the Whitianga tidal inlet and adjacent shoreline.

### ***3.1 Primary Elements of a Tidal Inlet***

Tidal inlets are classified by Boothroyd (1985) as 'large bodies of sand deposited and moulded by tidal currents and by waves'. They can form on any depositional shoreline where sediment supply is adequate, but are formed by a number of different processes. Most tidal inlets on sea coasts have formed, at least partly, as a result of littoral drift but others may have formed due to hurricane/storm activity, the direction of tidal wave propagation, or the geometry of a bay (Bruun, 1978). The majority of New Zealand tidal inlets are formed by the latter two situations and predominantly occur in the North Island. They are internationally diverse due to the characteristic low littoral drift on the coasts they form along, and the lack of anthropogenic modifications, such as engineering structures (Hume et al., 1992).

The size of an inlet entrance is determined primarily by an interplay of forces from alongshore sediment transport by wave action and tidal current discharge. Tidal inlet behaviour is generally controlled by mean sea level (MSL), tidal currents entering and exiting the inlet, wave climate, storm magnitude and frequency, freshwater inflow and sediment supply (Michel and Howa, 1997; Kruger and Healy, 2006). Bedrock arrangement and the configuration of the adjacent shoreline may influence the shape and location of an inlet. Bedrock acts as a barrier to growth and can also influence the location of the main ebb channel (Hicks and Hume, 1996) while the

shape and proximity of the hardrock shoreline influences the form of the ebb tidal delta.

No two tidal inlets are the same, however most inlets do comprise some basic common features. Based on the morphology and hydrodynamics, the primary elements of a tidal inlet are (Figure 3.1):

1. The tidal gorge or throat channel (Figure 3.1 (2)) is the narrow, deep section in the inlet through which the strongest currents flow. This section is typically the narrowest and has minimal wave action. The gorge acts as a balance between scouring out the inlet throat by tidal action and infilling from littoral drift (Sheffield, et al., 1991).
2. The Inner section (Figure 3.1(x)) is situated on the harbour side of the inlet and typically houses shoals and channels, with tidal currents being the primary driving force for sediment transport. This is typically where the flood tidal delta forms.
3. The Ocean section (Figure 3.1 (y)) which is located seaward of the inlet includes the main ebb channel, marginal shoals and flood channels and the ebb tidal delta. This is where wave energy is important for introducing littoral drift of sediment into the inlet (Hume and Herdendorf, 1988a).

Tidal inlets are dynamic equilibrium systems. They are continually being reshaped and resized due to the interaction of energy input to the system and sediment input. On microtidal coasts (tidal range <2 m), such as the east coast of New Zealand, waves are the dominant process and energy source (Hayes, 1973). On macrotidal coasts (tidal range >4 m) such as the northwest coast of Australia, tidal currents provide the majority of energy, and on mesotidal coasts (tidal range 2-4 m), such as those in the Wadden Sea, Netherlands, energy is provided by a mixture of waves and tides (Hayes, 1973). These processes work to keep the inlet at an equilibrium status but often fluctuations of environmental factors, such as climate and sediment supply, or human-induced modifications, can cause inlets to shoal or become shallower. This process is exacerbated if littoral drift is strong, relative to the tidal currents, bringing beach sands towards the inlet. If diabathic transport is dominant the inlet may choke up from offshore deposits.

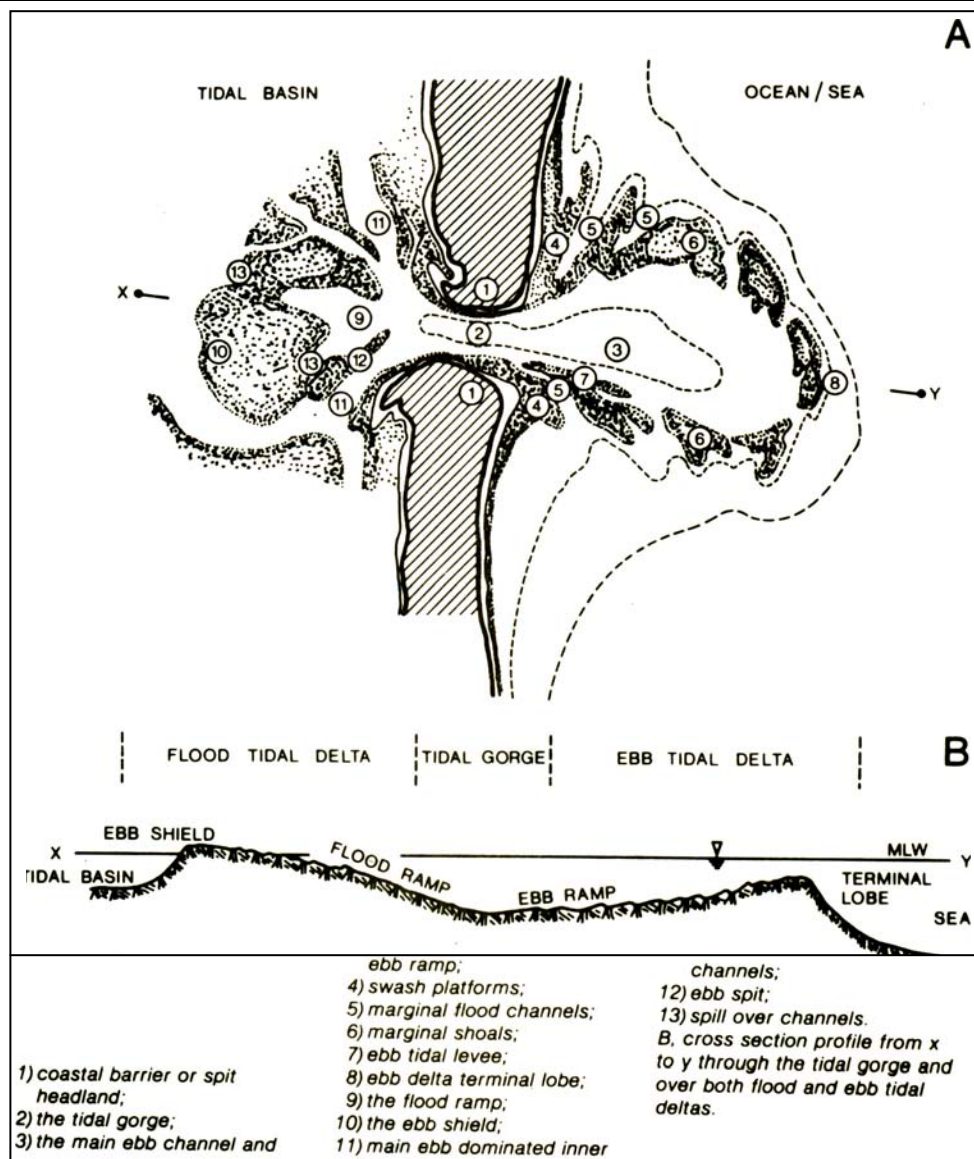


Figure 3.1 The principal morphological components of a tidal inlet on a sandy coast. Source: Hume and Herdendorf (1985).

All inlets are capable of shoaling to the point that they become closed off to the sea either temporarily or permanently (Bruun, 1978). Examples of this include the Hillsboro and Roca Baton inlets on the southeast Florida coast, which have both experienced temporary closure in the past due to shoaling across the inlet mouth (Stauble, 1993). Causes of inlet shoaling as given by Bruun (1978) include:

- prolongation of the inlet channel or channels;
- overwhelming deposits sediment material, particularly during storms;

- splitting up the main inlet channel into two or more channels, or formation of one or more additional channels from natural or artificial causes; or
- change in bay area from which water flows into the inlet or natural growth of the marshlands.

Tidal inlets are becoming increasingly affected by anthropogenic activities such as the maintenance of channels for navigation, the building of structures for docking and berthing of large vessels and the reclamation of land for marinas and port facilities (Elias and van der Spek, 2006). Such modifications can affect inlet stability and create regional problems because inlet processes have important implications for the evolution and morphology of the adjacent coast. This is primarily because inlets can act as a source or a sink of sediment in the coastal region, regulating sediment supply.

Sediment can be deposited on the ebb delta or inlet entrance channel from tidal, freshwater or wave induced currents (littoral drift) (Jimenez et al., 1997). Tidal inlets are also responsible for longer term loss of sediment as sand is transported into the backbarrier environment or deposited within prograding inlet channels (FitzGerald, 1988). Storm conditions with increased wave energy produce higher rates of sediment transport, and can increase the volume of sediment transported towards inlets from adjacent beaches and across the ebb tidal delta. Sediment transported seaward of the tidal inlet can be trapped and stored temporarily on the ebb delta from where it may be episodically released back onshore by tidal currents, or following storm events (FitzGerald, 1988).

### ***3.1.1 Ebb tidal deltas***

Ebb tidal deltas (Figure 3.1 (4-8)) are lobes of sediment deposited seaward of the inlet (Hayes, 1980). They represent a large sand reservoir and have significant control over sand exchange between estuaries and the open coast (Hicks and Hume, 1997). Coastal sands which are swept along the shore by wave action or littoral drift are commonly trapped by ebb deltas. However ebb deltas can also act as a source of sediment for the downdrift coast (Hicks and Hume, 1997). Some inlets incur sediment bypassing whereby sediment is transported from the updrift

side of the tidal inlet to the downdrift shoreline. This can occur due to three mechanisms (Fitzgerald, 1988):

- wave induced sand transport along the periphery of the ebb delta;
- transport of sand in channels by tidal currents, and,
- by migration of tidal channels and sand bars.

Sand shoals (Figure 3.1 (6)) associated with ebb tidal deltas can provide wave sheltering to adjacent beaches as they act as natural offshore breakwaters reducing wave energy reaching beaches landward of the delta (FitzGerald, 1988). The shape of an ebb tidal delta surface influences how wave energy is focused on the adjacent shoreline and how waves propagate into the inlet (Hicks and Hume, 1997). Through this ebb deltas can influence shoreline erosion on the adjacent beaches and erosion within the tidal inlet (Hicks and Hume, 1997).

The Florida coastline has many tidal inlets, of which a large portion have been modified. These have been studied for several decades (FitzGerald, 1988; Marino and Mehta 1988; Stauble, 1993) where it has been established that typically an increase in ebb delta volume is a result of increase in tidal prism, decrease in inlet depth/width ration and decrease in wave energy. Generally, ebb delta volume increases as wave energy decreases if the tidal prism remains the same (Boothroyd, 1985) and can be observed in New Zealand as the average ebb delta volumes on the west coast of the North Island are smaller than those on the east coast of the North Island, which receives lower wave energy (Hicks and Hume, 1996).

Hicks and Hume (1991) conducted a study of sand storage in New Zealand inlets, and found that the main control on the ebb delta volume was tidal prism. The tidal prism is regulated by the area and tidal range of the estuary, and the amplitude and phase of the tidal wave. They found the ebb delta volume also appeared to increase with other factors, such as decreasing wave energy, increased littoral drift rate, decreased throat depth and an increased angle of inlet outflow with respect to the shoreline.

### 3.1.2 Flood tidal deltas

Flood tidal deltas (Figure 3.1x) are not as well researched as their ebb counterparts. They are evident at most inlet systems but not all. A flood delta is a shield of sand that develops in the tidal basin landward of the gorge (Hume and Herdendorf 1985). Formed by decelerating flood currents, the flood tidal delta is typically composed of a flood ramp, flood channels, ebb shields, ebb spits and spill-over lobes. Ebb shields and ebb spits protect the flood ramp and channels from ebb current modification (Hayes, et al., 1972; Hayes, 1980). The flood delta is typically a similar shape and size to the ebb delta.

The dominant controls on flood delta formation, shape and size are:

- the shape and size of the bay landwards of the inlet throat with more space and a large tidal prism producing a large delta,
- the configuration of the headland-barrier,
- the route taken by the floodtide entering the inlet, and,
- the penetration of waves during storm events (Hume, 2003).

### 3.1.3 Inlet stability

A stable tidal inlet is defined by FitzGerald (1988) as having a 'stable inlet throat position and a main ebb channel that does not migrate'. There are two forms of stability within tidal inlets. *Positional stability* relates to the tendency for the inlet to migrate up and down coast. Most New Zealand inlets are positionally stable as they are typically sheltered by headlands which restrict inlet migration and provide a lower wave energy site for the inlet to emerge from (Hume and Herdendorf, 1992; Hume, 2003). *Morphological stability* relates to the cross-sectional area of the inlet throat which changes according to the availability of sediment and magnitude of hydrodynamic forces, particularly tidal currents. Morphological stability ensures the inlet has the ability to return to its original cross-sectional area after a disturbance such as a storm event (Hume, 2003). The tidal inlets of the northeast coast of the New Zealand are predominantly morphologically stable (Hume, 2003). Inlets are always changing and adjusting to changes in inlet geometry (i.e. littoral drift, sediment size, cross sectional area, and tidal prism) so no inlet is absolutely stable. However inlets which are not in equilibrium (unstable) experience erosion or

deposition in the inlet channel or lagoon as the processes struggle to adjust to changes.

### **3.2 Morphology of the Whitianga Tidal Inlet**

The Whitianga tidal inlet (Figure 3.2) is situated inside an embayment and is protected from swell by Whakapenui Point, thus making the tidal currents the dominant energy source. The narrow and elongated shape of the *ebb tidal delta* is influenced by the rocky shoreline of Whakapenui Point, which restricts lateral growth, and the sediment supplied from Buffalo Beach via littoral drift.

The Whitianga *flood tidal delta* is not clearly defined and there is limited information available about it. Aerial photos and the recent 1995 hydrographic chart were used to identify the approximate position of the flood delta (Figure 3.2). The flood delta is evidently located on the western side of the inlet and appears to have a similar long narrow shape to the ebb delta and comprises a narrow shoal or bank, aligned parallel to the main inlet channel.

The inlet gorge is located between the Whitianga wharf and the adjacent rocky shoreline. This is where the channel is narrowest and deepest and where the fastest currents are expected. There are two scour holes located approximately 100 m apart, which is not typical of most inlets and possibly an indication of instability in the inlet.

The morphology of the Whitianga inlet can be compared to other inlets along the north east coast of the North Island (Table 3.1). Ebb delta information, littoral drift rates, wave energy factors and runoff data was not available for Whangamata and Whangapoua so full comparisons cannot be made, but they were included to give an indication of east Coromandel coast inlet characteristics. The statistics for Whitianga were calculated using inlet bathymetry from 1979 and aerial photos prior to 1995, so new statistics have been estimated by the author, where possible, using recent aerial photos, and the 1995 hydrographic survey. There are some approximations with the new data associated with the location of the inlet throat.

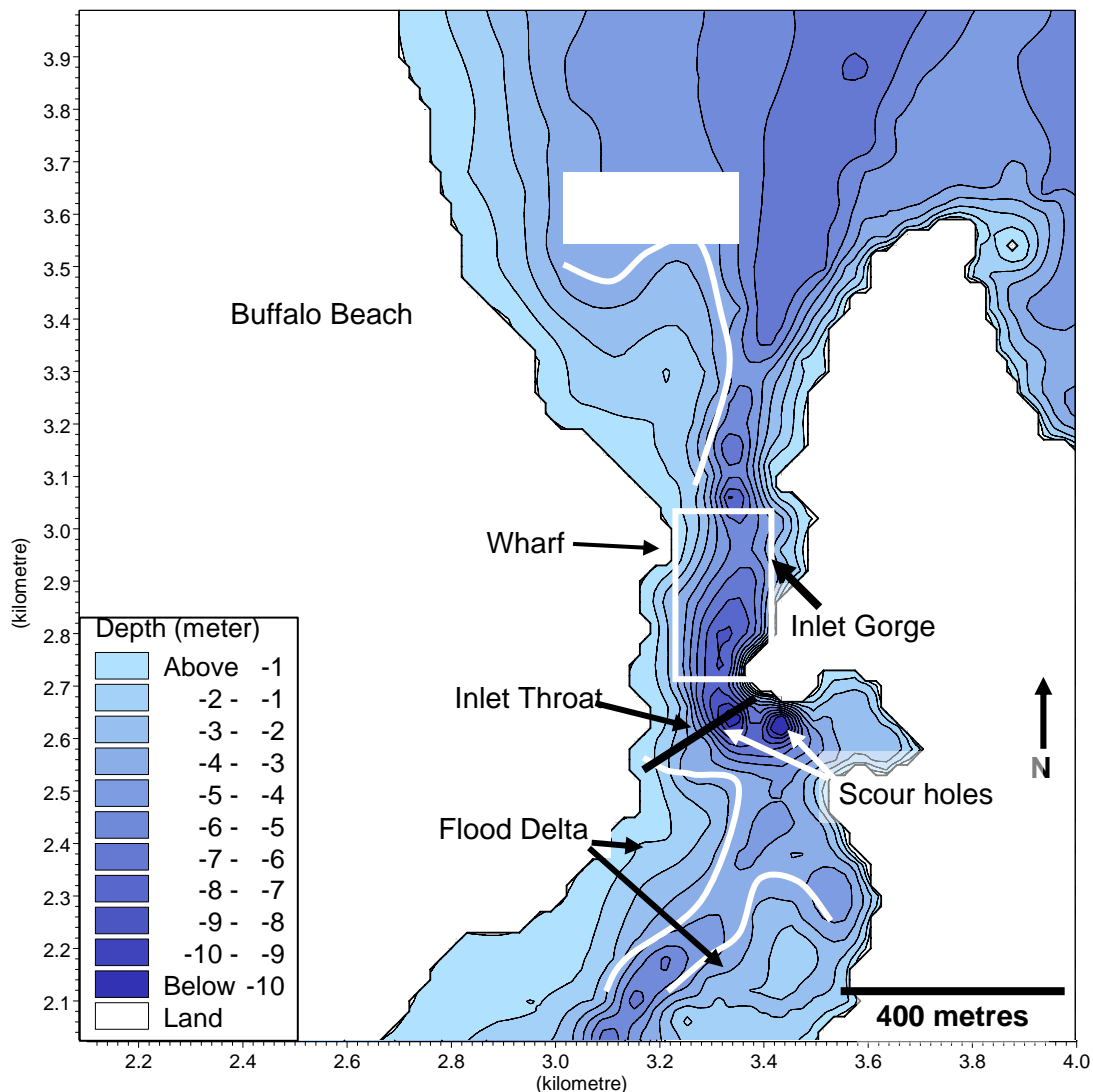


Figure 3.2 The digitised bathymetry and primary elements of the Whitianga tidal inlet system constructed using soundings taken in 1995. Datum: Mean sea Level (MSL).

The Whitianga inlet morphodynamics data suggest that the ebb delta has increased in volume by almost 60% in the 16 year period between the 1979 and 1995 surveys. This gives an ebb delta growth rate of approximately  $2000 \text{ m}^3$  a year. The throat has deepened by  $\sim 1.5 \text{ m}$ , which has increased the throat area by almost 60%. This may be a result of more detailed data used in this analysis or chosen location of tidal gorge. The tidal prism could not be properly estimated due to the lack of hydrographic data available for the upper estuary. It is likely the tidal prism follows a decreasing trend due to the high sedimentation rates within the estuary; however the prism may have increased recently due to the canal development upstream which saw the creation of artificial canal type channels, openly linked to the estuary. The increase in ebb delta volume calculated above is also suggestive of a reducing tidal prism.

Table 3.1. Characteristics of selected tidal inlets on the north east coast of the North Island. Inlet types after Hume and Herdendorf (1988b) are: 4 = single spit; 5 = tombolo; 6 = barrier island. Sediment sizes after (Hume and Herdendorf, 1992) are fs = fine sand; ms = medium sand; lag or shell or gravel lag. Ebb delta shape type: 2 = Constricted ebb delta, 3 = high angle half delta, 4 = low angle half delta. Data taken from Hicks and Hume (1996) and Hume and Herdendorf (1992 and 1993). Some data for Whangapoua and Whangamata are missing. Whitianga 2 refers to statistics calculated by the author for this study.

Inlet Type	Drainage Basin Area (km <sup>2</sup> )	Ebb Delta sand volume (10 <sup>6</sup> m <sup>3</sup> )	Ebb Delta Shape Type	Mean Spring Tide Range (m)	Mean Spring Tidal prism (10 <sup>6</sup> m <sup>3</sup> )	Spring peak Discharge (m <sup>3</sup> s <sup>-1</sup> )	Estuary area at high tide (km <sup>2</sup> )	Throat Width at Mid tide (m)	Throat Depth at Mid tide (m <sup>2</sup> )	Throat area at Mid tide (m <sup>2</sup> )	Annual Littoral Drift (m <sup>3</sup> )	Sand Size/ Type in throat	Wave Energy Factor H <sup>2</sup> T <sup>2</sup> (m <sup>2</sup> sec <sup>2</sup> )	Daily Mean Runoff (m <sup>3</sup> s <sup>-1</sup> )
Tauranga	851	47.3	2	1.6	131	8578	115.6	480	13	6260	70000	ms+lag	81	37
Tairua	271	2.15	3	1.6	5.02	436	6.1	130	3.31	430	5000	ms	16	15
Whangamataa	52			1.6	3.93	326	4.3	162	2.65	363		ms		
Whangapoua	109			1.72	8.54	600	13.1	454	2.15	980		ms+lag		
Whitianga 1	431	0.0384	4	1.6	12.56	960	15.6	240	5.42	1300	1000	fs+lag	4	2.3
Whitianga 2		0.065						240	9	2160				
Whangateau	41	0.277	4	2.2	10.5	840	9.2	174	3.49	660	13000	fs+lag	22	1
Whangerei	369	168	3	2.2	155	9057	98	790	18.5	14608	20000	mslag	22	12

The Whitianga harbour has a similar history to the Tairua harbour. Logging and milling occurred in both catchments which are steep and erodible in nature. The Tairua Estuary has a much smaller catchment area, about half that of the Whitianga catchment (Table 3.1) but a much larger daily mean runoff rate, littoral drift rate and a lot more sand on the ebb delta.

The Whitianga inlet has a relatively large drainage area compared to many of the other inlet systems; including Whangarei which is a much larger inlet with peak discharges almost 10 times that at the Whitianga inlet. An interesting constituent of the table is the ebb delta sand volume which is lowest for the Whitianga ebb delta. So in comparison with other inlets, the Whitianga ebb delta is small. The Whitianga inlet receives low annual littoral drift compared to the other north east coast inlets, which may reflect the small sand volume on the ebb delta. In comparison with the other inlets, Whitianga also receives very low wave energy due to the sheltering effect of Whakapenui Point.

The  $A$ - $\Omega$  relationship,  $A$  (cross sectional area) and  $\Omega$  (tidal prism) which assumes  $A$  and  $\Omega$  are proportional to one another, is one method of calculating the stability of an inlet (Figure 3.3). It assumes the cross sectional area of the gorge is the dominant cause of stability and therefore should not be used as a sole indicator of inlet stability but merely for, as advised by Bruun (1978), 'preliminary guidance for pre-evaluation of inlet conditions'. Many New Zealand inlets have had their stability specifically studied (Figure 3.3) but as yet Whitianga inlet has not been added to this list. Using the information from Table 3.1, Whitianga tidal inlet has been plotted on the Hume and Herdendorf (1988b) plot of  $A$  and  $\Omega$  for various tidal inlets.

The stability plot suggests Whitianga inlet has a tendency toward deposition in the inlet gorge. Deposition in the inlet gorge is characteristic of a decreasing tidal prism, resulting in slower tidal flow through the inlet thereby reducing scour at the inlet gorge (Bruun, 1978). In time, this will lead to continued reduction in the inlet cross sectional area. A second measurement of the  $A$ -  $\Omega$  relationship for Whitianga inlet stability (Figure 3.3 (2)) was calculated using the new approximate cross sectional area and the estimated decreasing tidal prism. This measurement suggests deposition in the inlet will continue in the future as tidal prism decreases.

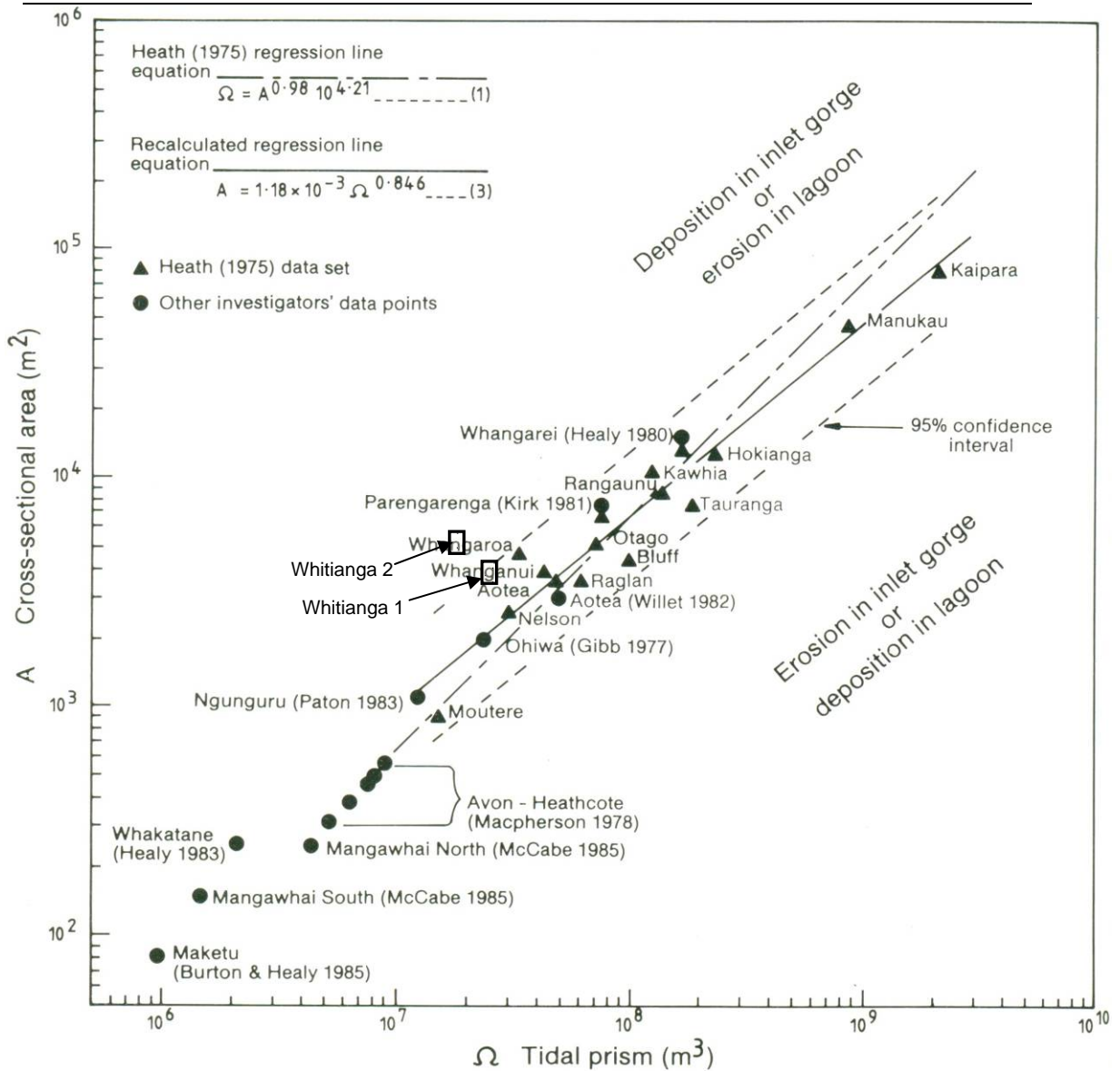


Figure 3.3 Logarithmic plot of the tidal prism versus cross sectional area (morphological stability) of selected tidal inlets in New Zealand as given by Heath (1975) and other named works. Source: Hume and Herdendorf, 1988b. The rectangle indicates Whitianga Inlet stability as calculated by the author. Whitianga 1 refers to the stability using data from Hume and Herdendorf (1992,1993) and Whitianga 2 refers to stability approximated using the area calculated by author and approximate estimated decrease in tidal prism.

### **3.3 Comparison of Aerial Photos to Identify Shoreline Change Adjacent to Inlet**

The morphology of Buffalo Bay is likely to have changed over the past 40 years, reflecting both naturally induced processes and the shifting landuse within the Whitianga estuary catchment, along Buffalo Beach and changes within the entire Mercury Bay catchment.

A series of aerial photos were collected to show changes in beach and inlet morphology within Buffalo Bay and also to highlight noticeable accretion and erosion trends within the Bay. Aerial photos were digitised and rectified, following which the area between the water line and the seaward vegetation line were mapped to find the position of the shoreline along Buffalo Bay. This allows for an estimate of erosion or accretion between the photos. The 1944 and 1990 photo can be compared as they were both taken on a similar tide and likewise for the 1995 and 2002 photos. All quantities and beach areas given are approximate only as there are possible errors associated with the rectification process and exact location of the water line.

The first photo (Figure 3.4) was taken in 1944 and illustrates the sparse development and housing at Whitianga. This photo does not include the northern section of Buffalo Beach and the photo attributed to this area could not be attained. The photo shows the southern section of beach is healthy and the ebb delta is barely visible. Extensive dune ridges are obvious on the farmland west of the township showing pronounced curvature and running parallel to the shoreline, indicative of a swell wave environment.

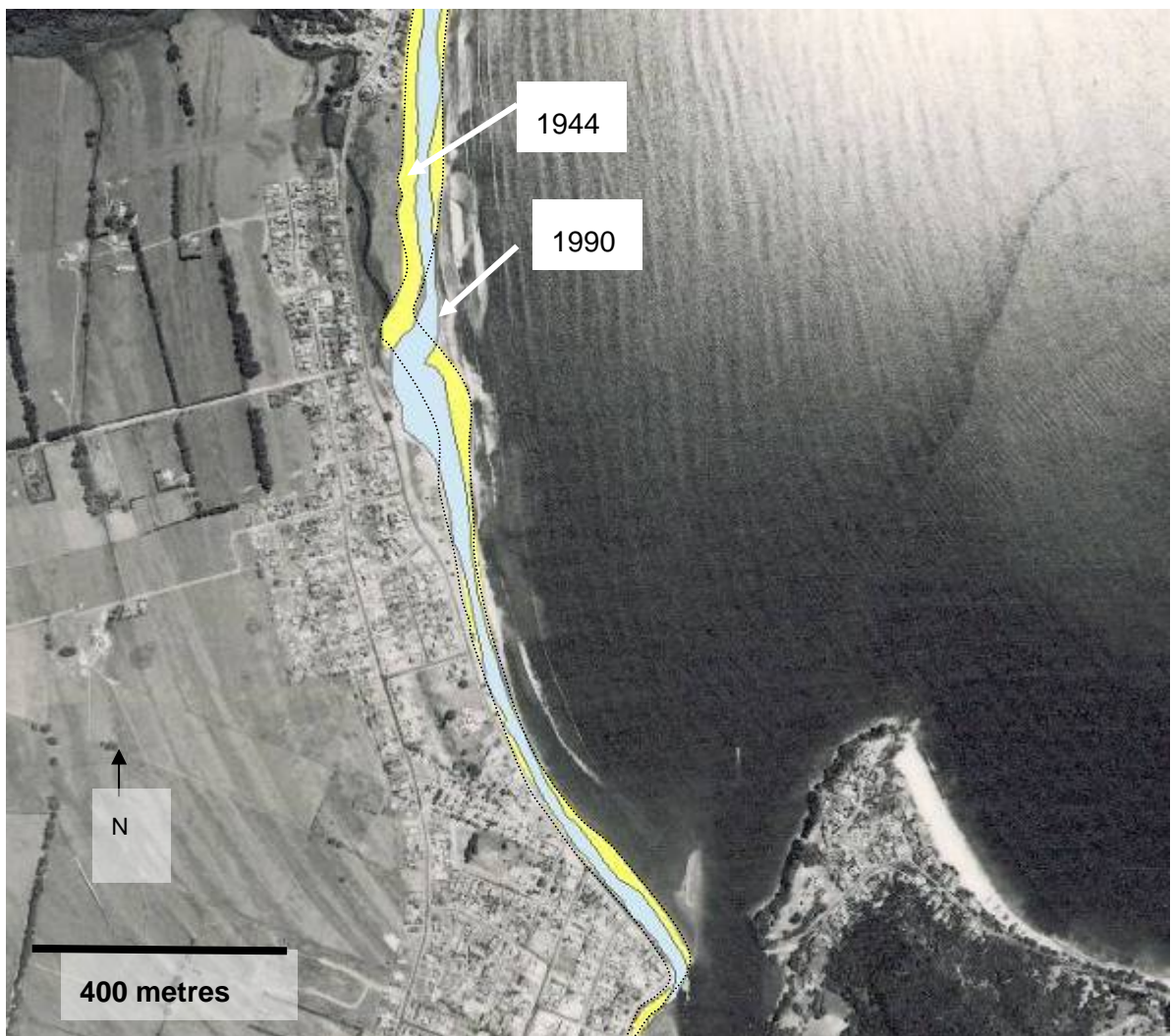
The next photo (Figure 3.5) dates from 1990, and shows the Whitianga inlet and the southern section of Buffalo Bay. The ebb delta is far more obvious in this photo and is clearly long and narrow in shape, building parallel to the headland on the western (barrier) side of the inlet, and orientated north-south. The approximate Mean Low Water Spring (MLWS) area of the ebb delta covers  $\sim 0.01 \text{ km}^2$  and it is approximately 200 m in length.



Figure 3.4 Whitianga township 1944. Note the extensive dune ridges. Source: *Environment Waikato, 2006*

The two beach areas (Figure 3.5) depict the area between the approximate seaward extent of vegetation and the water line. The primary changes identified by the beach areas between 1944 and 1990 are:

- The vegetation line has advanced seaward;
- The Taputapuatea stream mouth at the centre of Buffalo Beach has migrated south;
- The width of southern Buffalo Beach has narrowed;
- The mid-section of Buffalo Beach (top of the picture) has narrowed.



*Figure 3.5 The Whitianga township, inlet and southern Buffalo Beach in 1990. The dotted line area represents the beach area in 1944 and the solid line area is the beach area in 1990. Source: Environment Waikato, 2006*

The first available colour photo of Buffalo Bay was taken in 1995 (Figure 3.6). A noticeable aspect of this photo is the orange-brown colour of the sediment within the harbour and at the entrance which matches the colour of the bare soil seen near the bottom of the photo on the dune ridges. This photo shows a plume or build up of the same sediment in the littoral zone along Buffalo Beach and in the bay offshore from the Taputapuatea Stream discharge point which possibly alludes to the sediment transport within Buffalo Bay. The ebb delta appears to have migrated further into Buffalo Bay and is now orientated northwest-southeast.



Figure 3.6 Whitianga township, Inlet and Buffalo Bay 1995. Source: Environment Waikato, 2006



*Figure 3.7 Mercury Bay 2002 showing the large plume of sediment exiting the Whitianga Harbour. The green area shows the beach area in 1995 and the outlined area shows the beach area for 2002. Source: LINZ, 2006*

The most recent photo used (Figure 3.7) was taken on an ebb tide. This photo dramatically shows a plume of sediment exiting the Whitianga Harbour and moving into the greater Mercury Bay. The path of the plume in Buffalo Bay is similar to the isolated shallow sand shoal reported in the Notice to Mariners (2005).

To show the shoreline changes better, the photo has been split and blown up into two sections, the northern and the southern sections (Figures 3.8 and 3.9). The southern section of Buffalo Beach and the inlet (Figure 3.8) illustrate some interesting changes between 1995 and 2002. In order to better show these changes the photo is given twice, once with the 1995 beach area on top and once with the 2002 or most recent beach area on top.

It is obvious that most southern section of Buffalo Bay has widened between 1995 and 2002 (Figure 3.8 B) and the vegetation edge has moved seaward (Figure 3.8 A). The stream mouth (Taputapuatea Stream) along the centre of Buffalo Beach has migrated south again. It is difficult to define exactly where the ebb delta lies in this photo due to the plume or discharge exiting the harbour but its position can be approximated and is indicated (Figure 3.8A) by the white line. The MLWS area of the ebb delta estimated from this photo is approximately 0.04 km<sup>2</sup>, approximately 4 times larger than in 1990. The delta now extends approximately 400 m into Buffalo Bay, which is twice the length it was in 1990 and is orientated north-south.

The northern section of Buffalo Beach shows no major changes in the shoreline or the position of Taraporiki Stream that exits here.

In all the photos the southern extremity of Buffalo Beach is the widest and most healthy. This section suffered erosion between 1944 and 1990 but accreted between 1995 and 2002. By 2002, the adjacent ebb delta has extended approximately twice its 1990 length and the area has increased by almost 400%. Comparison of the aerial photos infer Ohuka Beach has maintained a similar position and has not changed noticeably over the 7 year period. The centre section of Buffalo Beach, where the Taputapuatea Stream mouth is located, has changed the most in each comparison, with the stream mouth appearing to generally migrate south. The width of the southern section and the growth of the ebb delta shown in this comparison provides evidence in support of the theory that sand is gradually travelling south down Buffalo Beach and depositing on the southern extremity of Buffalo Beach, and/or on the ebb delta.



Figure 3.8 The beach area change from 1995 to 2002 for the southern section of Buffalo Beach. The dark green area shows the beach area for 1995 and the aqua area shows the beach area for 2002. Photo A has the 2002 area over top of the 1995 area, and photo B shows the 1995 area on top of the 2002 area. The white line indicates the approximate position of the ebb delta. Source: LINZ, 2005



Figure 3.9 The beach area change from 1995 to 2002 for the northern section of Buffalo Beach. The dark green area shows the beach area for 1995 and the aqua area shows the beach area for 2002. Photo A has the 2002 area over top of the 1995 area, and photo B shows the 1995 area on top of the 2002 area. Source: LINZ, 2005

Healy et al., (1981) examined shoreline change at Buffalo Beach (Figure 3.10) by comparing aerial photos between 1944 and 1978. Their comparison shows that erosion is evident along a large portion of Buffalo Beach, most prominent around the stream mouth at the centre of Buffalo Beach (Figure 3.10). The photos compared above show a similar pattern around the Taputapuatea Stream migration, and at the southern section of Buffalo Beach between 1977 and 1990. Erosion is less pronounced in the comparison by the author in this study, however the comparison made by Healy et al. (1981) did not use rectified aerial photos and thus their results provide only an indication of erosion and accretion along Buffalo Beach. Photos of Ohuka Beach for 1944 and 1990 were not available and thus it is possible the erosion noted here by Healy et al. (1981) was correct but was not evident between 1995 and 2002 as indicated by the above comparison.

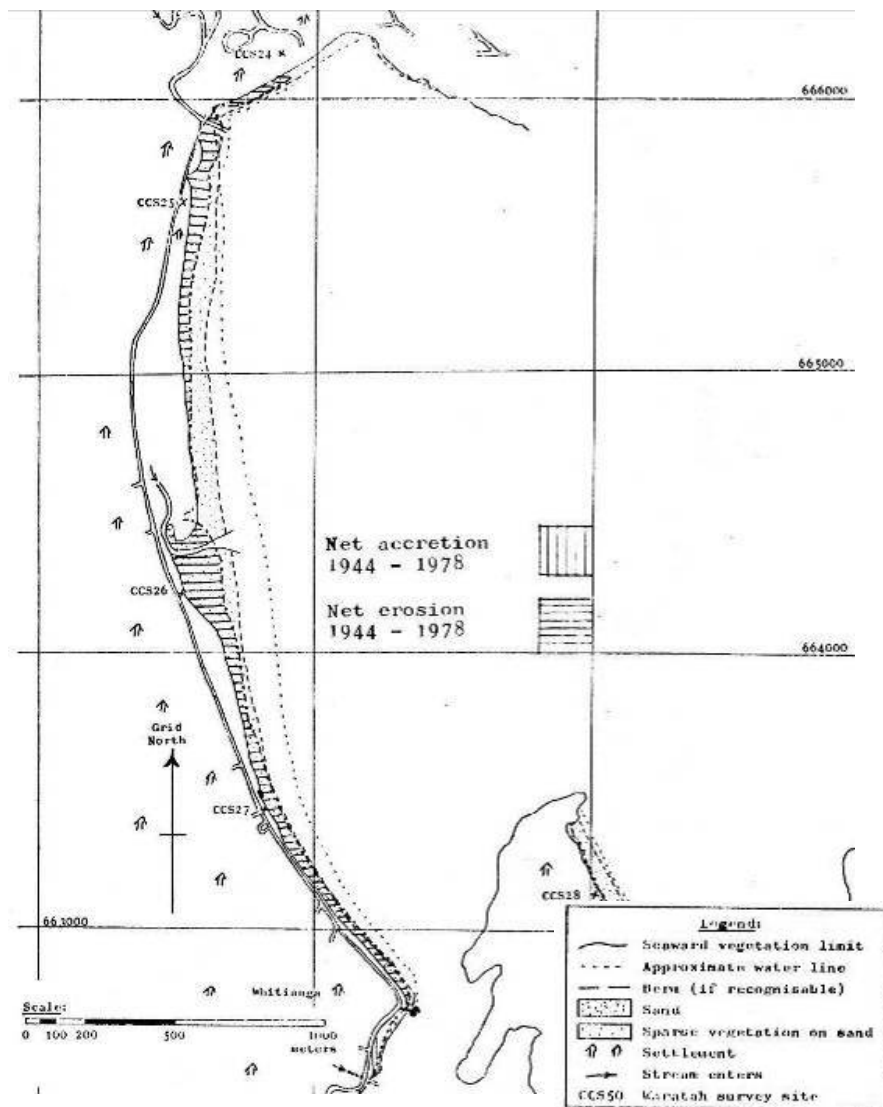


Figure 3.10 The shoreline change at Buffalo Beach between 1944 and 1978 attained through non-rectified aerial photo comparisons. Healy et al. (1981).

### **3.4 Bathymetry Comparisons**

A collection of past depth soundings and hydrographic charts are available for the Whitianga inlet and adjacent sea floor. Fair sheets of soundings were attained for the Whitianga inlet for 1963, 1979 and 1995. All of these were digitised relative to mean sea level (MSL) using the ARCVIEW GIS programme. Additionally a hydrographic chart of Buffalo Bay from 1945, which used soundings from 1938, was digitized to compare with the most recent hydrographic chart of Buffalo Bay. The most recent survey of the Whitianga tidal inlet was conducted in 1995 but Buffalo Bay and all of Mercury Bay were last surveyed in 1979. The 1979 bathymetry is primarily used in order to compare changes within Buffalo Bay between 1938 and 1979.

The same coastline (1938) was applied to each map to assess the bathymetry differences. There may be a degree of error associated with the 1938 bathymetry as measurements were possibly not as accurate as they are now. The surveyed depths were mapped in fathoms and feet in 1938, and when converted to meters, may have introduced a slight deviation. Additionally, the 1979 survey included detailed point depths for the inlet system whereas depth measurements were sparser in the 1938 survey.

The key morphological feature of the comparison of the 1938 and 1979 bathymetries (Figure 3.11) is the location and orientation of the inlet channel. This is orientated north to south in 1938 but shifted to northeast-southwest in 1979. This majority of the ebb discharge channel area in 1938 is 6-7 metres deep but in central places, the channel is up to 9 meters deep. In 1979 the majority of the channel is 5-6 metres deep with the deepest section only 8 meters deep.

The ebb delta is noticeably larger in 1979, compared to 1938, and is orientated parallel to the inlet channel. The zone of shoaling (extending from Pandora Rock to ~ 1 mile north in Buffalo Bay) identified in recent years by the Notice to Mariners (LINZ, 2005) is not evident in the 1938 or 1979 bathymetry, suggesting accretion has occurred here between 1979 and 2005 (when the Notice to Mariners was issued). This feature is investigated further in Chapter 6 from sediment transport modelling.

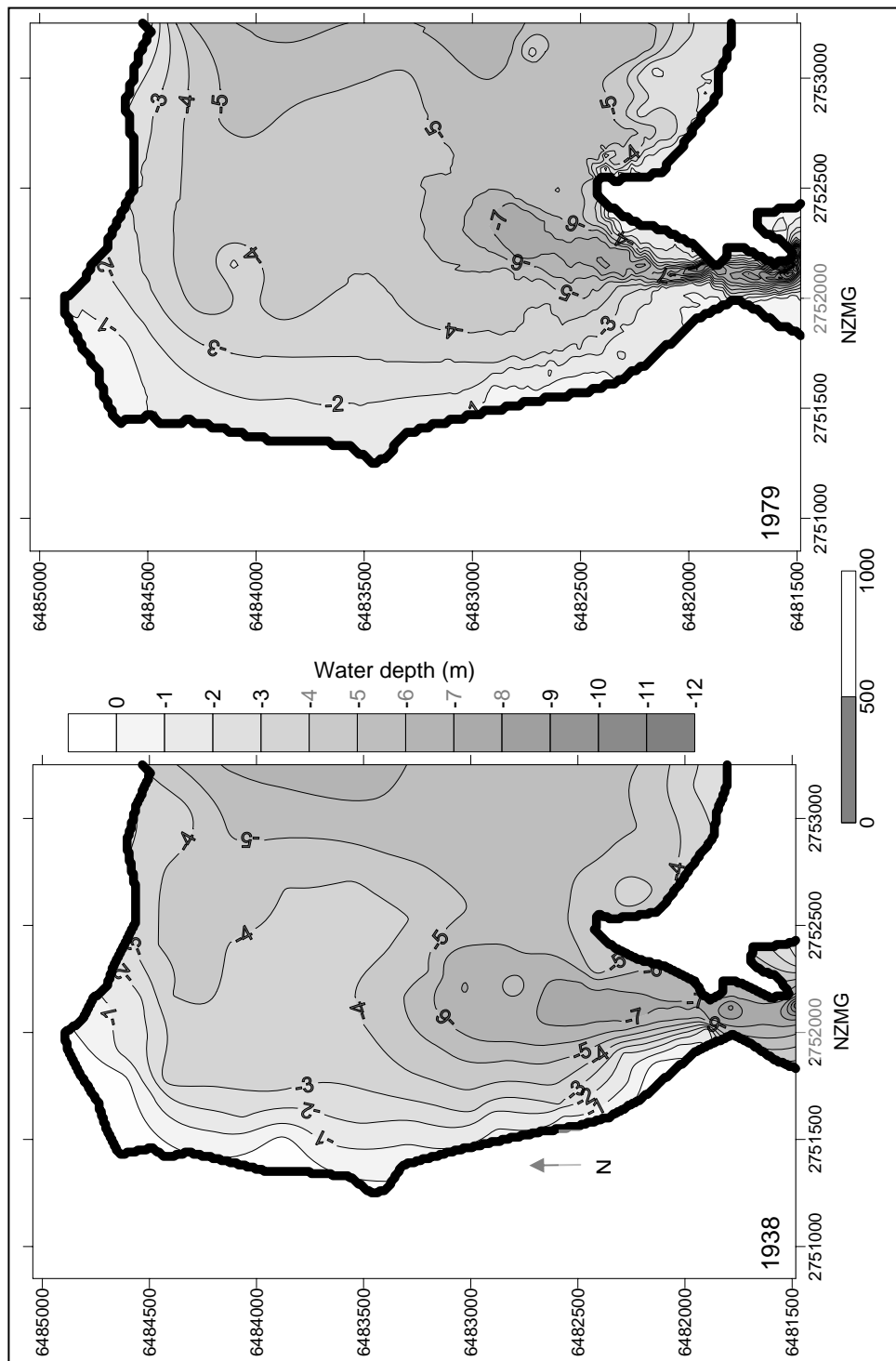


Figure 3.11 The digitised bathymetry of Buffalo Bay in 1938 and 1979 based upon soundings undertaken by the RNZN. Datum converted to MSL.

To show the areas of long-term accumulation and scour, a residual map illustrating the difference in depths between 1938 and 1979 was constructed (Figure 3.12) using Golden Software Surfer 7. The coastline from 1938 was also used for this so there may be some small areas near the coast that are falsely showing erosion or accretion due to the shape and orientation of the shoreline in 1938. This is evident at

the headland opposite the ebb delta, which is illustrating accretion of up to 4 meters, but an overlay of the 1979 bathymetry depicts this area as coastline. However, accretion contours on the seaward side of this 4 meter contour are not false.

This map identifies several zones of accretion in the vicinity of the inlet entrance, evidently associated with the ebb delta growth and tidal channel migration. The map implies up to 4 meters of accretion in these places, inferring a maximum vertical accretion rate here of  $10 \text{ cm y}^{-1}$ . It is apparent the inlet channel has shallowed in the 38 year period between 1938 and 1979, and has migrated approximately 100 m east towards the adjacent rocky shoreline (Whakapenui Point). It is likely the littoral drift system deposits sediment on the ebb delta west of the channel, and forces the tidal channel eastwards towards Whakapenui Point. Substantial accretion has occurred within Maramaratotara Bay, which is possibly due to local stream input or sediment input from the Whitianga estuary. An isolated spot of accretion located near the entrance to Buffalo Bay could be related to the shallow zone identified in Notice to Mariners (LINZ, 2005). The small circular section of accretion ~400 m offshore of northern Buffalo Beach is evident because the 1979 bathymetric chart observed a small circular shoal here whereas the 1938 bathymetry did not, probably due to the low resolution soundings. Additionally, a substantial area of accretion is noted near the Wharekaho headland. This is most likely to have been caused by the chosen coastline but could represent the lost sediment from northern Buffalo Bay.

Figure 3.12 illustrates there has also been erosion within Buffalo Bay. The majority of the erosion occurs near the coastline which suggests the erosion may be a result of the chosen 1938 coastline and therefore cannot be considered entirely accurate. However, the primary area of erosion, in the northern sector of Buffalo Bay, north of the Taputapuatea Stream entry, is realistic according to the digitised maps in Figure 3.11, and shows lowering of the seafloor by ~0.5 m. This is contradictory to the bathymetric comparison undertaken by Cooper (2003) who estimated approximately 1 m of accretion in the northern section of Buffalo Bay between 1852 and 1979. It is possible the 1852 soundings used in his comparison were of lower resolution and were not as accurate as the 1938 soundings used by the author in this comparison. However Cooper (2003) also undertook offshore beach profile sampling along Ohuka Beach, and results indicate scour offshore between 1991 and 2002.

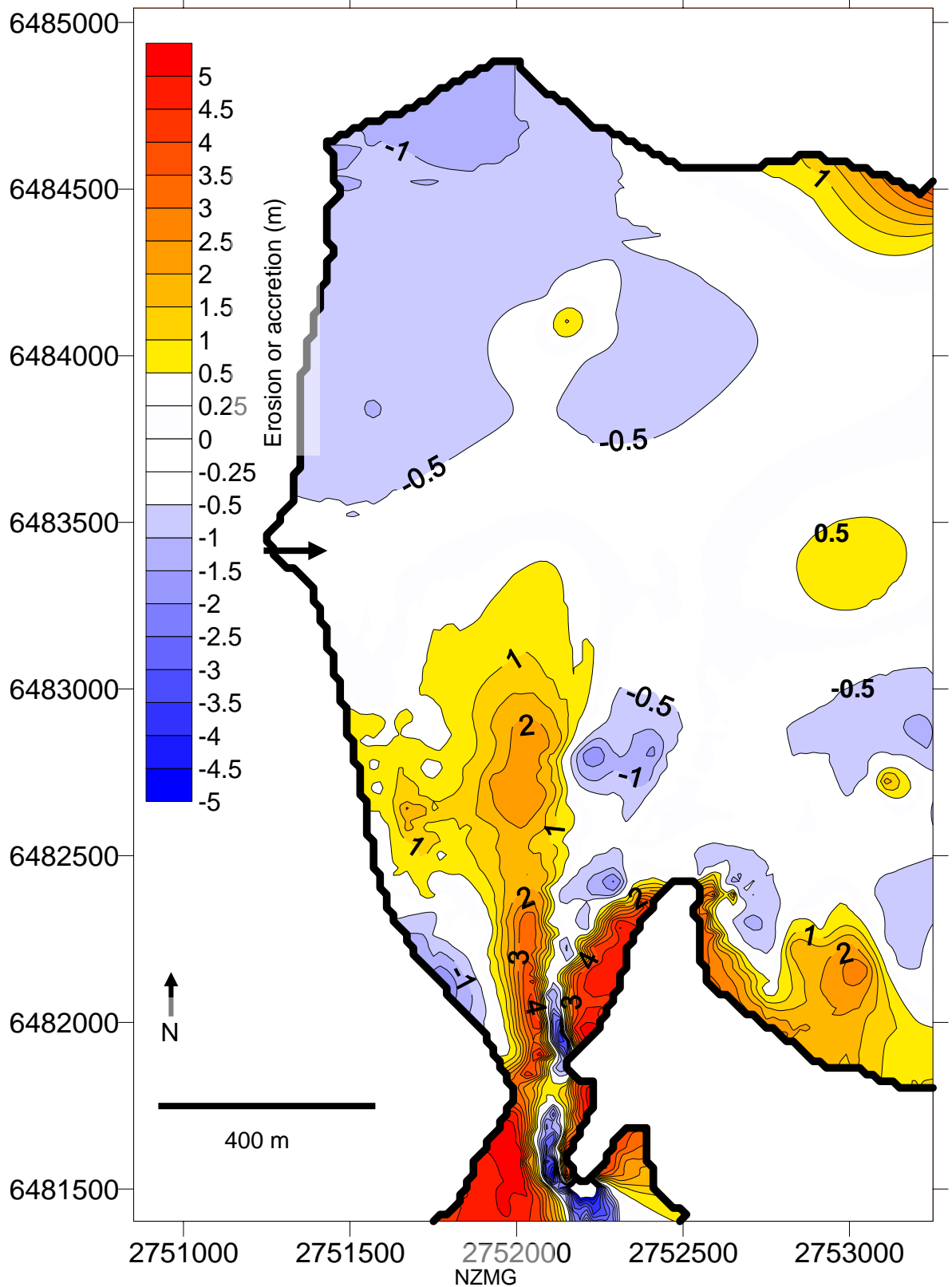


Figure 3.12 The residual map of Buffalo Bay showing areas of accretion and erosion between 1938 and 1979. White areas represent minimal or no change in depth. The two integers represent accretion and scour. Arrow indicates the Taputapuetea Stream entry.

There are two possible causes of the erosion in northern Buffalo Bay. Firstly, sediment in this section of the Bay may be slowly moved offshore by wave action and diabathic processes. This eroded sediment is not replaced due to the minimal sediment supply received from offshore and nearby streams. The other possibility is that the sediment is gradually moved southwards along Buffalo Beach in the net littoral drift and alongshore current systems to be deposited on the ebb delta. The erosion offshore in northern Buffalo Bay is not directly related to littoral drift or alongshore currents as these are limited to approximately 200 m offshore, within the active swash and surf zones. It is most likely the erosion is caused by waves entraining sediment, wherefrom it may be moved offshore by down-welling or ebb tide currents, or onshore by up-welling or flood currents and then be transported south down Buffalo Beach by the combination of littoral drift and alongshore currents.

Other areas of erosion include west of the ebb delta location, along the adjacent section of Buffalo Beach. It is likely this erosion has occurred due to the seawall which was first established in the 1960's but has been extended since. Scour is evident within the inlet gorge, probably associated with changing tidal channels. This erosion could be more apparent than real, caused by the sparse inlet soundings in 1938. There has also been some erosion offshore in Buffalo Bay, northeast of Whakapenui Point, which could be related to scour around Pandora Rock or it may have been induced by the new orientation of the ebb tidal discharge.

A comparison of the water volume change within Buffalo Bay between the two years suggests there has been approximately 700,000 m<sup>3</sup> of net accretion between 1938 and 1979 but only ~350,000 m<sup>3</sup> of net erosion within the whole of Buffalo Bay. This gives a gross accretion rate of ~18,400 m<sup>3</sup> per year within Buffalo Bay. The volume of accretion within the ebb discharge channel and ebb delta region over the 38 year period between 1938 and 1979 (~550,000) is approximately twice the volume of eroded material from northern Buffalo Bay (~280,000). It is likely the accretion around the inlet is caused by either a combination of sediment from the eroding northern Buffalo Bay (offshore of Ohuka) and sediment from within the estuary, or primarily due to sediment from the estuary. If the latter theory were true, the eroded sediment at northern Buffalo Bay may be lost offshore in diabathic transfer. Wave

attack in times of storm surge and onshore wind induced down-welling may erode and suspend the sediment wherefrom it could be moved offshore or alongshore. Bradshaw et al., (1991) did propose that up- and down-welling systems were a sediment transport mechanism within Mercury Bay, but the extent is unknown, however it is not likely to be the primary contributor. Healy (2003) provided evidence for a southwards littoral drift direction along Buffalo Beach, given in Chapter 2 (page 27), which suggests the accretion in the ebb discharge channel and ebb delta region is related to the erosion of the seafloor in northern Buffalo Bay.

A residual map was constructed to show the changing morphology of the inlet from 1979 to 1995 (Figure 3.13). This map provides a more accurate description of the areas of erosion and accretion in the inlet as the soundings in both surveys were to a high resolution. It appears the ebb discharge channel has migrated further east, towards Whakapenui Point, which has resulted in scour between the previous ebb discharge channel and Whakapenui Point and accretion of up to 4 m on the western side of the ebb discharge channel. The maximum vertical accretion rate for the ebb discharge channel and ebb delta area calculated by this residual map is  $\sim 25 \text{ cm y}^{-1}$ , twice the rate estimated in this area between 1938 and 1979. There has been accretion within the inner inlet channels and eastern estuary banks, likely to be a result of migrating tidal channels and the growth of the flood shield and flood spits. Erosion of up to 3 m has occurred on the western side of the inner inlet, which may coincide with the development of the Whitianga marina and subsequent dredging of the entrance in 1994, prior to the latest hydrographic survey of the inlet.

The two residual maps (Figures 3.12 and 3.13) suggest maximum vertical accretion rates on the ebb discharge channel and ebb delta region between  $\sim 10 - 25 \text{ cm y}^{-1}$ . It is possible the majority of Buffalo Bay is gradually accreting primarily due to the increasing fluvial input related to intensifying landuse within the catchment, and partly by onshore sediment creep from up-welling induced by predominant offshore winds (Healy 2003). Additionally, sediment moving south along Buffalo Beach in the net littoral drift direction, is deposited at the inlet and is thereby further increasing the sedimentation rate of the ebb tidal delta and ebb discharge channel.

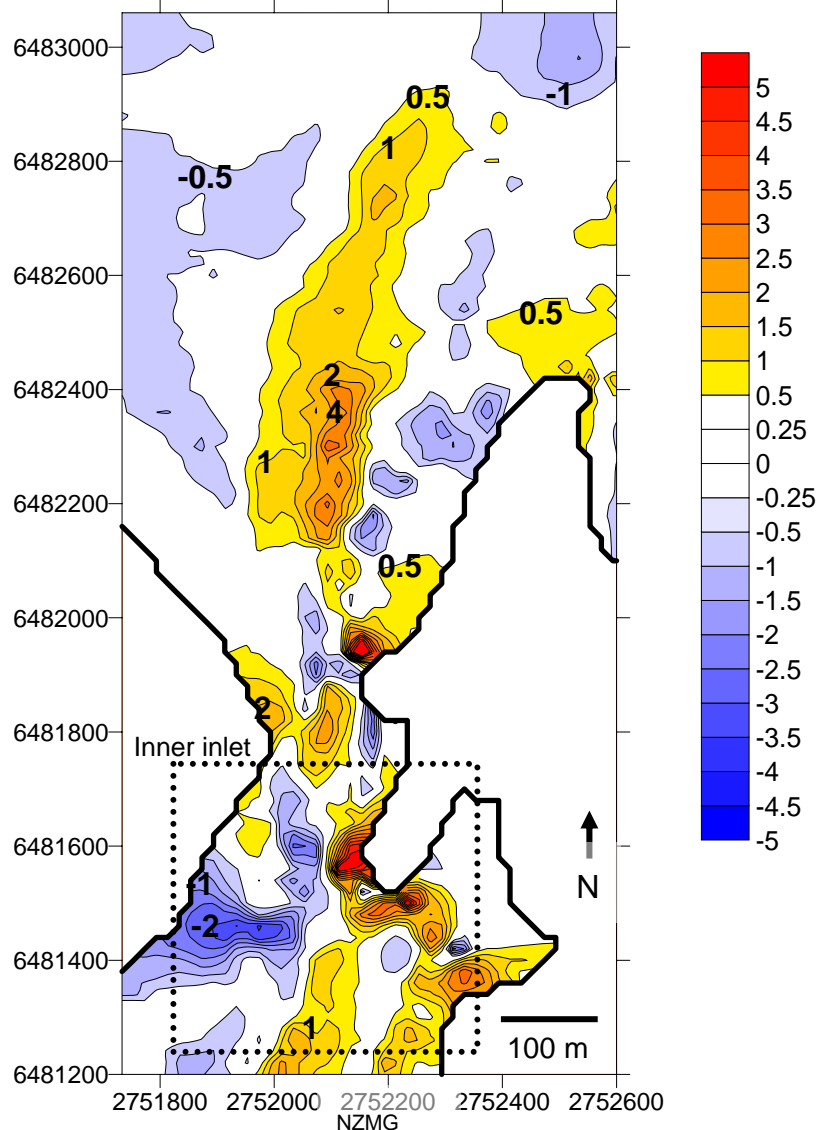


Figure 3.13 Residual map of the Whitianga inlet showing areas of accretion and erosion between 1979 and 1995. White areas represent minimal or no change in depth. The two integers represent accretion and scour.

A similar rapid sedimentation situation exists at the Maumusson Inlet and Marennes-Oléron Bay on the western coast of France, where a combination of human activities and natural processes have contributed to dominant accretion trends (Bertin et al., 2005). By comparing bathymetric surveys covering 171 years, the estimated annual accretion over this time was 619000 m<sup>3</sup> resulting in up to a 40% decrease in the tidal prism (Bertin et al., 2005). Landuse changes within the Maumusson Inlet catchment have significantly contributed to this volume change in recent decades (Bertin et al., 2005). In reasonable proximity, the Arachon Inlet system on the French Atlantic coast has also shown large scale changes over the last 300 years. This includes a large phase of accretion between 1768 to 1826

which resulted in ~5 km of accretion on the Cap Ferret Spit (Cayocca, 2001). These examples show that large scale accretion at inlet systems, whether in phases or as a general trend, is not uncommon internationally and in a lot of cases the rapid nature of this process can be attributed to human modifications and influence.

### **3.5 Conclusions**

The following conclusions can be drawn from this chapter:

- The Whitianga tidal inlet is protected inside Mercury Bay and experiences low wave energy and littoral drift. The volume of the ebb delta is estimated to have grown approximately 60 % between 1979 and 1995. The tidal prism is likely to exhibit a decreasing trend due to the high sedimentation rates within the estuary. This is suggested by the calculated increase in ebb delta volume.
- The aerial photograph comparisons show the southern end of Buffalo Beach has been the widest section of the beach for the 60 years previous to 2002. The MLWS area of the ebb delta is estimated to have grown over 400% in the 12 year period between 1990 and 2002. Ohuka Beach is relatively stable.
- Comparison of the 1938 and 1995 bathymetries show the tidal channel shifted from a north-south orientation in 1938 to northeast-southwest orientation in 1995. A residual map of Buffalo Bay and the inlet between 1938 and 1979 infers depths in the ebb discharge channel and ebb delta region have shallowed considerably, with maximum vertical sedimentation rates of up to  $10 \text{ cm y}^{-1}$  in the inlet channel between 1938 and 1979. Similarly, a residual map of the Whitianga inlet between 1979 and 1995 infers maximum vertical sedimentation rates of  $\sim 25 \text{ cm y}^{-1}$  in the ebb discharge channel and ebb delta region. The primary area of accretion in both maps is associated with the new inlet orientation and the primary area of erosion within Buffalo Bay occurs in northern Buffalo Bay which can be attributed to a combination of wave attack, wind-induced down-welling currents and the southwards net littoral drift along Buffalo Beach. Sediment accreted at the ebb discharge channel and ebb delta region is likely to have resulted due to the combination of sediment moved along Buffalo Beach in the net littoral drift and sediment input from the estuary. Growth of the ebb delta is assumed to

be the primary cause of the channel re-orientation and shallowing. The two residual maps identify the evolution of the inlet morphology. The ebb delta exhibits a northwards growth pattern and the ebb discharge channel subsequently slowly migrates east toward Whakapenui Point.

## Chapter Four – Analysis of Field Data

---

The previous chapter describes the morphological setting of the Whitianga tidal inlet system and the pattern of accretion within the inlet. In order to better understand the processes leading to the accretion at the inlet, a numerical sediment transport study was undertaken. The present chapter presents the field data collected, partly to calibrate the numerical model, but also to provide understanding of the processes leading to the sedimentation.

### 4.1 Field Deployments

The instruments deployed were S4 current meters, DOBIE water level gauges and sediment traps. The first deployment occurred from the 22<sup>nd</sup> of November 2005 until the 30<sup>th</sup> of December 2005. Four S4 current meters were deployed in positions around Mercury Bay (Table 4.1, Figure 4.1) to establish the direction of the circulation cell within Mercury Bay.

*Table 4.1 The Instruments used in the first field deployment, 22<sup>nd</sup> November to 30<sup>th</sup> December 2005 and the second deployment 21<sup>st</sup> March to 2<sup>nd</sup> May 2006.*

	Instruments Deployed			
	Name	Type	Depth (m)	Successful data collection
First deployment	Wharekaho	S4ADW	8	Yes
	Round Island 1	S4ADW	8	No
	South Channel	S4ADW	16	No
	Cooks Bay	S4ADW	7	No
Second Deployment	Buffalo Bay	S4ADW + sediment trap	4	Yes
	Wharf	S4ADW + sediment trap	8.5	Yes
	Entrance	S4ADW + sediment trap	4	Yes
	River	S4ADW + sediment trap	5	Yes
	Cooks Bluff	DOBIE	16	Yes
	Round Island 2	S4ADW	14	No

The second deployment occurred between the 21<sup>st</sup> of March 2006 and the 2<sup>nd</sup> of May 2006. Four of the instruments had sediment traps mounted on the frames. This deployment was to obtain boundary forcing data and calibration and validation data for the model, and to provide tide and wave data within Buffalo Bay and the entrance

to Whitianga estuary. An S4 and DOBIE were placed at the entrance to Mercury Bay to provide boundary conditions. The S4 at the entrance malfunctioned and was removed after a week and replaced with a DOBIE water level gauge. A further DOBIE provided model boundary data for the harbour.

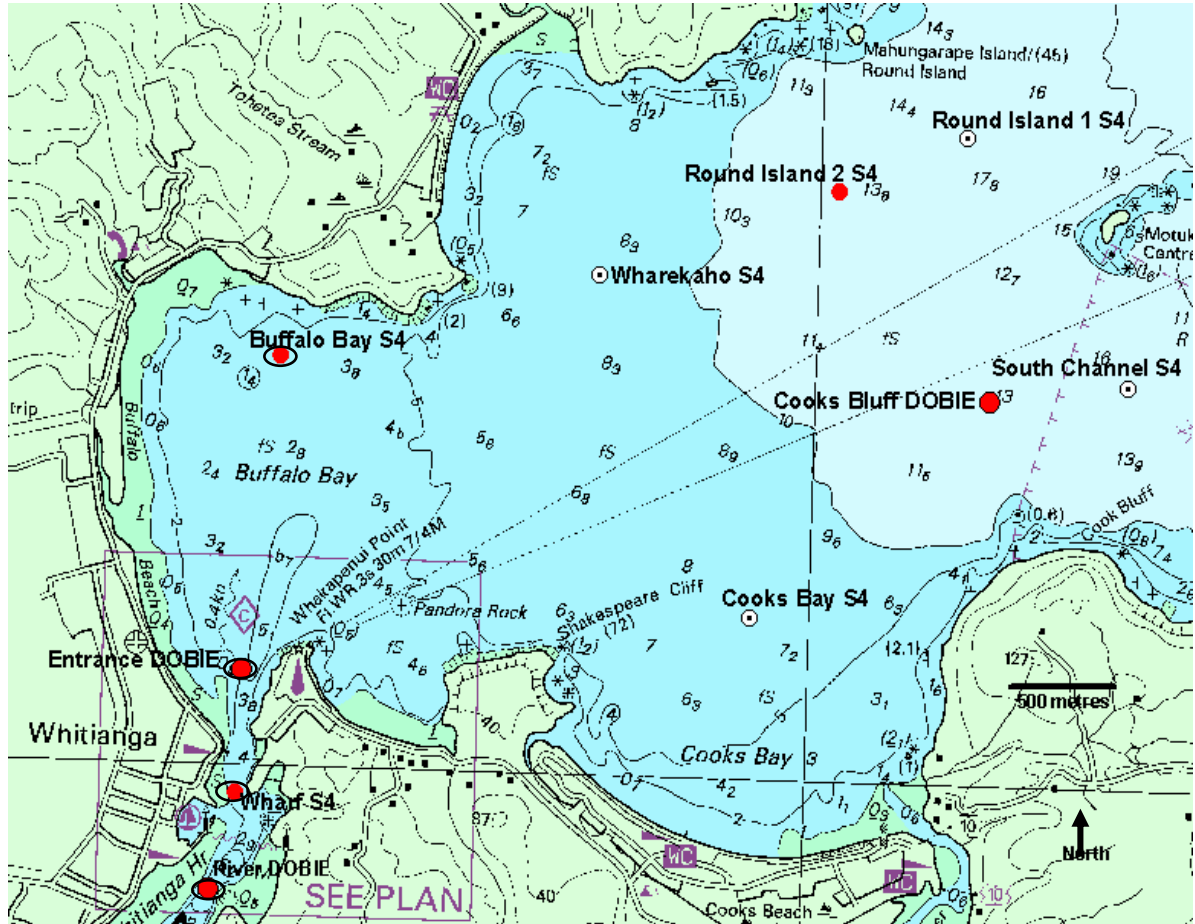


Figure 4.1 Map of Mercury Bay showing the instrument locations for the first deployment (22<sup>nd</sup> November to 30<sup>th</sup> of December 2005) indicated by white circles with solid centres, and second deployment (21<sup>st</sup> March to 5<sup>th</sup> May 2006) indicated by solid circles. Circles with rings around them indicate where sediment traps were attached to the instrument frame. Map adapted from LINZ (2005a).

#### 4.1.1 S4 current meters

S4 current meters are electromagnetic instruments, primarily used to measure currents and waves. Setting the instrument at different sampling intervals allows measurement of small scale changes (waves), or large scale changes (residual and tidal currents). The S4 measures absolute pressure in millibars which is converted automatically to depth by assuming atmospheric pressure is 1014 millibars (Hancock, 2003). Two pairs of electrodes, located symmetrically on the equator of

the sphere shaped instrument (Figure 4.2) enable the measurement of true magnitudes and direction of horizontal current motion (Interocean, 2006). Current data are then stored in a non-volatile solid-state memory (Interocean, 2006).



*Figure 4.2 The S4 current meter with its frame. Sediment traps were fastened to the sides, as seen to the left of the photo. Photo taken by author.*

For this deployment, the S4 used are capable of logging both waves and currents but they were primarily configured to log current information. Wave information can then be extracted using InterOcean Software. The S4 were set to sample in burst mode for 18 minutes every hour with a sampling frequency of 2 Hz (2 measurements per second). The S4 sit 1 m above the seabed.

#### **4.1.2 DOBIE**

DOBIES (Figure 4.3) can be deployed to measure wave and water level statistics (NIWA, 2001). A pressure sensor within the instrument measures the pressure over time. The sensor measures absolute pressure and the DOBIE software calculates dynamic pressure, once the data have been downloaded, by removing atmospheric pressure from the total measured pressure (NIWA, 2001; Hancock, 2003). The DOBIE undertakes error checking, and processes and compresses data prior to storage (Grant et. al., 1998).

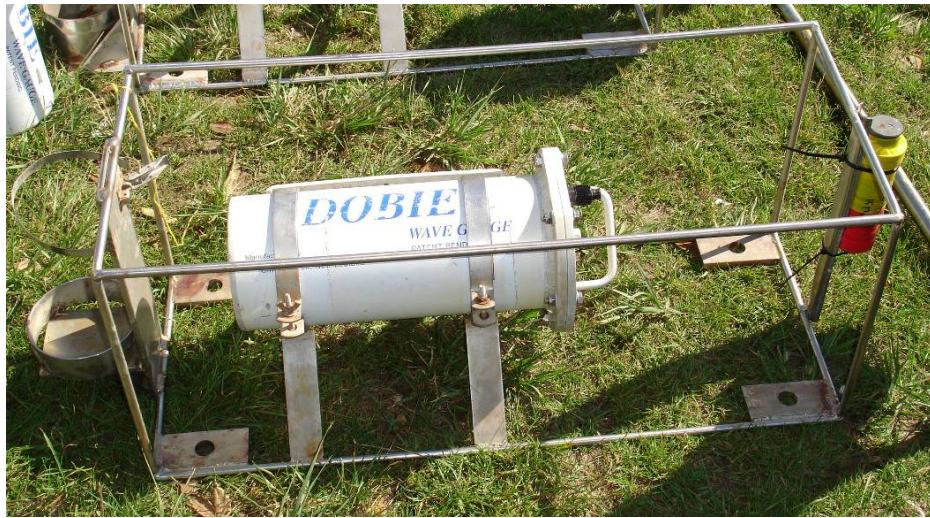


Figure 4.3 The DOBIE water level gauge in an ocean frame. Photo taken by author.

If the DOBIE is programmed to record wave data, then water depth, spectral width and deviation, significant orbital speed and significant wave height are all calculated. When recording water levels, the water depth is given as a mean water depth determined from burst-averaged pressure over the sample period (NIWA, 2001). For this deployment, the DOBIE instruments were programmed to record water levels and with a sample interval of 0.1Hz, 128 points per burst with a 10 minute interval between bursts. The DOBIE were deployed 0.30 m above the bed.

#### 4.1.3 Sediment traps

There are many different types of sediment traps. There is a general acceptance that cylindrical traps are the most accurate for measuring natural suspended sediment concentrations (Flint, 1998). The type used in this study (Figure 4.4), consisted of a PVC tube with a cap on the bottom and a cap on top that was removed once the instrument was deployed. The traps were mounted on the frames of the instruments (Figure 4.2). The traps can be used to obtain a time averaged vertical sedimentation rate of suspended sediment being transported by waves and currents. Traps were used only for the second deployment and were attached to four of the instruments frames. Traps were changed once during the deployment period.



*Figure 4.4 An example of the type of sediment traps used, seen attached to the S4 frame. The cap on top of the trap is removed after they are deployed. Photo taken by author.*

#### *4.1.4 Limitations of field work*

The instruments in the first deployment in Mercury Bay aimed to establish the direction of the current cell. For the second deployment (21<sup>st</sup> March to 2<sup>nd</sup> May 2006) instruments were configured to provide boundary data for model calibration and to ascertain current directions within Buffalo Bay. Unfortunately, an S4 deployed at the harbour entrance was found to be faulty 3-4 days after deployment. A DOBIE wave gauge was deployed in its place. The primary difficulty with this replacement was that the S4 was capable of providing valuable current flow data at the tidal inlet and the DOBIE which replaced it is only capable of logging water levels.

Further, upon downloading the final deployment data it was found that the Round Island 2 S4 did not log depth, which was needed to provide boundary water level data for the model, and to ascertain wave refraction patterns. As a result the model calibrations and boundary data are not as accurate as desired.

---

## **4.2 Results and Discussion of Instrument Data**

The data obtained by selected instruments are analysed in order to illustrate the physical processes occurring within Buffalo Bay. To find the dominant vector of sediment transport around the inlet, tidal elevation, current flows and wave characteristics are reviewed. Furthermore sediment characteristics from the instrument sites are evaluated.

### **4.2.1 Analysis of data**

S4 data were processed with InterOcean Software Version 4.1.1 to obtain current and tidal data. A magnetic correction of  $20^\circ$  was applied to achieve true north. This software converts the raw pressure data and logged current directions into depths and current speed and direction. An harmonic analysis was then conducted on the current and tidal data using the Matlab Tidal Analysis toolbox. The analysis gives the amplitude and phase of all tidal constituents found. The non-tidal currents are then separated from the tidal currents and predicted tidal water elevations are compared with measured total elevations. Julian days are given as the day of the year that the deployment took place. Julian days for the first deployment cover days 326-364 of 2005 and Julian days for the second deployment cover days 79-126 of 2006. The S4 off Wharekaho Beach was processed to obtain tidal, current flow, and wave data for the first deployment. For the purposes of this study, this S4 is not analysed as it covers a different time period. The Buffalo Beach and Whitianga Wharf S4 were processed for the second deployment as all other S4 instruments had insufficient data. DOBIE data was run through the Matlab programme Tidal Analysis also but only for model calibration purposes. The Wharf S4 has some erroneous data, probably caused by instrument tampering or interference (W de Lange, pers. comm., 2007). As a result the Wharf site data set finishes at day 115 and there is a gap between days 87-97.

Wave statistics were calculated from the S4 data using the InterOcean software WinWave. The wave data were processed to provide significant wave heights  $H_s$ , wave periods  $T$  and direction of wave approach for each site. Wave data was collected at the Wharekaho site but was excluded from the analysis as little information could be drawn from the data since it was taken over a different time period.

Sediment traps were emptied into plastic containers and weighed to find a total mass over time in grams (g) (Figure 3. 6). Further, each sample was put through the Rapid Sediment Analyser (RSA) to determine mean grain size, settling velocity, sorting and phi range values.

#### 4.2.2 S4 Tidal data

It is important to ascertain the significance of the tidal wave in the hydrodynamic setting of the Whitianga tidal inlet and Buffalo Bay. The tidal data provides information relating to tidal current speeds and the characteristics of the tidal wave as it enters Mercury Bay and Buffalo Bay.

The Matlab function `t_tide` (designed by M. G. Foreman and co workers, Institute of Ocean Sciences) produces a phase and amplitude for each tidal constituent. The function calculated the dominant tidal constituent at the Buffalo Bay and wharf S4 sites as the  $M_2$  tide, which has a period of approximately 12.4 hours. Using the calculated phase, a time lag between the two sites can be determined (Table 4.1) which enables an estimate of the travel time of the tidal wave.

Table 4.2 The phase and amplitude and the calculated phase lag of the  $M_2$  tidal constituent at each instrument site.

Location	M2 Tidal constituent		
	Amplitude (m)	Phase (degrees)	Lag
Cooks Bluff DOBIE	0.7207	213.51	2.4 minutes
Wharekaho S4	0.7409	214.67	48 seconds
Buffalo Bay S4	0.7328	214.28	1.7 minutes
Entrance DOBIE	0.7263	213.42	18 minutes
Wharf S4	0.7114	222.13	9 minutes
River DOBIE	0.6996	226.7	

Analysis of the phase lag between each instrument in a sequence indicates that the tidal wave slows as it enters the Whitianga inlet. This is to be expected as the

shallow entrance of the inlet induces more friction, the narrowing of the inlet retards the flow and there are also freshwater discharges into the estuary that can slow the flood tidal wave. In comparison, it only takes ~48 seconds for the tidal wave to move between the Wharekaho and Buffalo Bay sites, which is also to be expected as the sites are within close proximity and in reasonably deep water.

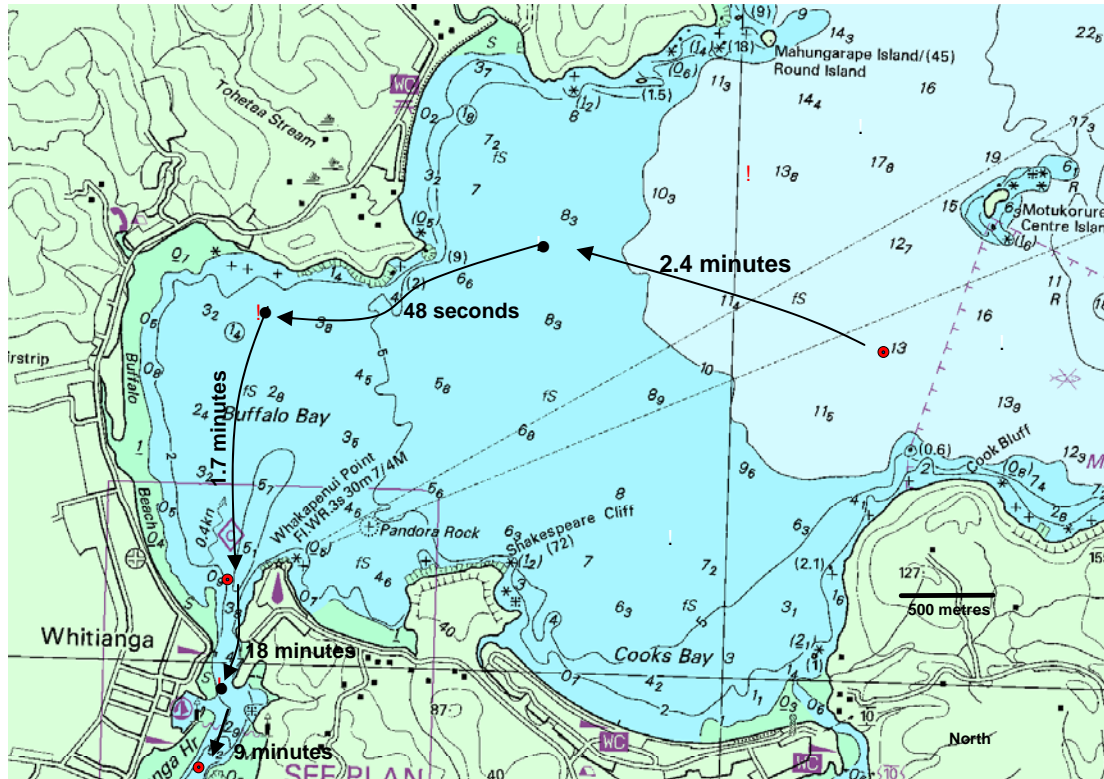


Figure 4.5 The lag times of the M2 tidal wave constituent between instrument sites within Mercury Bay using data from both deployments, 22<sup>nd</sup> November to 30<sup>th</sup> December 2005 and 21<sup>st</sup> March to 2<sup>nd</sup> May 2006. Note arrows do not necessarily indicate flow paths. Map adapted from LINZ (2005a).

The matlab 't\_tide' function uses the recorded tidal constituents (phase and amplitude) to predict the tidal elevation over the period of deployment and matches it to the measured sea level elevation. The discrepancy between the two represents any changes in the sea elevation not related to the tide (non-tidal).

The total and non-tidal elevation on the graph is relative to the depth the instrument was deployed at, and the tidal elevation on the graph is relative to the mean sea level of the tidal elevation data set which is calculated as the average of the tidal elevation time series. The Buffalo Bay tidal record (Figure 4.6) shows that the

predicted and actual surface elevations are similar, which suggests the total elevation recorded at this site is primarily derived from the tidal elevation. The mean ebb and flood tide have similar periods (~7 hours) and amplitudes (~0.6 m) at the Buffalo Bay site. The record also shows a very clear spring and neap tidal cycle with spring period occurring over days 85-95 and neap period over days 95-100.

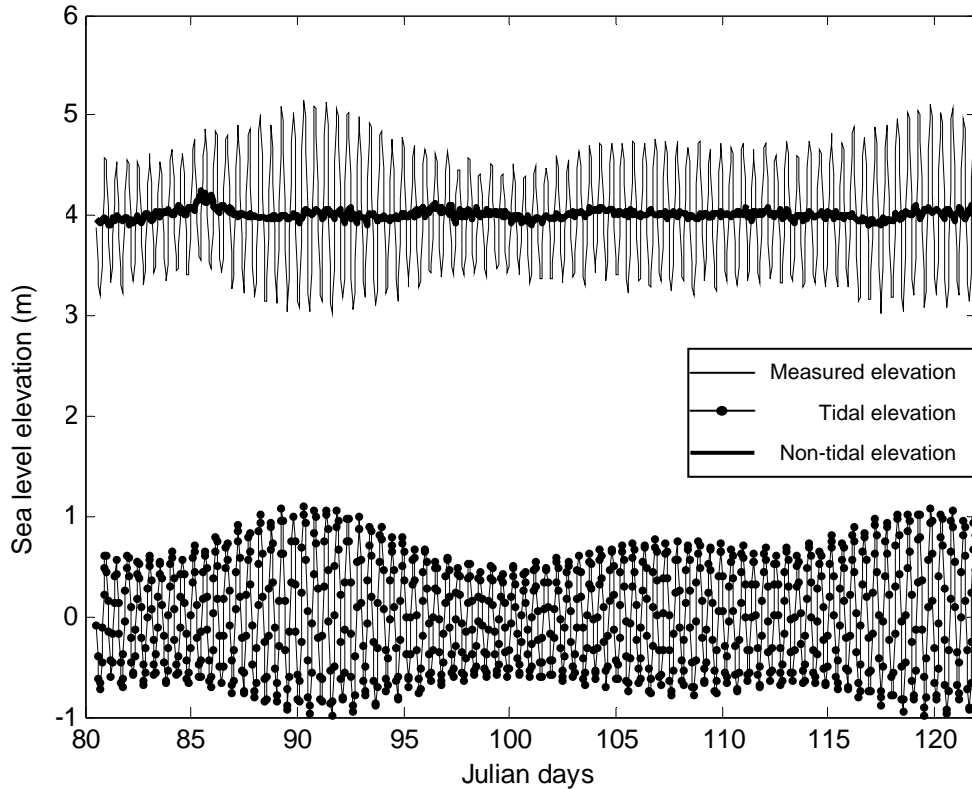


Figure 4.6 The total, tidal and non-tidal sea level elevation at Buffalo Bay for the second deployment (21<sup>st</sup> March to 2<sup>nd</sup> May 2006). The total elevation is relative to the depth the instrument was deployed at (4 m) and the tidal elevation is relative to the mean sea level of the data set.

A closer look at the non-tidal elevation record at the Buffalo Bay site (Figure 4.7) over the monitoring period, 21<sup>st</sup> March to 2<sup>nd</sup> May 2006, shows the occurrence of a long period (7-10 days) oscillation. A comparison with the atmospheric pressure time series for the period of the second deployment compares well over days 80 to 100 and days 117 to 122, with the oscillations in the non-tidal record (Figure 4.7). There is a lag (~24-48 hours) between the low pressure and the high water level. The  $r^2$  correlation between the atmospheric pressure and non-tidal elevation over days 80-100 is 0.1, allowing for a lag of approximately 24 hours.

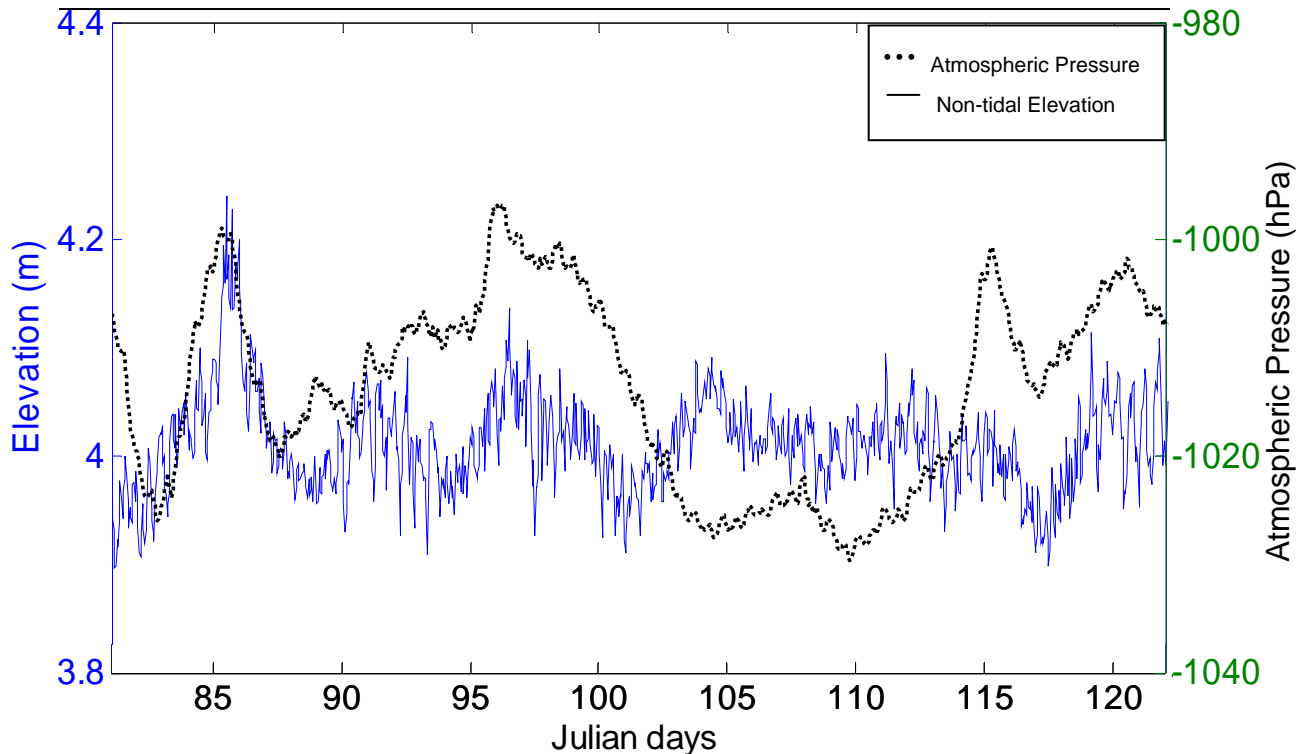


Figure 4.7 The non-tidal water level elevation at Buffalo Bay relative to the depth of the instrument (~4 m) and the inverse atmospheric pressure recorded at the Whitianga aerodrome for the duration of the second deployment 21<sup>st</sup> March to 2<sup>nd</sup> May 2006.

The atmospheric pressure data (Figure 4.7) was inverted to better show any relationship between pressure and water level as generally low pressure causes water levels to rise to counteract the low atmospheric pressure. This is known as the 'inverse barometer effect'. Atmospheric pressure is therefore likely to be the primary cause of the non-tidal oscillations in elevation at the Buffalo Bay instrument site, but not the sole cause. The non-tidal elevation that is not related to the pressure (i.e. days 100-117 Figure 4.7) is therefore a result of one or a combination of the following:

- Wind. In coastal situations, winds blowing offshore cause a stress on the ocean surface which can result in a setdown of sea surface elevation and vice versa for onshore winds. Therefore, wind may also contribute to the total elevation. The wind recorded at offshore Slipper Island during days 100-115 was predominantly from the south east (~127-184 degrees) which is onshore directed and may have caused set up of the water level at the Buffalo Bay monitoring site.

- Basin seiching or shelf waves caused by the natural shape of Mercury and Buffalo Bays.

The water level elevation at the Whitianga wharf site (Figure 4.8) is predominantly tidal. The flood tide at this site is approximately 30 minutes longer on average than the ebb tide but they have similar amplitudes ( $\sim 0.6$  m). It is likely the flood tide takes longer as the narrow inlet gorge retards the incoming flow.

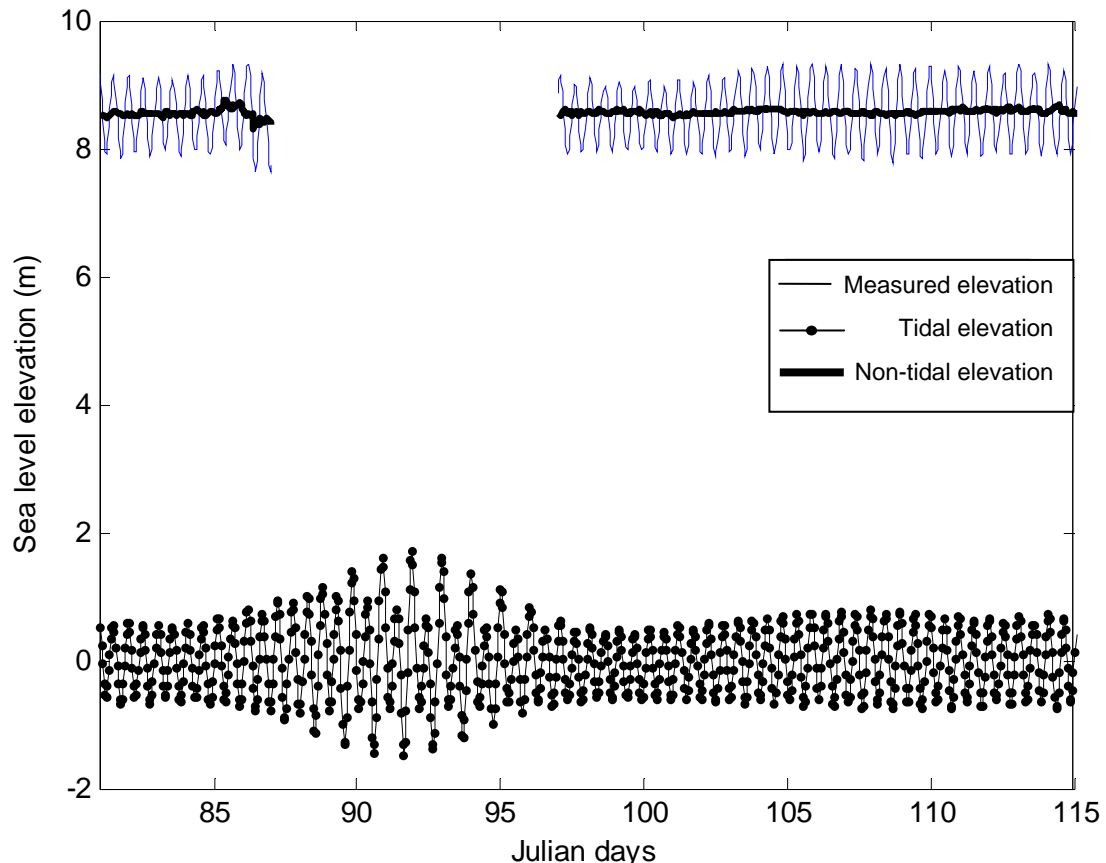


Figure 4.8 The total, tidal and non-tidal water level elevation at the Wharf for the second deployment 21<sup>st</sup> March to 2<sup>nd</sup> May 2006. Some data was removed due to errors. The total elevation is relative to the depth the instrument was deployed at ( $\sim 8.5$  m) and the tidal elevation is relative to the mean sea level of the data set.

### 4.2.3 Currents

The current at each monitoring site can be separated into tidal and non-tidal components. Non-tidal currents are induced by non-tidal processes such as increased freshwater input which causes density differences, wind stress on the surface or wind forcing (including up- and down-welling), longshore currents formed by oblique wave approach or bottom orbital currents induced by wave orbital motion. The current speed and direction (given as direction current is travelling to) (Figure

4.9) are very different at the Buffalo Bay and wharf monitoring sites. Current speed and direction at the wharf site are different due to the instrument's position within a harbour, which typically have a narrow and deep shape and experience freshwater discharge from land and river currents. The wharf S4 current data shows two dominant current directions ( $\sim 350^\circ$  and  $210^\circ$ ) clearly representing the ebb and flood tide. The ebb portion of the current exhibits the fastest current ( $\sim 1.3 \text{ m s}^{-1}$ ) with average current speeds of  $0.9 \text{ m s}^{-1}$ , and the flood portion of the tidal currents has an average current speed of  $0.7 \text{ m s}^{-1}$ . This is slower than the ebb current which is expected due to the dampening effect of the shallow and narrow inlet entrance. The ebb and flood currents are not in exact opposite directions because the flood and ebb tidal flow are controlled by inlet channel morphology and typically take different paths within an inlet. The  $t_{\text{tide}}$  analysis of the wharf site S4 data predicted that the tidal current at the wharf site accounts for over 97 % of the total currents. The 3 % of currents not attributed to the tidal wave are probably caused by freshwater input and wind or are actually tidal constituents not picked up in the analysis due to the short length of the data set.

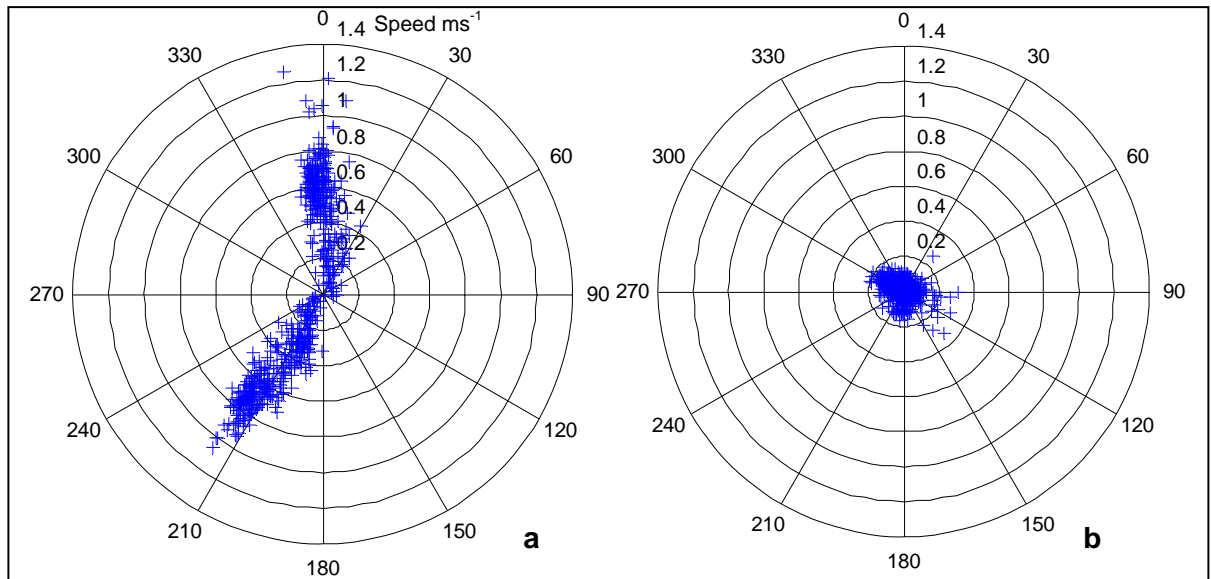


Figure 4.9 The current direction (degrees) (given as the direction the current is traveling towards) and speed ( $\text{m s}^{-1}$ ) at a) Whitianga wharf and b) Buffalo Bay sites between the 21<sup>st</sup> March and 2<sup>nd</sup> May 2006.

Current speeds at the Buffalo Bay site are very slow, only 25% of those recorded at the wharf site. Closer inspection of the Buffalo Bay current plot shows no dominant current direction. The direction of the tidal currents at this site were estimated by the  $t_{\text{tide}}$  analysis as being rotational, that is they do not move onshore and offshore but

rather flow around the Wharekaho headland and along Buffalo Beach. The ebb and flood tide have similar current speeds ( $0.05 \text{ ms}^{-1}$  and  $0.06 \text{ ms}^{-1}$  respectively) although the flood tide is faster by  $0.01 \text{ ms}^{-1}$ . The  $t_{\text{tide}}$  analysis of the Buffalo Bay site S4 data predicted only 40 % of the currents at this site are attributed to the tide. As with the non-tidal currents at the wharf site, some of the 60 % of the estimated non-tidal currents at the Buffalo Bay site could be explained by un-detected tidal constituents, but the majority of the non-tidal current is likely to be related to either wind, resonant seiching by the water body, freshwater input, or wave-induced alongshore currents. Due to the offshore location of this instrument it is unlikely to be the latter two. Therefore the non-tidal current is caused by either local wind, or wind offshore which induces alongshore, and up- and down-welling currents, or resonant seiching in the bay. No local wind data was available for the Buffalo Beach area but wind data was obtained from a wind station on offshore Slipper Island south east of Whitianga. A comparison of the non-tidal current speed and offshore wind speed (Figure 4.11) shows a fair correlation between days 115 and 122, with an  $r^2$  value of 0.08, but the rest of the time series does not match with the offshore wind data. Therefore, it can be assumed the majority of the non-tidal currents at the Buffalo Bay site are induced by the local wind speed and direction within Buffalo Bay, and possibly resonant seiching, for which some evidence is available in the model outputs, and was also detected in the tidal trace by Smith (1980).

The non-tidal current exhibits no clear dominant direction (Figure 4.10) with the exception of the period between 600 and 900 hours (~days 105-115) which show a north directed dominance, most likely related to local wind conditions or wave activity, which increased over this period (Figure 4.11). During this period, if sediment was entrained it could be carried north by this residual current, which is alongshore, towards the Wharekaho headland. Due to the typically multi-directional nature of currents at this site, the non-tidal current here is relatively insignificant in the sediment transport at this site.

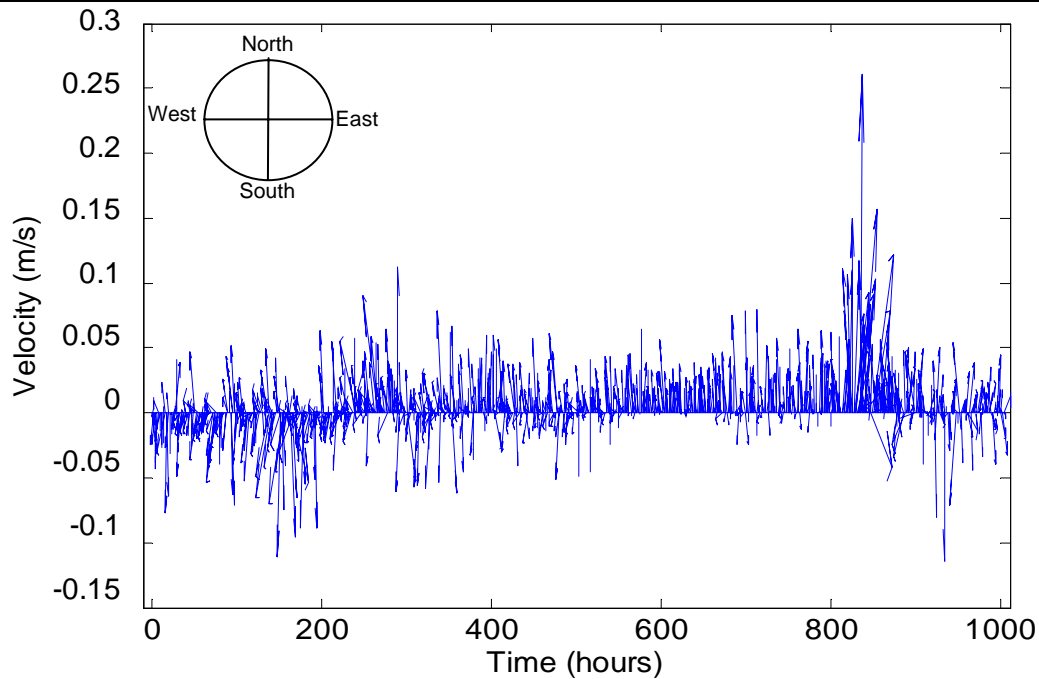


Figure 4.10 The non-tidal current speed and direction at the Buffalo Bay site. Directions are derived from U and V vectors which are positive or negative according to their direction relative to compass direction (0-360°). Positive values represent north and east current components and negative values represent south and west current components.

#### Implications for sediment transport

The threshold of a uni-directional current to entrain fine grained sediment is given by Miller et al. (1977) for grains with a diameter (D) less than 0.2 cm or  $1 \phi$ , using the equation:

$$\bar{u}_{100} = 122.6D^{0.29} \quad (1)$$

where  $\bar{u}_{100}$  is the velocity ( $\text{cm s}^{-1}$ ) measured 1 m above the bed, required to move sediment. The mean grain size recorded in this study at the inlet entrance and Buffalo Bay was  $\sim 0.015$  cm (0.15mm). Using this diameter the threshold velocity can be calculated as  $32.3 \text{ cm s}^{-1}$  or  $0.32 \text{ m s}^{-1}$ .

The current speeds at the wharf site 21<sup>st</sup> March to 2<sup>nd</sup> May 2006, as measured 1m above the bed, averaged  $0.52 \text{ m s}^{-1}$  with a maximum recorded speed of  $1.3 \text{ m s}^{-1}$  occurring during day 86. Tidal current speeds average  $0.6 \text{ m s}^{-1}$ , with a maximum of  $\sim 1.0 \text{ m s}^{-1}$ . Average non tidal current speeds extracted during the tidal analysis were

$\sim 0.21 \text{ m s}^{-1}$  with a maximum of  $0.37 \text{ m s}^{-1}$ . These non-tidal currents may have been caused by an increased water discharge or wind induced surface currents.

It is apparent that if the sediment transport threshold velocity is  $0.32 \text{ m s}^{-1}$ , average tidal currents at the wharf site are capable of transporting sediment. These current speeds are increased further with the addition of non-tidal currents occurring occasionally. Smith (1980) undertook current analyses in the gorge of the Whitianga inlet using a bucket wheel current metre. He found dominant ebb tidal flows 1 metre off the bed within the inlet gorge of around  $1.0\text{-}1.1 \text{ m s}^{-1}$  which is in agreement with the results attained for the inlet flow at the wharf site obtained in this study.

At the Buffalo Bay site 21<sup>st</sup> March to 2<sup>nd</sup> May 2006, as measured 1 m above the bed, the average current speed was  $0.06 \text{ m s}^{-1}$  with a maximum speed of  $0.34 \text{ m s}^{-1}$ . The maximum occurred over days 115-116 and again over 85-95, at times of larger wave heights. The average tidal current speed was  $0.03 \text{ m s}^{-1}$  and the maximum was  $0.09 \text{ m s}^{-1}$ . Non-tidal currents at this site, possibly formed by wind or wave activity or seiching, averaged speeds of  $0.03 \text{ m s}^{-1}$  and reached a maximum velocity of  $0.31 \text{ m s}^{-1}$ . During the period monitored in this study, sediment transport at the Buffalo Bay site would have been limited to days 85-95 and 115-116 where it appears wave activity induced faster total current velocities at 1m above the bed. Wave activity is a common driver in sediment entrainment, as wave orbital motion stirs up bed sediments which are lifted into suspension (Fredsoe and Deigaard, 1992). Any ambient current will then transport the suspended sediment. The Buffalo Bay site receives more wave activity than the wharf site but non-tidal currents at the Buffalo Bay site only averaged  $\sim 0.02 \text{ m s}^{-1}$ . Larger wave events occurring over days 85-87 and 115-122 show a reasonable agreement with the increased non-tidal velocities (Figure 4.11) so it can be deduced that larger swell waves have the ability to entrain sediment from this site.

Sediment entrainment under waves can also be estimated from linear wave theory (Komar and Miller, 1975) whereby the near-bottom orbital velocity of a wave,  $u_m$  is calculated as:

$$u_m = \frac{\pi H}{T \sinh(2\pi h / L)} \quad (2)$$

where  $H$  is wave height,  $T$  is wave period,  $h$  is water depth and  $L$  is the wave length.  $L$  is calculated for shallow water waves (such as the Buffalo Bay site in this study) (defined by ratio of water depth to deep water wave length  $= < 0.05$ ), as:

$$L = T \sqrt{gh} \quad (3)$$

where  $g$  is the acceleration due to gravity,  $\sim 9.81 \text{ m s}^{-2}$ . Using a water depth  $h$ , of 4 metres and the wave periods associated with the average and maximum wave heights at the Buffalo Bay site between 21<sup>st</sup> March and 2<sup>nd</sup> May 2006, of 8.4 and 9.0 seconds respectively,  $L = 52.6$  for the average wave and 56.4 m for the maximum wave recorded at the Buffalo Bay site in this study.

Therefore  $u_m$  can be calculated as:

$$u_m = \frac{\pi 1.6}{9.0 \sinh(2\pi 4 / 56.4)} = 1.21 \text{ ms}^{-1} \quad \text{For the maximum wave and;} \quad (4)$$

$$u_m = \frac{\pi 0.3}{8.4 \sinh(2\pi 4 / 52.6)} = 0.23 \text{ ms}^{-1} \quad \text{For the average wave.} \quad (5)$$

This illustrates that under the average wave conditions at the Buffalo Bay site between 21<sup>st</sup> March and 2<sup>nd</sup> May 2006, wave orbital velocities are not sufficient to entrain sediment as they do not exceed the threshold velocity of  $0.32 \text{ m s}^{-1}$  calculated above. Conversely, under large waves ( $T > 9 \text{ s}$ ) the orbital speed is sufficient to entrain sediments. Smith (1980) suggested wave orbital velocities of  $0.5 \text{ m s}^{-1}$  for a 10 second, 1 metre idealised wave in Mercury Bay. The velocity attained in this analysis of  $1.21 \text{ m s}^{-1}$  is considerably larger but is expected due to the larger wave height used and the shallow nature of Buffalo Bay compared to the greater Mercury Bay.

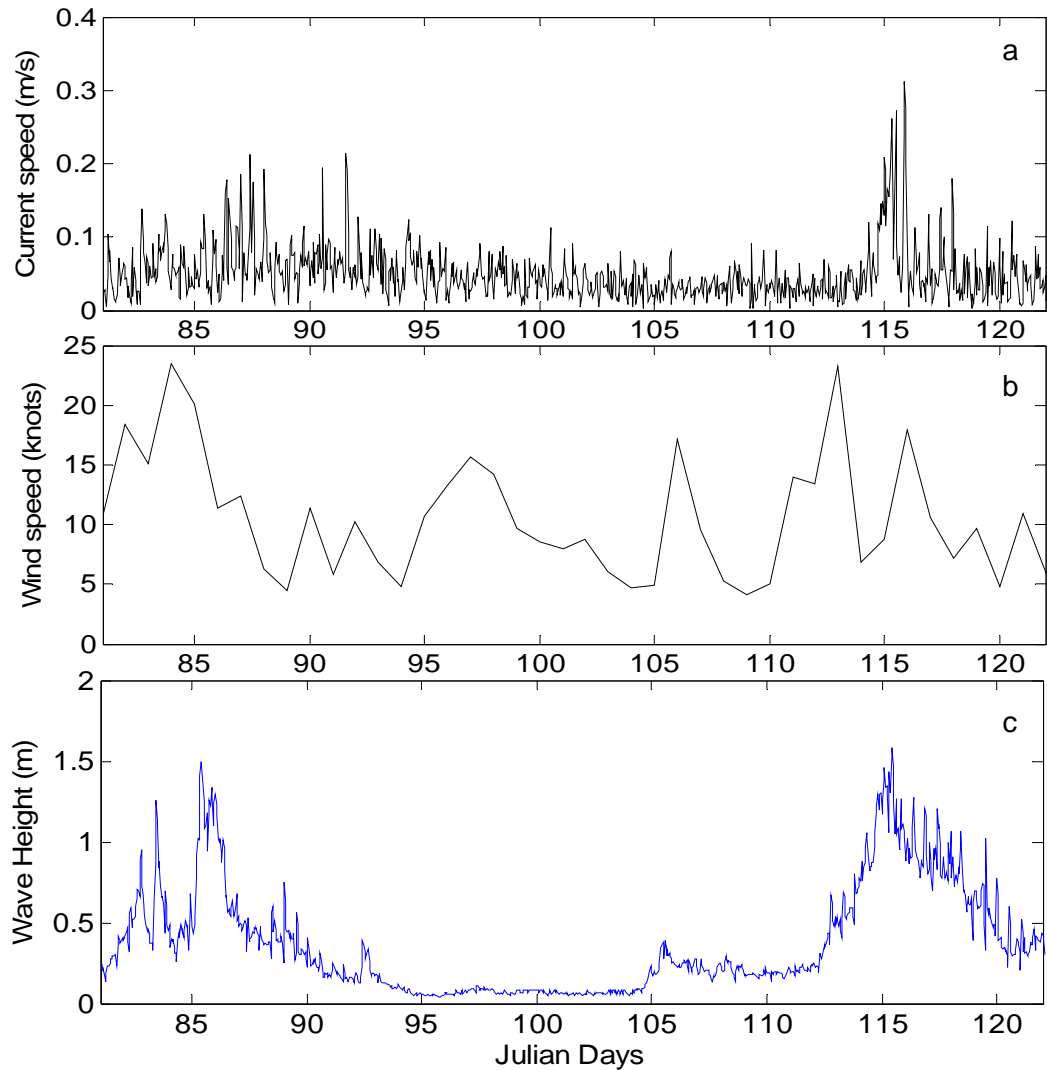


Figure 4.11 The a) non-tidal current speed at Buffalo Bay; b) the wind speed recorded at Slipper Island; and c) the wave height at Buffalo Bay for the second deployment, 21<sup>st</sup> March to 2<sup>nd</sup> May 2006.

Thus, during the monitoring period in this study, the Buffalo Bay site current speeds are slower than at the wharf site. The tide is the dominant driver of currents and elevation at the wharf site whereas small, non-tidal currents induced by local wind prevail at the Buffalo Bay. Maximum non-tidal and tidal currents alone at the Buffalo Bay site were not fast enough to transport sediment. However current speeds at the Buffalo Bay site are able to entrain sediment under maximum wave conditions recorded over the monitoring period.

#### 4.2.4 Wave data

The Buffalo Bay site received larger waves (Figure 4.12a) with longer periods (Figure 4.12b) on average compared to the wharf site. This is due to the sheltered position of the wharf site within the Whitianga Harbour, which received predominantly locally generated sea waves, boat wake and wind chop, while Buffalo Bay is more exposed and received swell waves generated offshore as well as larger sea waves produced within Mercury Bay.

*Table 4.3 The wave statistics for Buffalo Bay and Whitianga wharf sites over the second (21<sup>st</sup> March to 2<sup>nd</sup> May 2006) deployment.*

		March 21st to 5th May 2006	
		Buffalo Bay	wharf
Wave Height	Mean	0.4	0.08
H <sub>s</sub> (m)	Minimum	0.04	0.03
	Maximum	1.58	0.54
Wave Period	Mean	10.1	3
T (s)	Minimum	3.1	3
	Maximum	20.7	3.4
Wave direction	Mean	68.6	181
degrees	Maximum	154.8	359
	Minimum	36.3	0.4

The wave period at the wharf stayed relatively constant between 2 and 4 seconds and the wave heights were rarely greater than 0.2 m, making them insignificant for this analysis.

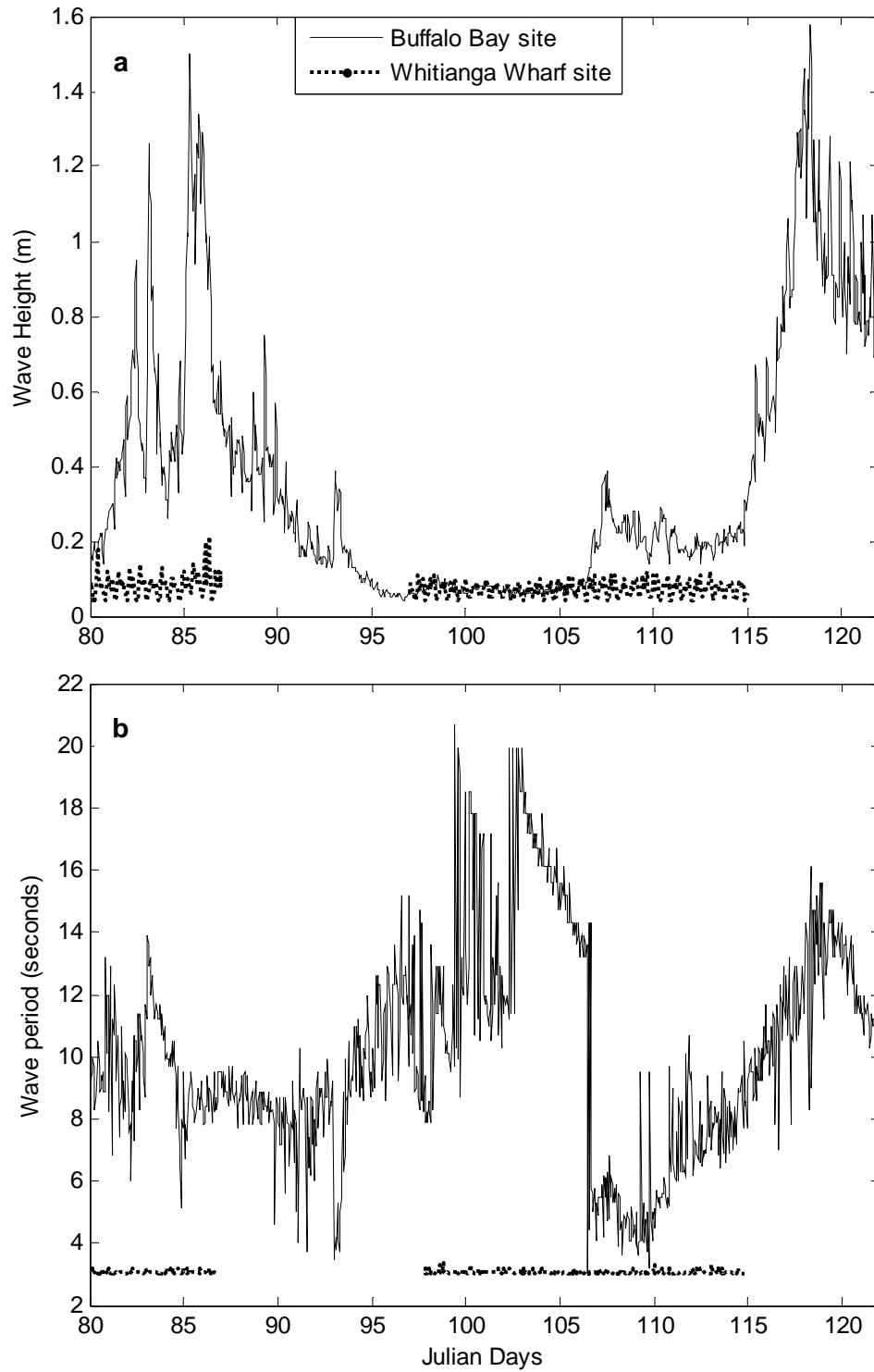


Figure 4.12 A The significant wave heights; and B, the wave periods recorded at Buffalo Bay and the wharf monitoring site during the second deployment from 21<sup>st</sup> of March to the 2<sup>nd</sup> of May 2006.

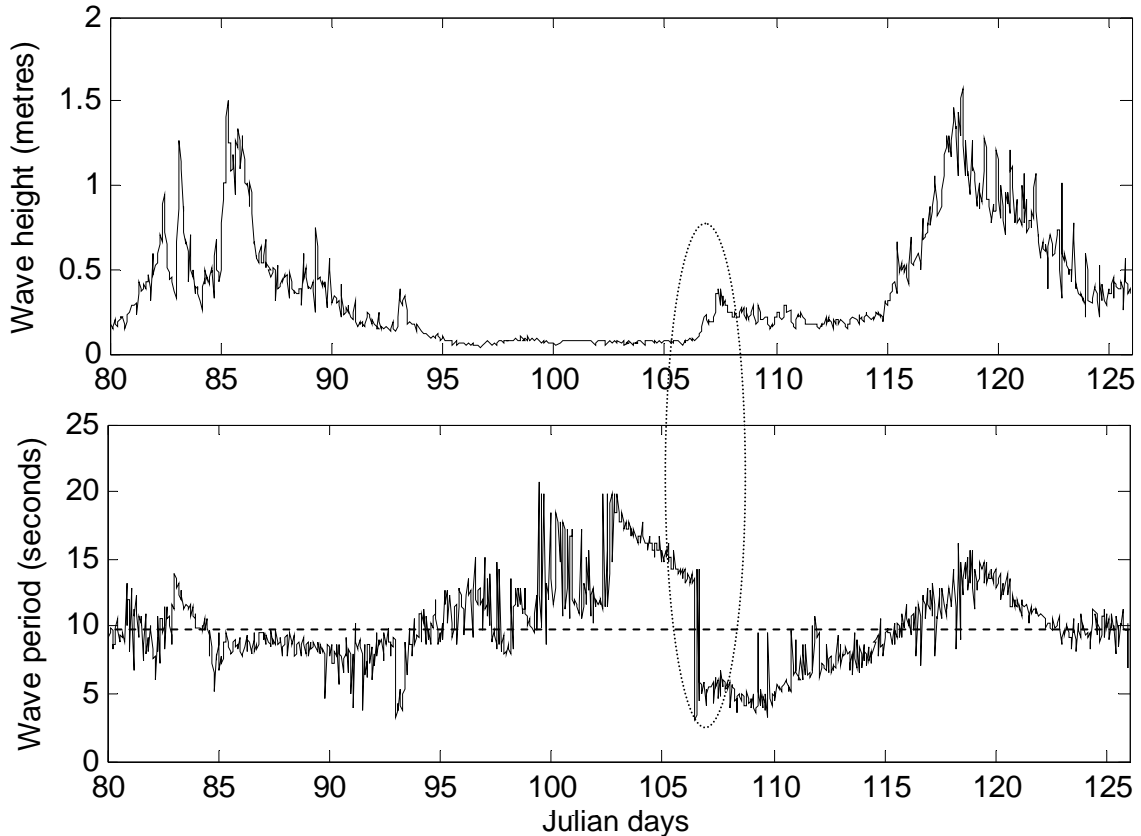


Figure 4.13 The wave height (top) and wave period (bottom) recorded at the Buffalo Bay site over the second deployment from 21<sup>st</sup> of March to the 5<sup>th</sup> of May 2006. The dashed line represents a 9 second wave period and dashed ellipse indicates the rapid drop in wave period.

During the period of observation, the wave period at Buffalo Bay starts to increase gradually around Julian day 94, where wave heights begin to decrease. Similarly wave heights start to increase on day 106 and wave periods drop dramatically. This is most likely to be due to local wind-generated waves, characteristic of storm conditions and comprising short periods. Comparison with situation maps and pressure data does not show a low pressure system over the north island during this time but the wind direction did change from southeast to southwest and wind speeds increased considerably over this time. Generally swell waves have periods of greater than 9 seconds (s) where as sea waves typically have periods less than 9 s. This wave analysis shows that both sea and swell waves are present in Buffalo Bay.

Data from Met Service gives the coastal forecasts over the time of deployment, including the predicted swell directions. Analysis of this data gives a swell direction

from the northeast for days 84-86 and 113-114 (2006). The dominant swell direction over the deployment period was equally north and northeast. An easterly swell was dominant over days 80-82, and again over days 115-122. These time periods coincide with the largest wave heights indicating that larger swell waves in Mercury Bay originate predominantly from an easterly direction. The smallest waves occurred over days 90-105 and are associated with a swell from the north.

The recorded wave directions (Figure 4.14) show that during the monitoring period, the majority of the waves at Buffalo Bay approached from between  $60^\circ$  and  $80^\circ$  degrees (indicated by the lines on Figure 4.14). The primary deviation from this occurs over days 95 to 106, with multiple fluctuations in wave approach direction. These fluctuations are most likely to be related to wind chop as the wave heights over this period were small (i.e. there was no swell waves over this time). In contrast, wave approach angles at the wharf are multi-directional which can probably be attributed to boat wake, wind chop and the narrow shape of the harbour.

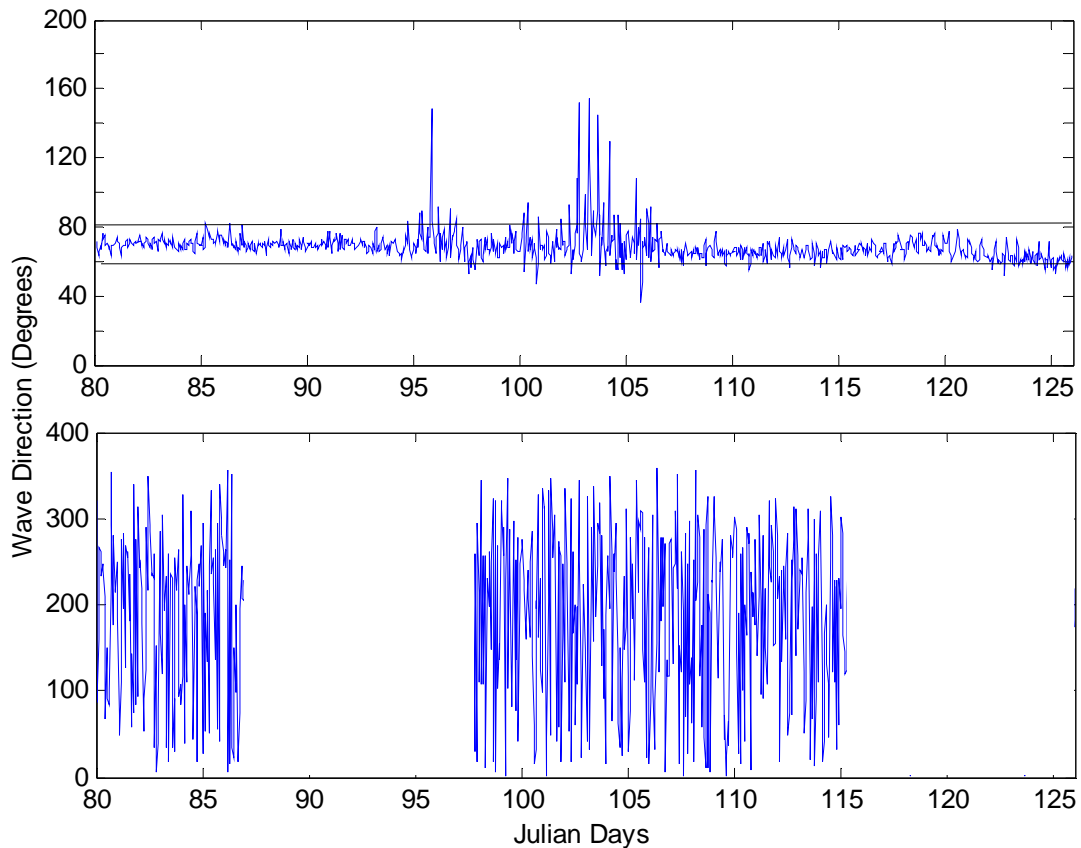


Figure 4.14 The recorded wave directions at the Buffalo Bay (top) and wharf sites (bottom) for the second deployment, 21<sup>st</sup> March to 2<sup>nd</sup> May 2006. Lines on the top graph indicate the location of the majority of wave approach directions from  $60^\circ$ - $80^\circ$ .

### 4.2.5 Sediment

In total 5 sediment traps were analysed for the two trap deployments occurring within the second deployment from 21<sup>st</sup> March to 2<sup>nd</sup> May 2006. By observation, the sediment samples collected at the river site were very fine and stained the white storage container reddy-brown, possibly due to a high iron oxide content. There was more sediment collected at this site in the first deployment than the second (Figure 4.15). The Harbour entrance site had only one sediment trap and this was relatively full. The sediment within the traps at the wharf site was minimal (less than 10 g) for the first deployment and empty for the second. Underwater photos taken at the time of instrument deployment at this site show the bed to be coarse material of primarily whole shells, with a thin covering of sand. This is a shell lag deposit overlying sand. The absence of fine sand here further supports the expectation that currents at the wharf site are too fast and turbulent to allow sand deposition, as is typical within the narrow tidal gorge of a tidal inlet (Black et al., 1989). This fast-velocity-coarse-sediment relationship is also evident in the Tauranga inlet (Davies-Colley and Healy, 1978) and the Whangerei inlet (Black et al., 1989). The shell lag was also noted by Smith (1980) and Cooper (2003) but the actual shape and extent of this lag deposit within the inlet is unknown.

The Buffalo Beach site sediment trap had the most sand collected for both deployments. This trap was located within the area identified by the bathymetric residual map (Figure 3.12) in Chapter 3 as undergoing erosion between 1938 and 1979. The entrance and Buffalo Bay site samples exhibited a large proportion of organic material, black and bark-like in nature in various sizes. Some very fine particles of this organic matter were evident within the river samples, which also appears to be bark. The Whitianga wharf is not used to load or unload logs or any forestry product and there is no large-scale deforestation taking place in Buffalo Bay so one could assume the bark originated from the Whitianga estuary catchment and the forestry sector within.

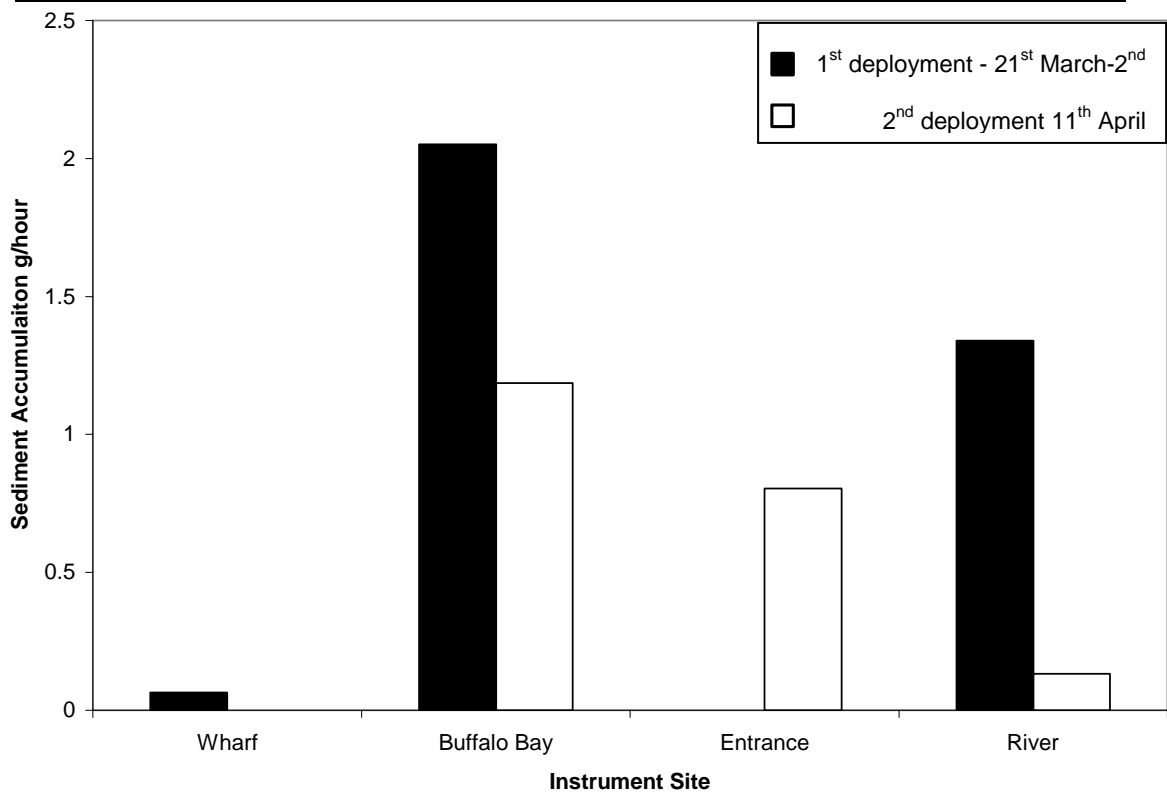


Figure 4.15 The sediment accumulation rate for each sediment trap site for the second deployment, 21<sup>st</sup> March to 5<sup>th</sup> May 2006.

Sediment traps are indicative of the amount of suspended matter, not of the actual rate of accretion, as it is possible for sediment to be suspended but not deposited. The accreted sediment at the Buffalo Bay site has two possible sources. Firstly, it may have been advected here from another source, namely the inlet. However, if the sediment was transported from the estuary then the entrance trap could be expected to be fuller and contain coarser sediment compared to the Buffalo Bay trap, as the sediment would settle out as the current flowed out of the inlet and suspended load would be finer once the current reached the Buffalo Bay site. Secondly, the sediment accumulated in the trap may have been in a sediment 'puff'. Sediment puffs form as a result of wave activity lifting them into suspension, then sediment settles out and is re-suspended again with the next wave (Aagaard and Greenwood, 1995; Brun-Cottan et al. 2000). Therefore the trapped sediment at this site may not have been transported here, but rather it may represent a period of sediment entrainment and uplift under wave currents. Sediment transport at this section of Buffalo Bay is small, due to the low velocity currents which are typically unable to entrain sediment. However orbital velocities of larger swell waves (e.g. days 112-120 Figure 4.13) combined with background tidal currents, can entrain sediment,

which can then be transported by any ambient current in the vicinity, but is unlikely to be transported far due to the slow and multi-directional nature of currents at this site (as identified above). This interpretation of the data agrees with Smith (1980) and Bradshaw (1991) who hypothesised wave action was important for suspending and reworking nearshore sediments in Mercury Bay and may be the cause of the identified erosion in northern Buffalo Bay in Chapter 3.

A portion of sediment from each trap was analysed using the RSA to obtain mean grain size and textural properties of sediments. Buffalo Beach sediment overall was moderate to poorly sorted and strongly coarse skewed with a mean grain size of 2.47 phi (~0.15 mm). The entrance sample showed moderately sorted sediments that were near symmetrical with a mean size of 2.52 (~0.15 mm). The RSA results suggest that the sediments at the Buffalo Bay instrument site are similar to those at the entrance instrument site, having similar grain sizes. The river sample was too fine to put through the RSA so the Malvern Mastersizer was used to analyse the river sediment and the entrance and Buffalo samples were also analysed for calibration purposes (Appendix 3). Samples from the Buffalo Bay and entrance sites had very similar grain size distributions with mean grain sizes of around 0.15 mm, and both samples contained grains of up to 2 mm diameter. The mean grain size of sediment from the river site was 0.14 mm but the sample contained a portion of very fine (0.003 mm) sediment with minimal coarse grains.

Previous sediment studies (Smith, 1980; Cooper, 2003) found similar grain sizes, although mud deposits were found in northern Buffalo Bay by Smith (1980) and Bradshaw (1991). In his beach and offshore sampling, Cooper (2003) noted the likelihood of a fluvial sediment origin for the sediments. The fine nature of the sediment in this study, and absence of shell matter is suggestive that the sediment originates from the Whitianga catchment. The poor sorting of sediment in the Buffalo Bay site sample may be attributed to several sediment sources at this site, such as sediment from the inlet, sediment reworked offshore and possibly sediment from local river inputs from nearby Taraporiki Stream. Further, the moderate sorting at the entrance site could be attributed to two sources of sediment, as some sediment is deposited at the entrance during the ebb tide as the flow decelerates while additional

sediment is deposited after moving down Buffalo Beach in the net littoral drift system.

### **4.3 Conclusions**

Two field monitoring deployments were undertaken (22<sup>nd</sup> November to 26<sup>th</sup> December 2005 and 21<sup>st</sup> March to 2<sup>nd</sup> May 2006) to obtain current, water level, wave and sediment information. Based upon the available data the following conclusions were drawn.

- The M<sub>2</sub> tidal constituent dominated at the Buffalo Bay and wharf sites. Sea level elevation at the Buffalo Bay and wharf sites is predominantly due to the tidal wave. There is some non-tidal elevation at the Buffalo Bay site, likely to be caused by the combination of atmospheric pressure and wind.
- Currents at the wharf site are primarily driven by the tide and are on average, capable of transporting sediment. The Buffalo Bay site has weaker currents which, on average, are not fast enough to transport sediment. However, the combination of non-tidal and tidal currents can result in transport. At the Buffalo Bay site, non-tidal currents dominate and are attributed to local and offshore wind speed and direction. Near bottom wave orbital velocities over the monitoring period (21<sup>st</sup> March to 2<sup>nd</sup> May 2006) are fast enough during the maximum recorded swell conditions ( $H_s \approx 1.5\text{m}$  and  $T \approx 9\text{ s}$ ) to transport sediment. The lack of a dominant current direction at this site suggests sediment transport here would be minimal.
- Wave heights averaged 0.3 meters at the Buffalo Bay monitoring site with the dominant wave approach direction from the east. Waves at the wharf are probably the product of wind chop and boat wake.
- Sediment traps at the Buffalo Bay and entrance sites accumulated the most sediment and both sites have similar textural characteristics with an average grain size of  $\sim 0.15\text{ mm}$ . The sediment accumulated in the trap at the inlet entrance is presumed to be from the estuary whereas the amount accumulated in the Buffalo Bay site trap is thought to be caused by suspension events under waves.

The raw analysis identified wind and pressure as contributing factors to the hydrodynamic setting, but hydrodynamics are primarily regulated by the tidal wave.

## ***Chapter Five – Hydrodynamic Modelling of the Whitianga Inlet***

---

Modelling represents a useful way of exploring process-response interactions and allows insights into the structure and functioning of intricate systems (Lakhan and Trenhaile, 1989). It is important to remember, however, that coastal systems are complex and therefore models can not be assumed to be 100% correct (Bird, 2000). The primary steps in coastal numerical modelling are (Lakhan, 1989):

1. Specify the problem to be investigated and objectives of the model simulations. These factors will determine various components to be included in the model.
2. Accurately define the boundary conditions to insure all systems relative to the simulated area are included.
3. Identify which processes operating within the model area are essential to give a satisfactory description of the system.
4. Collect and prepare data over a continuous and long time period to run, calibrate, and validate the model with real time processes.
5. Calibrate and validate the model to ensure the accurate simulation of known processes.
6. Experimental design incorporates experiments to attain information relating to spatial and temporal changes in the model area.
7. Results are interpreted to ascertain their accuracy and logicity in the real world.

The numerical model used for this study is the DHI MIKE 21 modelling suite. MIKE 21 encompasses many different modules that are capable of simulating wave-related, current, and sedimentological processes. The MIKE 21 model simulates variation of water levels and flows in response to a variety of forcing conditions (e.g. wind, tidal forcing, radiation stresses) (de Vriend et al., 1993). The primary inputs to the model are the bathymetry, bed resistance, eddy viscosity, wind and boundary

conditions. The MIKE 21 models solve the vertically integrated equations of continuity and momentum in two horizontal dimensions (Somes et al., 1999).

A total of four modules were used in this research. These models and the governing equations are all outlined in the MIKE 21 and MIKE 3 reference manuals so are not reiterated here. The MIKE 21 Hydrodynamic (HD) module calculates the flow field from the solution of the depth-integrated continuity and momentum equations for shallow water (Nicholson et al., 1997; Kerper et al., 2002). Currents are driven by gradients in radiation stresses (Pechon et al., 1997). MIKE 21 HD was used to simulate the elevation and current speed and directions for Buffalo Bay. The water level elevations and currents within Buffalo Bay are tidally dominated, so attention was focused on reproducing a tidal model.

Wave refraction, diffraction and reflection was modelled using the MIKE 21 Parabolic Mid-Slope (PMS) module which accounts for the effects of shoaling, diffraction and refraction, directional spreading, forward scattering and bed friction, and breaking. As sufficient wave data was not collected, calibration of the wave behaviour in Mercury Bay is not undertaken but the results are considered a reasonable approximation.

In this chapter a description of hydrodynamic (tidal and wave) model inputs, the application of the calibration data and set up of the model for hydrodynamic applications are detailed and results and implications from the hydrodynamic modelling are presented.

## **5.1 Tidal Model Set Up**

### *5.1.1 General model inputs*

The objective of this model is to ascertain the water circulation patterns and sediment transport pathways at, and adjacent to, the Whitianga inlet. This model defines the various input parameters which can be specified by the user. The most

significant model variables are given below, and will be referred to in the following sections. Further information is given in the MIKE 21 HD reference manual.

#### *Courant number*

The Courant number expresses how many grid points the information moves in one time step (DHI, 2004). The Courant number is calculated using the following equation:

$$C_R = c \frac{\Delta t}{\Delta x} \quad (1)$$

where  $t$  is the time step,  $x$  the grid spacing and  $c$  the celerity given as:

$$c = \sqrt{gh} \quad (2)$$

where  $g$  is acceleration due to gravity and  $h$  is the water depth. A maximum courant number of 5 is recommended as anything over this causes stability problems. For this study the courant number was kept below 2.

#### *Sources and sinks*

Many model domains include rivers, intakes and outlets i.e. stormwater, power stations, drinking water etc. This functions allows the source location (grid points), discharge and direction to be specified (DHI, 2004). This variable was not included in this study.

#### *Flooding and drying*

Flooding and drying allows computation of flow in an area which sometimes dries out and sometimes is flooded (e.g. tidal flats). This function was enabled for this study using default settings of 0.2 m drying and 0.3 m flooding depths.

#### *Eddy Viscosity*

The eddy viscosity represents the momentum fluxes due to turbulence, vertical integration and sub grid scale fluctuations (DHI, 2004). The eddy viscosity value depends on a combination of wind speed, the density of water, the depth of the sea and the coriolis force (Ramming and Kowalik 1980). Eddy viscosity provides damping of short wave-length oscillations, and generally alters the current speeds and turbulence. MIKE 21 has 3 methods for applying eddy viscosity. Firstly a constant value can be applied to the whole grid. Secondly the eddy viscosity can be constant in time but specified in space by constructing a grid of eddy viscosity as a

dsf2 or grid file. The more sophisticated method, the Smagorinsky formula, uses a time varied function of the local gradients in the velocity field (Somes et al., 1999). Types one and three were trialled in this study but the best calibration was obtained using the Smagorinsky formula.

#### *Bed Resistance*

Bed resistance introduces friction which primarily affects the elevation data. In MIKE 21, either Manning or Chezy Numbers can be chosen to represent bed resistance. Manning numbers are calculated as follows:

$$M = \frac{gu|u|}{C^2} \quad (3)$$

where  $u$  is velocity and  $C$  is the Chezy Number (DHI, 2004). Bed resistance is applied as a value to each grid point within the model. All points can have the same value or a map of bed resistance can be imported to introduce different resistance values to the grid area. If no information is available a constant Manning number of  $32 \text{ m}^{1/3}/\text{s}$  is recommended (DHI, 2004) and was used in this model due to the lack of bed resistance data. The model definition of the resistance means that a smaller resistance number increases the bed resistance and vice versa.

#### *Wave Radiation*

This variable allows inclusion of the wave induced flow in the model area. Wave radiation can be included as stationary or quasi stationary but both settings require a grid or dsf2 file (grid file) of radiation stresses,  $S_{xx}$ ,  $S_{xy}$ ,  $S_{yy}$  and bathymetry. This file can be created from wave model results. Wave radiation stresses were not included in this model application for simplification.

#### *Wind Conditions*

The wind can be specified in 3 ways (DHI, 2004). Firstly with wind speed and direction constant over the whole grid. Secondly with wind speed and direction varying in time but not space which requires a time series file input, and thirdly with wind speed and direction varying in time and space. The latter requires wind be defined for every grid point in the area by creating a dsf2 file. Wind does affect the elevation and currents within Buffalo Bay, however a time series of local wind over the deployment period (21<sup>st</sup> March to 2<sup>nd</sup> May 2006) was not available to include in the model. Therefore in this modelling exercise the effects of wind were modelled to

establish their effect from different directions etc, but wind was not primarily included as a model input.

### 5.1.2 Bathymetry

The bathymetry is very crucial to the model's precision and accuracy of simulations so must be as accurate as possible. The most recent survey of the Whitianga tidal inlet was in 1995. Buffalo Bay and Mercury Bay were last surveyed in 1979. The latest hydrographic chart available, published in April 2005 combines both the 1979 full Mercury Bay survey and the smaller 1995 inlet survey. This chart was digitised using ARCVIEW GIS software and a series of DEM's (Digital Elevation Model's) with 10, 20 and 30 metre grid spacing were created then transformed into grids in DHI. As the nested grid option was not available for this study, the hydrodynamic model was first run using the Buffalo Bay bathymetry and then later the entire Mercury Bay (Figure 5.1) bathymetry was modelled. The reference level for all the bathymetries was converted to MSL. The bathymetry in Buffalo Bay could have changed in the 27 year period since the 1979 survey, and likewise the inlet bathymetry would have changed considerably in the last 11 years since the 1995 survey. The inlet could be up to ~250 cm shallower in places if the approximate maximum vertical sedimentation rate in the inlet calculated in Chapter 3 of  $\sim 25 \text{ cm y}^{-1}$  is correct. However a multibeam survey or similar bathymetry sampling of the study area was not feasible for this study, so the most recent bathymetry was used. This may provide difficulty in calibration as depths may have changed, so water level elevation and current speeds and direction may all be different.

In order to have a straight boundary, the bathymetry was rotated 55 degrees anticlockwise using Surfer 7 software and the sides were blanked. The Whitianga marina was left out of the model grid as a 20 m grid spacing was too small to adequately identify the marina entrance.

#### *Grid sizing*

Grid spacing is an important variable as it determines the extent at which processes can be identified. Finer resolution is best in order to identify small scale processes, but this creates large files and takes a long time to run (Chau, 2003). Grid sizing is specified when creating the bathymetry and cannot be changed in the model setup. For this research the grid spacing was trialled at 10, 20 30 and 50 metres and the

final model was set at 20 metres which did mean that model runs were lengthy as the resolution was high, but enabled small areas such as the inlet entrance to be studied and observed in detail.

### 5.1.3 Boundary conditions

The placement of the boundary is an important decision and affects the accuracy and validity of the model. As mentioned previously, when deciding on the correct place for a boundary one must consider all the systems and processes operating around the study area and decide if they should be included in the model (Holland and Capotondi, 1996). Often a model domain includes a larger area than the actual study area. Within the boundary conditions there are certain aspects that need to be specified also. The water level at the boundary must first be specified and there are five options. The water level can be constant, where elevation remains the same at all grid points along the boundary in time and space. Secondly, the elevation can be given as a sine series using the amplitude and phase of the tidal wave. The water level is calculated for each time step but is constant in space. Thirdly, water level can be given in a time series file where water level along the boundary varies in time and space but is the same at each grid point (dsf0 file). Similarly the boundary can be given as a time series where each value along the boundary is specified and varies in time (dsf1 file). Alternatively, conditions from previous model runs can be used along the boundary (transfer file). In this study both the sine series of the  $M_2$  tidal constituent derived from the harmonic analysis of field data, and tidal time series data based on the field survey, were used as boundary conditions. The Flux Along the Boundary (FAB) must be specified which relates to the type of flow at the boundary. The flow can be perpendicular to the open boundary (0), or either obtained by extrapolation from the flow one grid point inside the boundary (1) (DHI, 2004) or the direction of the flow at the boundary is explicitly given (2) (DHI, 2004). Typically the FAB is set to 2 or 12 which is a combination of 1 and 2.

As a boundary is often comprised of different depths, sometimes currents forced at the boundary begin to flow into the model then turn around and flow back out again due to bathymetry changes, or wind or coriolis effects. The tilting function within the boundary conditions allows the boundary profile to be tilted to stop these returning currents. The user can specify non-linear or linear tilting about a grid point along the

boundary, usually the deepest point. Linear tilting assumes the water level to follow a straight line which can be rotated around the tilting point. With non linear tilting the amount of tilting is calculated in each grid pint on the boundary based on the Navier Stokes equations which is a more theoretically correct approach. Both types of tilting can be trialled to see which gives the best calibration.

Finally there is an option to specify the flow direction at the boundary in a dsf1 file. Typically the direction is not specified and is perpendicular to the boundary by default.

The boundary in this study was first placed along the entrance to Buffalo Bay (Figure 5.1) in order to save computing time and output file size. This introduced problems when calibrating the model, particularly with the speed and direction of currents. The boundary was therefore shifted to the entrance to Mercury Bay and the grid was rotated to create a straight boundary and allow flow perpendicular to the model area. The sides of the model were filled in to create equal boundary conditions. Incorporating this larger area resulted in better model calibrations. This illustrates the interaction of hydrodynamic conditions between Mercury Bay and Buffalo Bay. A second open boundary was placed across the Whitianga estuary where the river DOBIE was situated.

The Mercury Bay grid was used for all model runs and experiments but only a small output area or sub grid of Buffalo Bay was saved to reduce computing time and output file size.

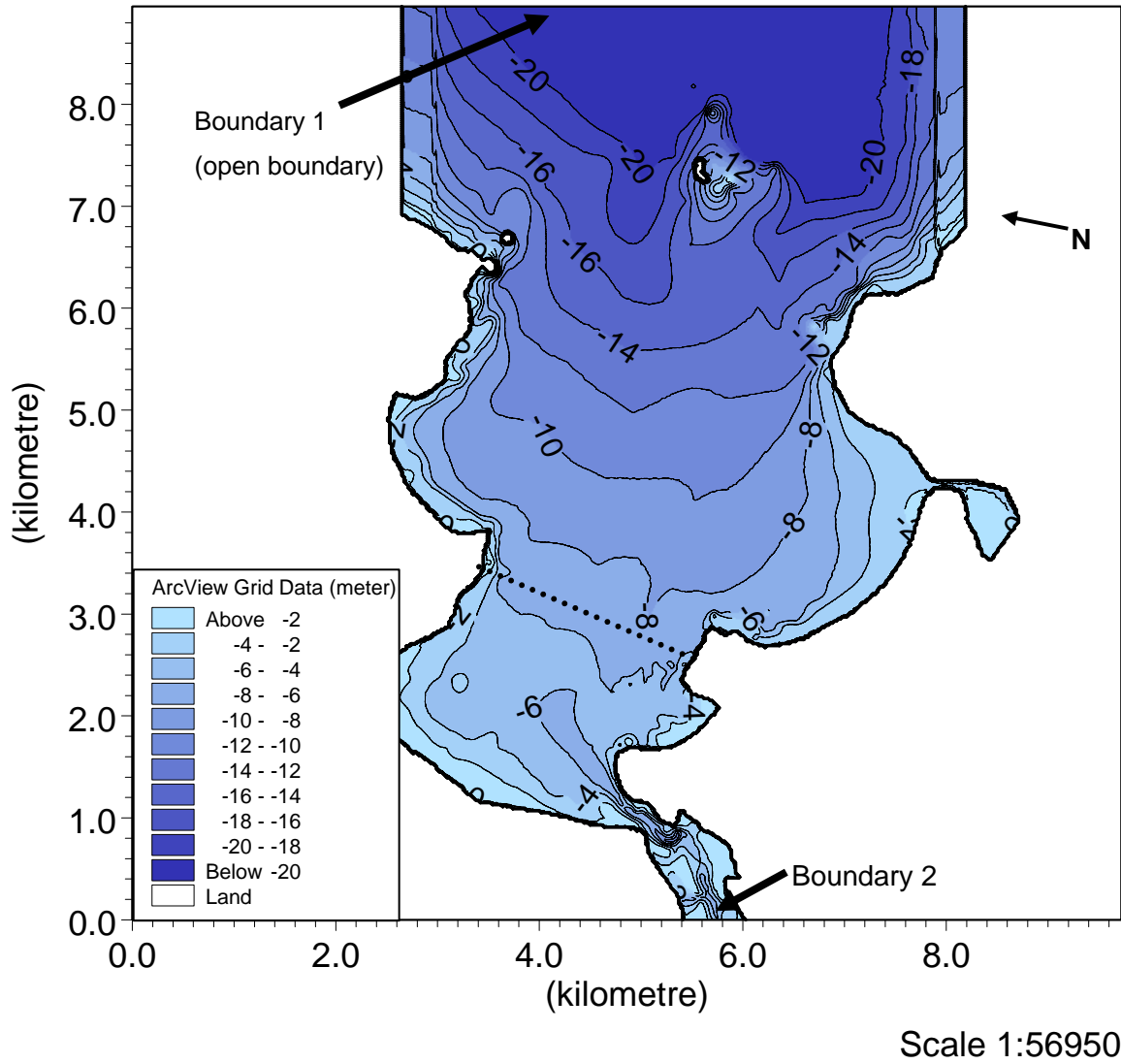


Figure 5.1 The Bathymetry used to model Mercury Bay and Buffalo Bay. Dotted line indicates the initial open boundary placement for Buffalo Bay.

## 5.2 Tidal Model Calibration

Time series data of sea level elevation was used to force the model at two open boundaries, (Figure 5.1). Tidal data (elevation and current speed and direction), from field survey measurements using DOBIE and S4 instruments were then used to calibrate the predicted elevation and current speed and direction. Calibration requires a time period of at least 10 days in order to capture the spring and neap tidal cycles. The first three days of model output are discarded as a warm up period, so the final time period used for calibration was from 12:00 am on 8<sup>th</sup> April, 2006 to 12:00 am on 18<sup>th</sup> April, 2006. Firstly the elevation was calibrated using the entrance DOBIE, and Buffalo Bay and wharf S4. Once the model simulated the elevation, current speeds and direction were calibrated using the wharf and Buffalo Bay S4. By changing the eddy viscosity and applying tilting along the open boundary, predictions of current speeds and directions compared better with the measured data. The calibration settings can be seen in table 5.1.

Table 5.1 The input variables for the hydrodynamic model calibration.

Input variable	Value
Time step	2 seconds
Courant number	1.5
Simulation period	12:00 am 3 <sup>rd</sup> April 2006 to 12:00 am 18 <sup>th</sup> April 2006
Flood and Dry	Drying depth = 0.2 m, Flooding depth = 0.3 m
Boundary manipulation	Applied non-linear tilting about the deepest boundary point
Boundaries	Flux Along Boundary type 12, undefined flow direction 1. Forced with elevation data from river DOBIE 2. Forced with elevation data from Cooks Bluff DOBIE
Eddy viscosity	Smagorinsky Formula with constant of 0.5
Bed resistance	Manning number 32 m <sup>1/3</sup> /s
Wind	No wind

### 5.2.1 Elevation

To calibrate the model properly to elevation, a different range of bed resistance values are typically used. In this model, the elevation showed the best calibration using the default Manning number of 32 m<sup>1/3</sup>/s.

Simulated and measured elevation compared well at the Buffalo Bay and entrance sites (Figure 5.2) and the spring and neap were evident at all sites. Buffalo Bay (Figure 5.2a) was the best fit with a maximum error of  $\pm 0.21$  m. The entrance elevation (Figure 5.2b) had a maximum error of  $\pm 0.3$  m and the wharf elevation (Figure 5.2c) was the least accurate with a maximum error of  $\pm 0.43$  m. The model-simulated elevation at the wharf site is in phase with the measured elevation but the simulated water level elevation was approximately 20 cm less than the measured for the majority of the calibration period. This is discussed in section 5.4 below.

The Mean Absolute Error (MAE) is a suitable method of determining the accuracy of a model prediction (Sutherland et al., 2004). The MAE is calculated as the mean difference between the model and measured values and thus represents the average difference between collected field data and model simulation. The MAE values obtained in this calibration compare well with hydrodynamic modelling studies undertaken in similar situations (e.g. Stoschek and Matheja, 2000; Siegle et al., 2002; K. Spiers, pers. comm., 2007).

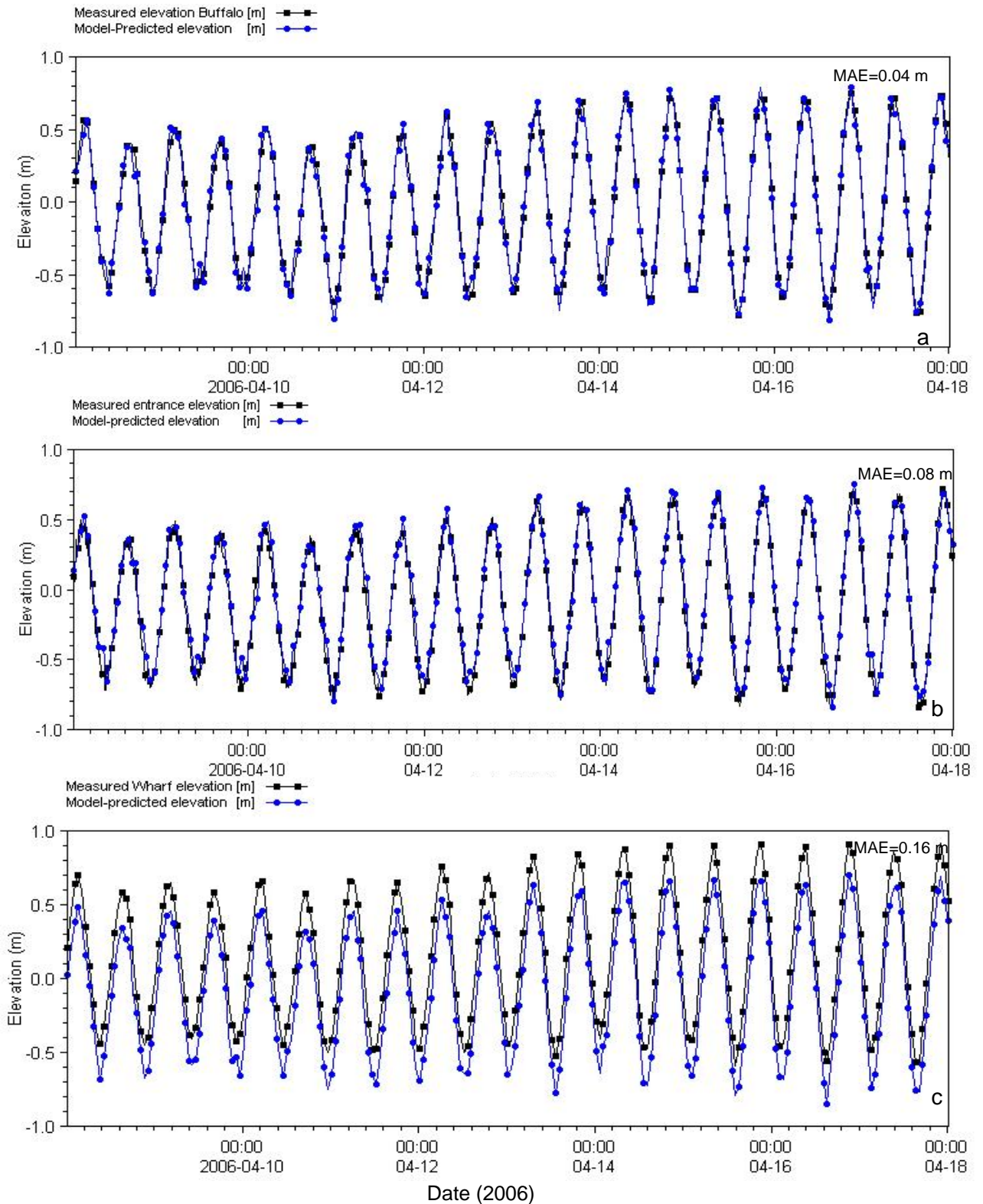


Figure 5.2 The model predicted and measured tidal water level elevation at a) Buffalo Bay, b) the entrance, and c) the wharf sites over the 10 day calibration period, 8<sup>th</sup> -18<sup>th</sup> April 2006. Measurements are plotted hourly for the model-simulated elevation and for the elevation at the wharf and Buffalo Bay sites. The measured elevation at the entrance site is plotted at 10 minute intervals. The Mean Absolute Error (MAE) is given also.

### 5.2.2 Current speed and direction

The accuracy of the predicted current speed and direction is very important as this will greatly influence the simulation of the sediment transport model also. Bathymetry has a significant impact on the current speed and direction and the model may not accurately simulate present hydrodynamic conditions using historical bathymetry.

The current speed of the MIKE 21 HD model outputs is depth averaged velocity, whereas in reality the current speed and direction vary over the flow depth (Ponce and Yabusaki, 1981). In this research the measured velocity using S4 recording current meter represents velocity as measured 1 metre off the bed. Therefore, the measured velocity must be depth-averaged in order to calibrate more accurately. The measured velocity at 1 m above the bed was converted to depth averaged velocity using the equation:

$$u_0 = u^* / k \times \left( \ln \frac{\text{depth}^{*0.4}}{z_0} \right) \quad (4)$$

where  $k$  is the von Karmens constant of 0.41, depth is the time series of measured depth and  $z_0$  is the bed roughness (0.0001 m for planar beds (Black et al., 1989) such as the Buffalo Bay site, and 0.001 m for estuarine beds (Black et al., 1989) such as the wharf site).  $u^*$  is calculated using the equation:

$$u^* = \frac{u \times k}{\log(z / z_0)} \quad (5)$$

where  $u$  is the measured velocity at 1 m above the bed and  $z$  is the height of the instrument above the bed (1). Depth averaging increased the velocities at the wharf site (Figure 5.3) but at Buffalo Bay they remained relatively the same.

Various bed roughness factors were trialled, namely at the wharf as the instrument sat on a shell bed which introduces a different bed roughness length but 0.001 m gave the model result for the wharf dataset. The profile of velocity with depth was plotted to ensure the depth-averaged velocity was realistic, then the depth averaged velocity can be compared with the model-predicted velocities (Figure 5.4).

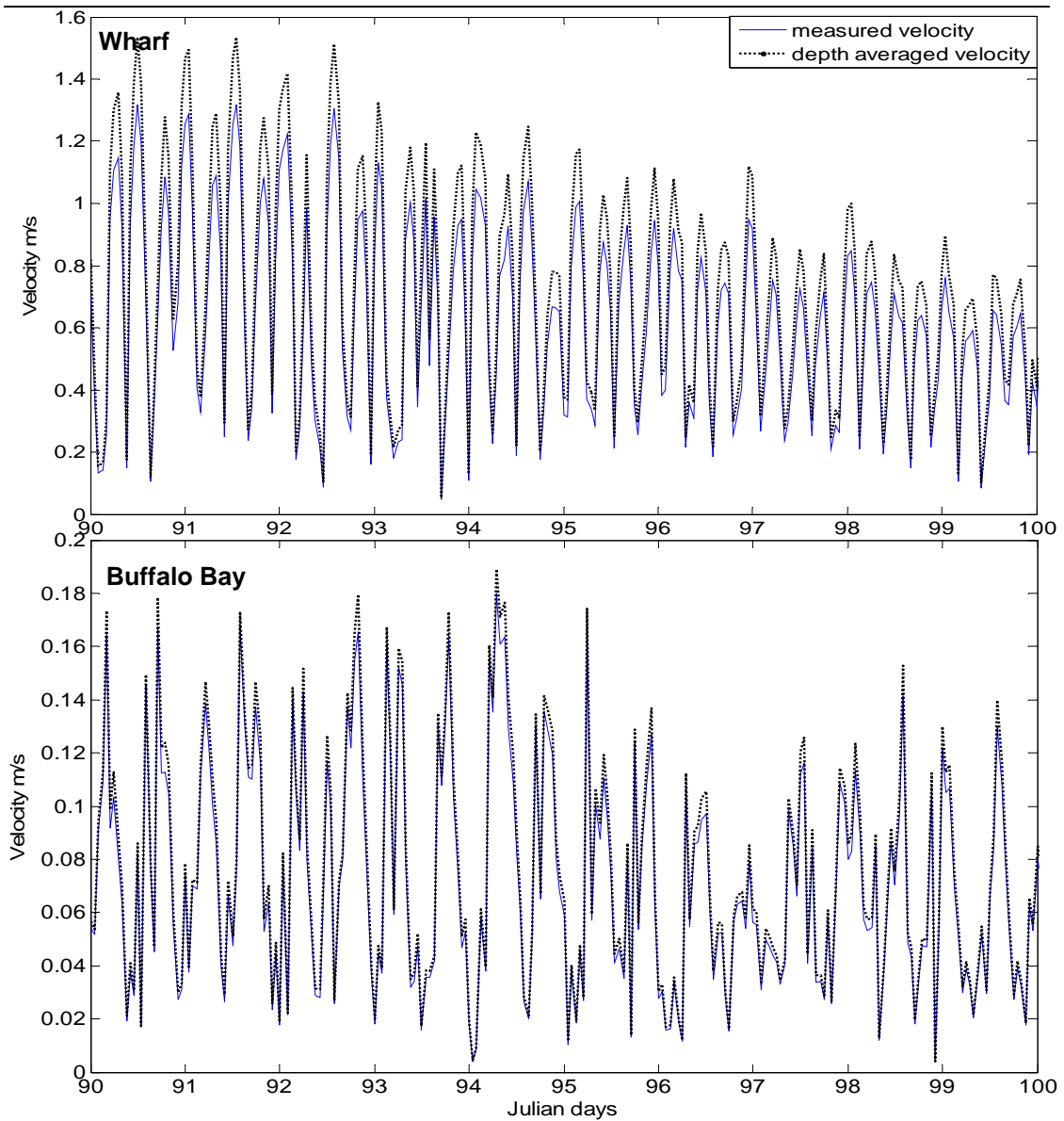


Figure 5.3 An example of the time series of measured current speed 1 m off the bed at a) the wharf and b) Buffalo Bay sites, and depth averaged speed (derived from the measured current speed recorded by an S4 current metre 1 m off the bed), at a) the wharf, and b) Buffalo Bay.

The simulated and measured wharf current speeds (Figure 5.4a) exhibit a similar pattern. The speed values have a similar range but the simulated currents speeds are lower than the measured depth-averaged speed. The maximum error of the current speed at the wharf is  $\pm 0.22 \text{ m s}^{-1}$ .

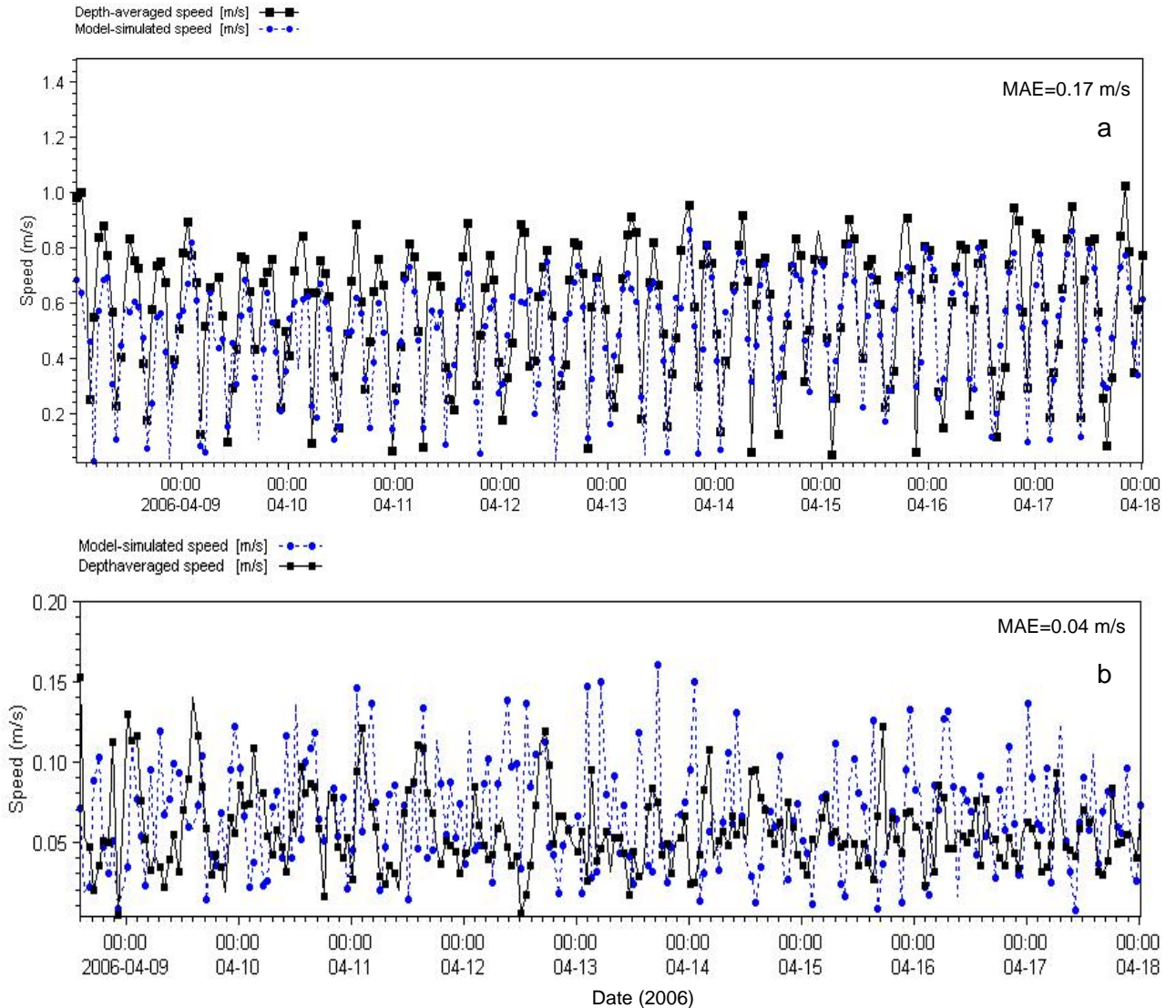


Figure 5.4 The model-simulated and measured current speed at a) the wharf site and b) the Buffalo Bay site for the 8<sup>th</sup> - 18<sup>th</sup> April 2006. The model-predicted speed is depth averaged and the measured depth averaged speed is derived from the measured current speed recorded by an S4 current metre 1 m off the bed at the Buffalo Bay site. Measured and simulated speeds are plotted hourly.

At the Buffalo Bay site (Figure 5.4b), the model does not predict the correct pattern of speed with over and under prediction. However the time series of model predicted current speed does show a similar range in speed values with a maximum error of  $\pm 0.18 \text{ m s}^{-1}$ . The speed at this site is particularly hard to calibrate to as the model does not include wind which may have a significant effect on the current speed and direction as noted in Chapter 4. In addition, as shown later from the snapshots of the spatial pattern, this site is likely subjected to bay seiche effects, which could affect the current speeds illustrated in Figure 5.5.

Current direction was corrected by 55 degrees due to the rotation of the bathymetry grid. Further the DHI software had assigned the bathymetry an orientation of 27.5 degrees which is probably an artefact of the original input grid and could not be changed. Therefore, in total, 82.5 degrees was added to the current directions so they are relative to map north. Simply adding 82.5 degrees to the calculated directions alters the shape of the rose plot as directions are derived from the current speed value (negative or positive U or V). Therefore the rose plots were rotated once they were constructed.

Rotating the wharf rose plot by 83 degrees clockwise is not quite enough to match up correctly with the measured direction, leaving an error of ~7 degrees. This can be incorporated into future model runs by always applying an 83 degree correction.

Buffalo Bay predicts a similar shape to the measured plot but the directions do not match up. Rotating this plot by 82.5 degrees clockwise does provide a slightly better match but directions are still up to 110 degrees out. Both the wharf and Buffalo Bay plots show a better match up with the measured current rose plots when rotated 90 degrees. The extra 7 degrees may be due to a problem with the orientation of the bathymetry grid or possibly a problem with the instrument derived north direction or it may be related to the differences in bathymetry.

The rose plots illustrate the model-predicted current speeds are similar to the measured speeds with both sites predicting the approximate calmness within 5 %.

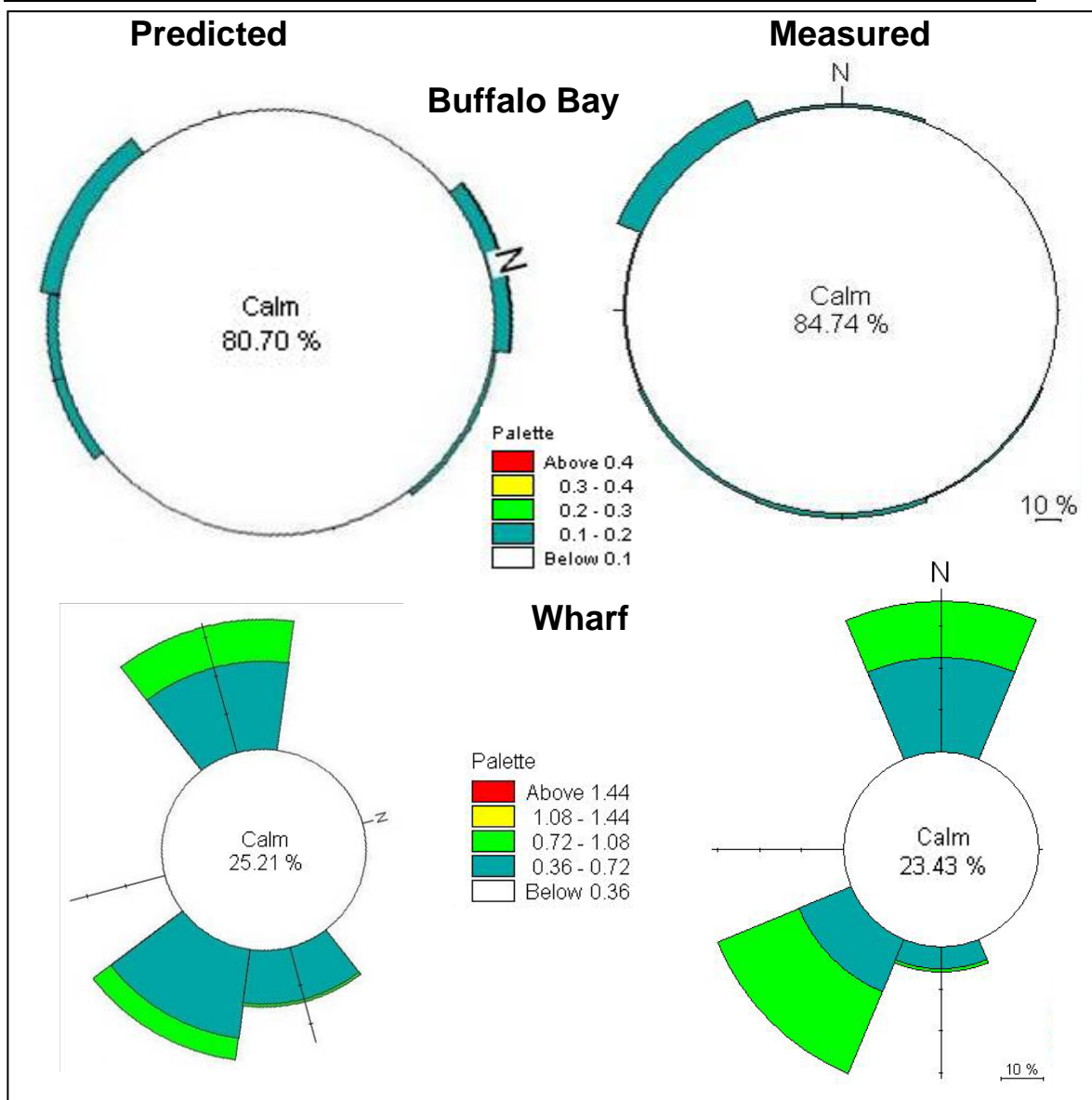


Figure 5.5 Rose plots of the model simulated and measured current speeds and direction (moving to) at a) Buffalo Bay, and b) the wharf over the calibration period. The model simulated plots have been rotated 82.5 degrees clockwise. Calm is defined as the percentage of the speed below 0.1 m/s for Buffalo Bay and below 0.36 m/s for the wharf site. 10 % represents the percentage of currents at each speed. The palette for each site is given in  $\text{ms}^{-1}$ .

### 5.3 Tidal Model Validation

Once a model is calibrated against a time series data from field measurements, the model must be verified against measured field data also. The same variables and model constituents are included to ensure the model is capable of predicting events outside of the calibration period.

Ideally the model should be validated against both spring and neap tides. For this study the model was validated for three days over the neap tide cycle which occurred from 12:00 am on 19<sup>th</sup> of April 2006 to 12:00 pm on 21<sup>st</sup> April 2006 and three days over the spring tide cycle from 7:00 pm on 28<sup>th</sup> of April 2006 to 4:00 pm on 1<sup>st</sup> of May 2006. Due to the erroneous data from days 115-122 in the wharf S4 dataset, the model-simulated elevation and currents over the spring tide were validated to the tidal elevation and tidal current speeds extracted from the harmonic analysis of elevation data carried out in Chapter 4 instead of the total sea level elevation and total currents speeds. This is not ideal but as the wharf site is tidally dominated and the dataset was incomplete, was a logical option.

The elevation (Figure 5.6) compares well for both the neap and spring tide periods at Buffalo Bay. The spring tide at the entrance site is out of phase with the tide by ~20 minutes but the neap tide compares well. A 20 cm difference is again evident between the simulated and measured water elevation at the wharf site for the neap tide. The spring tide has a similar difference even though the model was validated to the tidal elevation. This suggests the 20 cm difference is not from wind or freshwater effects which were not incorporated in the model, but could be due to model input values or bathymetry changes which is discussed in section 5.4.

The rose plots (Figure 5.7) show the neap period predicts an almost perfect match with the model-simulated calmness at Buffalo Bay within 0.5 % of the measured and model-simulated calmness at the wharf matching exactly. The spring period is not as good however, with Buffalo Bay calmness over 20 % less than measured and the wharf calmness over 5% less than measured. The general shape of the plots are satisfactory, although still approximately 7° different.

The model can now be applied to establish sediment transport pattern within Buffalo Bay.

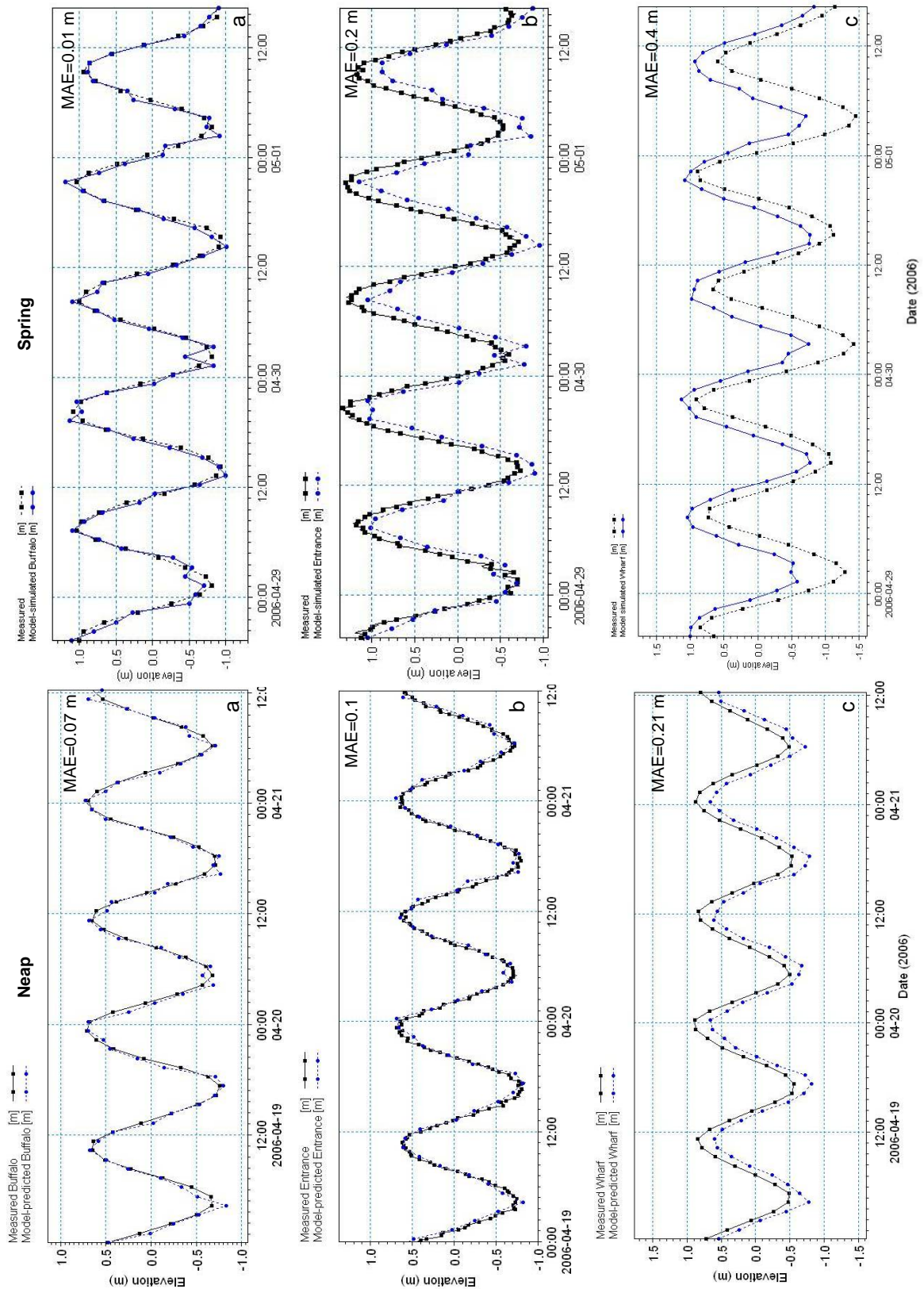


Figure 5.6 The model simulated and measured elevation at a) Buffalo Bay, b) the entrance and c) the wharf site over the spring and neap cycles. Measurements are plotted hourly for the model-simulated elevation and for the elevation at the wharf and Buffalo Bay sites. The measured elevation at the entrance site is plotted at 10 minute intervals.

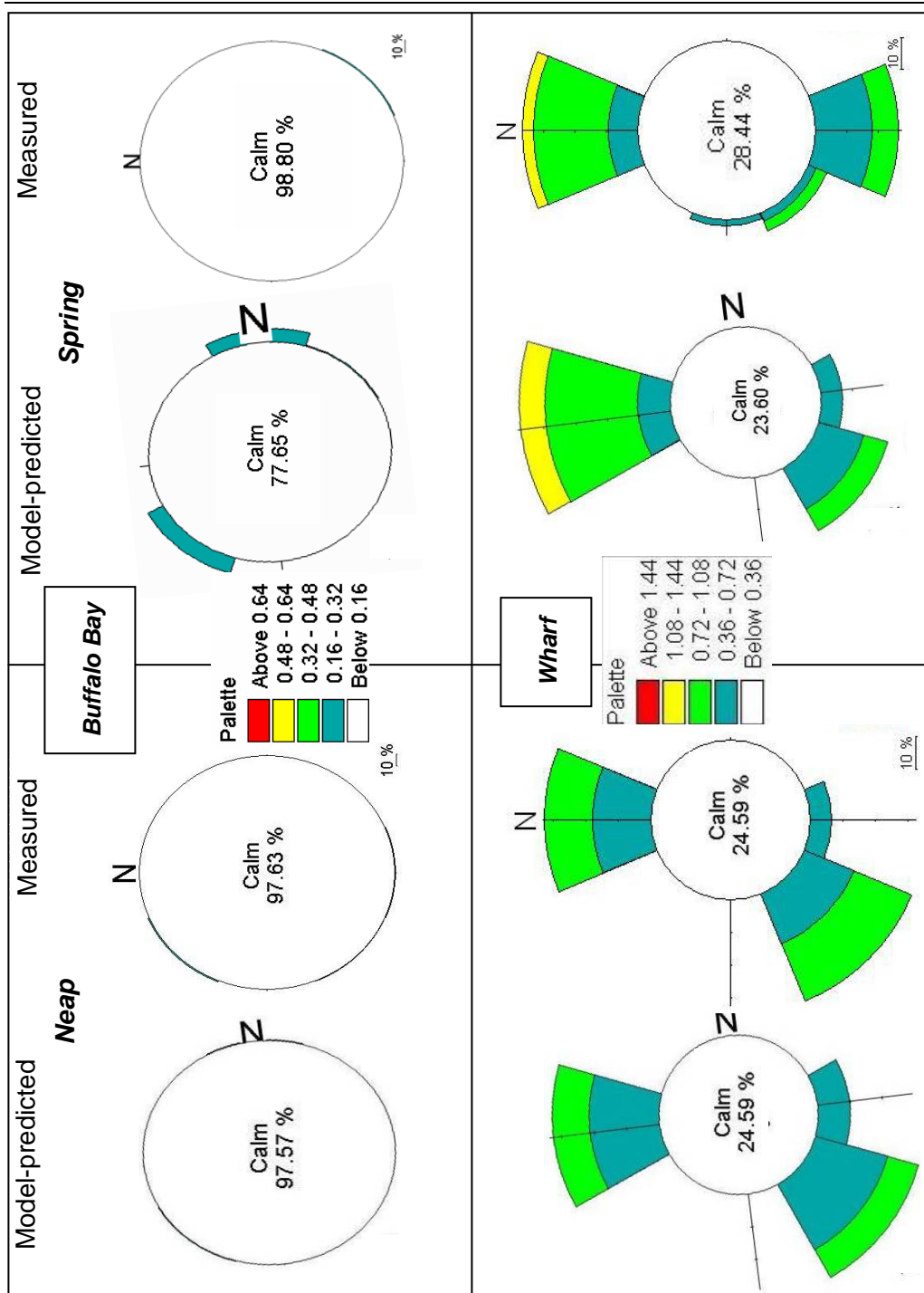


Figure 5.7 Rose plots of the model simulated and measured current speeds and direction at a) Buffalo Bay, and b) the wharf over the validation period. The model simulated plots have been rotated 82.5 degrees clockwise. Calm is defined as the percentage of the speed below 0.16 m/s for Buffalo Bay and below 0.36 m/s for the wharf site. 10 % represents the percentage of currents at each speed. The palette for each site is given in  $ms^{-1}$ .

### 5.4 Experimental Design

In order to determine the reason for the elevation difference at the wharf, a number of simulation experiments were conducted in which input variables were altered. Firstly as identified in Chapter 4, the total elevation at the wharf site is primarily determined by the tidal elevation. Therefore, it is unlikely the difference is caused by

non-tidal elevation, resulting from factors such as atmospheric pressure, freshwater influences or wind. However different wind conditions were trialled to establish their role in the difference between simulated and measured current speeds. The dominant wind direction and average speeds were trialled first but there was no change in speed or elevation at the wharf site. Various wind speeds and directions were trialled also. Maximum recorded wind speeds along Buffalo Beach of  $12 \text{ ms}^{-1}$  (Cooper 2003) combined with a wind blowing from the west did produce a difference in current speeds (Figure 5. 8). Therefore, wind does not account for the majority of difference but current speeds when wind was applied, matched the measured speed approximately  $0.15 \text{ ms}^{-1}$  better, and reduced the phase difference from approximately 1 hour to 30 minutes.

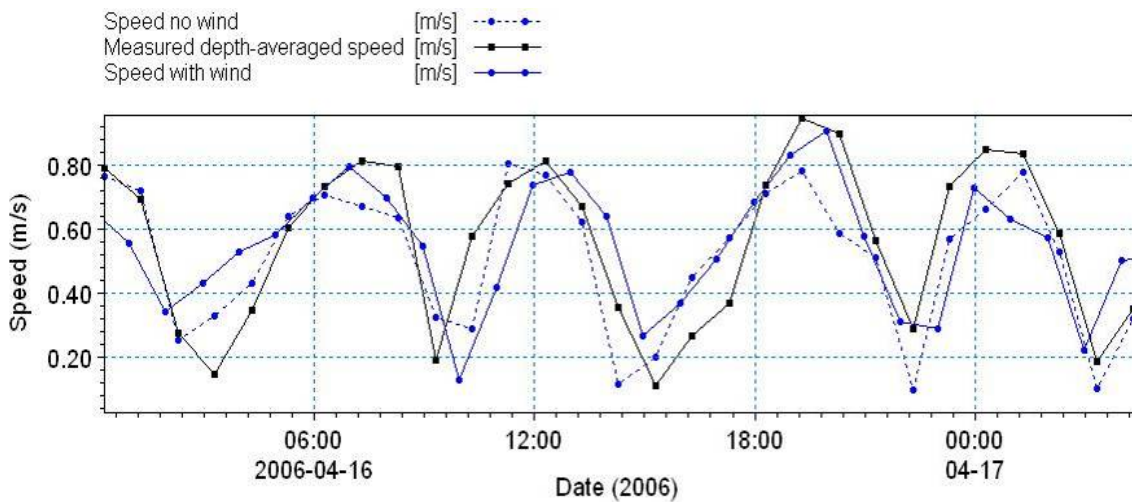


Figure 5.8 Comparison of the measured current speed at the wharf and model simulated current speeds with no wind and with a wind from the west of  $12 \text{ m/s}$ . The model-simulated speed is depth averaged and the measured depth averaged speed is derived from the measured current speed recorded by an S4 current metre  $1 \text{ m}$  off the bed at the wharf site.

Secondly the bed resistance was altered to find a better match with elevation data. Manning numbers of  $25 \text{ m}^{1/3}/\text{s}$  and  $40 \text{ m}^{1/3}/\text{s}$  were both trialled but neither altered the elevation data. Different eddy viscosity values were trialled also but did not alter the model-simulated elevation or speed. Therefore, based on these results and those obtained in Chapter 4, the difference in elevation is likely to be caused by a change in bottom topography which is highly probable at this site due to the likely re-orientation of the tidal channel and high sedimentation rate in the estuary, or due to a model schematisation effect. Model schematisation effect occurs when a series of

bumps, holes or sudden changes in bathymetry, which can be expected within an inlet, lead to instabilities in model flow and water level predictions (DHI, 2004).

## **5.5 Model Results of Tidal Flow**

Once the model has been calibrated and validated, the output can be interpreted to give results and conclusions relating to the circulation pattern and the sediment transport pathways in Buffalo Bay, and in particular, identify the cause of inlet shoaling and the isolated shallow zone.

### **5.5.1 Mercury Bay**

One challenge in modelling such a large area is trying to represent real processes. In Mercury Bay, the dominant hydrodynamic process is the clockwise circulation cell operating within (Smith, 1980). This cell is thought to be the result of the combination of many processes as discussed in Chapter 2. Eddy-type formations (Figure 5.9a) are observed on the seaward and landward sides of the ebb discharge which extends into Mercury Bay, and also around the Wharekaho headland. As the tide continues to exit the Bay, the eddy diffuses (Figure 5.9b) and an anti clockwise cell can be noted within Buffalo Bay. The model does simulate elements of a clockwise rotating cell in Mercury Bay, as suggested by Smith (1980), particularly on the ebb tide as the ebb tidal discharge from the inlet pushes water along the northern side of the Bay (Figure 5.9b). There are a lot of complex processes operating within Mercury Bay worth studying and modelling. However only those that impact upon the Whitianga inlet are considered in this study as the scope would otherwise be too broad.

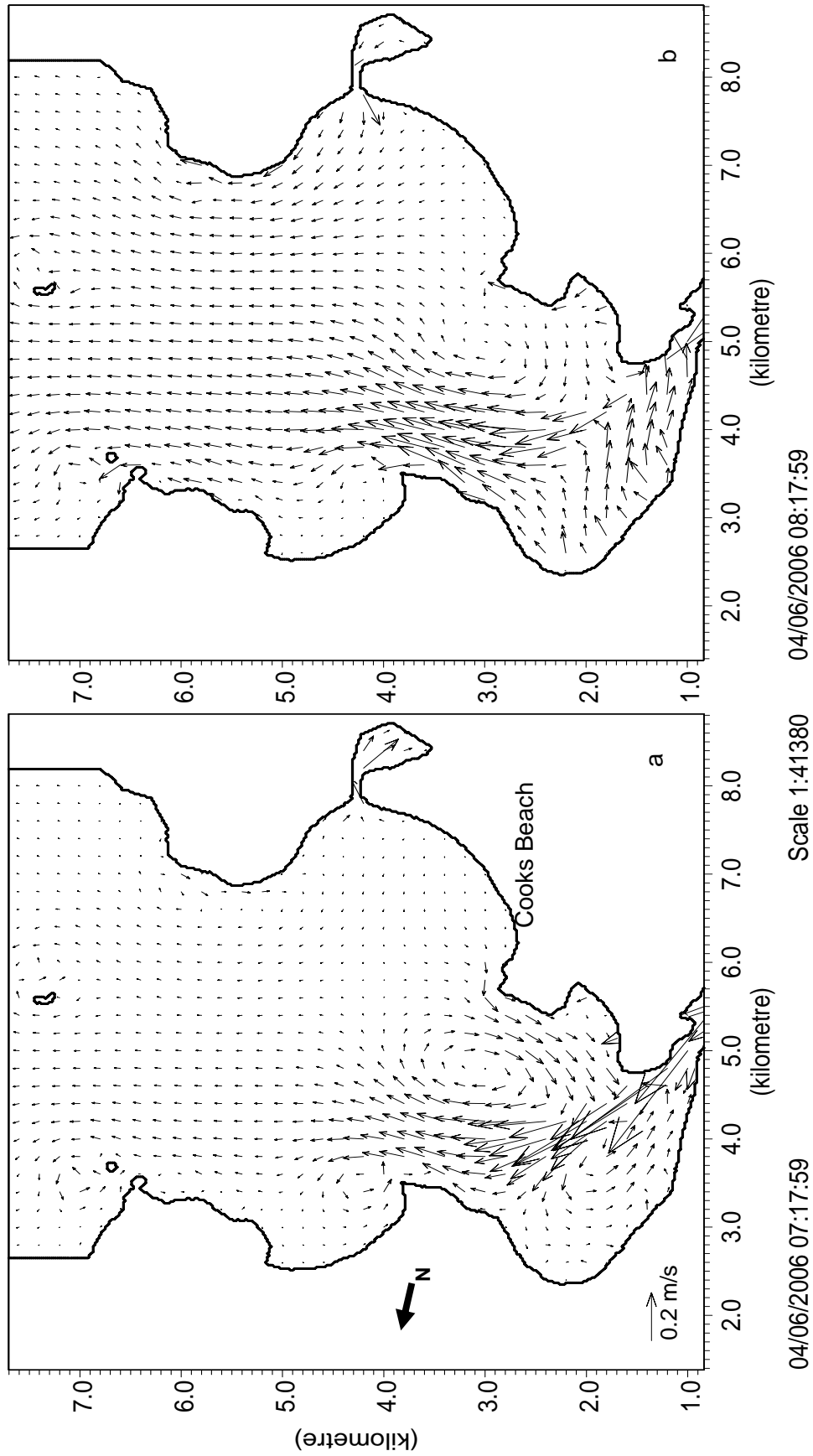
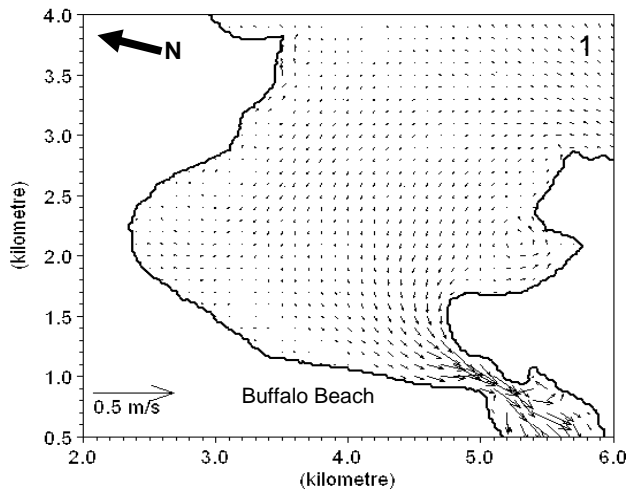


Figure 5.9 Frames of the hydrodynamic model output for Mercury Bay on the ebb tide, illustrating the eddy on either side of the ebb jet as well as behind the Wharekaho Headland.

### *5.5.2 Buffalo Bay and Whitianga tidal inlet*

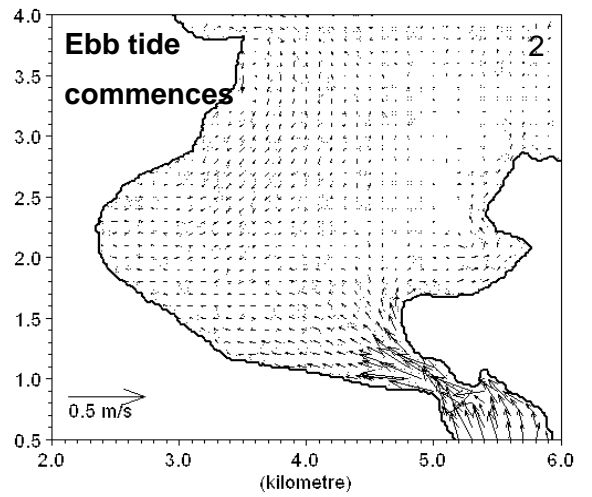
The model has highlighted a number of interactions of hydrodynamic conditions within Buffalo Bay. A sequence of snapshots over an ebb tidal cycle and part of the flood cycle (Figure 5.10), shows these conditions which are largely controlled by the ebb discharge from the inlet. Over the time period the following points are evident:

- The ebb discharge starts gradually. The fastest flow occurs in the inlet entrance and across the ebb delta, then dissipates as it enters Buffalo Bay. Northern Buffalo Bay has very slow currents in comparison.
- As the ebb discharge increases, an eddy begins to form seaward of the inlet, into Maramaratotara Bay in a clockwise direction and is clearly visible between frames 7 and 13. The eddy moves north with the ebb discharge and gradually spreads further into Mercury Bay.
- Northern Buffalo Bay experiences slight currents but the model shows a second eddy or rotating cell, moving anti-clockwise landward of the ebb tidal discharge path, evident in frames 8-14. Both eddy-like formations move spatially with the path and strength of the ebb discharge. They are formed by shearing of the main ebb jet and are thus transient and free-moving.
- Eventually the ebb jet slows and the flood tide begins, initially deflected to the side of the ebb jet. The flood tide pushes water down Buffalo Beach and into the inlet.
- On the flood tide, between frames 19 and 24, the tidal current appears to pulse. In frame 20 fast currents enter the southern section of Buffalo Bay but slow in frame 21, then increase again in frame 22. This type of pulse behaviour is characteristic of resonant seiching and the topographic configuration of Mercury Bay, which apparently facilitates seiching phenomena.



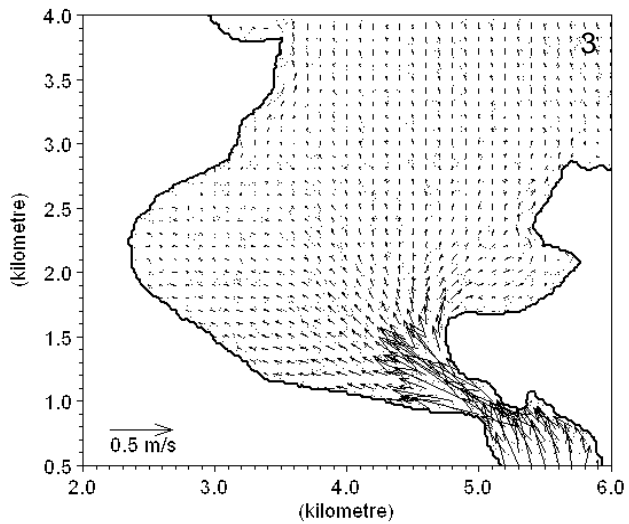
04/16/2006 21:57:59

Scale 1:27790



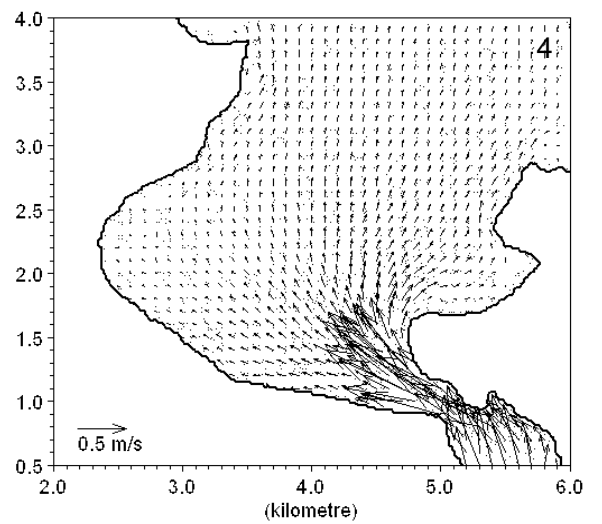
04/16/2006 22:17:59

Scale 1:27790



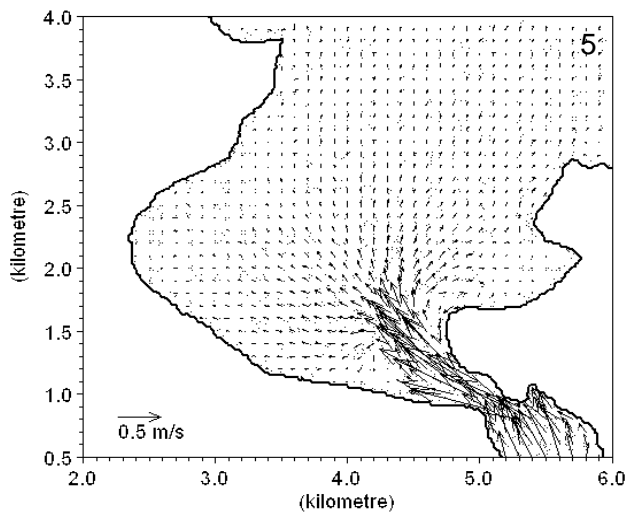
04/16/2006 22:37:59

Scale 1:27790



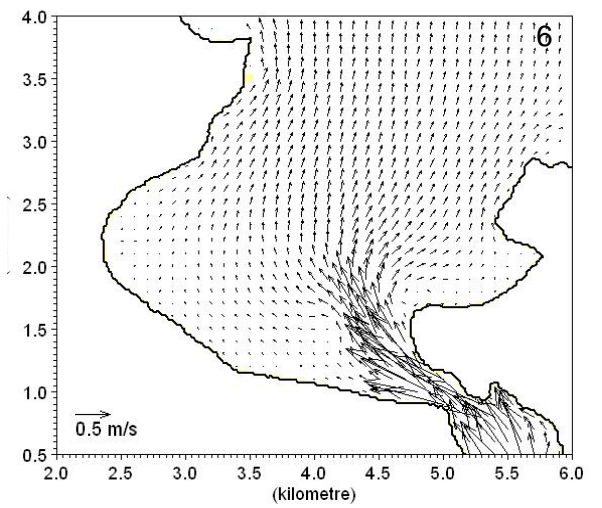
04/16/2006 22:57:59

Scale 1:27790



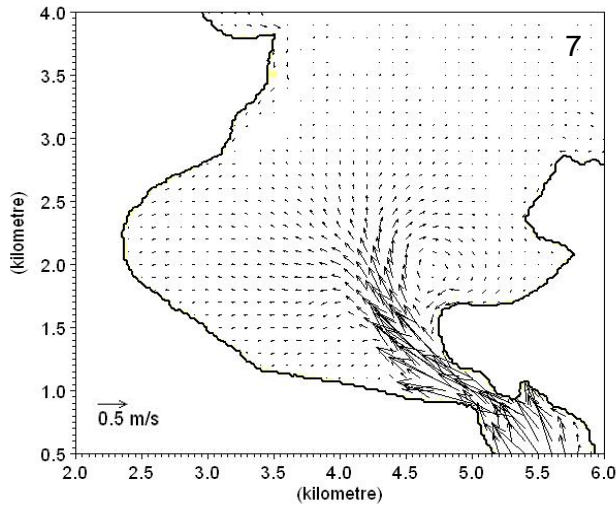
04/16/2006 23:17:59

Scale 1:27790



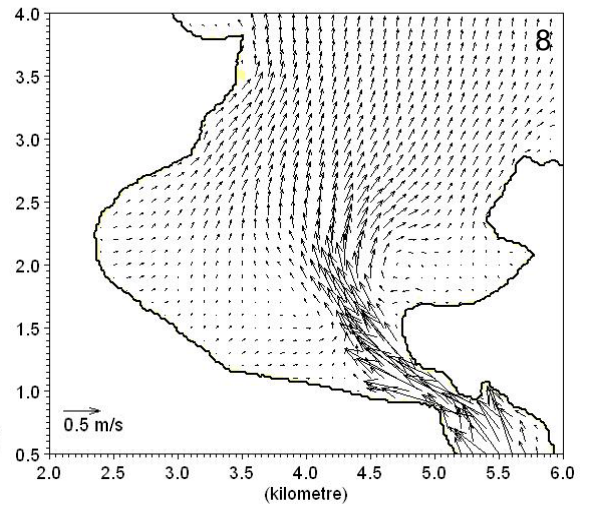
04/16/2006 23:37:59

Scale 1:25000



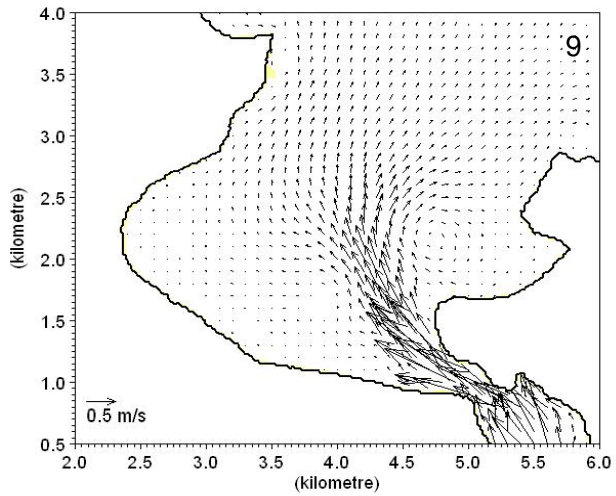
04/16/2006 23:57:59

Scale 1:25000



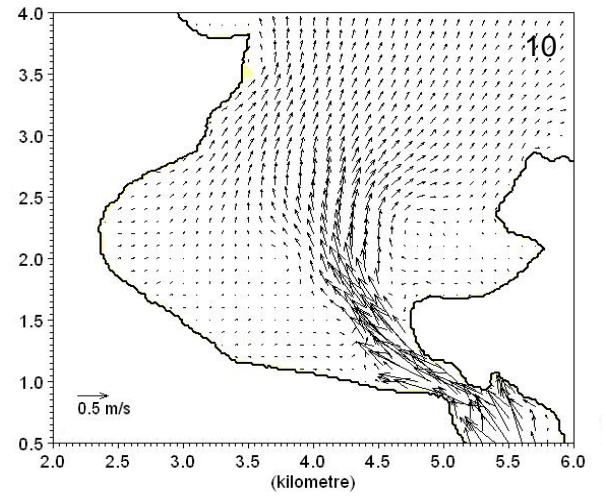
04/17/2006 00:17:59

Scale 1:25000



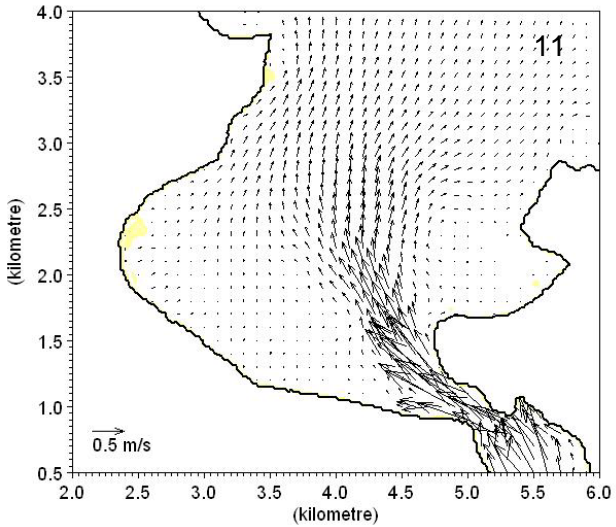
04/17/2006 00:37:59

Scale 1:25000



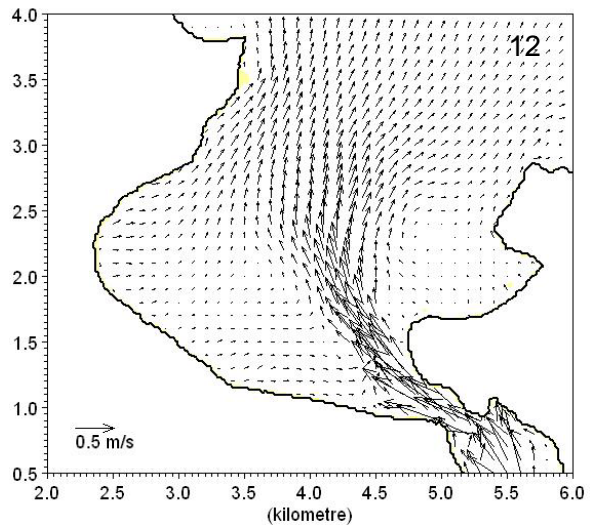
04/17/2006 00:57:59

Scale 1:25000



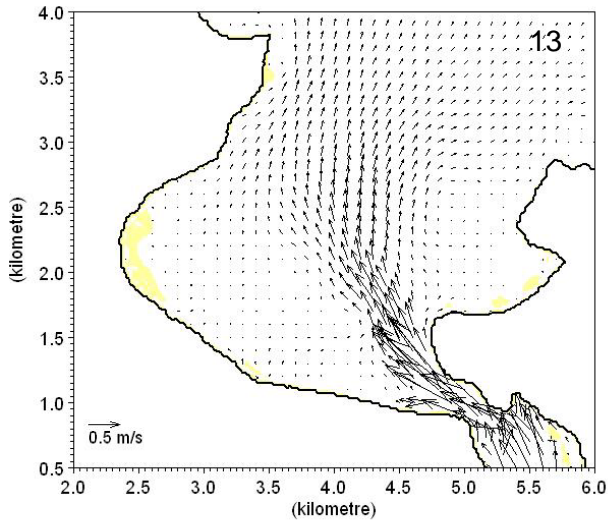
04/17/2006 01:17:59

Scale 1:25000



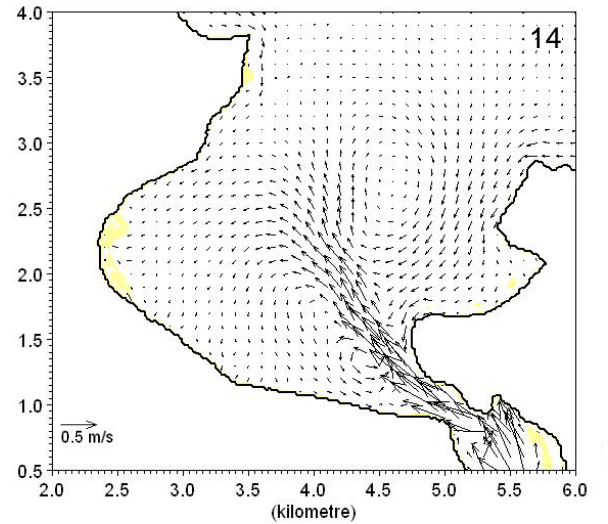
04/17/2006 01:37:59

Scale 1:25000



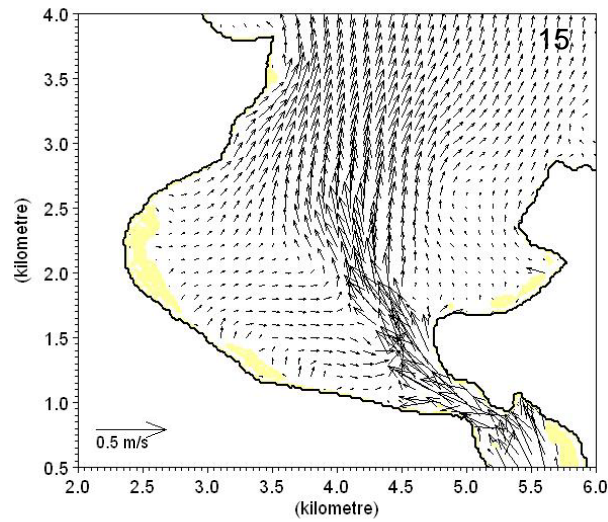
04/17/2006 01:57:59

Scale 1:25000



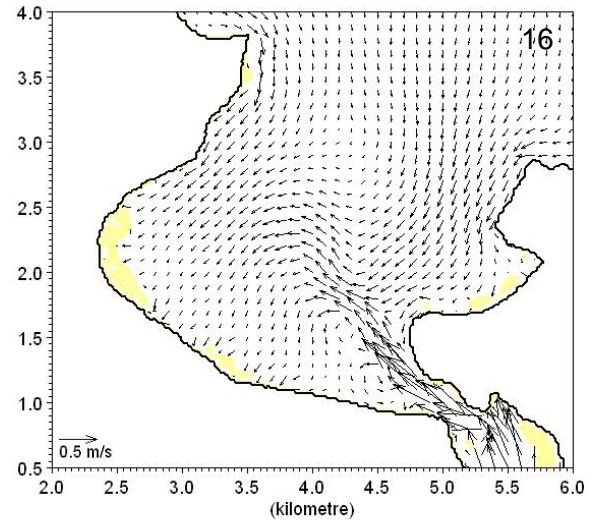
04/17/2006 02:17:59

Scale 1:25000



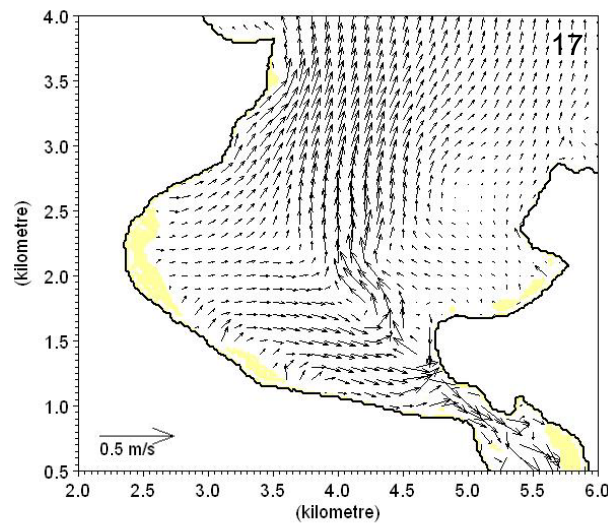
04/17/2006 02:37:59

Scale 1:25000



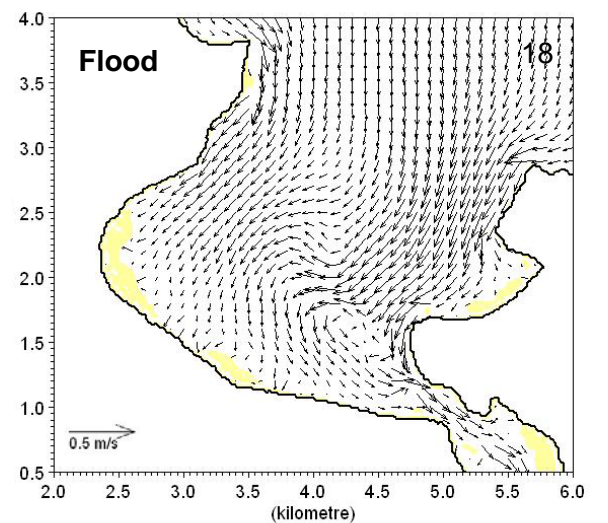
04/17/2006 02:57:59

Scale 1:25000



04/17/2006 03:17:59

Scale 1:25000



04/17/2006 03:37:59

Scale 1:25000

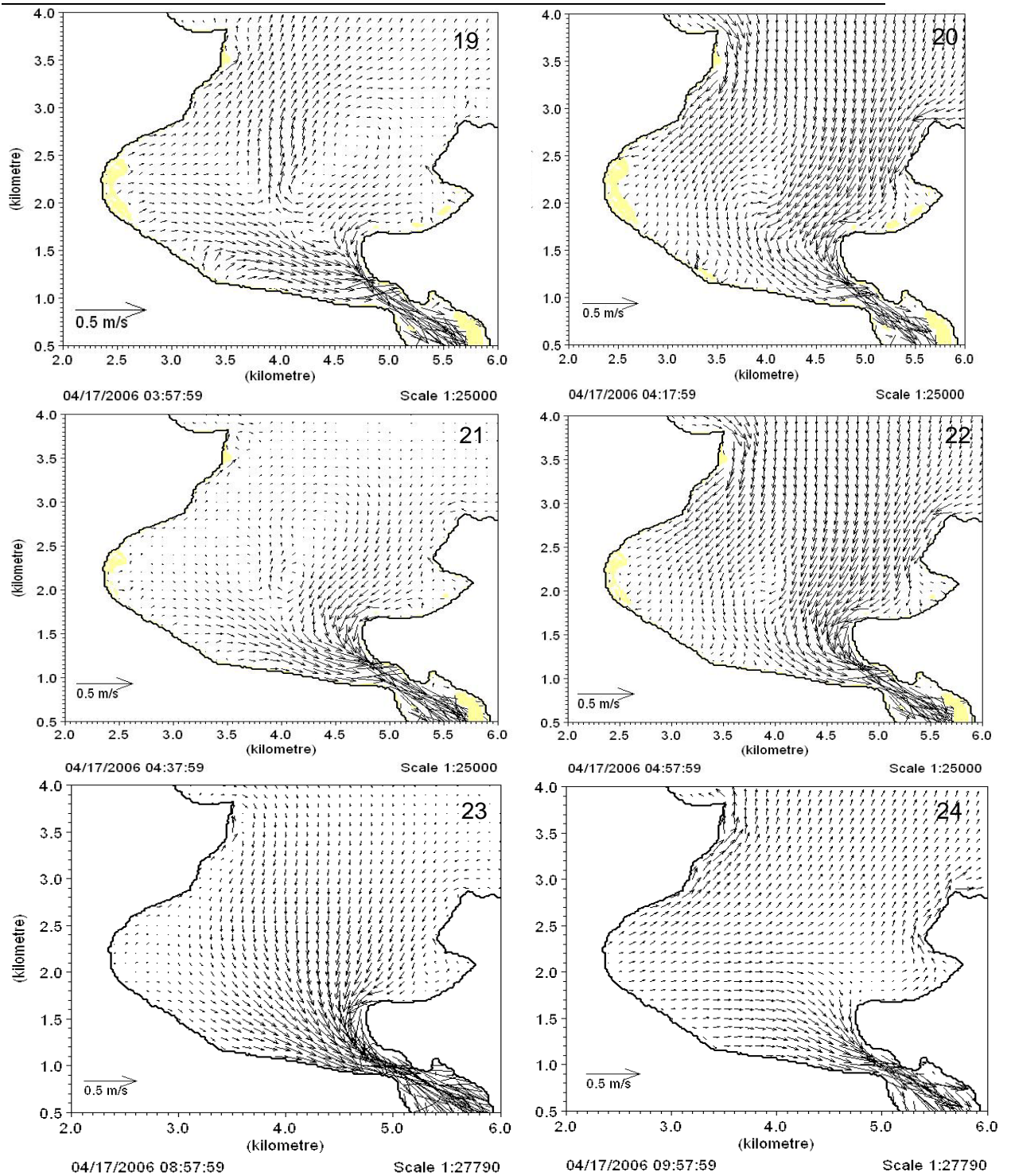


Figure 5.10 Sequence of snapshots of the hydrodynamic model output for Buffalo Bay over an ebb tide and part of the flood tide.

Focusing upon the detail of the tidal inlet (Figure 5.11) some additional trends over the tidal cycle are evident. The inlet gorge has the fastest current speeds as the inlet narrows and flow is pushed through. The flow moves into Buffalo Bay and

decelerates as it flows over the ebb delta due to the shallow nature of the delta, which induced greater friction. Behind the ebb delta the flow is low and parallel to the inlet channel. The bottom of the landward Buffalo Bay eddy is visible in the last snapshot, moving water along Buffalo Beach towards the inlet where it is moved out into Buffalo Bay again by the ebb tidal discharge.

The tidal currents can be averaged over the time period between two high tides to establish the mean or residual tidal current speed and direction over Buffalo Bay (Figure 5.12). This is the average circulation pattern within Buffalo Bay which appears to be ebb dominated. Current velocities within Buffalo Bay are fastest within the inlet which is to be expected. Two residual eddy systems are apparent within Buffalo Bay. Along Buffalo Beach the mean current flows towards the inlet which is probably a combination of the landward eddy during ebb tide and the flood tide direction along Buffalo Beach.

Within the inlet a large portion of the grid is flood dominated with speeds highest in the gorge and upper estuary reaches. This is to be expected as the flood tide flows from the large Buffalo Bay into the narrow inlet.

Deposition of sediment is likely to occur in places where the current moves from high to low velocity or where two opposing currents meet, such as over the ebb delta and in Buffalo Bay, northeast of the inlet entrance. Scour is likely to occur where current vectors move out of, but not into an area, such as northern Buffalo Bay and along southern Ohuka (mid-*Buffalo Beach*).

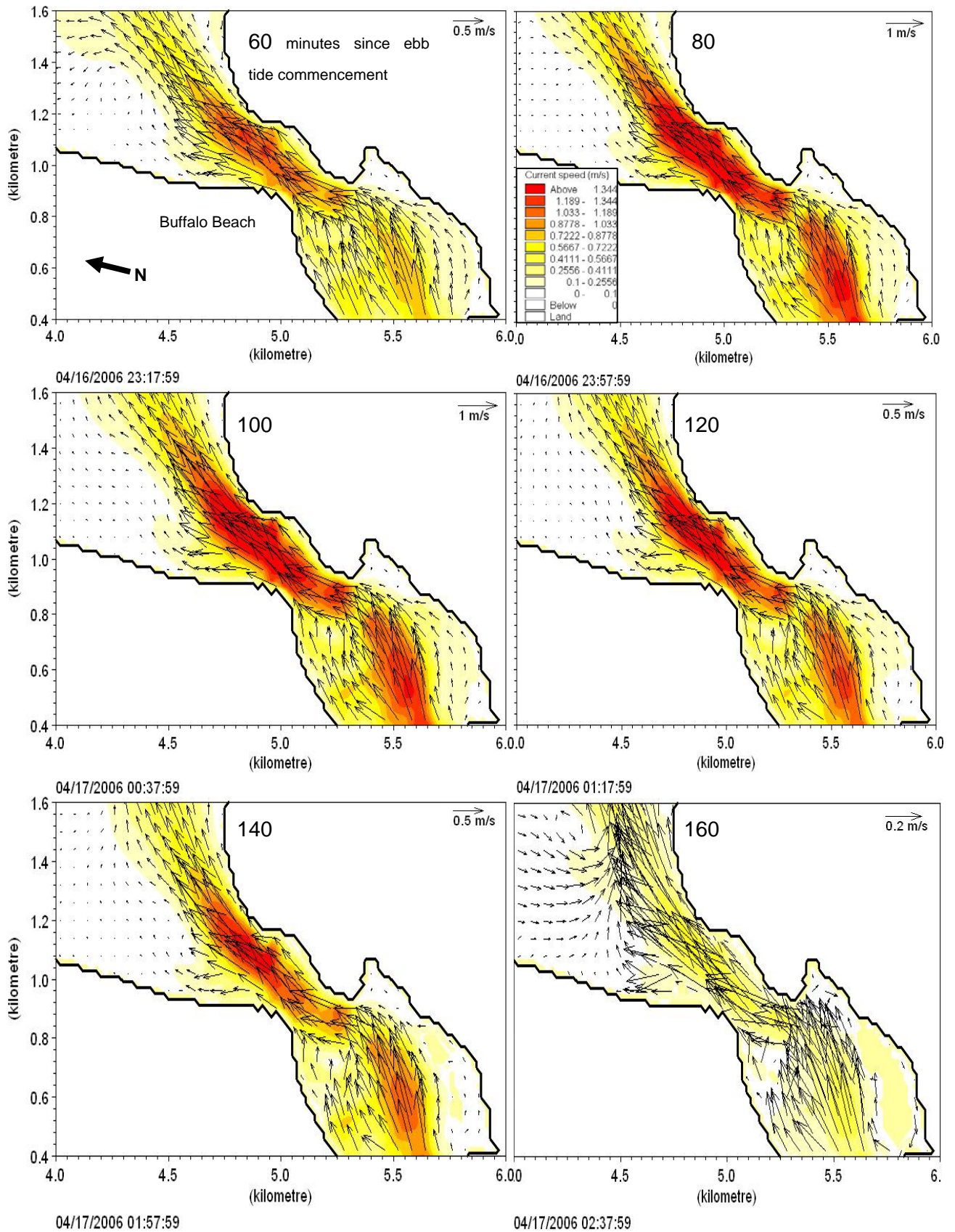


Figure 5.11 Sequence of snapshots of the speed and direction of currents at the Whitianga inlet over an ebb tidal cycle. Numbers represent minutes since ebb tide commenced.

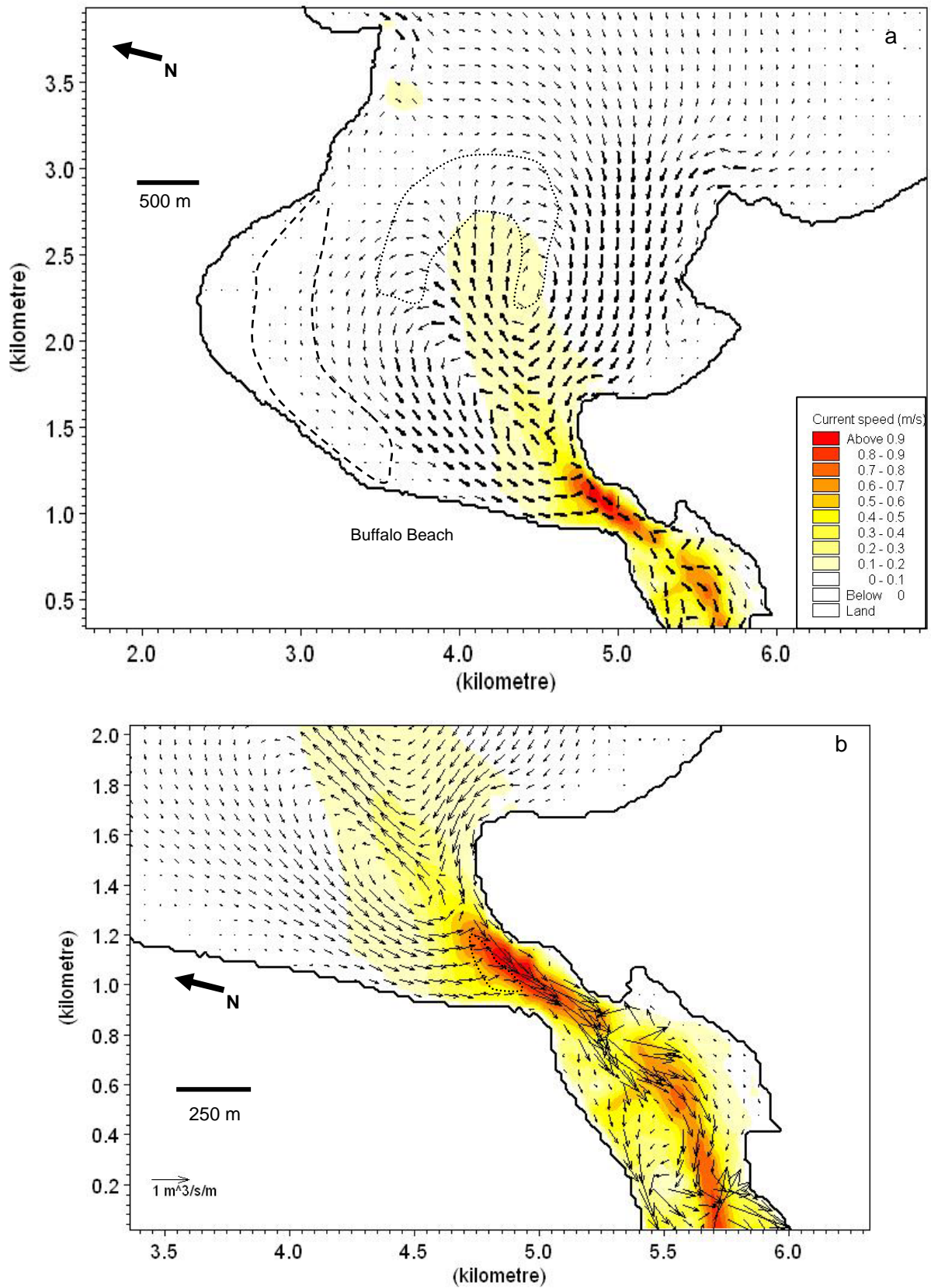


Figure 5.12 The residual circulation within a) Buffalo Bay and b) the tidal inlet over an average tidal cycle. Dashed line indicates likely areas of scour and dotted line indicates likely areas of deposition.

In order to establish the evolution of the sediment transport pathways the same model parameters were employed to run a hydrodynamic model using 1938 bathymetry of Buffalo Bay (Figure 5.13). The primary difference between the two model outputs is the path of the ebb tidal jet discharge from the inlet. In 1938 the jet is aligned almost adjacent to the beach and exits Buffalo Bay towards the centre of the open boundary as opposed to the northern end of the boundary as in the 1995 output. Two eddy systems are still apparent, but the seaward eddy is less pronounced and confined within Maramaratotara Bay. The landward eddy appears to get larger as the tide discharges from the estuary and is possibly stronger than is predicted in the 1995 model.

The 1938 model can only be used to suggest past hydrodynamic behaviour. As there was no elevation data available for this time period there were problems with the location of the boundary, and additionally the model cannot be calibrated. However the model output seems, for the most part, realistic considering the bathymetry differences iterated in Chapter 3.

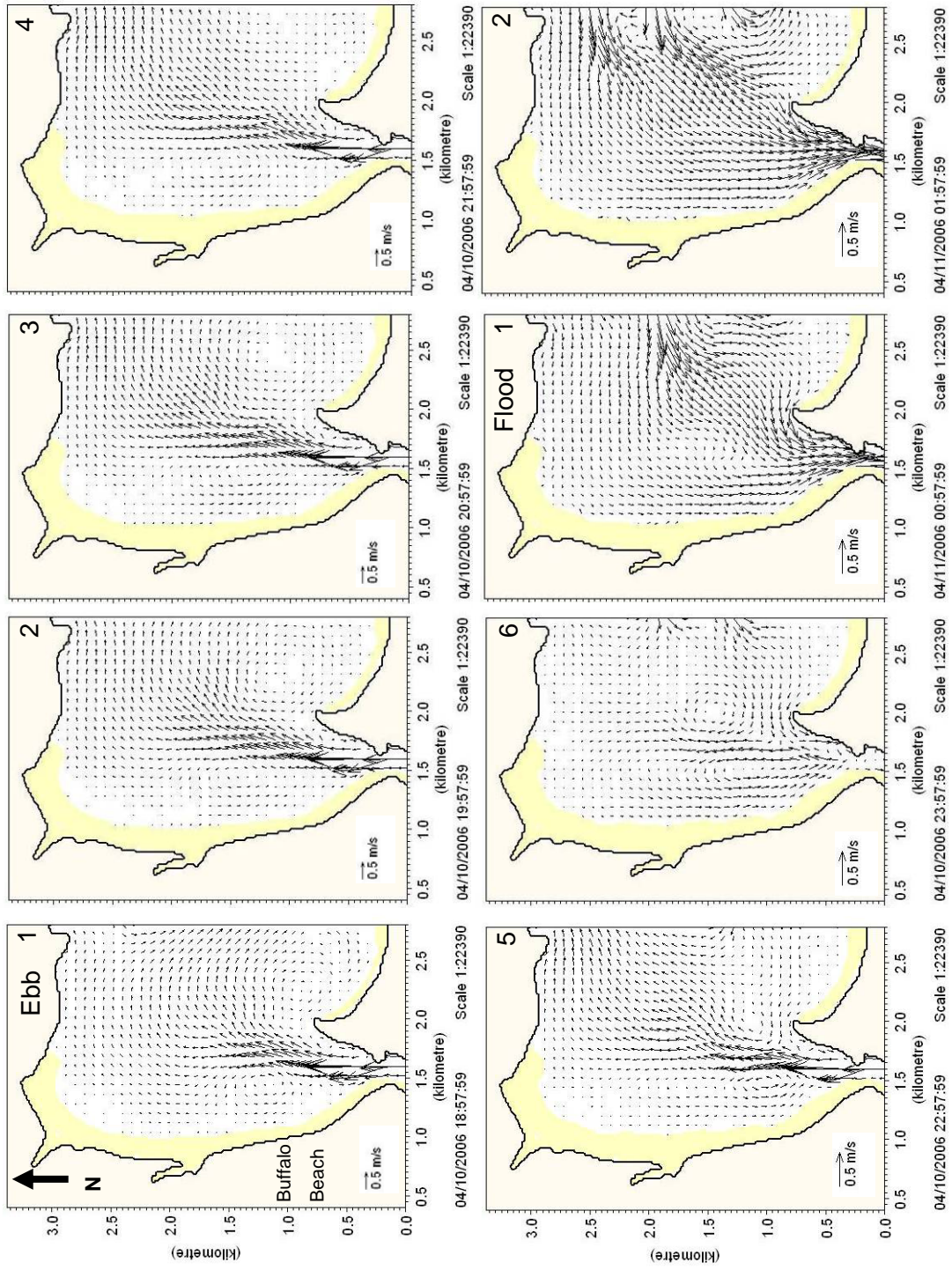


Figure 5.13 Sequence of snapshots of the hydrodynamic model output for Buffalo Bay over an ebb tide for 1938 bathymetry.

## 5.6 Discussion and Implications of Tidal Model Results

The primary driver of circulation, identified by the model within Buffalo Bay and also Mercury Bay is the ebb tidal discharge from the inlet. Shearing from the ebb jet causes the two eddy circulation systems within Buffalo Bay and contributes to a portion or the majority of the Mercury Bay net circulation. Both Buffalo Bay eddies are transient, moving with the ebb discharge and are asymmetrical. The seaward eddy within Buffalo Bay originates within Maramaratotara Bay then moves north (Figure 5.14) as the path of the tidal discharge is pushed further towards the headland between Wharekaho Beach and Buffalo Bay. Tidal eddies are a common feature of the coastal environment especially near headlands, and they play an important role in transport of a variety of materials including pollutants and sediment (Galloway et al., 1996).

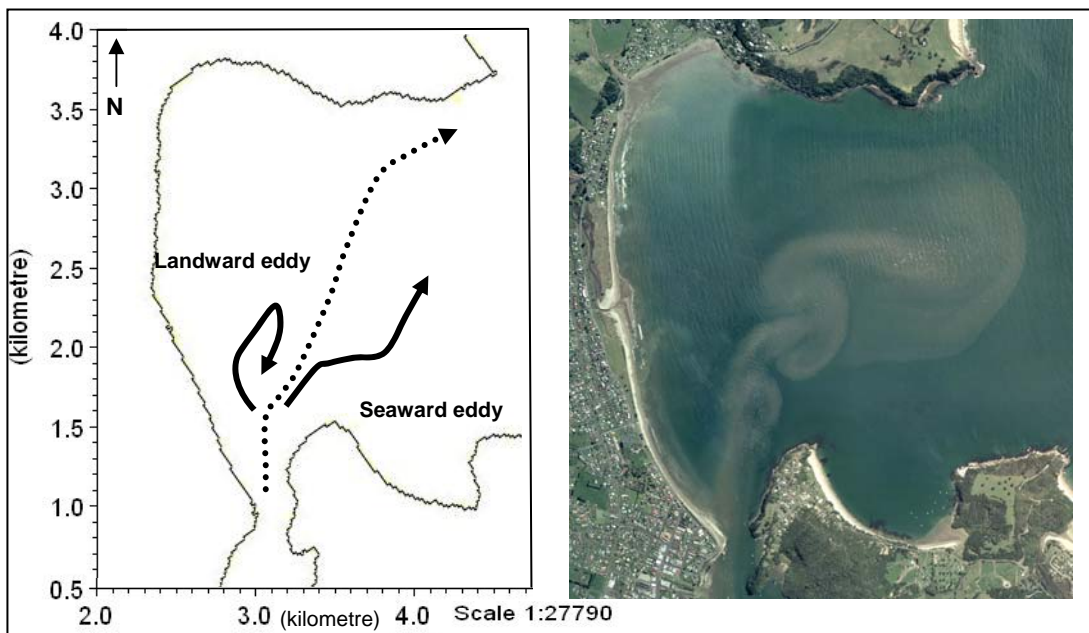


Figure 5.14 the path of the two eddy formations during the ebb tidal cycle at Buffalo Bay. The path of each eddy was determined by mapping the pathway of the centre of the eddy formation. The dashed line shows the path of the ebb jet and main tidal discharge from the inlet. The model-simulated pathways are compared with the 2002 aerial photo of Buffalo Bay.

The formation and evolution of eddy systems in the vicinity of a headland is described by the production, advection and dispersion of vorticity. Vorticity can be simplified as the rotation of the current. In the area around a headland, shallow water depth and rapid bathymetry gradients generate vorticity within the flow (Signell

and Geyer, 1991). The headland then causes flow to separate, whereby streamlines break away from the coast, carrying high vorticity fluid from the lateral boundary into the low vorticity interior of the flow (Signell and Geyer, 1991). The gradient in vorticity causes a rotating flow, or eddy, around the obstacle. There are many examples both locally and internationally of eddies forming in this manner such as at Portland Bill (Pingree and Maddock, 1978) and Start Point (Pingree and Maddock, 1979) off the northwest Europe coast and locally transient eddy formations around a headland have been identified and at cape Rodney (Hume et al., 1997), the Whakatane headland (Saunders, 1999), at around Mount Maunganui (K. Spiers, pers. comm., 2007).

Eddy systems can be broken into residual and transient eddies. Residual eddies are tidally induced and are formed by the transfer of vorticity from the tidal current to the mean current (Zimmerman, 1981). Transient eddies are produced by the tide but migrate with the tidal path (Park and Wang, 2000). A residual eddy circulation is apparent within Buffalo Bay but the transient eddy is more important in sediment movement and circulation. The three principal controls on transient eddy formation are (Signell and Geyer, 1991) :

- The aspect or sharpness of the headland as a sharper aspect increases the flow at headland tip, which means flow is more likely to separate.
- The bottom friction given by the Reynolds number, which determines the velocity available for the eddy; and,
- The advection relative to local acceleration given by the Keulegan-Carpenter number.

As the tide progresses, the original eddy is advected downstream (Signell and Geyer, 1991), as is the case for the Buffalo Bay landward and seaward eddies, or is dissipated and the flow in the lee of the headland becomes stagnant (Signell and Geyer, 1991).

The lifetime of a transient eddy primarily depends on the magnitude of vorticity available and its dissipation by bottom friction (Imasato, 1983). For example, an

eddy within a basin with large bottom friction would diminish in 1-2 hours whereas an eddy in a basin with small bottom friction would remain strong at the time of the ebb tide (Imasato, 1983). The lifespan of the landward eddy in Buffalo Bay is approximately 1.5 hours, whereas the seaward eddy has a lifespan of approximately 2.25 hours.

The seaward eddy identified in this study has formed due to the adjacent headland. The eddy moves downstream with the tidal flow but is eventually dissipated by the flood tide. Eddies formed in the vicinity of headlands generally form on alternate sides with the reversal of the tide. Here though, both the landward and seaward eddies within Buffalo Bay are only evident with the ebb tide. Eddy turbulence is a known contributor of sediment accretion. The eddy forming here on the ebb tide is the most likely cause of the isolated shallow zone. This will be discussed in Chapter Six.

The landward eddy is not formed by a headland but it is likely the ebb delta acts as a partial headland, creating vorticity due to the shallow bathymetry. This eddy moves north also but unlike the seaward eddy, it moves back along Buffalo Beach again towards the inlet entrance as the ebb tide weakens. This occurs because the path of the ebb discharge moves north east (seaward) as it progresses.

It is said to be a test to any tidal model to correctly simulate non-linear features such as the tidal eddies associated with headland promontories (Pingree and Maddock, 1978). In this study, the tidal model of Buffalo Bay does simulate the formation of an eddy around the Whakapenui Point. Further, the eddy system may have changed in the 11 years since the last hydrographic survey due to changes in the bathymetry influencing the ebb jet shearing, but it is likely the eddy system will still occur due to the adjacent headland. Eddy systems derived from headlands can often be mapped using plankton distribution, satellite infrared images or satellite images of turbidity patterns (Wolanski et al., 1984). The 2002 aerial photo of Buffalo Bay can be used to map the eddy as it shows the migration of the seaward eddy system north (Figure 5.14). This matches well with the model-predicted path. The photo shows a series of mushroom-shaped plumes that are likely to represent the path of the rotating eddy at

each time step as it gradually moves north. This is why the most northward plume is the largest as the eddy is well developed and encompasses a larger area as the ebb tide progresses (Figure 5.10 (14)).

The landward eddy is not shown in the aerial photo but is still realistic. It is possible the observed net littoral drift direction of south is in fact the return current of the eddy formation which transports sediment south along Buffalo Beach and back to the ebb delta. This is also detailed more in the following chapter.

The model output highlights the likely occurrence of a resonant seiche superimposed on the tidal wave within Mercury Bay. This is particularly evident on the frames of the flood tide. This seiche wave may explain the poor current speed and direction calibration at the Buffalo Bay site. Smith (1980) first suggested the presence of seiche waves within Mercury Bay, likely due to the box-like shape of Mercury Bay.

The model shows that the ebb delta channel marginal linear bar acts as a hydraulic groin, training and slowing currents in its vicinity. Therefore the ebb delta may be trapping sediments exiting the inlet from the estuary, and also sediment moving south along Buffalo Beach. Prior to the growth of the ebb delta it is likely the ebb currents flowed along Buffalo Beach with greater strength and then dissipated in Buffalo Bay.

Chapter 3 identified areas of deposition and scour within Buffalo Bay. These can be compared to the areas outlined in Figure 5.12. Scour is likely to occur in northern Buffalo Bay due to the dominant south-directed currents which transport sediment along Buffalo Beach to the inlet. Any sediment removed is not replaced as there are minimal currents entering this section of Buffalo Bay. This is consistent with Figure 3.12 which identified this area of erosion also but only applies to southern Ohuka as Figure 5.12 illustrated northern and mid Ohuka have low velocity mean tidal currents. The primary area of accretion in Buffalo Bay identified by Figures 3.12 and 3.13 was the ebb discharge channel. The residual currents also suggest this is an area of

deposition due to the sudden decrease in current velocity. The dominant area of accretion derived from the residual map northeast of the inlet entrance in Buffalo Bay, is caused by decelerating tidal currents. This area was not identified as accreting in Chapter 3 but does compare well with the sandbar defined in Chapter 1 by the Notice to Mariners (2005).

The 1938 tidal model provides an estimation of the circulation pattern prior to the growth of the ebb delta. The landward eddy appears to be stronger than the seaward eddy which is small and resides in Maramaratotara Bay. In Chapter 3 the ebb delta is barely visible in the 1944 aerial photo and likewise for the 1938 bathymetry data. The eddy formations in the 1938 model are similar but evidently of a smaller scale. It is likely the ebb delta growth has trained the ebb tidal discharge from the inlet so it now flows further into Buffalo Bay. The path of the ebb tide could be pushed further east if the ebb delta continued to grow seawards beyond the adjacent headland. However the isolated shallow zone around Pandora Rock and shallow nature of Maramaratotara Bay also potentially train the flow on the seaward side. The 1938 bathymetry provides an insight into the evolution of Buffalo Bay, which suggests the evolution of the channel marginal ebb delta has caused the tidal stream to realign toward the east (Figure 5.15).

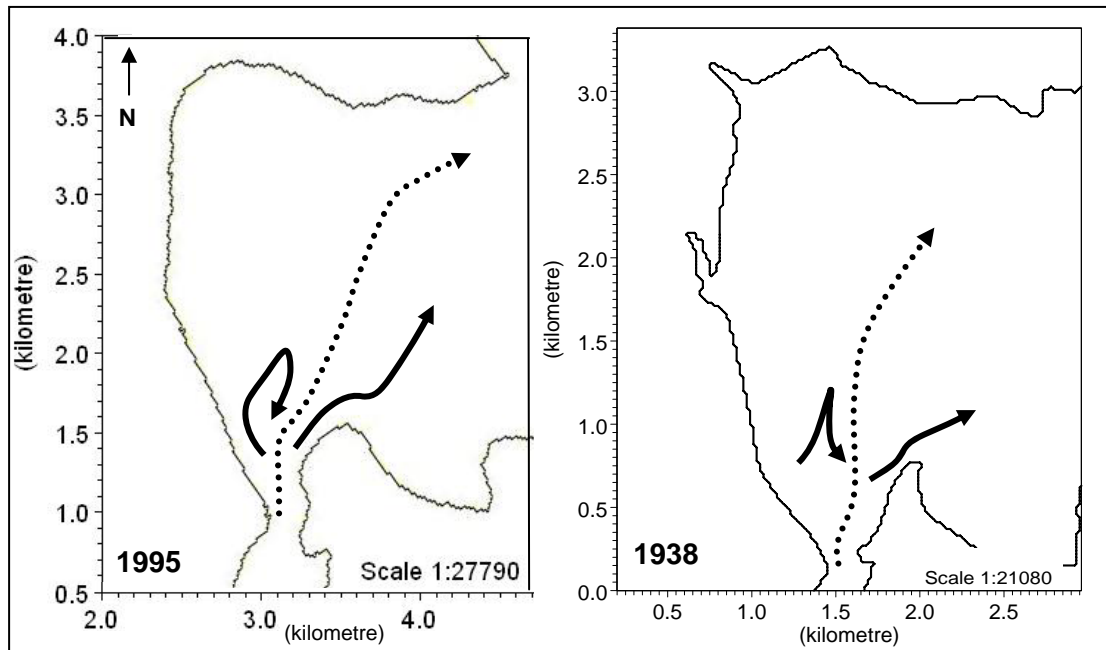


Figure 5.15 The path of the two eddy formations during the ebb tidal cycle at Buffalo Bay using 1995 and 1938 bathymetry. The path of each eddy was determined by mapping the pathway of the centre of the eddy formation. The dashed line shows the path of the ebb tidal discharge from the inlet.

## **5.7 Wave Model Inputs**

Wave models were used to establish wave behaviour within Buffalo Bay to primarily establish the best suited location of a new boat loading ramp along Buffalo Beach. Secondly the wave behaviour may provide reasons for the sections of erosion along Buffalo Beach. The MIKE 21 PMS model was used for this due to the coastal position of the study site. The model output cannot be directly calibrated due to lack of data, but can be approximated on the basis of visual observation, aerial photos and logic. This section provides a description of the input parameters used. Further details of these inputs and the PMS model are given in the MIKE 21 PMS reference manual

### *Bathymetry*

MIKE 21 PMS model requires the open offshore boundary be on the west and land on the east so the grid was rotated a further 90° anticlockwise from the tidal bathymetry data.

### *Simulation Period*

There are two available simulation types in MIKE 21 PMS, stationary and quasi-stationary. Stationary is used if only one wave event is simulated whereas quasi-stationary is used to simulate several sets of wave events derived from a time series of offshore wave boundary conditions

### *Boundary Conditions*

Two types of boundary conditions must be specified in MIKE 21 PMS. Firstly the offshore boundary is where waves are generated. The conditions at this boundary can be specified as a constant wave height, period and approach direction, obtained from a time series file, or from a dsf2 file containing wave energy distribution for the boundary. Secondly the lateral boundary defines the behaviour of waves at the top and bottom of the grid. Waves can either be reflected, absorbed or symmetrical.

### *Solution parameters*

These cover the type of parabolic approximation used in the PMS model. There are three options, simple, Pade and Minimax models.

### *Bottom Dissipation*

Bottom dissipation is an important variable as it determines the amount of energy a wave loses as it propagates. The bottom dissipation can be given as a constant bed roughness (m) or specified for each grid point in dsf2 file.

#### *Wave breaking*

Wave breaking is another important factor in energy dissipation of waves when they get too steep, and can also be incorporated into the model as a constant or in a dsf2 file. Constant values can be constant for each grid point, calculated using the Battjes and Stive method derived from water depth or the Nielson method, derived from bed slope.

The model inputs for this study are outlined in table 5.2.

*Table 5.2 The input variables used for the MIKE 21 PMS model*

<b>Input variable</b>	<b>Value</b>
Simulation type	Normal
Simulation Period	Stationary
Offshore Boundary type	Param. Random
Lateral Boundary Type	Both Symmetrical
Solution Parameters	Minmax Model - Aperture 60, exclude filtering
Bottom dissipation	Nikuradse roughness constant Kn of 0.002
Wave breaking	Include constant values Gamma1 = 1 Gamma2 = 0.8 Alpha = 1

## **5.8 Wave Model Output**

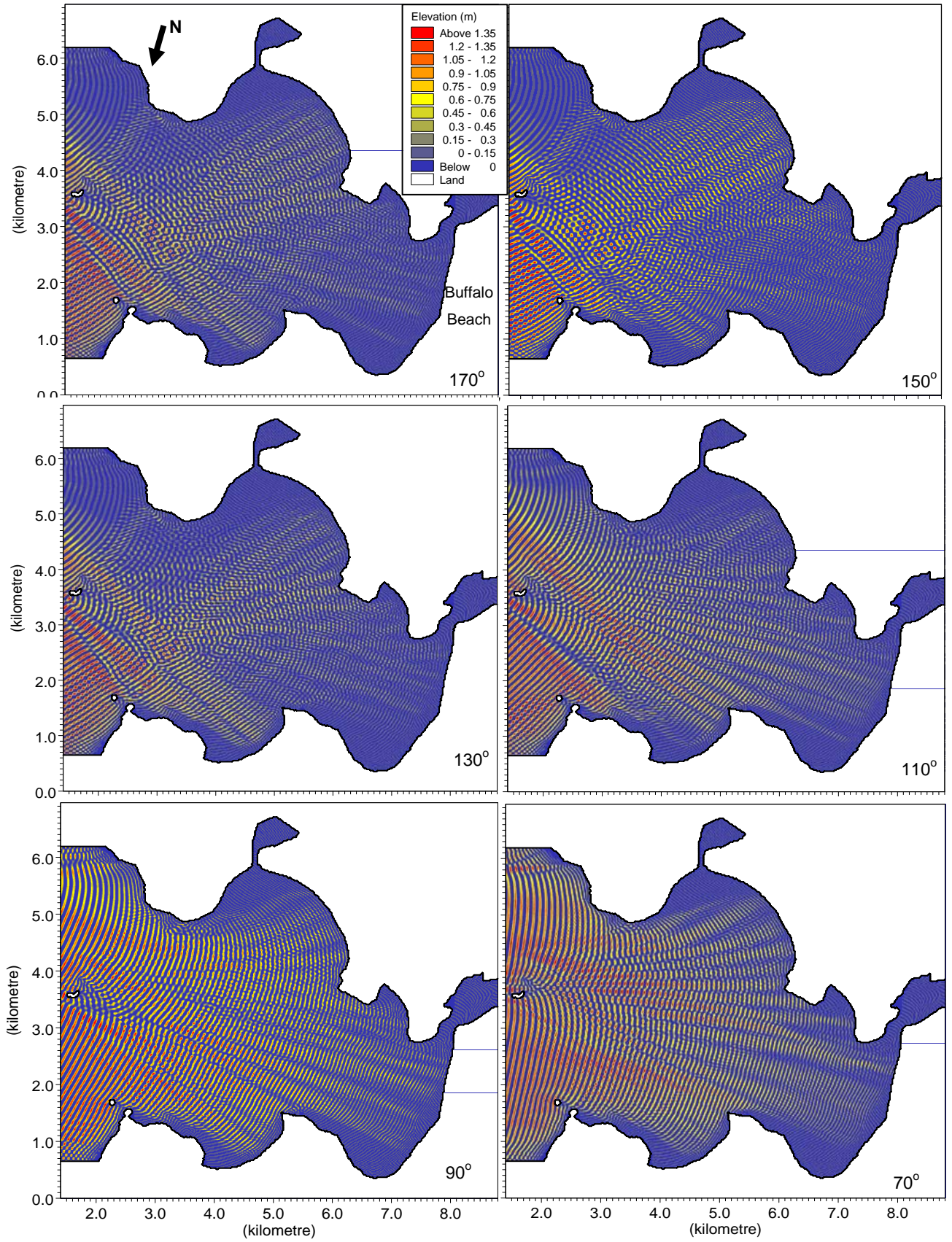
The MIKE 21 PMS model calculates the wave height and period for each grid point, and also the elevation, and velocity in the x and y directions. The model outputs here are shown in elevation in order to illustrate the behaviour of wave lines as they enter Mercury Bay. Various wave height and periods were trialled (Table 5.3) with wave directions from 0 - 180 degrees. The approach angle is the governing factor of wave behaviour as it determines the amount of wave energy that can reach Mercury Bay. To reiterate from chapter 4; a typical swell entering Mercury Bay would have a period of approximately 9 seconds and a wave height of ~1.5 m approaching from the northeast. The model outputs (Figure 5.16) shown used a wave height of 3 m and period of 9 seconds in order to better illustrate the behaviour at different angles.

This is within the range of a typical wave scenario but would only occur with a moderate-large swell. Using the larger wave height is agreeable as wave refraction behaviour is very similar under different wave heights but alters with different wave periods. This is because the wave period affects the wavelength which determines the shoaling depth. Therefore, the wave period must be carefully considered when setting boundary conditions. The chosen period of 9 seconds is within typical limits given by tables 2.1 and 4.3. Longer and shorter periods were trialled (table 5.3) for all approach angles also, and snapshots of all wave period and height combinations can be seen in appendix 5.

*Table 5.3 The wave statistics used to generate wave behaviour models*

Wave height (m)	Wave period (s)	Wave approach angle (deg)
0.6	5	10-170
	9	10-170
	13	10-170
1.5	5	10-170
	9	10-170
	11	10-170
3	9	10-170
	11	10-170
5	9	10-170
	11	10-170

The elevation snapshots (Figure 5.16) show swell best imposed on Mercury Bay when propagating from an easterly quarter, between 50 and 100 degrees. The highest elevations within Buffalo Bay occur with an easterly swell (90°) whereas a swell from the south-southeast (~150-170°) hardly enters Mercury Bay. Wharekaho Beach receives the largest waves in the bay when swell is approaching from the east, whereas Cooks Beach receives the largest waves with a swell approaching from the north (~10°). The pictures illustrate the importance of Centre Island as a control on wave behaviour within Mercury Bay.



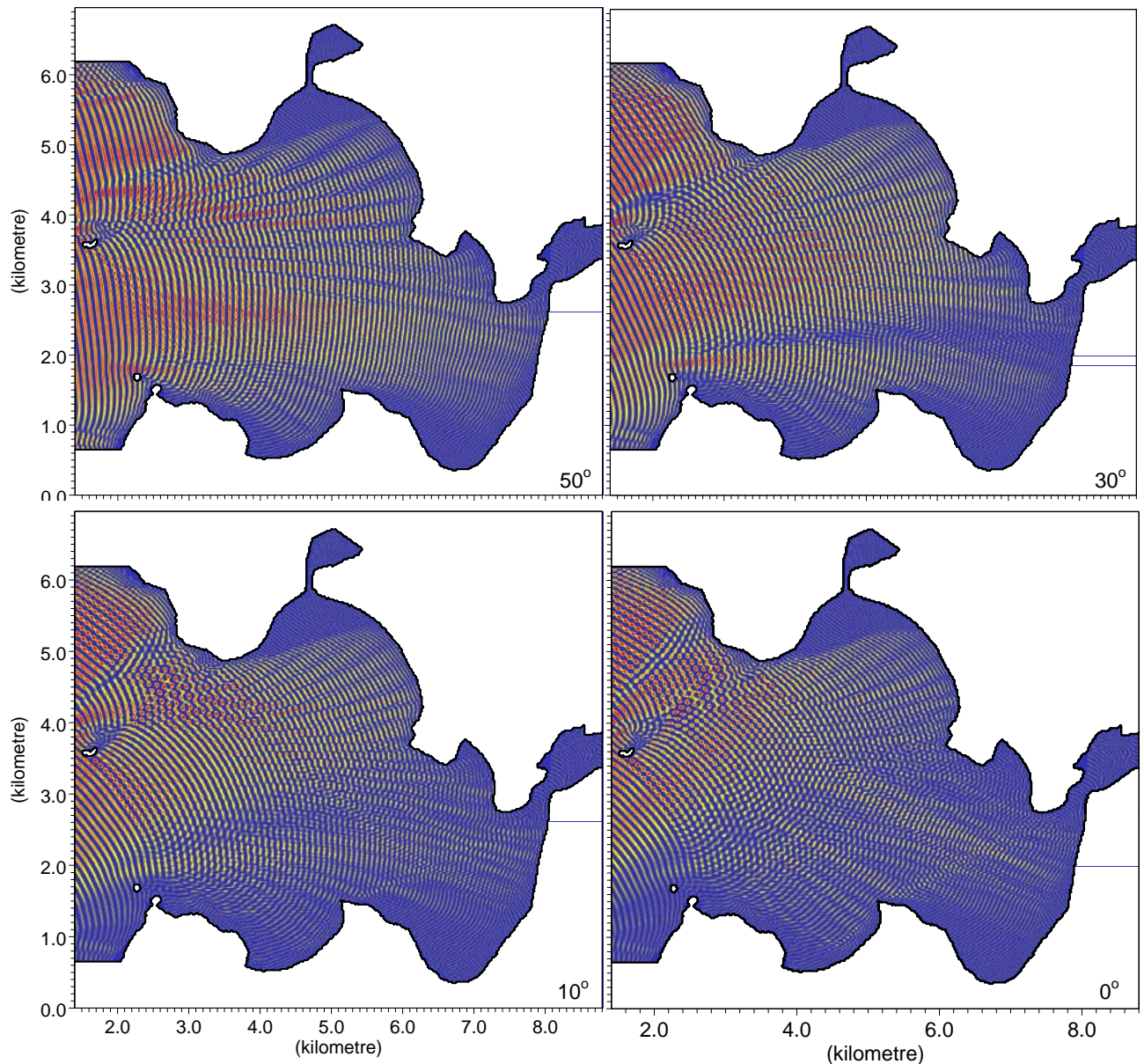


Figure 5.16 The wave behaviour within Mercury Bay with approach angles ranging from true north ( $0^\circ$ ) to true south ( $160^\circ$ ) using a wave height of 3 m and wave period of 9 seconds on the open boundary.

The headland separating Buffalo and Wharekaho Beaches appears to reflect waves, which are then focused on the inlet entrance. A closer inspection of elevation within Buffalo Bay (Figure 5.17) reveals the possibility of edge waves propagating along the beach. This behaviour is evident for all wave angles as they all cause similar wave behaviour within Buffalo Bay. It is possible this edge wave effect is an artefact related to the modelling grid creating a coarse coastline, or wave reflection after breaking. Whakapenui Point provides protection for the tidal inlet although medium

wave heights still reach the inlet via refraction around the headland. There is some indication waves propagate perpendicular to the beach in the southern section of Buffalo Beach but near the mid-section secondary waves form and begin to propagate north along Buffalo Beach where they are dissipated at Ohuka Beach. Wave heights over the ebb delta are small compared to the wave heights on either side illustrating the sheltering effect the ebb delta channel marginal linear bar it has on the southern most section of Buffalo Beach.

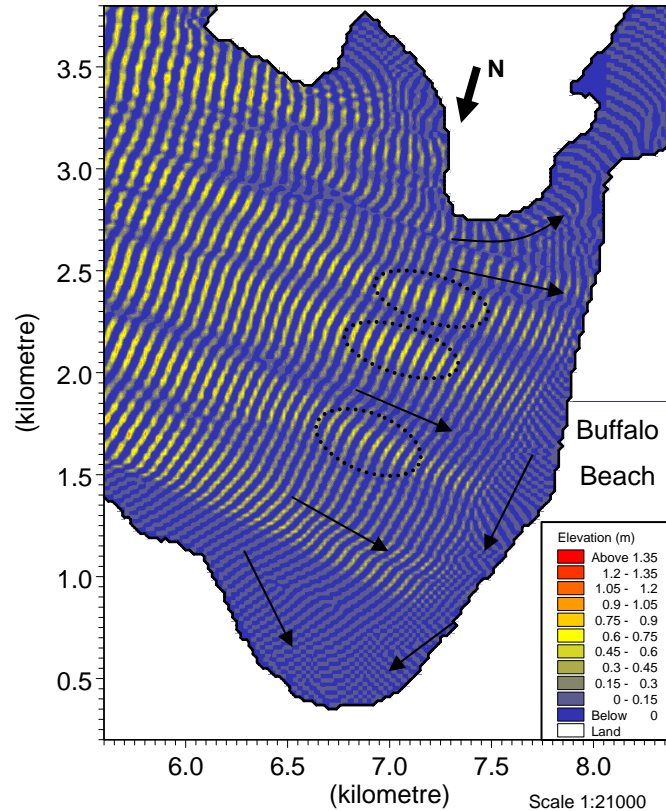


Figure 5.17 The elevation of Buffalo Bay with a wave height of 3 m, wave period of 9 seconds and approach from  $90^\circ$  at the entrance to Mercury Bay. Arrows indicate wave propagation direction and ovals indicate areas of wave energy convergence.

When the wave height at the offshore boundary is increased to 5 m (appendix 5), wave heights reaching Buffalo Beach are the same as with a 3 m wave height at the offshore boundary. This is because the waves are significantly reduced in height as they approach Buffalo Beach by diffraction and refraction around the headlands and shoaling on the gradually shallowing seabed. It is only once the wave period has been increased that wave heights reaching Buffalo Beach are increased as refraction depends on the phase speed  $C$  which is a function of depth and period. Wave periods of up to 11 seconds were trialled as any period larger than this is not

typical within Mercury Bay. The larger period (Figure 5.18) produced slightly larger wave heights along Buffalo Beach and waves were able to refract to a greater extent around the headland separating Wharekaho and Buffalo Beaches. The wave heights are similar but the 11 second wave penetrates further into Ohuka and also further into Maramaratotara Bay around the Shakespeare Cliff headland. The 11 second wave focuses more energy on the mid section of Buffalo Beach but less to the southern section and inlet area. More of the beach receives high wave energy with an 11 second wave period. There are only two primary zones of large waves focused along Buffalo Beach compared with ~5 with the 9 second wave. The 11 second wave is more able to refract around headlands, and brings higher energy to the Buffalo Beach shoreline.

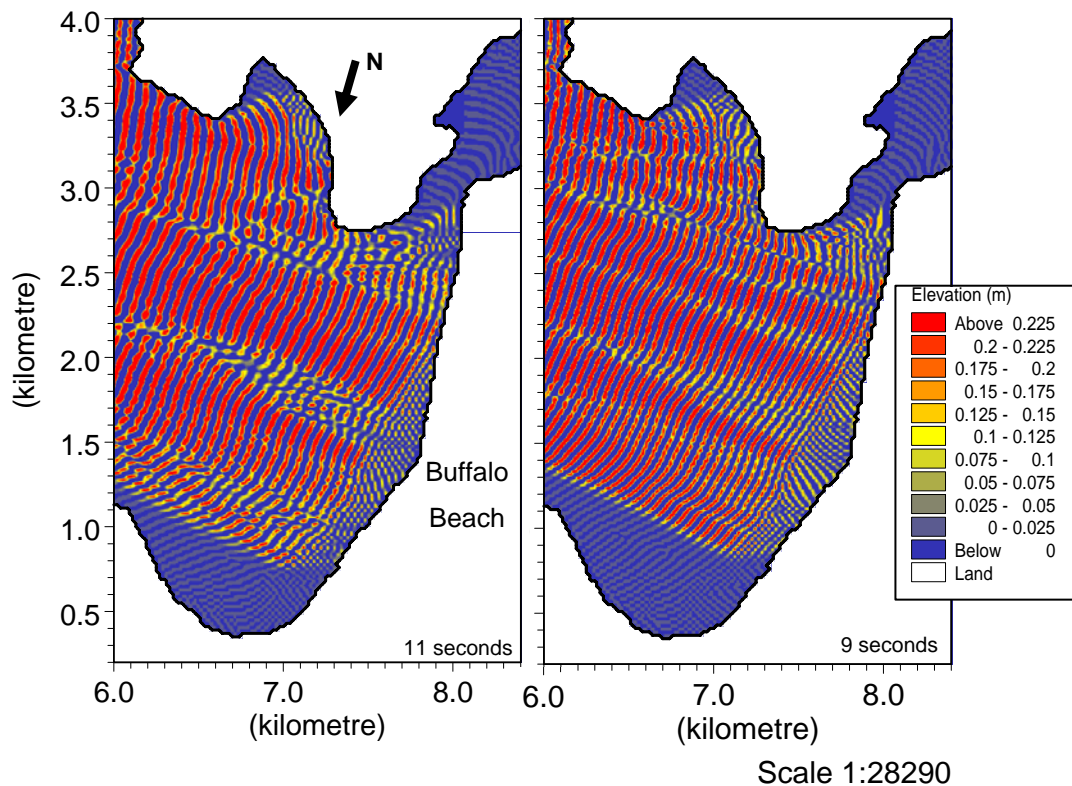


Figure 5.18 The elevation within Buffalo Bay with a 3 m wave height and 11 and 9 second wave period at the open boundary propagating from 90°.

Due to Centre Island and the headlands within Mercury Bay, Buffalo Beach receives a variation in wave heights (Figure 5.19). The largest waves enter Buffalo Bay with a swell from 70° at the Mercury Bay entrance. Wave heights along Buffalo Beach are enhanced with wave approach angles from between 30-70° and also for 90°. The wave height at the boundary was 3 m and wave heights along Buffalo beach are

simulated at over 1.5 metres with a 30-90° approach angle with waves of over 2 m high reaching the Buffalo Beach shoreline with a 70° swell approach angle. The inlet receives waves of up to 1 m for all directions. The largest wave heights are experienced at the southern section of Buffalo Bay near the seawall, where wave energy concentrates from most approach angles. Ohuka Beach (the northern section) receives minimal wave energy from all angles, due to shelter from the Wharekaho headland. Remarkably the Wharekaho headland causes wave reflection onto the southern section of Buffalo Beach, increasing the wave energy here.

The approximated wave breaking zone is widest with the larger waves which occur from between 50-90°.

The refraction patterns within Buffalo Bay can be compared to aerial photos (Figure 5.20) to show the areas of wave energy convergence and direction of wave propagation. The aerial photo shows the propagation angles within Buffalo Bay are very similar to those depicted in the elevation snapshots (Figure 5.16). The areas of wave energy convergence also show a reasonable match with the greater wave heights (Figure 5.19) and elevation (Figure 5.16). The bottom picture also shows the lack of wave energy at Ohuka.

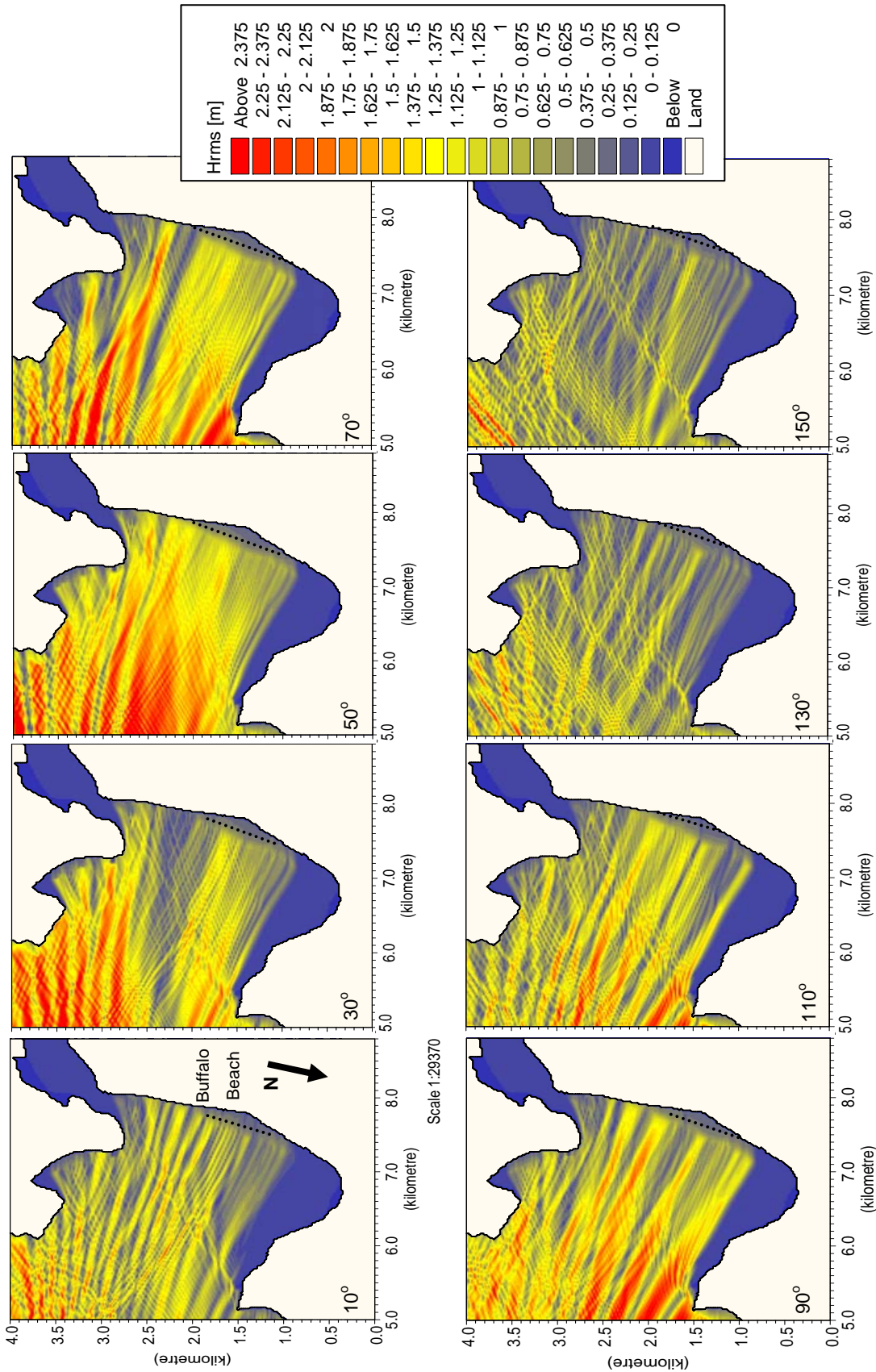


Figure 5.19 Sequence of snapshots of the wave height distribution within Buffalo Bay with approach directions of 10 – 150 degrees. A wave height of 3 m and period of 9 seconds were used at the open boundary. Note the reflection effect of the Wharekaho headland which causes larger wave heights at the southern end of Buffalo Beach. Dotted line indicates the potential breaking wave zone.

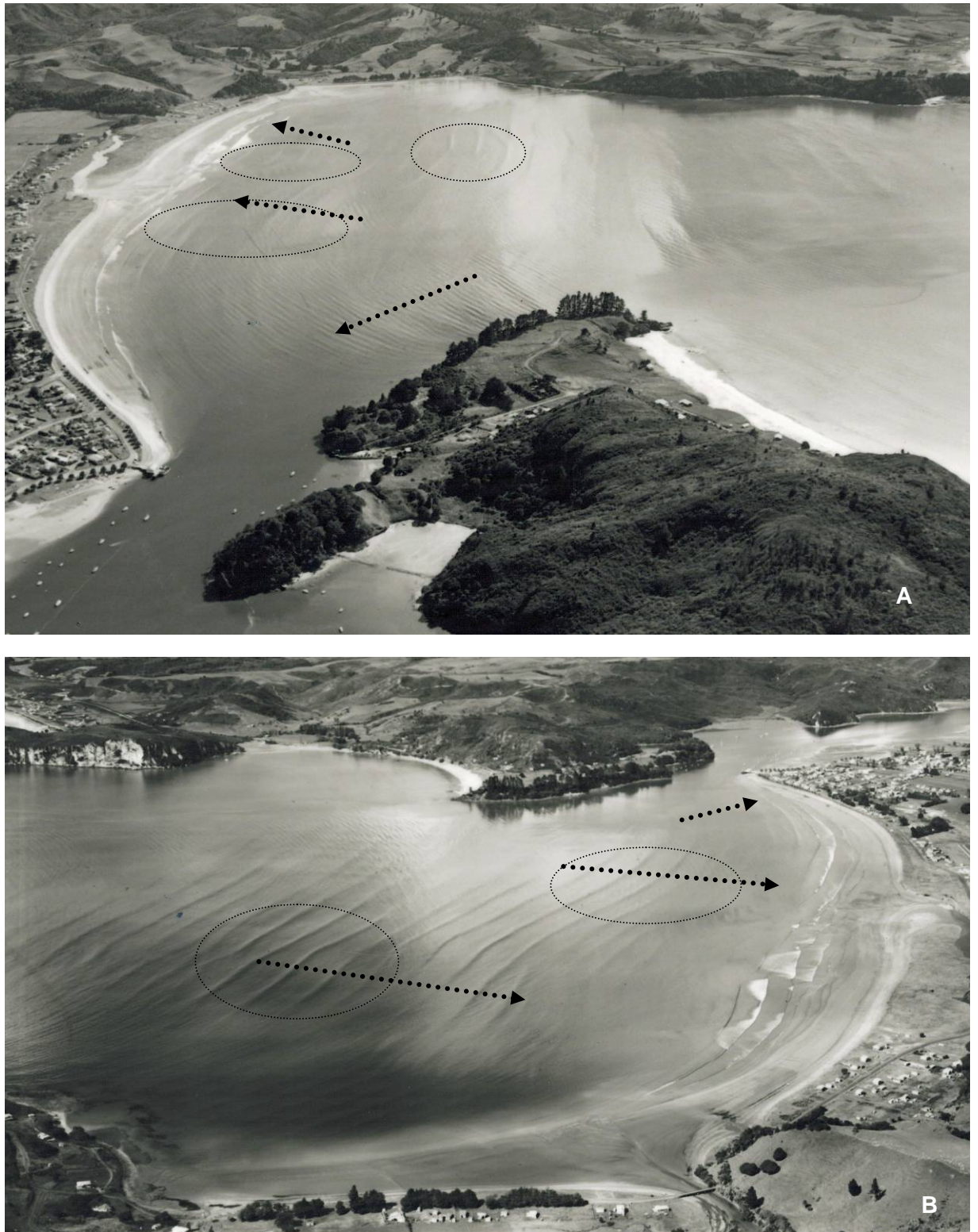


Figure 5.20 The wave energy convergence within Buffalo Bay. Oblique aerial photos taken in 1962 looking a) north and b) south. Arrows show direction of wave propagation and ovals show areas of wave energy convergence. Source: Environment Waikato 2006

### *5.8.1 Boat loading facility*

The potential suitability for a new boat loading/unloading facility is investigated as a component of the study. It has already been shown from the wave refraction study that wave energy for the 3 wave periods modelled is in each case minimised by the shelter of the Wharekaho headland in northern Buffalo Beach and Ohuka. Accordingly, three breakwater designs were trialled at northern Ohuka Beach to ascertain their effect in further reducing wave energy. The three designs assume a breakwater of approximately 500 m which is much larger than one would expect to be constructed but enables a better visualisation of the effect on wave behaviour.

The first and second designs (Figure 5.21) represent linear breakwaters at different angles to the beach and the third design mimics an artificial headland. The wave energy modelling shows that due to the natural shelter provided by the adjacent headland, Ohuka Beach is the best location for a boat ramp along Buffalo Beach, receiving minimal wave activity over all angles. Therefore, a breakwater or similar protection would provide additional protection from sea waves for example. In this instance a linear breakwater type structure protruding perpendicular to Buffalo Beach (design 2) would be best suited, causing the least disruption to wave behaviour.

Although this section of Buffalo Beach is the best location for ramp along Buffalo Beach, there are of course negative aspects associated with this site. Boat loading facilities need to be functioning on low and high tides so generally need a steep incline. The primary issue is the shallow platform-like nature of the beach which may not be steep enough for a boat loading facility and possibly may not be used on a low tide.

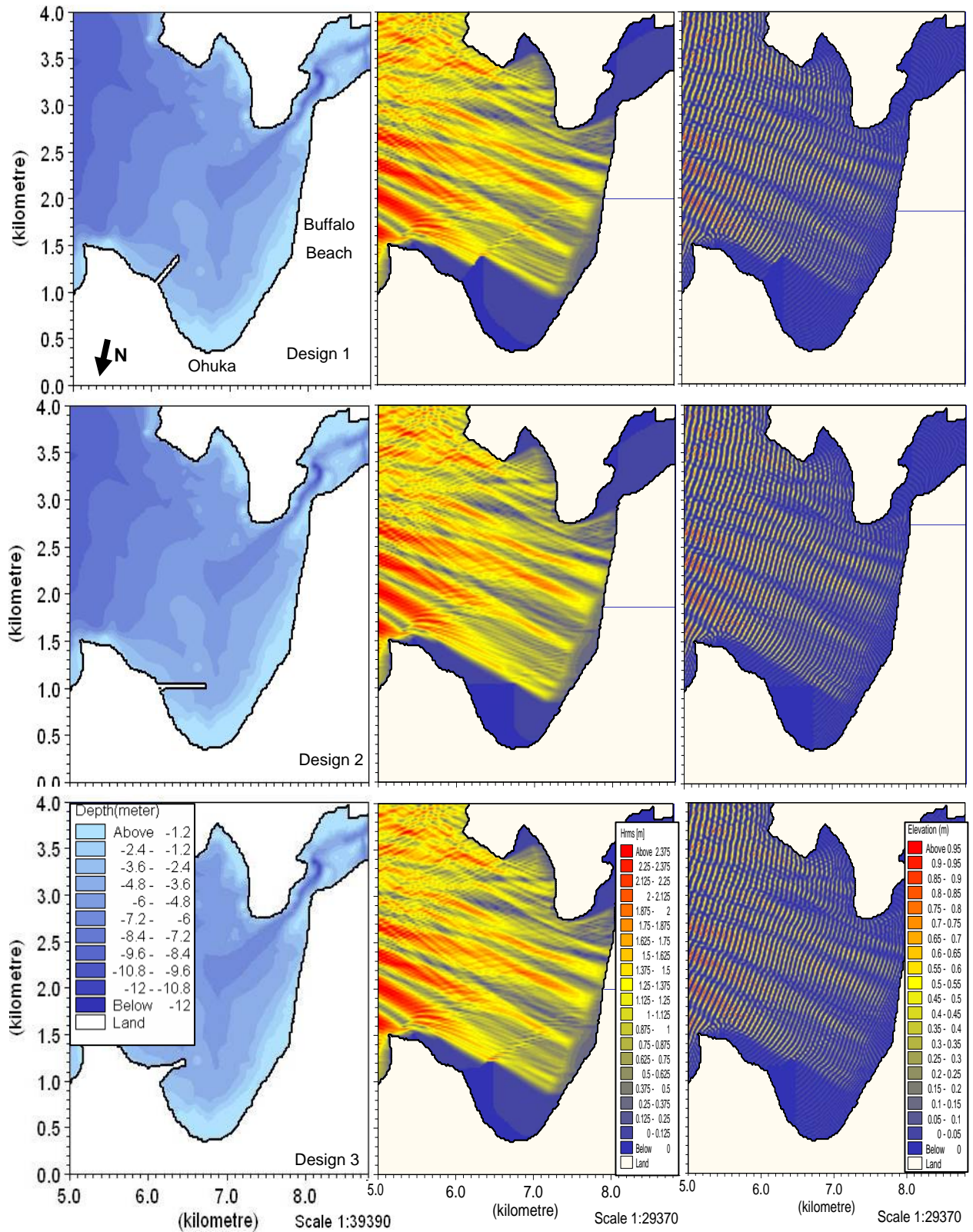


Figure 5.21 The 3 breakwater designs trialled at Ohuka Beach and the wave height distribution and elevation within Buffalo Bay due to the three hypothetical breakwater designs at Ohuka.

## **5.9 Discussion and Implications of Results**

The highest waves within Mercury Bay occur when the wave approach angle is from between  $30^\circ$  and  $110^\circ$ , with the largest wave heights occurring around  $70^\circ$ . The dominant swell direction entering Mercury Bay is from the northeast, around  $45^\circ$  with easterly swells (propagating from  $90^\circ$ ) also common (Pickrell and Mitchell, 1979). The results of the modelling show that waves approaching from between  $50$  and  $90^\circ$  cause the highest waves within Mercury Bay, including at the Whitianga inlet and along Buffalo Beach. That is, the typical swell conditions approaching Mercury Bay cause large wave heights along Buffalo Beach compared to other swell approach directions (i.e. from  $0-30^\circ$  and  $110-150^\circ$ ).

Within Buffalo Bay wave energy converges predominantly at the southern section of Buffalo Beach in the same position as the large sea wall revetment placed here. Therefore, wave energy focusing is the cause of this eroded section of beach and it is likely the seawall is causing waves to scour the beach face here, which is why the beach had not widened between 1990 and 2002 (Chapter 3). The growth of the ebb delta over the last 60 years has evidently provided increasing shelter to the adjacent beach, which is why the southern extremity adjacent the ebb delta is the widest section of Buffalo Beach.

Waves along Buffalo Beach break parallel to the shore, which can enable edge waves to form. Edge waves are standing oscillations that propagate along the coastline and form due to resonance between the waves approaching the shoreline and the waves already reflected from it (Bird, 2000). The observed northwards propagation of waves at the mid section of Buffalo beach likely indicates the presence of an edgewave. Edge waves are thought to cause variations in wave height along a beach as waves arriving at the coast can be amplified if the wave crest meets the edge wave crest, and dampened if the wave trough coincides with the edgewave trough. Paton (1993) found evidence of edgewaves along Buffalo Beach in wave data attained from an S4 (as mentioned in Chapter 2) so the model prediction of edgewaves is consistent.

Typically waves with an oblique approach to the coast generate an alongshore current which drives the littoral sediment transport. Within Buffalo Bay waves refract and tend to break almost parallel to the shore. However the variation in wave heights along Buffalo Beach causes a gradient in energy dissipation. The gradient causes a superimposed lateral dispersion on the longshore currents to form in the near shore zone. This gradient presumably varies so the longshore current may not be continuous, but flow from an area of high wave energy to an area of lower wave energy (Figure 5.22a). The variation in wave height along Buffalo Beach is the same for every wave angle which suggests littoral drift is rare along Buffalo Beach causing localised zones of littoral transport. This promotes the theory the observed net littoral drift direction is a combined function of the breaking waves interacting with the return flow of the well-defined landward tidal eddy system in Buffalo Bay, or flood tidal currents. Occasional longer period waves may induce more longshore transport as less variation in wave height occurs. With an 11 second wave (Figure 5.22b) the mid, southern and northern parts of Buffalo Beach receive low energy which generates a stronger, more continuous alongshore current from the high to low energy areas.

The northern end of Buffalo Beach was identified in Chapter 3 as suffering long term erosion. It is advisable that this scour is the result of offshore diabathic sediment transfer by high energy waves in times of large, northeast swells. These waves erode and suspend the sediment from northern Buffalo Beach wherefrom it is probably moved offshore by the ebb tide or down to the ebb delta by the flood tide current or landward eddy associated with the ebb tide.

The bathymetry used did not include the isolated sandbar near Pandora Rock. It is likely, based on visual observation, the Notice to Mariners (LINZ, 2005), and anecdotal evidence from local inlet users, that the sandbar causes waves to shoal early and occasionally swell waves would break on the sandbar. For most swells, the waves would typically shoal over the sandbar then reform to break on the southern section of Buffalo Beach. Longer period waves have larger wavelengths, so they can break in deeper water (waves break when depth is approximately half the wavelength). Long period waves are not typical in Buffalo Bay but do occur and in this instance would produce hazardous breaking waves in the sandbar area.

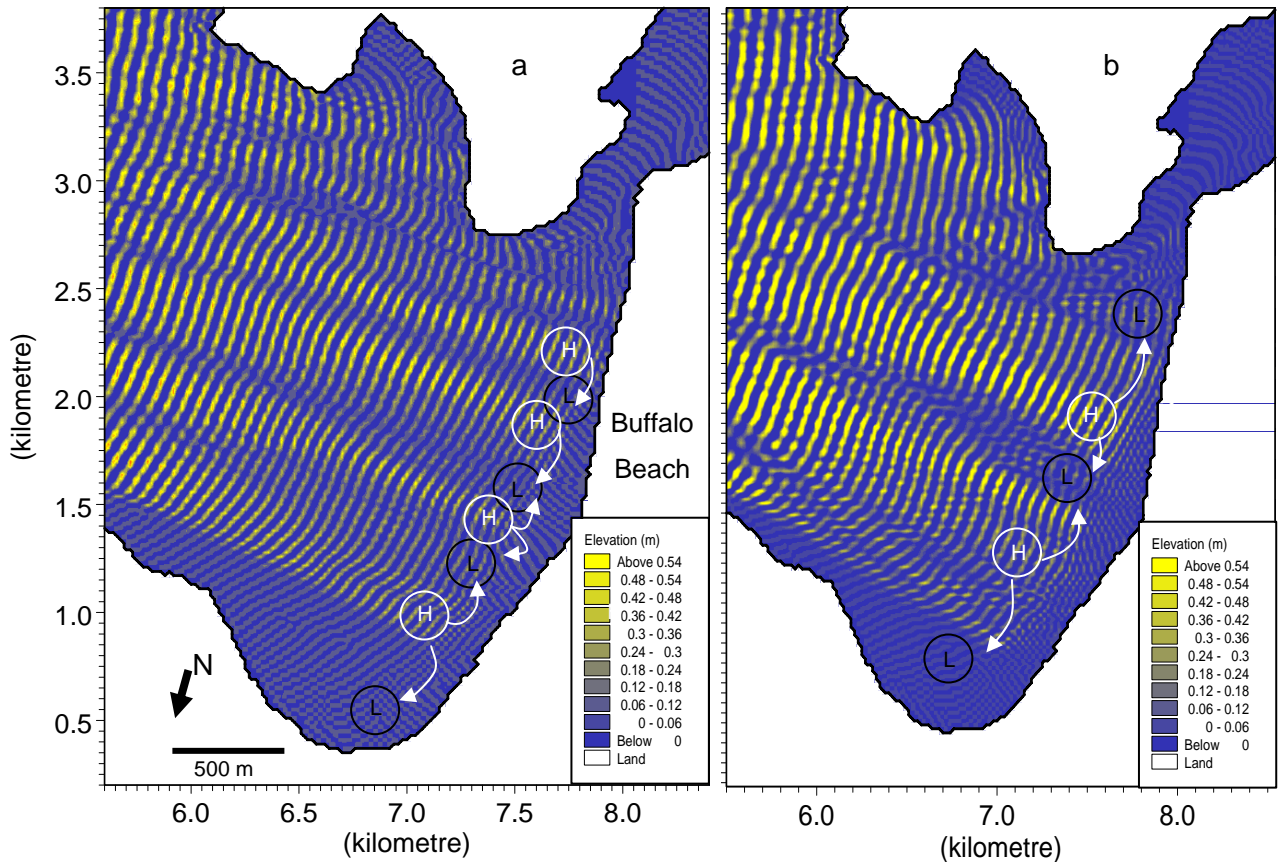


Figure 5.22 The areas of high and low wave energy (H and L) and the resultant long shore current directions along Buffalo Beach for a) a 3 m and 9 second wave at the entrance to Mercury Bay and b) a 3 m and 11 second wave at the entrance to Mercury Bay.

This modelling exercise suggests Ohuka Beach would be the best position for a new boat loading facility along Buffalo Beach due to the shelter provided by the adjacent headland from all swell directions. Along Ohuka, placing the facility as indicated by Figure 5.23, would minimise wave approach at an angle to the boat ramp, which produces a navigation hazard for boat users. The waves reaching any part of this section of beach will be small, with a maximum of 0.15 m reaching Ohuka, even when a 5 m and 9 second swell enters Mercury Bay from 70°. Design 2 provides the best shelter to Ohuka Beach and causes minimal reflection and diffraction and maximum protection. The other two designs create similar reflection patterns and cause waves to focus on the mid section of Buffalo Beach while providing only a small amount of wave shelter.

The final boat ramp position will depend on other factors such as infrastructure demands and social aspects, but Ohuka Beach provides a sheltered and safe

environment for such a facility. If it was unfeasible to install the boat loading facility here, optional locations are minimal along Buffalo Beach.

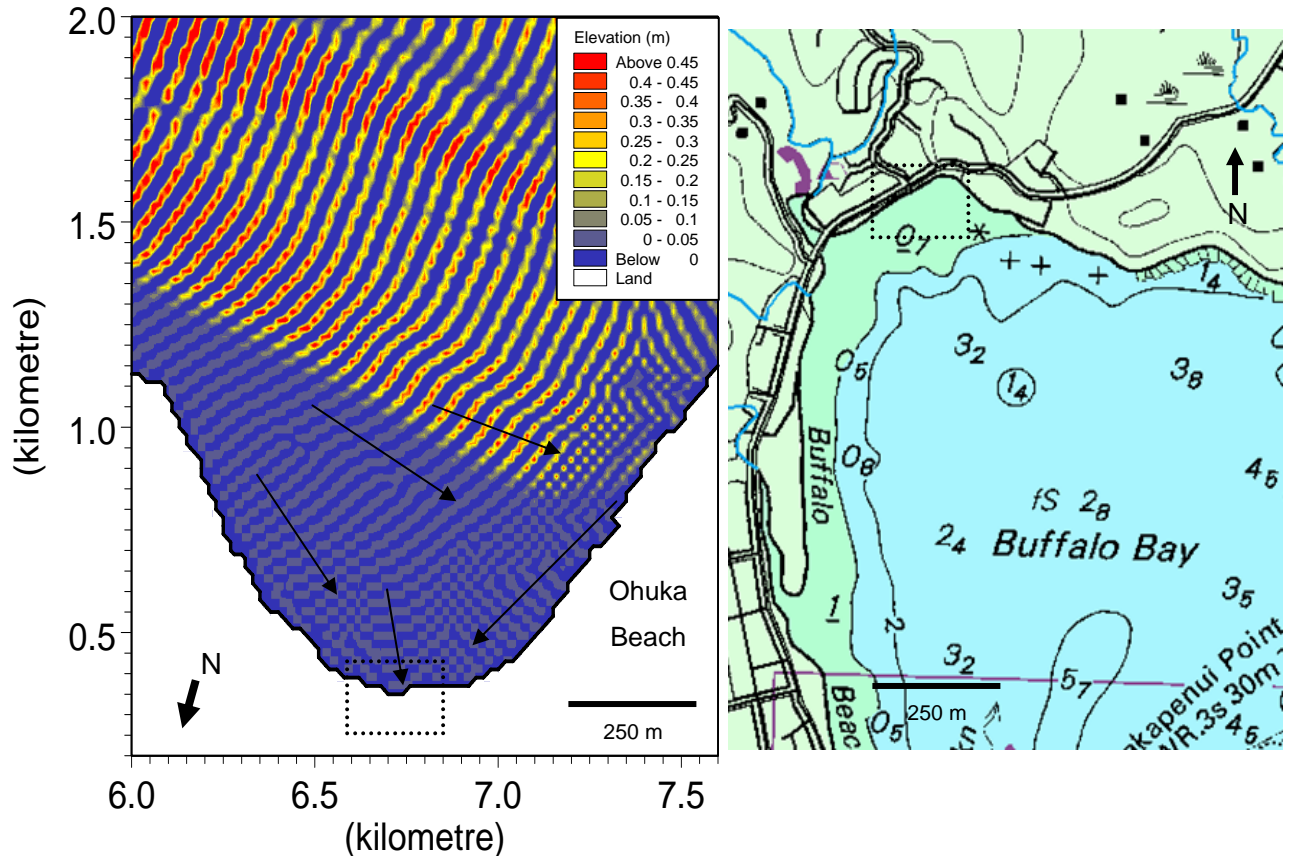


Figure 5.23 The wave propagation direction at Ohuka beach for a 3 m 9 s wave, and the ideal location for the boat loading ramp (indicated by the dotted square).

## 5.10 Conclusions

Numerical models provide an efficient and passive method of studying the marine environment. The objective of the modelling in this study is to identify sediment transport pathways. The primary conclusions of the hydrodynamic model exercise are:

- The calibration and validation of the model were successful with elevation MAE's ranging from 0.04-0.16 m in calibration and from 0.01-0.4 m in validation.
- Altering the bed resistance depth and eddy viscosity did not provide a better calibration match with the elevation data, although adding wind does adjust

the current speed. The difference in elevation and speed is likely to be caused by model schematisation or changes in bottom topography.

- Two eddy systems are present in Buffalo Bay with the ebb tide. The seaward eddy is the likely cause of the isolated shallow zone in Buffalo Bay and the observed net littoral drift direction south is likely to be enhanced by the southward return flow of the landward eddy.
- In 1938 the ebb tidal jet discharge from the inlet was aligned north to south and it is likely the growth of the ebb delta pushed the ebb jet northeast. The landward eddy was apparent and stronger than the seaward eddy which was short-lived and resided predominantly in Maramaratotara Bay in 1938.
- Seiching is evident within Mercury Bay in the model output sequence, likely arising from the topographic configuration of the Bay
- The residual current speed and direction indicates areas of scour in northern Buffalo Bay and southern Ohuka Beach, which correlates with erosion identified in this area in Chapter 3. The residual map also suggests accretion is likely to occur offshore, northeast of the inlet entrance and in the vicinity of the ebb delta channel marginal linear bar, which is consistent with the results of bathymetric change noted in Chapter 3.
- Waves approaching Mercury Bay from between 50-90 degrees induce the largest wave heights within Buffalo Bay, with wave energy focusing on the mid-southern section of Buffalo Beach for most wave approach directions. The ebb delta protects the southern tip of Buffalo Beach from large waves.
- A new boat loading facility along Buffalo Beach would be best located in the lee of the headland at Ohuka due to the high degree of shelter here.

These summations of the hydrodynamic conditions can now be used to investigate and draw conclusions on the sediment transport system within Buffalo Bay.

## ***Chapter Six –Modelling of Sediment transport***

---

The MIKE 21 non-cohesive sediment (sand) transport model (ST) combines the wave and hydrodynamic models to predict average sediment transport rates and average rates of bed level change (over the simulation period) and a time series of transport rates e.g. daily or hourly. The ST model accounts for a plane or rippled bed, and graded or uniform bed material (Siegle et al., 2007). Wave induced sediment transport can be calculated using the MIKE 21 PMS model and then incorporated into the ST model. However, there was no calibration data available for wave heights, periods or wave orbital velocities which all affect the sediment suspension and transport by waves. Local and offshore wind has also been previously identified (chapters 2, 3 and 4) as a likely contributor to sediment transport, particularly in the Buffalo Bay region. However lack of wind time series data meant MIKE 21 ST model was simulated with tidal hydrodynamic data only.

The MIKE 21/3 Particle/Spill Analysis model is a particle tracking module which simulates the pathway of a grain from a specified point. This model was used to establish sediment transport pathways within Buffalo Bay. Both the ST and PAP models are described in detail in the MIKE 21 ST and MIKE 21/3 reference manuals.

This chapter describes the ST and PAP model inputs and the results obtained in relation to establishing sediment transport pathways within the Whitianga inlet. The results are compared and discussed in relation to the HD output and conclusions and implications are made pertaining to the combined results of chapters 5 and 6.

### ***6.1 Sediment Transport Model***

#### ***6.1.1 Model setup***

##### *Model parameters for simulation of current only*

The choice of sediment transport formula can have a pronounced effect on the resulting model morphology output (Nicholson et al 1997). The MIKE 21 ST model gives the following five calculation options.

- The Engelund & Hansen total-load transport theory;

- The Engelund & Fredsøe total-load (bed load plus suspended load) transport theory;
- The Zyserman & Fredsøe total-load (bed load plus suspended load) transport formulation;
- The Meyer-Peter & Müller bed-load transport theory;
- The Ackers & White total-load transport method.

The chosen method will depend on the study area and modelers preference. Once the type of calculation is chosen, the relative density of sediment, critical Shields' parameter and the water temperature can all be specified or left as default values.

The Chezy or Manning bed resistance can then be given as a constant or varying in space by a dsf2 file to account for bottom friction. The sediment properties such as grain diameter, porosity and grading can be given as constants or in a dsf2 file of the model area. The non-erodible bed parameter in this section allows for a depth to be specified by the user which equates to the maximum depth of bed erosion. Lastly the morphological parameters are specified whereby the lateral boundary conditions, morphological scheme and filtering method can be adjusted. The inputs used in this ST model are given in table 6.1.

Table 6.1 The input variables for the MIKE 21 ST model

Input variable	Value
Pure Current Theory	Engelund and Hansen Density of sediment - 2.65 Critical shields Parameter - 0.045 Water Temp - 20°C
Bed resistance	Constant Manning Number $32\text{m}^{1/3} \text{s}^{-1}$
Sediment Data	Spatial constant Porosity - 0.4 Size - 0.15 mm Gradation - 1.1
Morphological parameters	Non-erodible surface excluded Lax-Wendroff method, no filtering zero sediment flux gradient for outflow specified gradient

### *6.1.2 Model output – Bed level change*

The chosen current theory of Engelund and Hansen means the transport of sediment simulated in the ST model output for this study is total load, not only suspended load transport.

The bed level change provides a visual record of areas of tidally induced erosion and accretion within Buffalo Bay and the Whitianga inlet (Figure 6.1) over a 10 day period. The change refers to the total bed change so exact quantities of erosion and accretion cannot be derived. In order to derive the quantities of bed change the bed roughness within the inlet and grain size would need to be established, but the output plot shows the pattern of erosion and accretion under the selected parameters. The model output suggests the primary area of tidally-induced bed change in Buffalo Bay is within the inlet, with minimal bed change and sediment transport simulated over for the rest of the Bay over this time. There is no zone of sedimentation apparent around Pandora Rock or within Maramaratotara Bay, although it is likely the model does not hold the necessary capabilities to simulate sediment transport in eddy formations. The bed level change within the inlet area was plotted with the average sediment transport direction over the 10 day mean tidal flow period at the Whitianga inlet (Figure 6.1). Accretion primarily occurs where two opposing currents meet, which occurs in the vicinity of the ebb delta. The opposing currents here suggest the ebb delta receives sediment from both the estuary on the ebb tide, and also from Buffalo Beach, possibly due to both the flood tide, and the landward eddy on the ebb tide. The fastest area of sediment transport occurs in the inlet gorge and coincides with the fastest current velocities (Figure 6.2b). This suggests that although this section of the inlet is flood dominated, the ebb tide results in the greatest sediment transport here.

The eastern side of the inner inlet appears to be dominated by ebb tidal deposits, most likely originating from the Whitianga estuary catchment, whereas the western side likely receives sediment in flood tidal flows, possibly from the inlet entrance or Buffalo Bay.

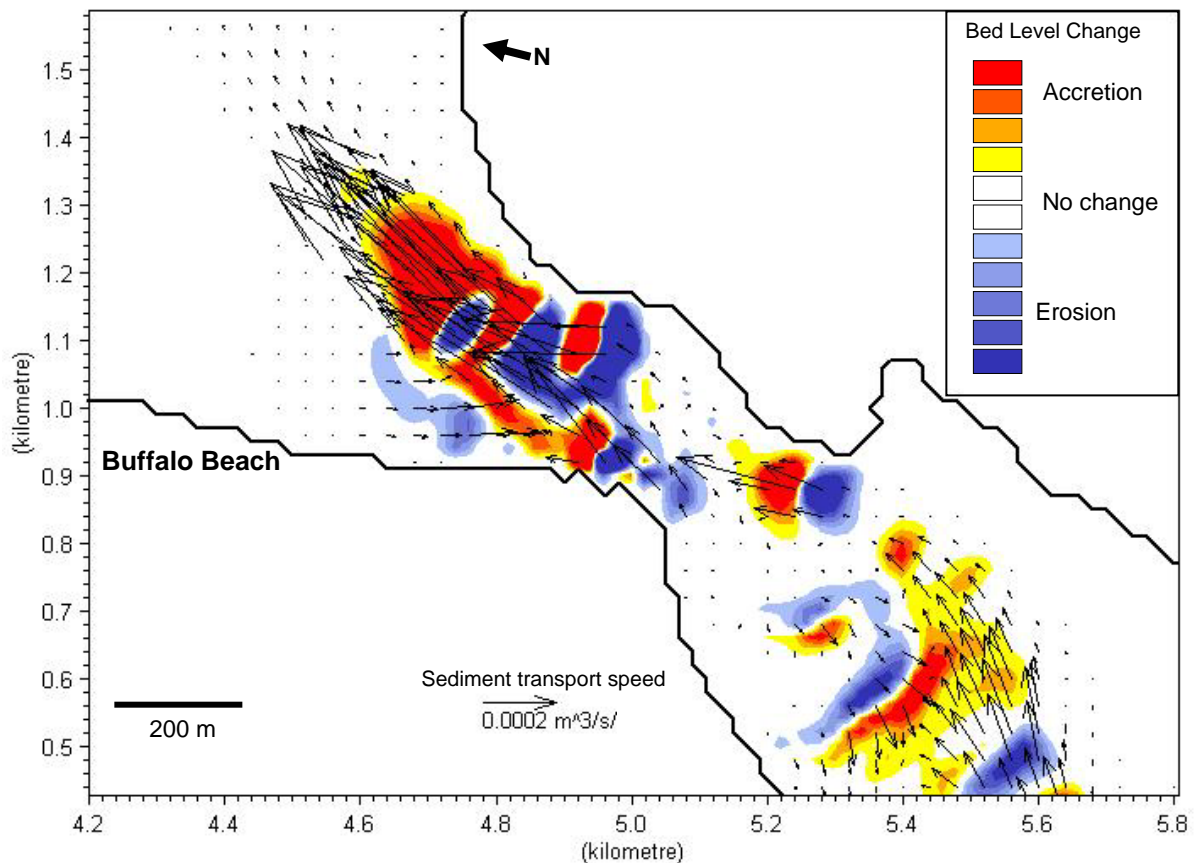


Figure 6.1 The simulated average bed level change and direction of total sediment transport drawn by mean tidal flows over a 10 day period within the Whitianga inlet using a  $d_{50}$  of 0.15 mm. The speed and direction of each arrow is taken at the base or origin of the arrow.

In comparison, areas of erosion are generally located where fast currents flow out from.

A closer perusal at the inlet bed change (Figure 6.2a) reveals the possible shape and position of the flood tidal delta in the Whitianga inlet. The residual velocity map (Figure 6.2b) further strengthens this theory as the area where the possible flood delta is situated is flood dominated. Further, alternative zones of erosion and accretion are evident within the inlet gorge and are consistent with the possibility of sandwaves, although these bedforms have not been previously identified in the side scan survey undertaken by Cooper (2003). The areas of change within the inlet are situated in faster velocity areas, most likely to represent the inlet channel (Figure 6.2b).

The simulated accretion and erosion is quite dependant on the grain size used. The median measured grain size ( $d_{50}$ ) from sediment trap data of 0.15 mm was used for this model, but smaller and larger grain sizes were trialled (Figure 6.3) in order to establish the effect of grain size on bed change, in the instance that grain size was not uniformly 0.15 mm.

The plots show the same zones of sediment deposition and erosion within the inlet but to varying extents. The larger grain size ( $d_{50} = 1.0$ ) resulted in bed level change within the inlet, and the smaller grain size ( $d_{50} = 0.1$  mm) caused more pronounced erosion and deposition, compared with the bed change using  $d_{50} = 0.15$  mm.

There is a lack of detailed surficial sediment and bed form data available for this area of the inlet. The most detailed previous study (Cooper, 2003) identified coarse sand and gravel deposits in the inlet gorge. Therefore the uniform  $d_{50}$  grain size of 0.15 mm is not likely to represent the grain size for the entire inlet. It is possible then, that the bed level change, particularly in the inlet gorge where coarser sediments have been identified, is less, as coarser sediment increases the threshold velocity needed to entrain sediment. The largest grain size (Figure 6.3,  $d_{50} = 1.0$ ) shows that bed level change is less but identifies similar zones of bed level change.

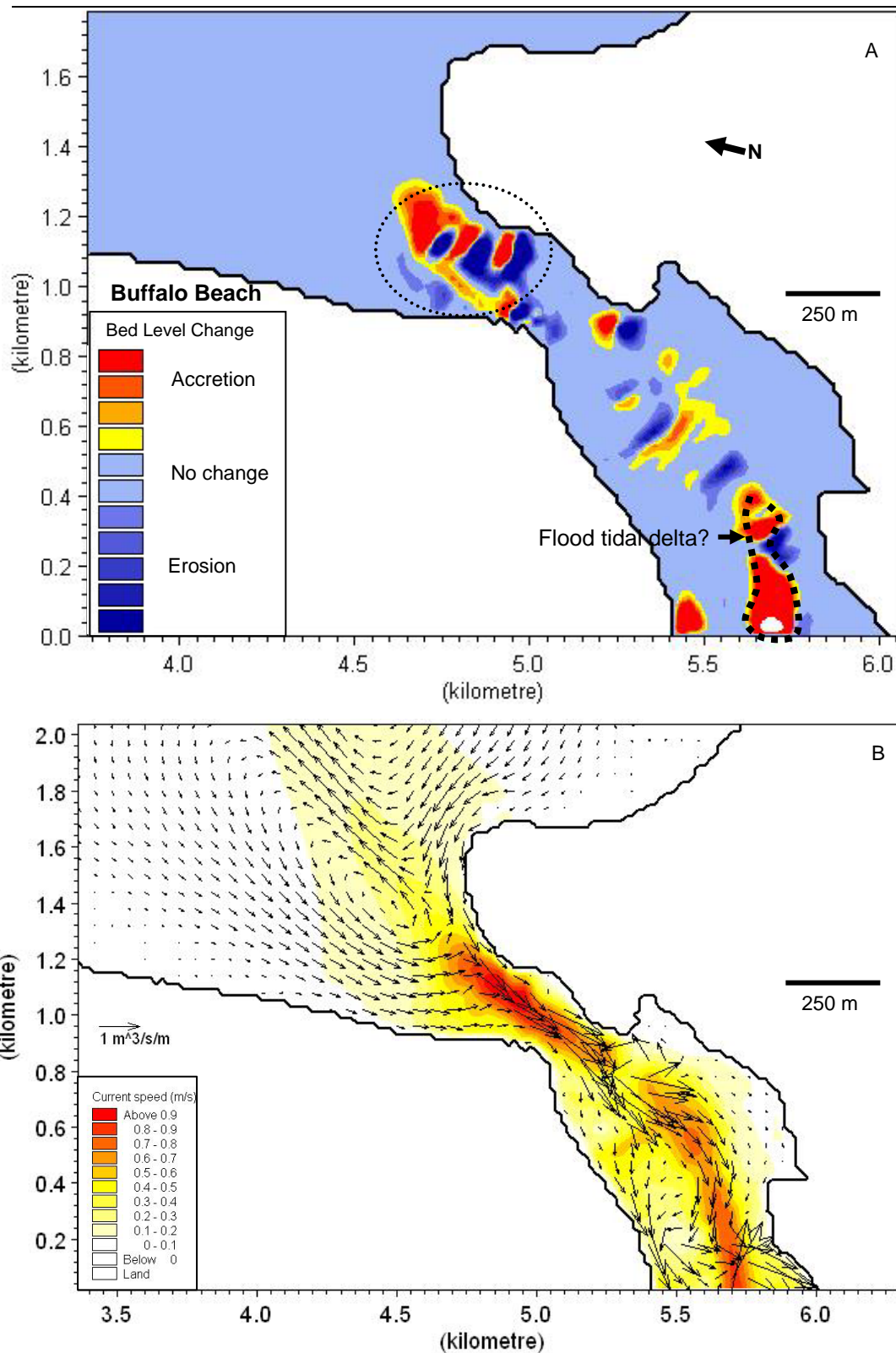


Figure 6.2 A. The simulated bed level change averaged drawn by mean tidal flows over a 10 day tidal cycle within the inlet using a  $d_{50}$  of 0.15 mm. The thick dotted line indicates the approximate flood delta position and the oval indicates possible sandwave bedforms. B. The residual tidal cycle velocity vector pattern within the Whitianga Inlet.

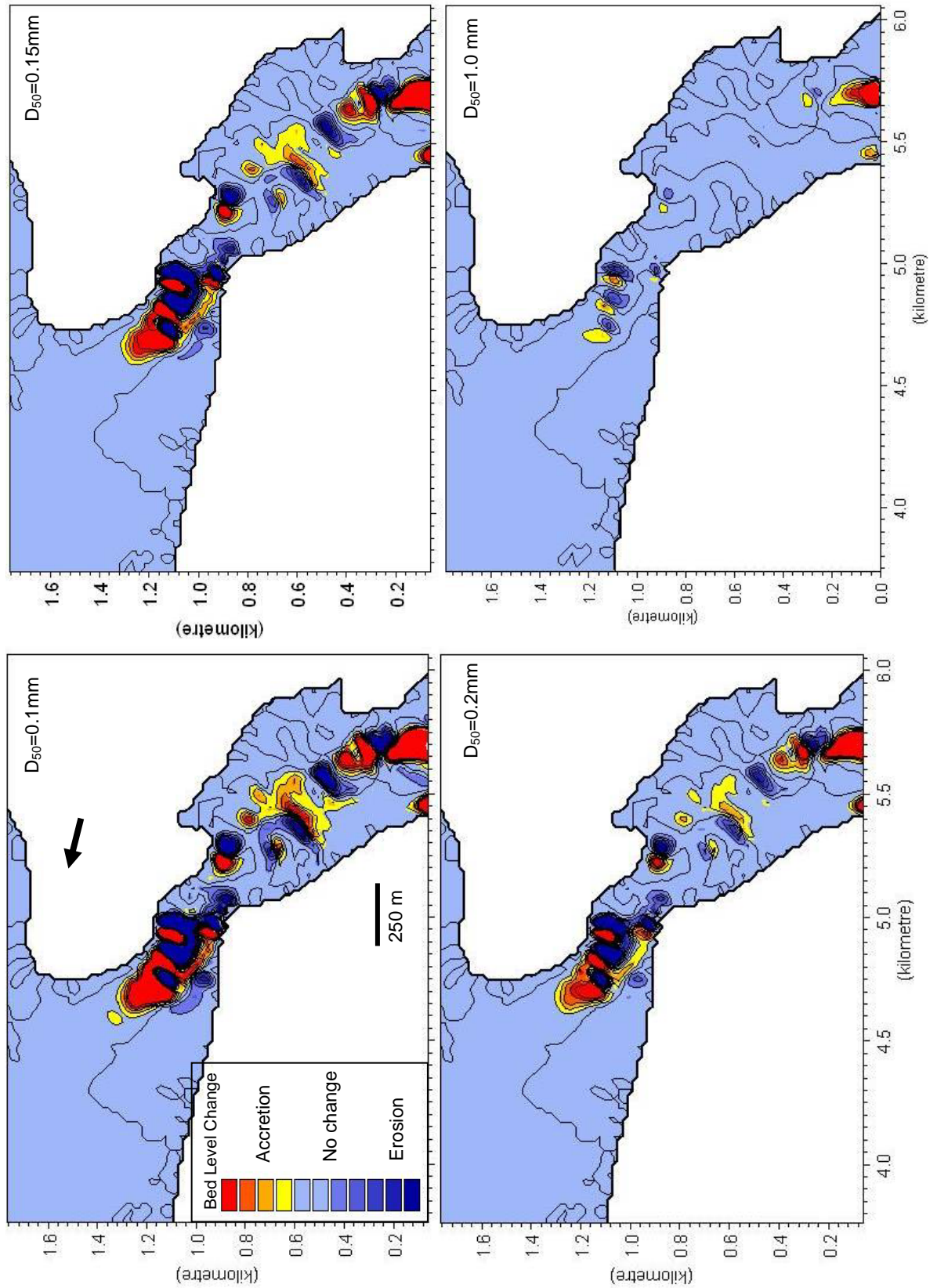


Figure 6.3 The simulated tidally induced bed level change drawn by mean tidal flows averaged over a 10 day period within the Whitianga inlet using a sand diameter ( $d_{50}$ ) of 0.1, 0.15 0.2 and 1.0 mm. All plots relative to same scale.

## 6.2 Particle tracking Model

### 6.2.1 Model set up

MIKE 21/3 PAP is a useful tool in the coastal sector due to its predictive capabilities of oil spills, coastal discharges and suspended particle tracking. The primary model inputs used in this study are outlined below. Inputs used in this modelling exercise are given in table 6.2.

#### Basic Parameters

The PAP model allows up to 64 individual sediment sources to be specified in the model. These are given as grid co-ordinates. The number of particles released each time step can be manipulated and a maximum particle age can also be specified, whereby after such a time the particle is taken out of the simulation.

The dispersion of the particles can be defined as independent of the current or scaled to match changes in the hydrodynamic conditions. The eddy and logarithmic velocity profile is used to specify a bottom roughness which adjusts the vertical dispersion of sediment. This is set to default unless a Logarithmic Velocity Profile was specified in the simulation.

Table 6.2 The input variables for the MIKE 21/3 PAP model

Input variable	Value
Hydrodynamic data type	Hydrodynamic, Varying in time and space 2D
Sources	1 particle per time step, age not specified
Dispersion	Independent of the current, constant of $1\text{m}^2\text{ s}^{-1}$
Eddy and logarithmic velocity profile	Logarithmic constant 0.1m
Water properties	Temperature = constant $20\text{ }^{\circ}\text{C}$ and Salinity = constant 10 psu
Type of Particle	1 order process - particulate matter
Settling velocity	Minimum sediment mass - 0.01 kg Constant 0.003 m/s

Water temperature and salinity can be specified if sufficient data are available. However, if using the PAP model for sediment transport from a MIKE 21 HD file, only constants can be specified. For other modules they can be given as a time series.

### *Sediment Parameters*

The model allows specification of the type of particle used such as dissolved or particulate matter or non-cohesive or cohesive mud. The settling velocity can then be given as a constant or changing with settling or size distribution.

#### *6.2.2 Model output – Particle tracks*

The model outputs a time series of the dispersion of each particle released over the run period. The MIKE 21/3 PAP model outputs also include particle tracks, which give an approximate path of the suspended particle over the time of model run, which was 10 days of mean tidal flow in this instance, in order to show the long-term sediment transport pathways.

Figure 6.4 illustrates the tidal-current-derived sediment transport pathways within Buffalo Bay for a 10 day period. The sediment along the northern half of Buffalo Beach (particles 1-2 Figure 6.4 (a)) does not travel very far from the source, particularly at Ohuka (particle 2 Figure 6.4 (a)) where the model shows the majority of particles stay within a 20 m radius of the original source. The simulation shows a general northwards tendency for particles on the lower northern section (particle 3 Figure 6.4 (a)) with some movement offshore. Particles from the mid to northern section of Buffalo Beach (particles 1-4 Figure 6.4 (a)) are not transported into Buffalo Bay and do not make it into the ebb tidal flow path or either eddy system. Particles 1 and 3 in the northern section are dispersed offshore, approximately 200 metres from their source.

It is possible that particle tracks in northern Buffalo Bay differ from those simulated in this section due to the existence of non-tidal currents identified at the Buffalo Bay monitoring site in Chapter 4. Wind-induced currents and wave activity, which were not included in this modelling exercise, both may play an important role in the sediment transport pathways here although the amount of sand transported will still be minimal due to the low currents typical of northern Buffalo Bay, as reported in Chapter 5 and established for the Buffalo Bay monitoring site in Chapter 4.

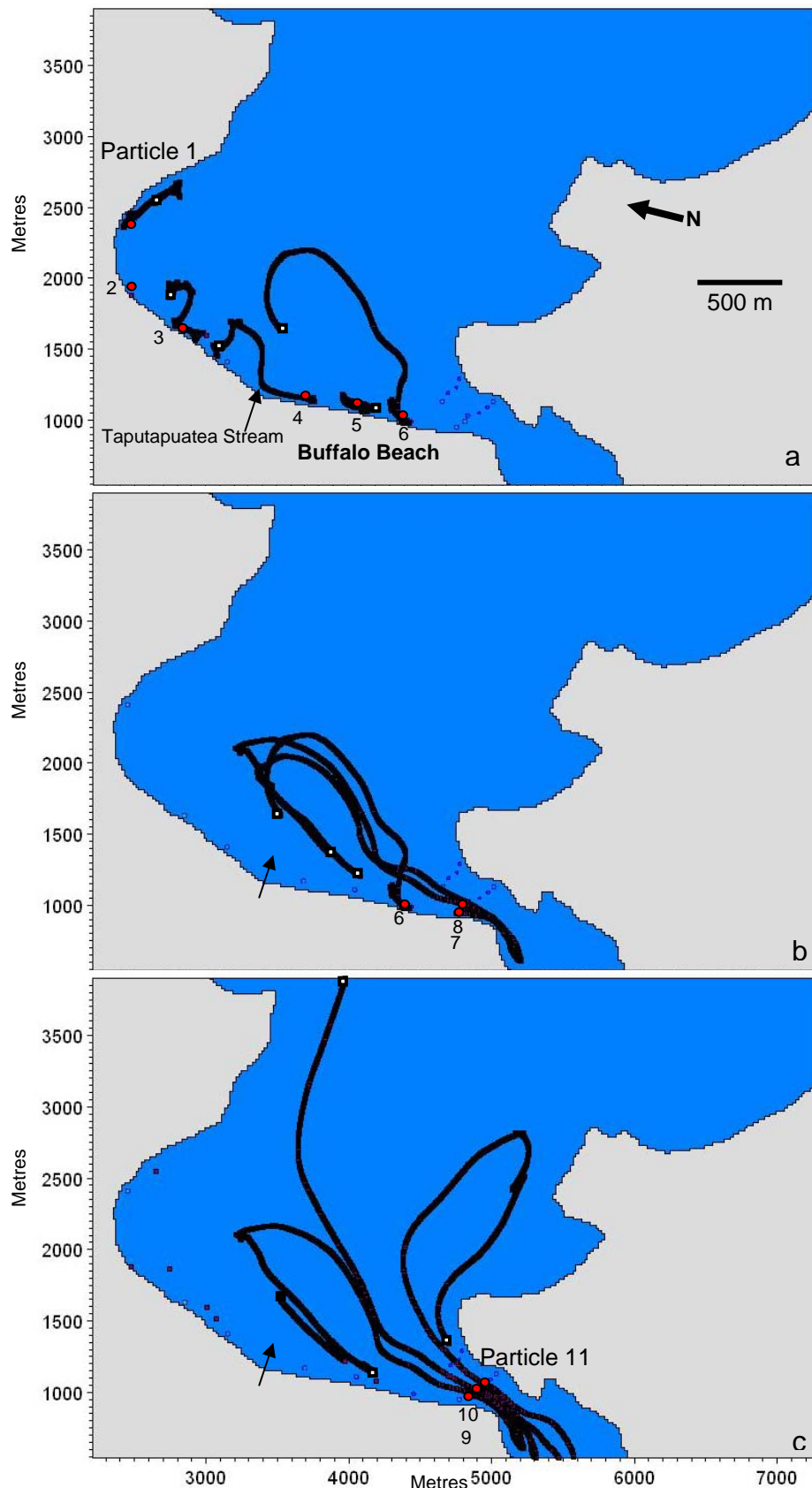


Figure 6.4 The suspended particulate matter particle tracks along Buffalo Beach and across the inlet gorge over a 10 day mean tidal flow period. Solid circles indicate the starting position of each particle. White squares indicate final position of particle.

The particles in the southern section of Buffalo Beach (particles 6-8 Figure 6.4 (b)) have a southward migration tendency towards the inlet. Particles between 500 m south of the Taputapuatea Stream entry and the ebb delta (particles 6-9 Figure 6.4 (b and c)) are moved south down the beach where they are then moved either into the inlet or out into Buffalo Bay and back around in the landward eddy system. These particles are most likely moved south along Buffalo Beach due a combination of the landward eddy system and the flood tide, which pulls water south along the beach into the inlet. Particles in the inlet channel and ebb delta vicinity (particles 8-11 Figure 6.4 (c)) are all moved into Buffalo Bay and are then transported out onto Mercury Bay or circulated in the seaward eddy system.

Therefore, three primary zones of sediment dispersal can be identified in the inlet entrance (Figure 6.5). Sediment on the southern section of Buffalo Beach is moved into Buffalo Bay and transported in the landward eddy system. Sediment deposited on the ebb delta (particle 9 Figure 6.4(c)) is most likely to be moved out into Buffalo Bay then recycled back onto the ebb delta, whereas suspended sediment in the inlet entrance (particles 10-11 Figure 6.4(c)) will be moved into Buffalo Bay and either transported out into Mercury Bay or circulated in Buffalo Bay via the seaward eddy.

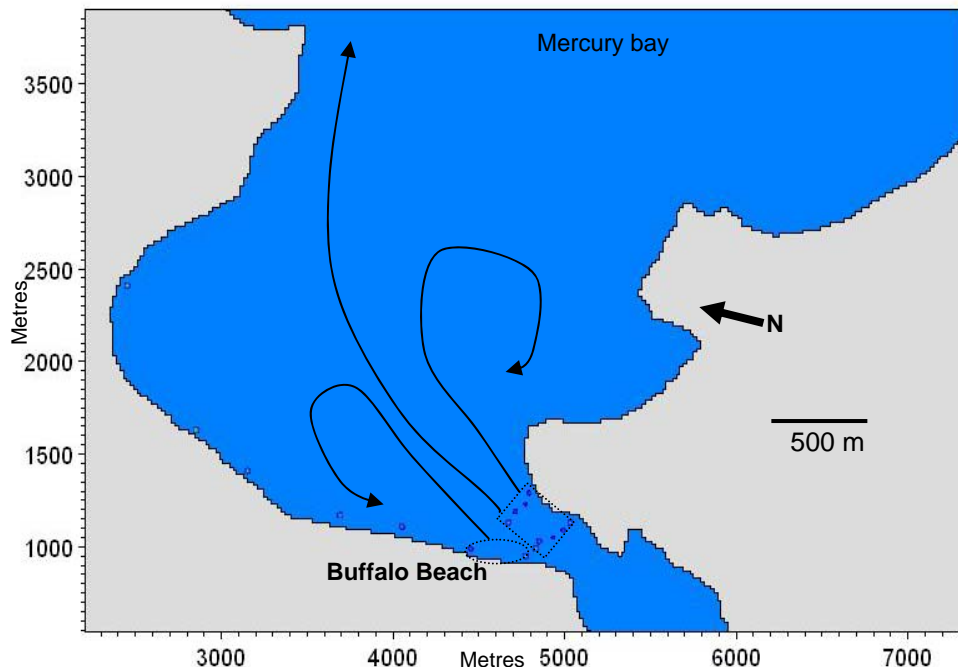
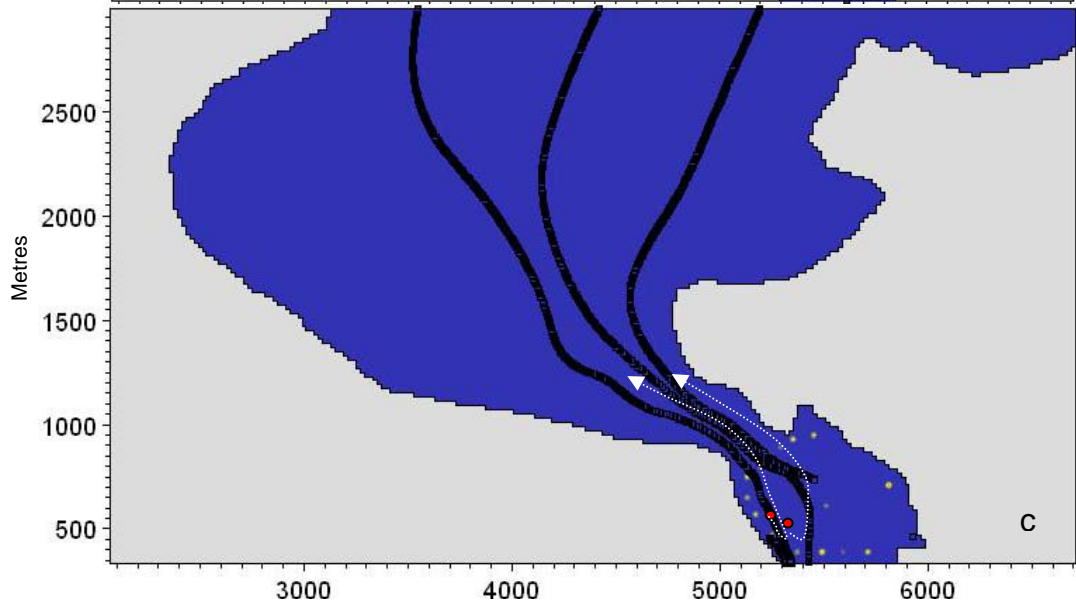
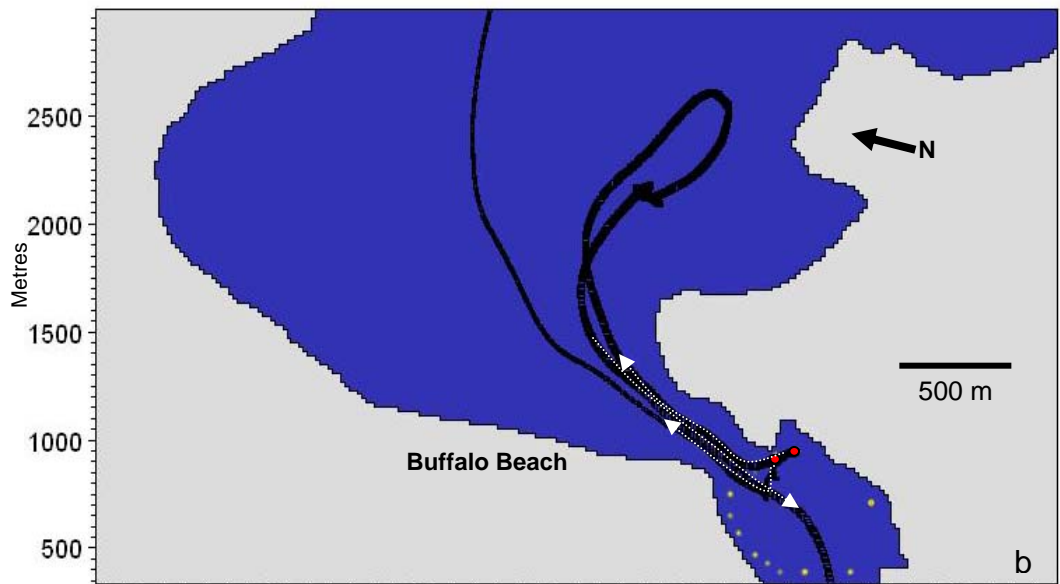
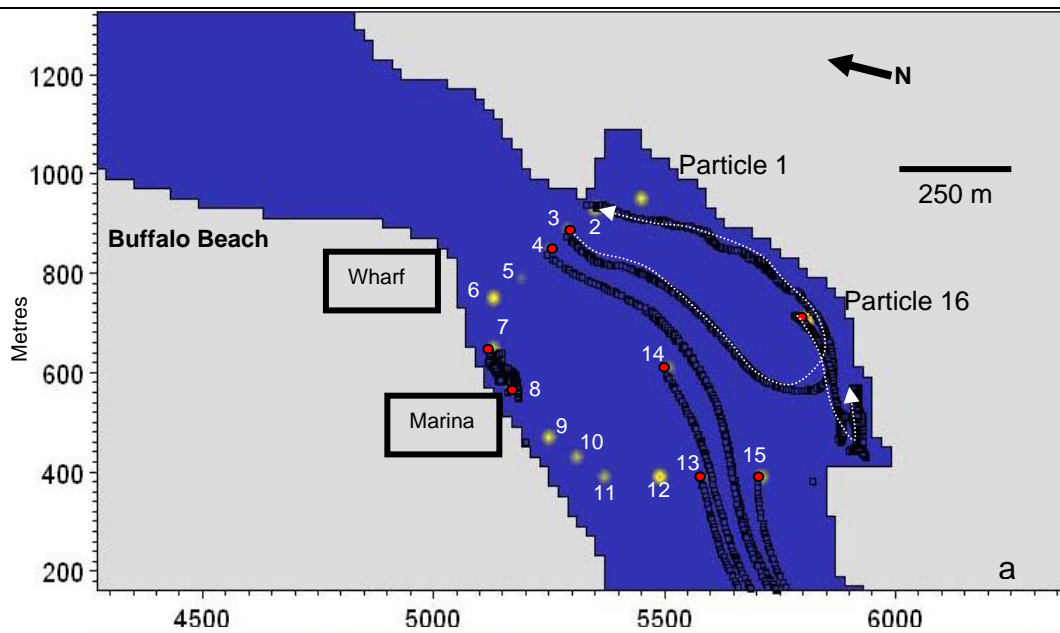


Figure 6.5 Simulated zones of suspended particle ebb tidal transport pathways in the inlet entrance vicinity.

The three zones of dispersal occur due to current separation once the flow has exited the inlet and entered Buffalo Bay. Some of the sediment travelling into Mercury Bay could potentially be carried out of Mercury Bay onto the shelf if down-welling currents were prevalent.

Particles released within the inlet (Figure 6.6) move in a very complex matter with no obvious relationship between particle location and the coincident transport pathway. The only two inert areas are the embayment opposite the marina and the Whitianga wharf beach area (particles 7, 8 and 16). Particles 3, 4, 13, and 14 all move up the estuary and do not exit the inlet although particle 3 most likely enters the pathway of particles 1 and 2 and flows out with them.

The remainder of the particles are moved out of the inlet and into Buffalo Bay where they are transported in the landward or seaward eddy systems. Some particles (5 and 6) were moved out into Buffalo Bay with the ebb tide and then returned to the inlet system with the flood tide to be deposited within the inner section of the inlet. It is therefore possible the inlet is accreting due to sediment inputs from the estuary on the ebb tide and sediment re-circulated from Buffalo Bay on the flood tide, which was suggested in section 6.1.2 also.



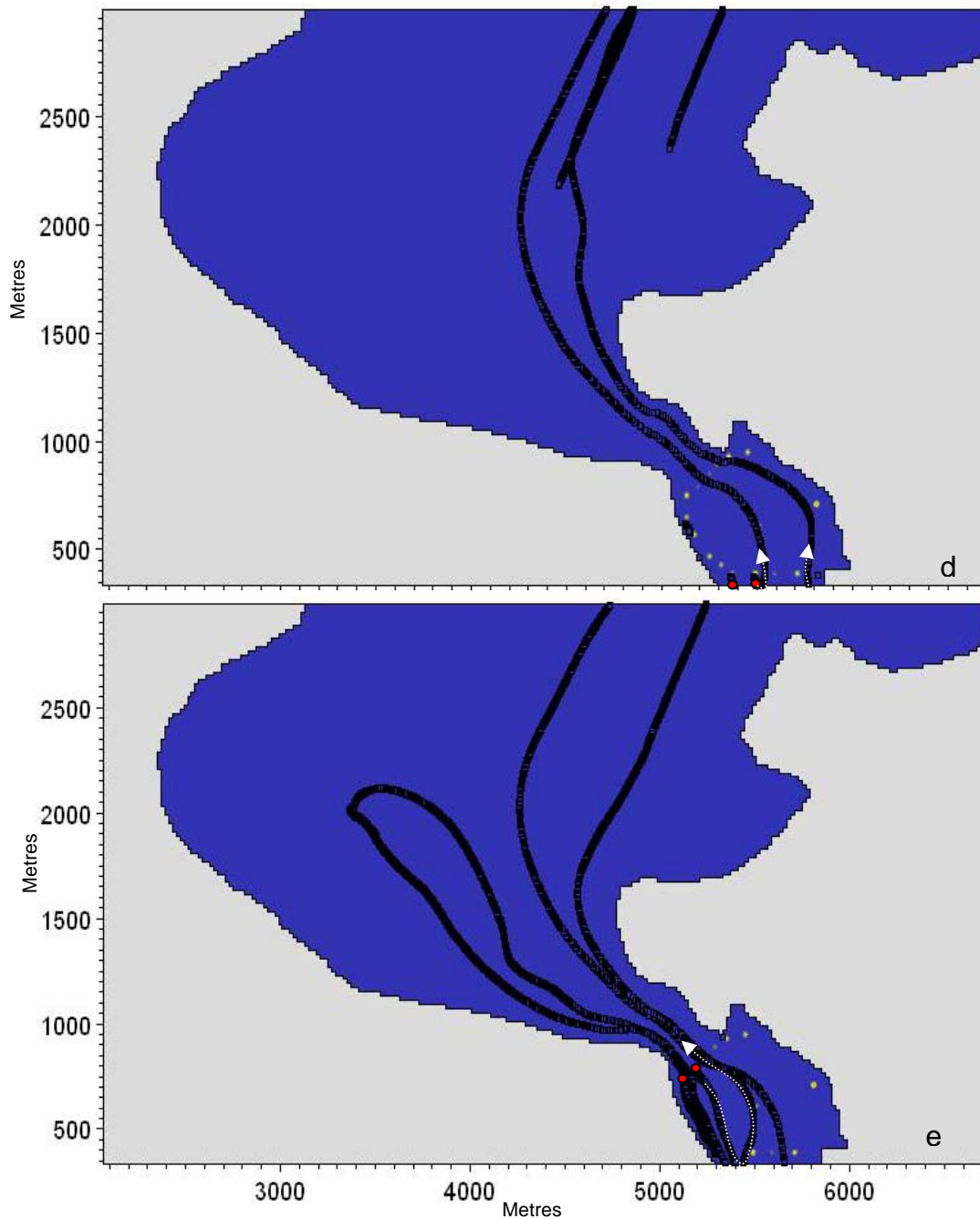


Figure 6.6 Simulated tidally derived suspended particulate matter particle tracks within the Whitianga inlet over a 10 day mean tidal flow period. Solid circles indicate the starting position of each particle. Arrows indicate direction of particle track where two tracks are overlaid.

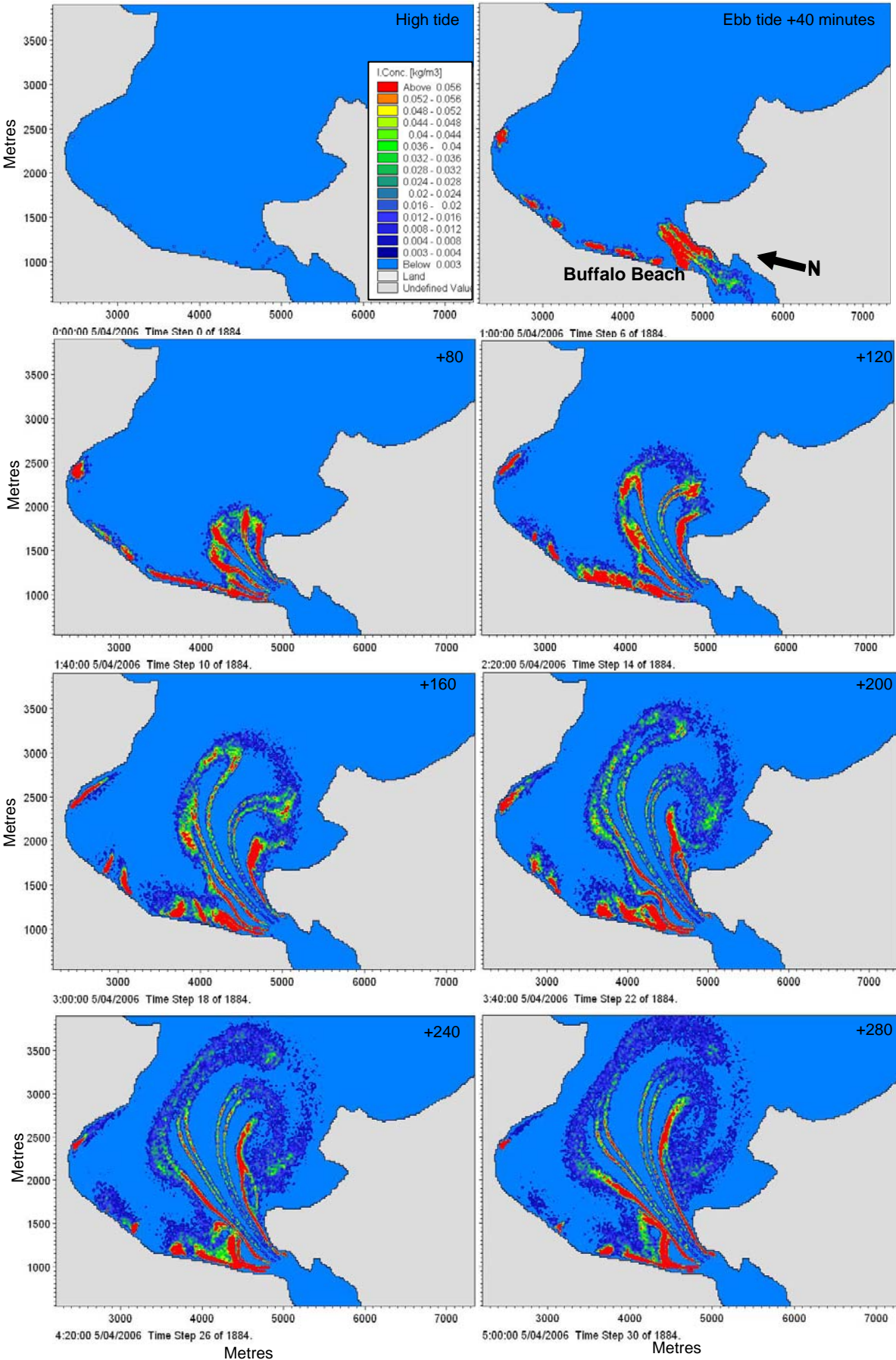
### 6.2.3 Model output – Sediment Dispersal

The simulated tidally-derived sediment transport within Buffalo Bay is largely dominated by the ebb tidal discharge. The sediment dispersal snapshots (Figure 6.7) indicate sediment concentration through the tidal cycle. The highest zones of concentration are on the seaward and landward sides of the ebb tidal discharge from

the inlet. Most particles dispersed from the inlet are transported in either the landward or seaward eddy system. Sediment along Buffalo Beach stays in similar concentrations for the duration of the ebb cycle and on the flood tide.

During the flood tide minimal suspended sediment transport is evident within Buffalo Bay. The concentration of suspended particles gradually declines and the particles moved into the Bay by the previous ebb discharge slowly sink offshore from the mid section of Buffalo Beach. The majority of transport on the flood tide occurs within the inlet with highest sediment concentrations noted in the low velocity areas on the banks of the estuary and on the ebb delta also. Suspended particles along southern Buffalo Beach are gradually pulled south by the flood current towards the inlet.

Some sediment, in low concentrations, is observed past the Wharekaho headland which is a long way for sediment to travel and may be a function of the chosen settling velocity, although the sediment dispersion pattern matches that shown in the 200s aerial photo (Figure 6.18).



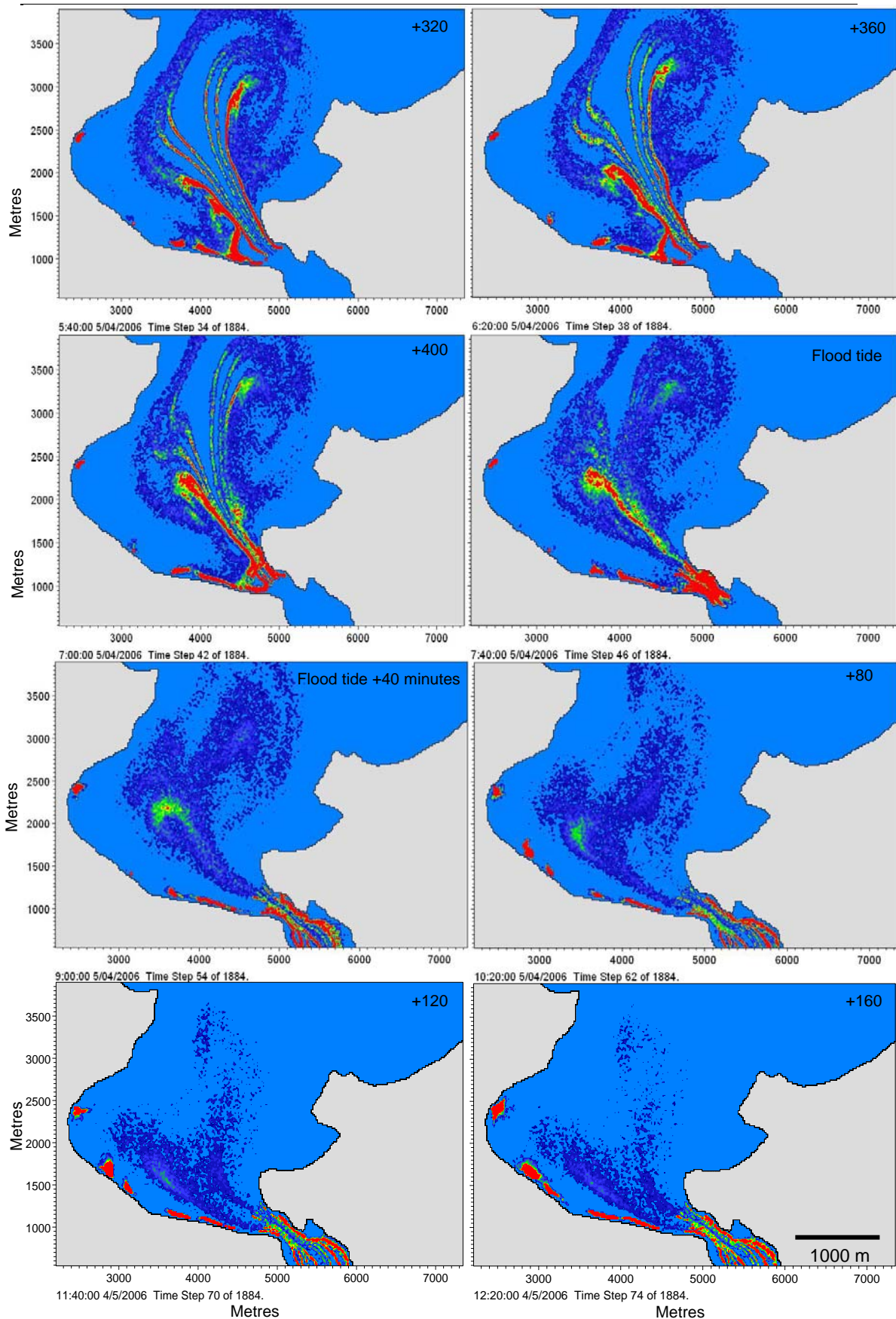


Figure 6.7 Snapshots of the suspended total sediment transport pathways at different stages of the tide within Buffalo Bay, as simulated in the PAP model.

## **6.3 Discussion and Implications of results**

### **6.3.1 Bed level change**

Sediment transport is typically a result of wash load, bed load and suspended load. Wash load is very fine particle transport, bed load is sediment which is in constant contact with the bed, and suspended load is sediment moving without continuous contact with bed due to agitation of fluid turbulence (Fredsoe, 1993). Deposition of suspended and wash load sediment typically occurs in areas of low flow (Figure 6.8) (Hoyal et al., 2003). However the bed load transported out of an inlet is most likely to be deposited adjacent to high velocity areas (Hoyal et al., 2003) (Figure 6.8) such as the boundary between the channel and ebb delta, the inlet gorge or up the estuary. This would explain the pattern of areas of accretion next to areas of erosion within inlet channel in (Figure 6.2) which are moving sand out of the inlet as bedload.

The pattern of alternating deposition and scour in the tidal gorge is suggestive of the presence of sandwaves, although these morphological features are not positively identified in this study. However, it is known that sandwave bedforms strongly affect the flow resistance through changing the bed roughness height (Boothroyd, 1985). Their presence affects the entire flow structure and resulting sediment transport capacity of the flow. Sandwaves typically develop due to a dynamic balance between available sediment, tidal currents and wave energy (Catano-Lopera and Garcia, 2006; Dyer, 1986). The alignment and geometry of bedforms provide a method of determining the direction of net bedload sediment transport particularly for large bedforms as they are less likely to change orientation due to tidal forcing (Fitzgerald et al., 2005).

The simulated tidally-induced average bed level change is minimal in Buffalo Bay compared to within the inlet. This is not consistent with the long-term accretion identified in this area in Chapter 3. However, as the bed level change is only a result of the tidal currents, so the stable condition under tidal flows further suggests the observed erosion in Chapter 3 (Figure 3.12) at northern Buffalo Bay is a result of wave scour and/or down-welling currents, which were not incorporated in this model. The residual tidal current velocity plot (Figure 5.12) indicated a small offshore area of northern Buffalo Bay and the southern section of Ohuka Beach may experience

erosion due to the combination of flood tidal currents and the return flow of the landward eddy during the ebb tide.

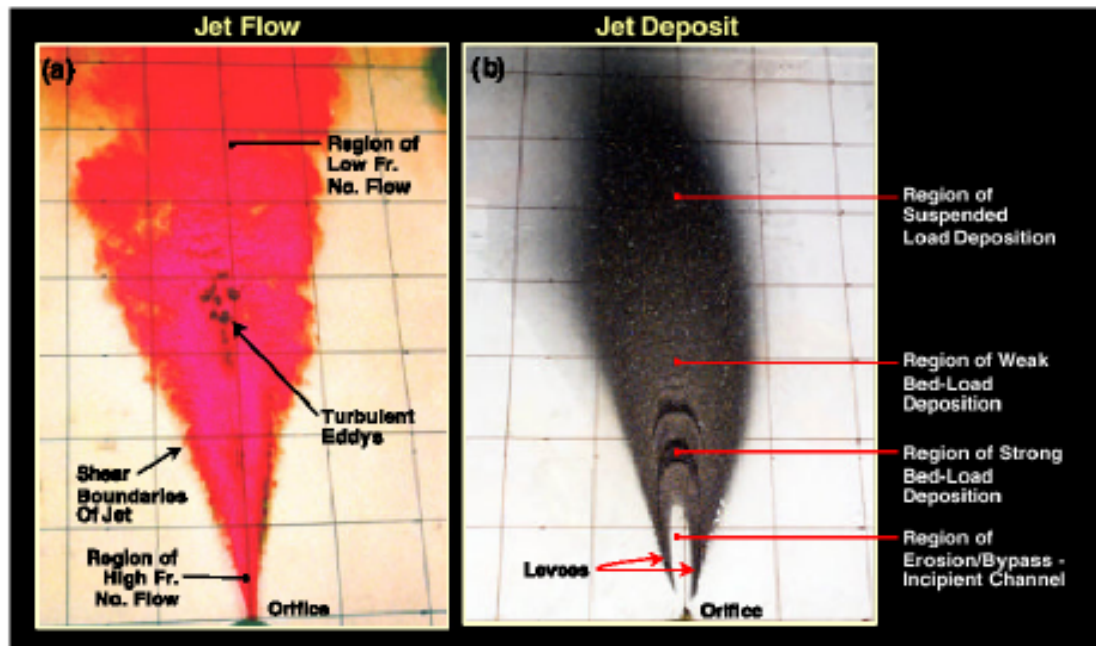


Figure 6.8 The relationship between a) velocity and b) areas of deposition from a wall jet-plume. Source: Hoyal et al., 2003.

### 6.3.2 Sediment transport

The PAP model accounts for suspended and particulate matter that is transported in Buffalo Bay. The sediment transport within Buffalo Bay can be separated into 2 primary zones, the inlet and Buffalo Beach. The inlet has an active and complex sediment transport system whereas along Buffalo Beach sediment is only transported from its original position if it lies along the southern section of the Beach. The results of the sediment transport model show northern Buffalo Beach is almost a closed system, with little interaction with other areas of Buffalo Bay. No sediment is transported into this area and no sediment is moved out by the ebb and flood tides. It is likely the erosion in this area, identified in Chapter 3, is caused by wave scour or wind-induced diabathic transfer alongshore or offshore (down-welling). As established in Chapter 5, wave-induced littoral drift along this section of Buffalo Beach would be minimal due to the variation in wave heights along the beach, and the landward eddy does not affect the northern section of Buffalo Beach either. Therefore sediment eroded from northern Buffalo Beach by wave scour or down-welling, is probably transported either alongshore by the flood tidal currents or offshore when ebb tidal current and down-welling processes combine. The amount

of sediment eroded from here is thus probably not great as it depends on the combination of many processes, but the erosion is pronounced due to the minimal supply of sediment to this section of Buffalo Beach. Particles 1 and 3 in the northern section are dispersed offshore, approximately 200 metres from their source. This indicates that if a breakwater structure was placed in this vicinity, as mentioned in Chapter 5, sediment could be transported out to the breakwater and deposited on the landward side, creating a shallow zone.

The net direction of transport along southern Buffalo Beach is south towards the inlet. This is due to a combination of the ebb tide-generated landward eddy and the flood tide which propagates along Buffalo Beach and into the inlet. Any transport that does exist occurs predominantly with the ebb tide. As identified in Chapter 5, waves provide zones of sediment transport along Buffalo Beach but the amount appears insignificant and within confined areas, propagating tides are the dominant sediment transport mechanism.

Particles within the inlet that did not move far from their source (particles 7, 8 and 16, Figure 6.6(a)), were typically located in areas with low velocity over the ebb and flood cycles (Figure 6.9) which have similar velocity distributions. Particles released in higher velocity areas of the estuary (particles 3, 4, and 13-15 Figure 6.6(a)) do not flow out into Buffalo Bay but move up the estuary and out of the model area. This may be because they are in the direct path of the flood tide. The residual plot (Figure 6.2) shows the inlet is flood dominated so upstream migration would be expected for particles within the inlet.

The remaining particles all exit the estuary and flow into Buffalo Bay. From here they either flow into Mercury Bay (particles 1 and 9 Figure 6.6(b and c)), are deposited in Buffalo Bay by the seaward eddy (particles 11 and 12 Figure 6.6(d)), or are returned to the inlet (particles 10 and 2 Figure 6.6(b and c)). These particles are all in areas where the current velocity is moderate.

Some of the particles are moved up the estuary by the flood tide and possibly moved into faster flowing areas, so that when the ebb tidal flow commences these particles are carried out of the estuary (particles 5 and 6). Therefore although most particles

are transported a small distance by the flood tide, they tend to travel further with the ebb tide.

The flood dominance in the inner inlet, and the observation that particles enter the inlet on both the flood and ebb tide, suggest long term infilling of the estuary.

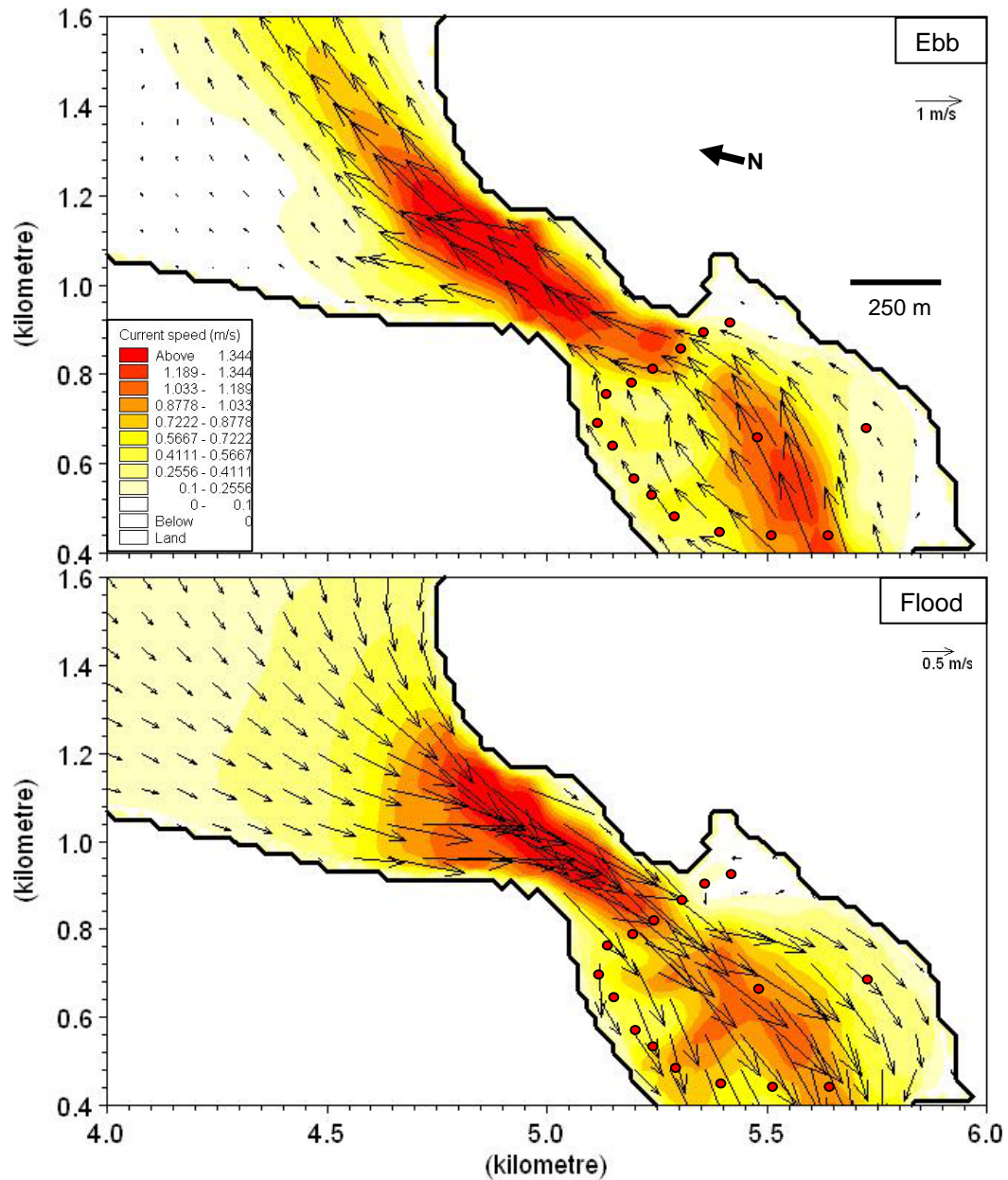


Figure 6.9 The maximum speed and subsequent direction of flow within the Whitianga estuary for the flood and ebb tide. Solid circles indicate position of particles released in the PAP model.

Dredged material (~60,000 m<sup>3</sup>) from the Whitianga marina development was placed on the dunes near Taputapuatea Stream in 1994, and in 2002 the wharf beach was

dredged and spoil was deposited on Ohuka Beach dunes (Cooper, 2003). Similarly sections of Ohuka have been renourished recently with dredged material from the canal development in the upper estuary reaches. Approximately 10,000 m<sup>3</sup> of sand was placed at Ohuka Beach 2004 (V. Pickett, pers. comm., 2006). There is likely to be two more similar renourishments in this section before 2008 so the particle tracking can provide scientific-based knowledge and an approximation of where this sediment may be transported. The 2004 renourishment has occurred around particles 1 and 2 (Figure 6.4). Results from the sediment transport modelling in this study suggest sediment deposited on the beach face here would be relatively stationary, only being transported away when non-tidal processes combine to move it offshore, or when scour occurs in small amounts due to the flood tidal and landward eddy currents, as indicated by the residual plot in Chapter 5 (Figure 5.12). The low rate of sediment transport away from this section of Buffalo Beach makes it the ideal location for renourishment. If enough sediment was placed here it may counteract the amount removed by wind and wave induced processes and the beach may start to accrete. In contrast, the eroding section of southern Buffalo Beach (at the seawall) would not benefit so much from renourishment as the sediment deposited here would soon be transported down toward the inlet and the wedge of sand linking to the ebb tidal delta.

The growth of the southern extremity of Buffalo Beach is likely to be due to a combination of the mean southward current direction towards the inlet, and the wave shelter provided by the ebb delta. One of the simulated sediment transport pathways indicate that sediment is moving around in a continuous motion from the inlet, out into Buffalo Bay and then back around to be deposited on the southern tip of Buffalo Beach. The channel marginal bar of the ebb delta acts as a groin or headland, trapping sediment on the up drift side and widening this section of beach. The delta can also trap sediment from within the inlet on an ebb tide because the ebb flow decelerates as it moves over the ebb delta from the inlet, and sediment therefore settles out. If left to continue, the net southwards drift and expanding wave protection will likely result in the further widening of the southern tip (Figure 6.10a), and the southern section of Buffalo Beach. This may also cause the inlet channel to become narrower, and it may realign against the adjacent hard rock shoreline of Whakapenui Point, as it did between 1938 and 1995 due to the growth of the ebb delta (Figure 6.10b).

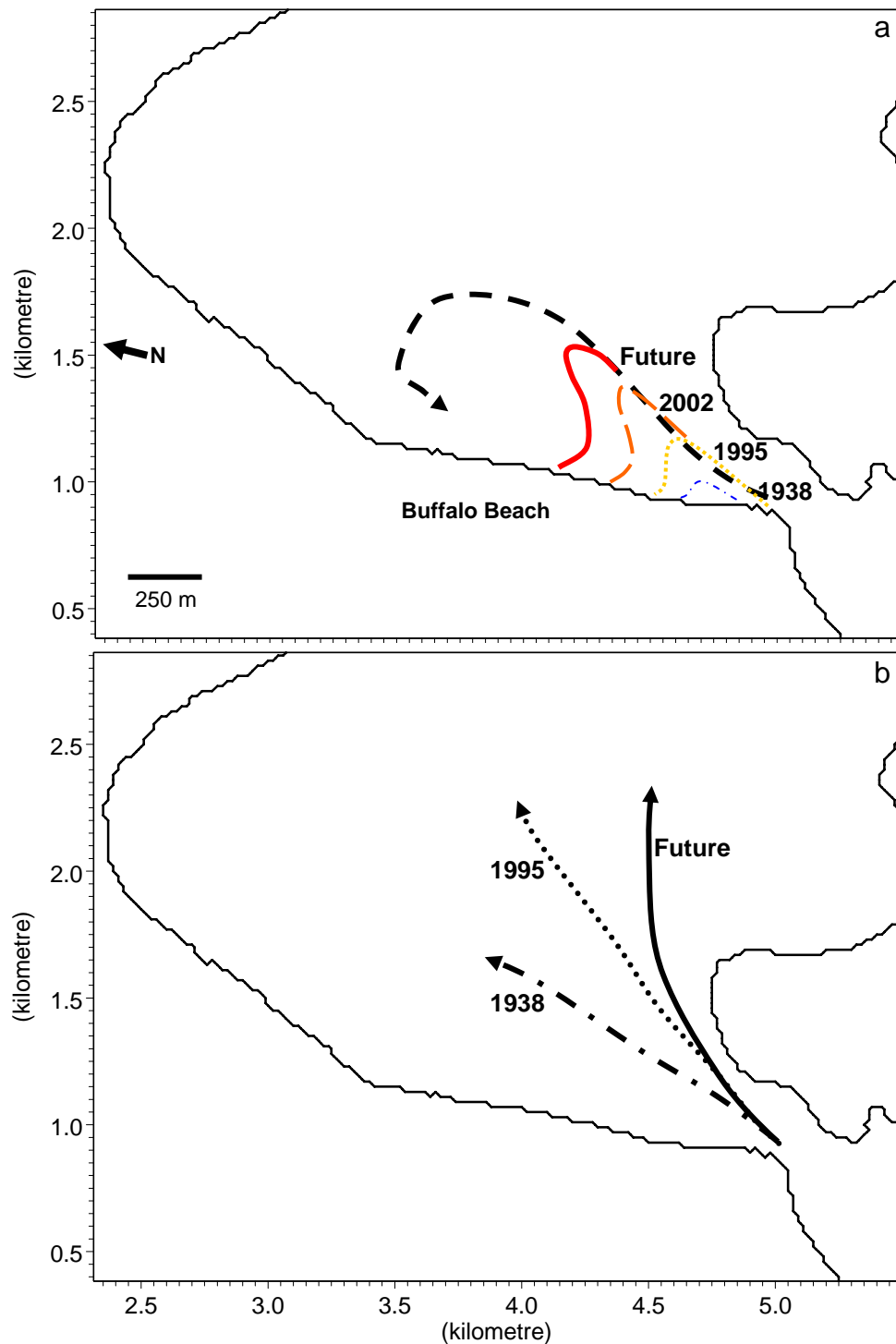


Figure 6.10 The probable progression of a) the ebb delta shape and size and b) the tidal channel orientation. A. (--) indicates the approximate current ebb delta location, based on 2002 and 2005 aerial photos. (••) indicates the approximate 1995 ebb delta position based on 1990 and 1995 aerial photos and 1995 hydrographic soundings. (-•) indicates the approximate ebb delta position in 1938 based on the 1944 aerial photos and 1938 hydrographic soundings. The solid line indicates the approximate future shape of the ebb delta in 10 years if left to evolve naturally. The arrow shows direction of sediment transport in this section of Buffalo Bay. B. (-•) indicates the tidal channel position in 1938 based on hydrographic soundings. (••) indicates the approximate orientation of the tidal channel in 1995 based on the 1995 and 1979 hydrographic surveys. The solid line indicates the approximate future tidal channel realignment if ebb delta growth continues.

*Remediation of ebb delta growth*

The continued growth of the ebb delta causes navigation problems within the inlet and decreases the gorge cross sectional area and will eventually choke up the tidal inlet. Two initial remediation options to prevent further accretion of the ebb delta into the inlet channel may be considered. Firstly the tip of the ebb delta could be dredged to maintain its current shape and prevent further accretion on the southern tip of Buffalo Beach without significantly altering the hydrodynamics in this area. Detailed soundings of the present-day ebb delta shape would be required before dredging could be carried out to ascertain the location of the tip of the ebb delta, where dredging should be concentrated. Dredging would be continuous, occurring probably every 2-3 years.

The second option involves using a hard structure to train the flow out of the inlet and prevent further accretion of the ebb delta into the inlet channel. Conceptually, a rounded groin could be installed, following the shape of the ebb delta (Figure 6.11 (1 and 2)). The placement of a groin here was previously suggested by Raudkivi (1981) when the Whitianga marina was designed. The groin was to provide a southern headland to increase stability along southern Buffalo Beach. The groin was not installed due to concerns raised by many parties about factors such as tsunami hazard, previous groin destruction in the vicinity, and the likeliness the groin may increase erosion of the beach.

However, using the morphodynamic information available now for the inlet, the groin could be established to ensure ebb currents exiting the estuary flowed out into Buffalo Bay and not onto the ebb delta where suspended load may be deposited. Similarly sand deposited on the ebb delta by the landward eddy system, flood tidal currents and littoral drift would not add to the growth of the ebb delta towards Whakapenui Point, and would instead result in ebb delta growth concentrated on the southern end of Buffalo Beach.

Further particle tracking modelling was carried out to provide an indication of the effect the groin would have to sediment transport pathways, namely the landward eddy system, and flood currents along Buffalo Beach as flood tide currents may become trapped in the lee of the groin until the ebb delta has filled in this space.

Two shapes were trialled with the first groin following the shape and the length of the ebb delta perimeter. The second groin configuration is longer and has a hook on the seaward end, orientated north west. This would ideally stop eddy formation around the end of the groin which could cause accretion in this area.

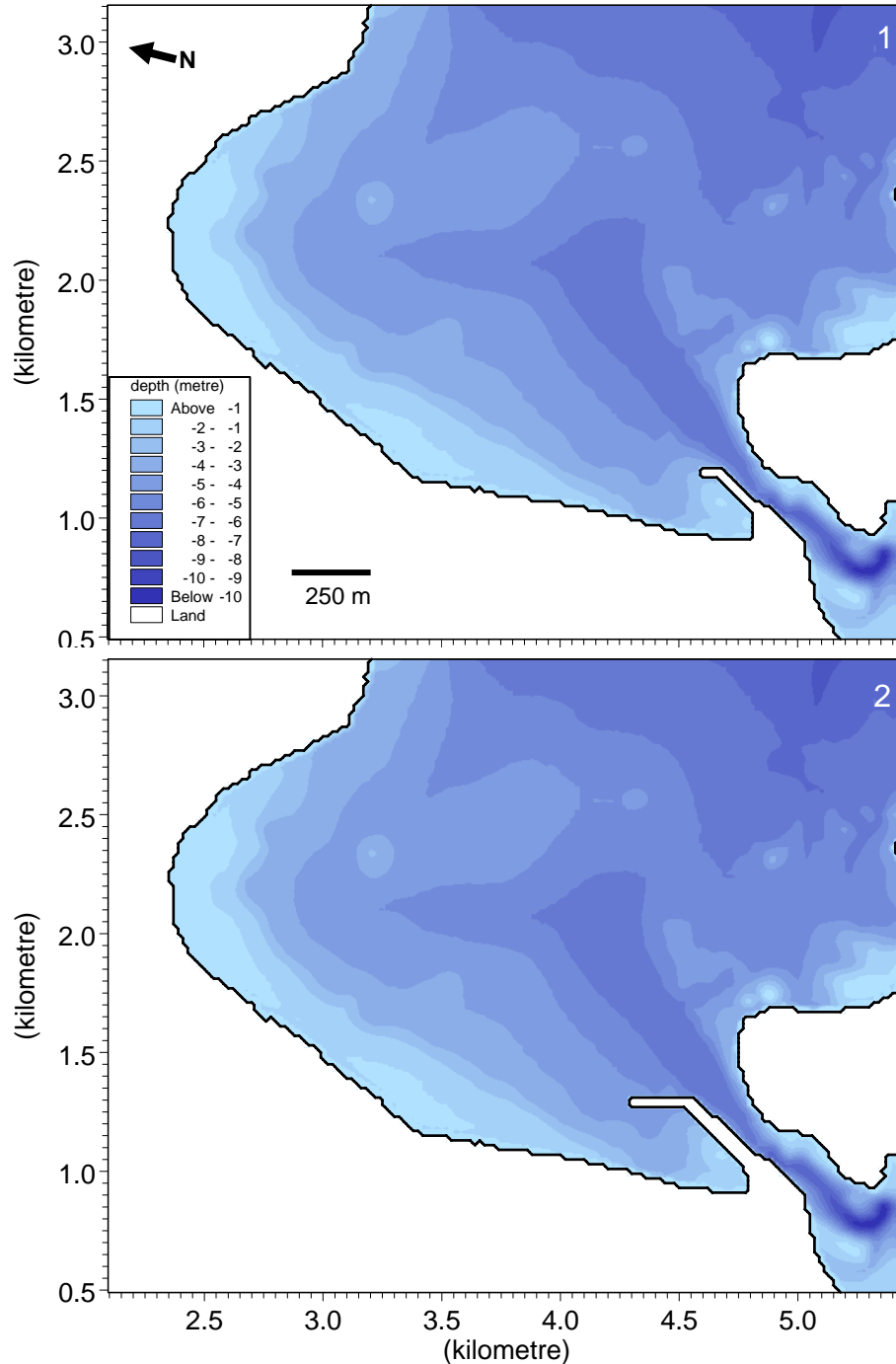


Figure 6.11 The two possible groin shape options (1 and 2), which were modelled to establish their effect on Buffalo Bay hydrodynamics.

Before the sediment transport pathways could be established, the hydrodynamics were modelled using the same model inputs as the HD model in Chapter 5.

Snapshots taken during the ebb and flood tide show that groin option 1 induces a small eddy system around the seaward end of the groin on the ebb tide. The path of the flood tide is not altered considerably, with a low velocity zone forming landward of the groin.

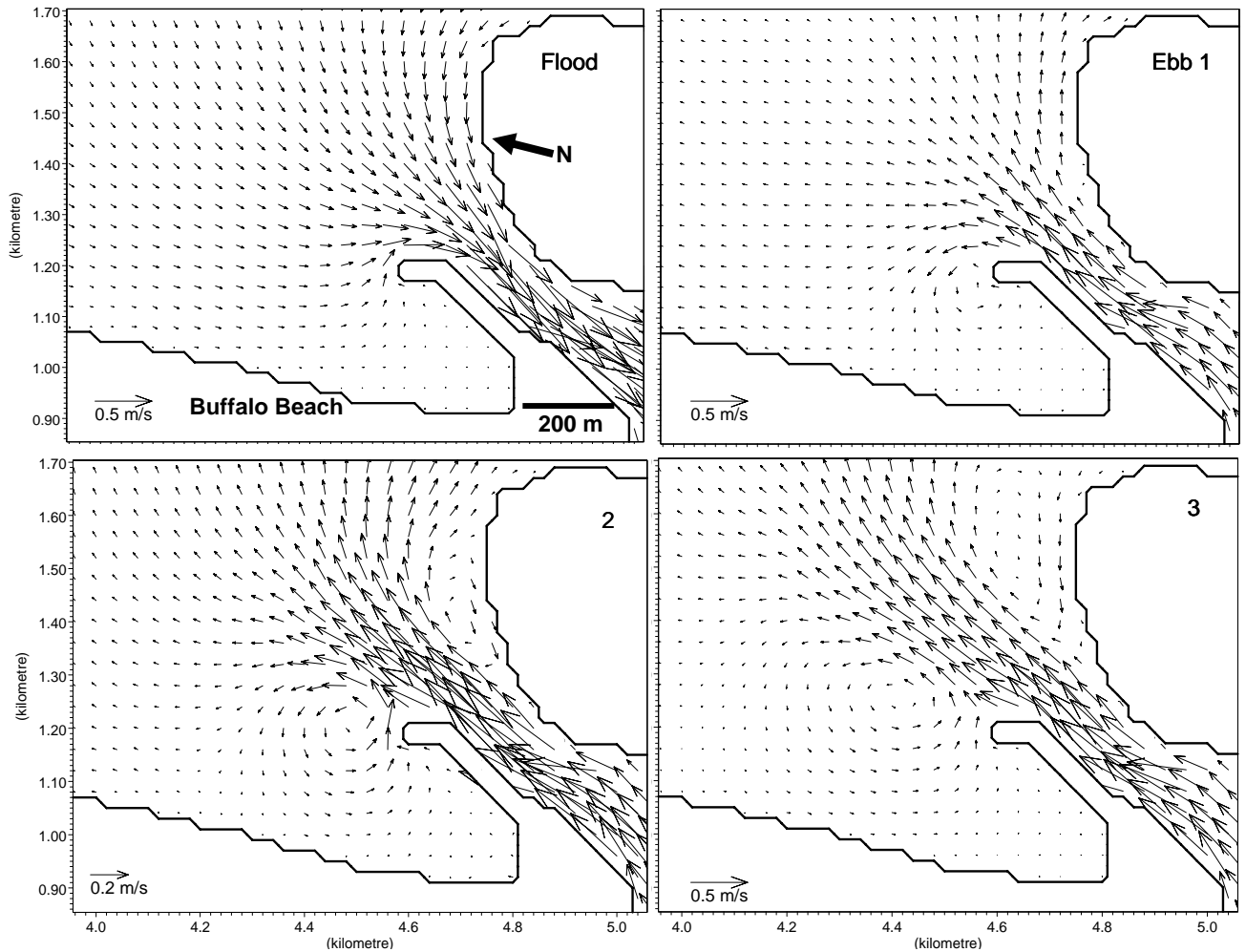


Figure 6.12 The current speed and direction around groin option 1 at the Whitianga inlet.

Groin option 2 extends further into Buffalo Bay. The hook on the seaward end dampens the eddy seen in groin option 1, although a small eddy system still appears to develop with the ebb tide. The flood tide follows a similar path to the flood tide in Figure 6.12.

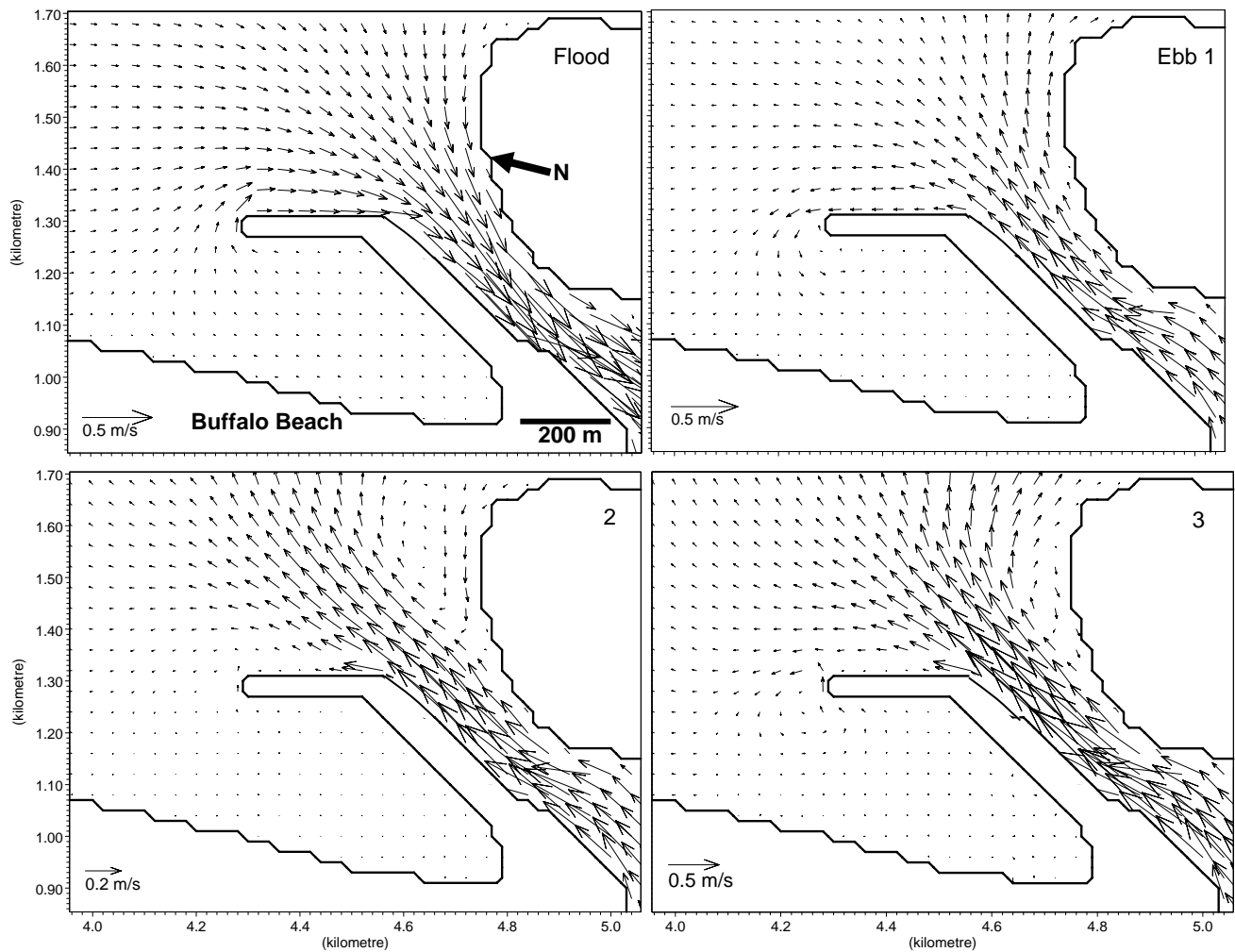


Figure 6.13 The current speed and direction around groin option 2 at the Whitianga inlet.

The sediment concentration patterns show groin option 1 creates similar sediment transport patterns as seen in Figure 6.7, and sediment is dispersed evenly into southern Buffalo Bay. The zone of highest sediment concentration on the landward side of the inlet is reduced and moved seaward with groin option 1, when compared to Figure 6.7. Groin option 2 results in higher sediment concentration (Figure 6.15) near southern Buffalo Beach. The area of highest landward sediment concentration in Figure 6.15 is larger than in Figure 6.14 with groin option 1, and is located closer to the beach.

Sediment on northern Buffalo Beach and in northern Buffalo Bay (Figure 6.15) does not move far from the source with either groin option, illustrating a small offshore tendency (~200 m), as seen in Figure 6.7.

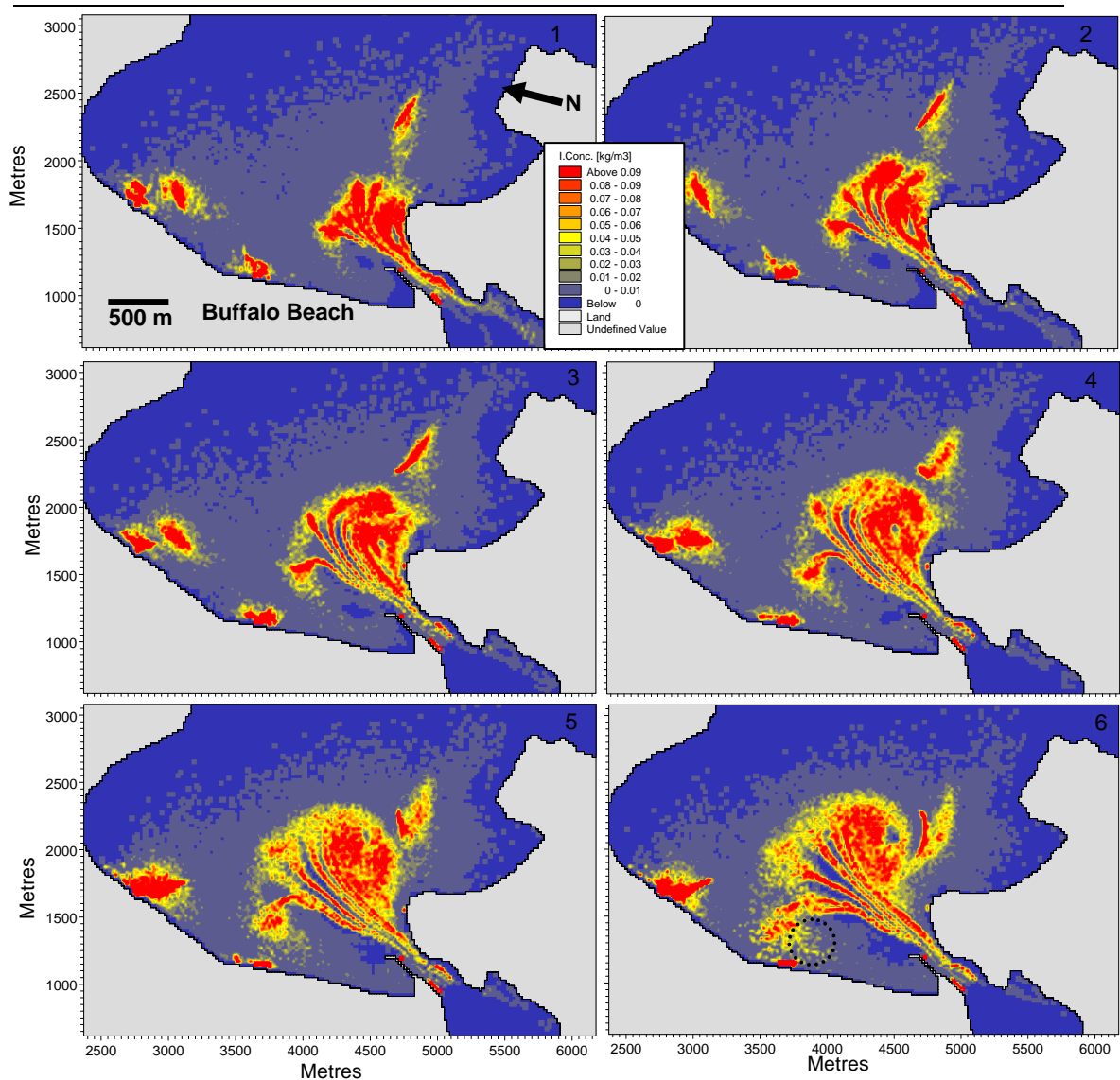


Figure 6.14 Snapshots of the suspended sediment transport pathways at different stages of the tide within Buffalo Bay using groin option 1, as calculated in the PAP model. Dashed oval on snapshot 6 shows the area of highest sediment concentration on the landward side of the groin.

Particle tracks were modelled (Figure 6.16) using the same grid co-ordinates used in section 6.2.2. Particles released on the eastern side of the inlet entrance, near Whakapenui Point, follow the same tracks as seen in Figures 6.4 and 6.6 for both groin designs. Particles on the western side of the inlet entrance, near the proposed groin (particle 2 in Figure 6.16), move out into Buffalo Bay then back into the inlet with groin option 1. Particles released near groin option 2 flow out into Buffalo Bay also but then move south along Buffalo Beach in the landward eddy system with groin option 2. The particle circulates in the landward eddy and is likely deposited in the middle of Buffalo Bay, north of the groin.

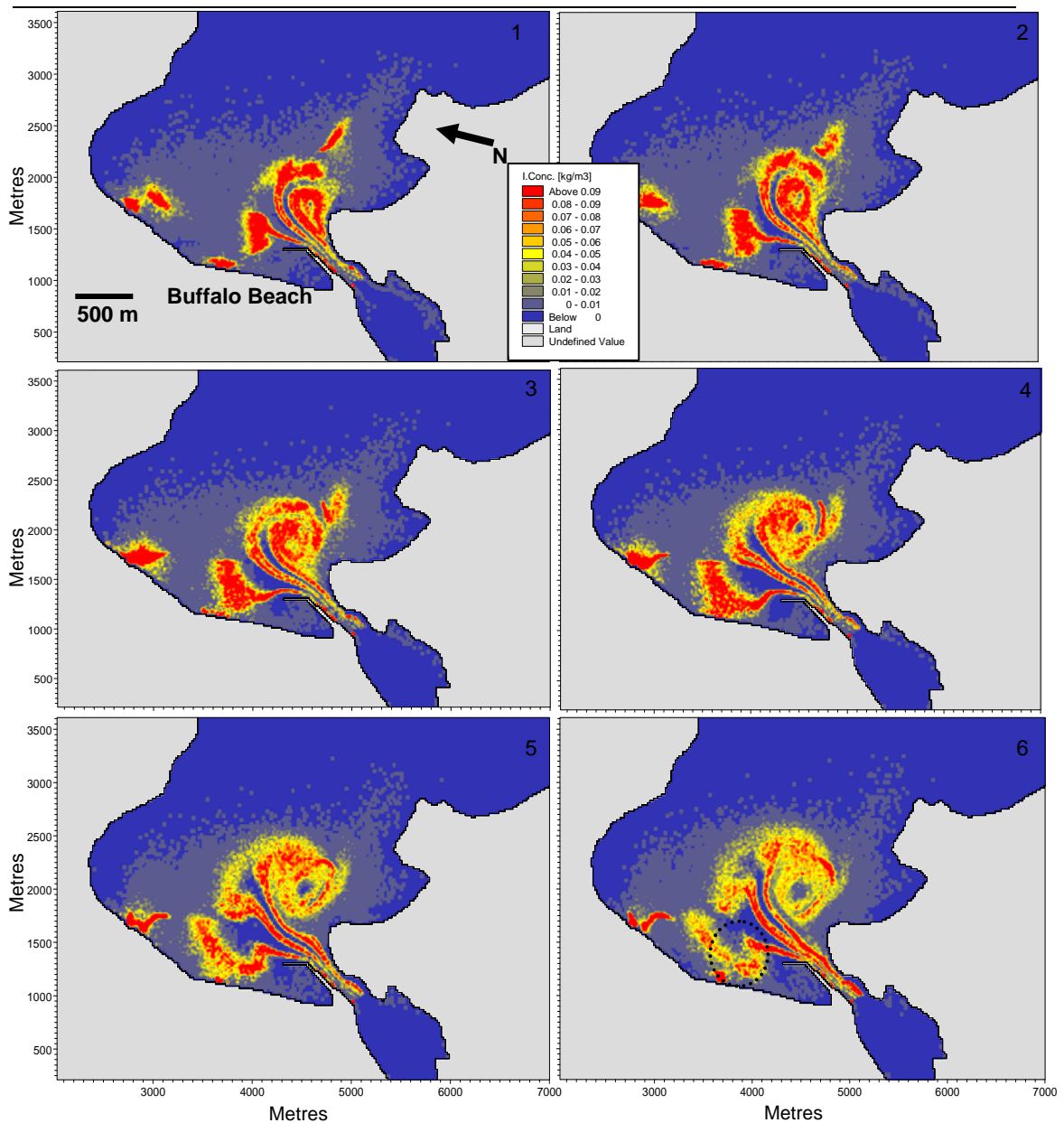


Figure 6.15 Snapshots of the suspended sediment transport pathways at different stages of the tide within Buffalo Bay using groin option 2, as calculated in the PAP model. Dashed oval on snapshot 6 shows the area of highest sediment concentration on the landward side of the groin.

Particles released on southern Buffalo Beach (particle 1 in Figure 6.16) are transported south along Buffalo Beach into the inlet and then out into Buffalo Bay with groin option 2, but do not move far with groin option 1. This is most likely due to the extension of the landward eddy caused by groin option 2, which forces high sediment concentrations closer to the adjacent beach (Figure 6.15) and closer to the position of particle 1. Thus particle 1 is easily transported south along Buffalo Beach. This may suggest that groin option 2 will accelerate accretion behind the

groin with sediment from further up Buffalo Beach included in the landward eddy return current.

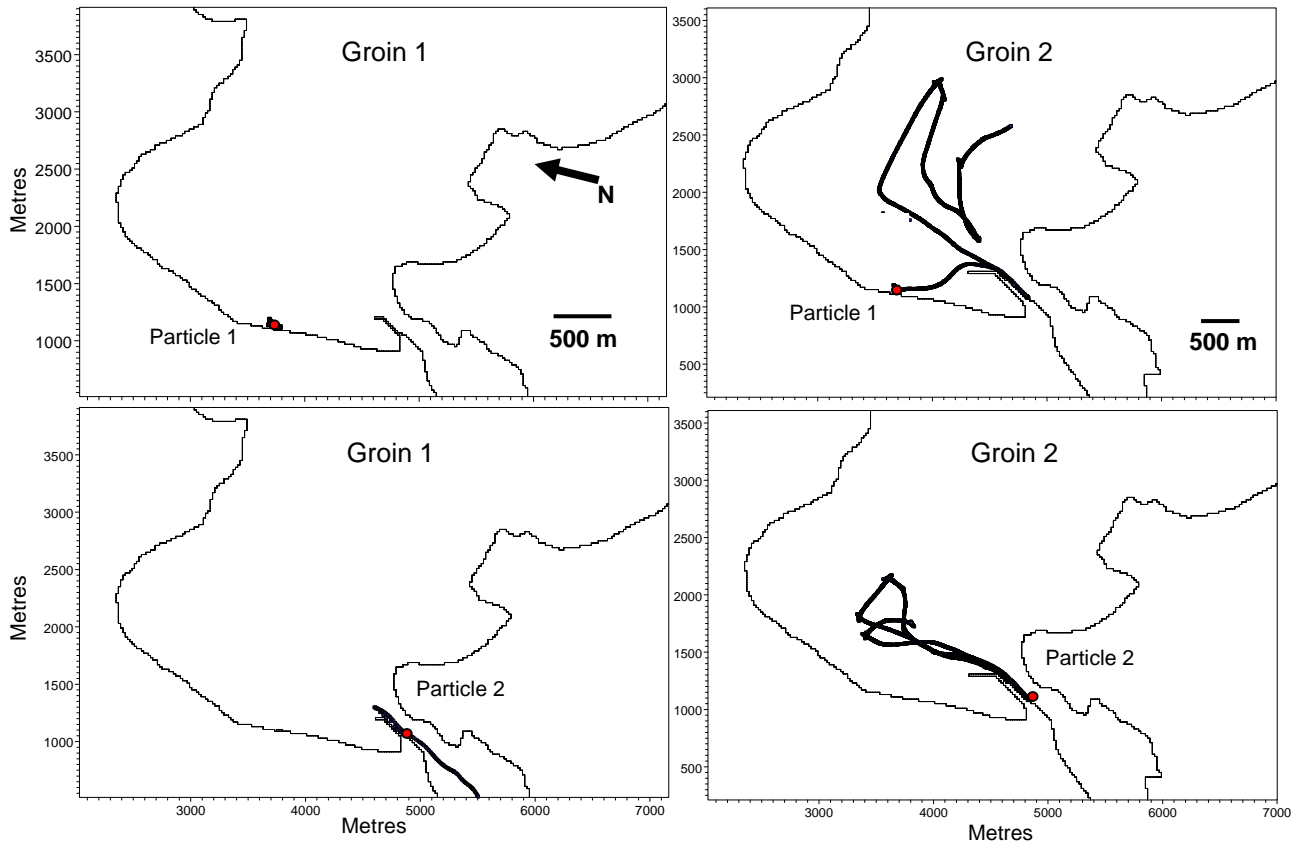


Figure 6.16 Snapshots of the particle tracks with sediment released within the inlet gorge and along Buffalo Beach for groin options 1 and 2.

Groin option 1 results in similar sediment transport pathways as seen in section 6.2.2 with no groin. The eddy that forms near the tip of the groin does not appear to induce high sediment concentrations or deposition. The zone of highest sediment concentration on the landward side of the ebb jet is moved seaward and offshore, although the particle tracks indicate groin option 1 may result in more accumulation within the inlet. In comparison, groin option 2 does not produce an obvious eddy near the tip but does cause higher sediment concentrations along the adjacent beach. The particle tracks indicate particles in suspension in the inlet gorge are likely to be deposited in Buffalo Bay, accelerating accretion offshore. Therefore groin option 1 would be a preferred configuration of the two groin options trialled, in order to train the ebb currents exiting the Whitianga inlet but create minimal disturbance to the hydrodynamic behaviour of the inlet and Buffalo Bay.

A similar groin was installed at Ti Point, Omaha in the late 1970's in order to stabilise the migrating Mangatawhiri Spit which was assumed to be influencing the tidal flow direction in Whangateau Harbour (Beca Carter Hollings and Ferner Ltd, 1976). The spit had experienced accelerated erosion since 1953 (Dames and Moore, 1977). The curved groin extends 570 m in a shape similar to that of the natural spit shape and has successfully stabilised the previously-eroding spit. Similar systems have also been implemented in the Hillsboro and Fripp Island Inlets internationally (Dames and Moore, 1977).

The groin options investigated here provide only an approximate indication as to likely hydrodynamic behaviour. Prior to further consideration of such a solution, detailed bathymetry data and intensive high resolution modelling of hydrodynamic processes within the inlet area and Buffalo Bay would need to be carried out, to ascertain various design parameters, such as groin length and height and specifically address the wave energy in the groin vicinity and the structures effect on wave behaviour.

#### *Remediation of eroding southern section*

If left to naturally evolve, eventually the ebb delta will grow out in front of the adjacent beach and protect this eroding area from large waves, which typically induce erosion here. This would occur over a long time scale, creating problems within the inlet. However, it is possible the sediment moved south along Buffalo Beach in the landward eddy system is enough to warrant replacing the existing seawall with the installation of a groin field or similar structures to counteract the erosion and seawall scour occurring in this section now, in order to increase the amenity value of the beach. Groin fields were installed along this section of beach in the 1960's but either disintegrated or became buried. The transport pattern identified in this study makes the latter theory possible but still unlikely. The high level of wave convergence at this section of Buffalo Beach is the probable cause of the destruction of the groin field. Groin fields are not preferable where wave energy is high (Headland et al., 2000), and therefore at southern Buffalo Beach, where wave energy is moderate-high (based on Chapter 5), the combination of groin field and offshore breakwater to dissipate wave energy at this section of the beach is a possible option. However, the placement of the breakwater would likely cause

navigation issues in the nearby inlet so an alternative protection method may be the installment of artificial headlands (Figure 6.17).

Artificial headlands are an extension of groins but their main purpose is to reduce the amount of wave energy reaching a beach by providing gradients in wave energy that promote sediment deposition between headlands (Headland, et al., 2000). A singular headland can be used to trap sediment but commonly two headlands or a series of headlands are used to form pocket beaches between them. A headland series may utilise natural headlands in the area also and work with them. The addition of renourishment material on the section of beach between the headlands would also act to stabilise and protect this section of Buffalo Beach.



Figure 6.17 An example of an artificial headland from the Kashima Coast Japan (from Committee of coastal engineering and Japan Society civil engineering, 1994).

There are examples of artificial headlands internationally and locally. In 1988 plans were made to erect a series of headland structure on the severely eroding shore of Te Atatu, Peninsula in Waitakare. Headlands were decided as the best method to protect the coast as they would ultimately use natural beaches to protect coast and restore the natural, eroded headlands along the coast. The headlands caused little construction disruption and the added benefit of high community amenity (White, 1998). Recently a series of natural looking headlands were installed at Kohimaramara Beach by Auckland City Council and provide an aesthetically pleasing but functional coastal protection method (Priestly, 2006) (for more details see issue 33 of NZCS Coastal News).

Artificial headlands act as traps where they don't provide storm protection but rather help to build up the beach to decrease the extent of storm damage (Headland et al., 2000). However, when design conditions are not thoroughly examined, and the specific dimensions and consequences of such structures are not suited to the natural surroundings, these structures can result in erosion of the shoreline that they have been built to protect. If the regional council or Whitianga community decide to update the existing seawall at the southern end of Buffalo Beach to a more robust coastal protection method, the author suggests the use of artificial headlands in conjunction with renourishment be thoroughly investigated.

### *6.3.3 Sediment Concentration*

The time series of sediment concentration shows the development of mushroom shaped plume exiting the harbour over an ebb cycle. The plume gradually moves into Mercury Bay as it gets larger (Figure 6.18) and compares well with aerial photos of the area taken on an ebb tide. The shape and path of this feature follows that of the seaward eddy system. Eddy systems are a known cause of coastal sedimentation. The sedimentation occurs as the centre of the eddy experiences low velocity whereas the outside of the eddy has higher velocity. The gradient in velocity causes the particles to be sorted and the centripetal acceleration pushes them towards the middle where they sink, according to their settling velocity (Zimmerman, 1981). Therefore as the eddy moves north, the zone of sediment accretion moves also, following the centre of the eddy. The path of the centre of the eddy (Figure 5.13) therefore identifies the zone of expected accretion. This zone matches the isolated shallow zone identified in the Notice to Mariners (LINZ, 2005) and explained in Chapter 1.

There is no detailed bathymetry available for the new shallow zone so the centre path of the seaward eddy cannot be compared with the orientation, shape and size of the isolated shallow zone. However the literature suggests the eddy system will cause accretion and it is likely the accretion here will continue to form a shallow sandbar that will create increasing navigation and safety issues.

Accretion in the centre of the landward eddy has not been reported by the local populous, but this is probably because this area of Buffalo Bay is not as heavily used by boat traffic. The accretion caused by the landward eddy is probably not as

pronounced because the centre of the eddy moves back down towards the inlet as the ebb tide weakens. The aerial photo does not show the landward eddy but it is possible the landward eddy had decayed or had not formed when the photo was taken as it is only evident for ~1.5 hours of the ebb tide. The accretion of the southern tip of Buffalo Bay, combined with the possible accretion in the centre of the eddy will result in a large shallow zone offshore from the southern section of Buffalo Beach.

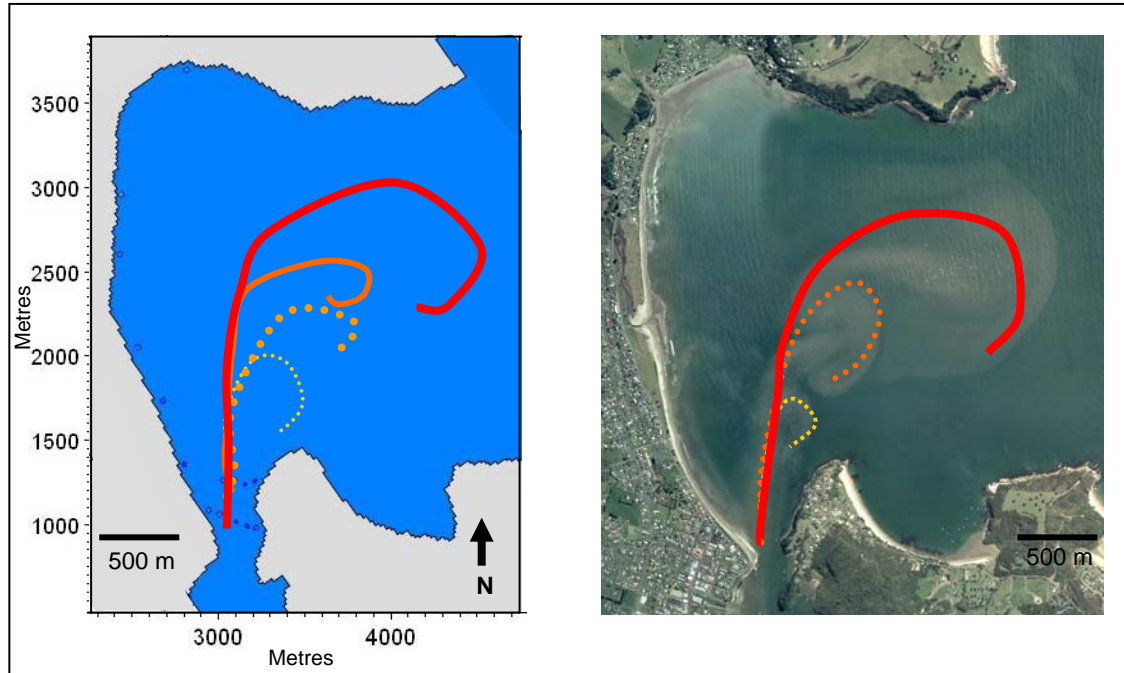


Figure 6.18 The mapped pathway of the model-simulated sediment dispersal over an ebb tidal cycle matched with the 2002 aerial photo. The more solid the line, the more time in the ebb tidal cycle has elapsed.

## 6.4 Conclusion

- The primary area of tidally-derived bed level change in Buffalo Bay is within the inlet. Bedforms resembling sandwaves are evident in the inlet gorge, indicating a bed load transport mechanism. The ebb delta appears to have formed as a result of ebb and flood tidal deposits.
- Sediment transport in Buffalo Bay is governed by the ebb tidal discharge which creates landward and seaward eddy systems. It is highly likely the two eddy systems cause accretion in their centres which migrate with the ebb tide.
- Sediment within the inlet is transported according to the velocity distribution. Faster flowing areas are typically flood dominated and therefore

predominantly move sediment up the estuary, or move in close proximity of their source. Sediment in zones of moderate currents move into Buffalo Bay and are then transported back towards the inlet via the landward or seaward eddy. Some particles are transported out into Mercury Bay.

- Along Buffalo Beach, not much sediment is moved by the tidally generated currents. Only sediment in the mid-southern section is transported in the net tidal current south towards the inlet. Renourishment material and dredge spoil should ideally be placed in the northern section of Buffalo Bay which is essentially a closed system, receiving and providing minimal sediment to Buffalo Bay and Buffalo Beach.
- The southern tip of Buffalo Beach is accreting rapidly due to the ebb delta's role as a natural groin, trapping sediments on both ebb and flood tides. The modelling suggests that the ebb delta will likely continue to grow and cause the southern section to widen and inlet channel to narrow and migrate further north east. Dredging of the ebb delta tip and the installment of a rounded groin such as Figure 6.11(1) are two options that may prevent this from happening.

## ***Chapter Seven – Conclusions***

---

The Whitianga tidal inlet is used by many recreational and commercial vessels. In recent decades, subdivision intensification within Mercury Bay has seen this number rise. In September 2005 shallow zones within the inlet were identified and began to create difficulties for larger vessels, and treacherous conditions in times of high swell.

The primary aim of this study is to investigate the sedimentation processes within Buffalo Bay, particularly within and adjacent to the Whitianga inlet and to ascertain the cause of the shoaling of the Whitianga tidal inlet and the reasons for shoaling around Pandora Rock. Specific aims of the study were to:

- Identify morphological change around the inlet and adjacent shoreline,
- Establish the sediment transport pathways within Buffalo Bay,
- Investigate wave behaviour within Buffalo Bay: and
- Estimate future inlet morphology.

This chapter addresses these specific issues and provided suggestions for further research in the Whitianga/ Buffalo Bay area.

### ***7.1 Physical Setting***

The physical setting of the study area produces a naturally high sedimentation rate. This is due to a steep land and soft rock catchment which experiences frequent intense rain events. The sediment within Buffalo Bay is predominantly fine sand, of fluvial origin, but some mud deposits are evident in northern Buffalo Bay, which are attributed to stream input. Coarse sand and a shell lag are apparent in the Whitianga tidal inlet channel.

The sedimentation rate within the estuary catchment has been exacerbated in the last century due to changes in land use, beginning with Kauri milling in the late 1800's.

Sediment transport within Buffalo Bay is dominated by the ebb tidal discharge from the inlet, and the net littoral drift direction south along Buffalo Beach. Swell direction ranges from north to southeast and wave heights range from about 0.9 metres in fair weather conditions to about 5 metres in storm conditions. Wave refraction and diffraction behaviour is controlled by the shape and bathymetry of Mercury Bay.

## **7.2 Morphological Change**

The Whitianga tidal inlet receives low wave energy due to its position within Mercury Bay, and the adjacent Whakapenui Point headland. The inlet is evidently infilling in the channel due to a decreasing tidal prism driving reduced peak current flows. Comparison of aerial photos show the southern end of Buffalo Beach immediately adjacent to the inlet is the widest section of Buffalo Beach. Mid and northern sections have remained relatively stable. The aerial photo comparison demonstrates a growth of the ebb delta above chart datum between 1990 and 2002 from 0.01 km<sup>2</sup> in 1990 to 0.04km<sup>2</sup> in 2002.

Analysis of the historic hydrographic data indicates that the bathymetry of Buffalo Bay shallowed up to 4 metres in places between 1938 and 1979. Average vertical sedimentation rates of up to 10 cm y<sup>-1</sup> were calculated in the inlet ebb discharge channel between 1938 and 1979. In contrast, the primary eroded area within Buffalo Bay between 1938 and 1979 occurred in northern Buffalo Bay and along northern Ohuka Beach. This erosion can be attributed to a combination of wave attack, wind induced down-welling currents and the southwards net littoral drift transporting sediment away from northern Buffalo Bay.

Average vertical sedimentation rates of up to 25 cm y<sup>-1</sup> were calculated in the ebb discharge channel and ebb delta area between 1979 and 1995. During this time the ebb jet discharge channel migrated northeast towards Whakapenui Point. Sediment accretion on the ebb delta is attributed to the combination of southwards net littoral drift along Buffalo Beach, and sediment input from the Whitianga estuary catchment. The primary cause of the channel re-orientation and shallowing is due to the growth

of the ebb delta which subsequently forces the ebb discharge channel to gradually migrate northeast against the rocky shoreline of Whakapenui Point.

### **7.3 Buffalo Bay Hydrodynamic Monitoring**

Tidal, wave, and current behaviour were all investigated based upon field deployment of recording instruments at several sites. The  $M_2$  tide dominated at all instrument sites. The water level elevation at the wharf and Buffalo Bay sites is primarily represented by the tidal elevation. Tidal currents were dominant at the wharf site with average speeds of  $0.56 \text{ m s}^{-1}$  during the monitoring period able to transport sediment. The Buffalo Bay site experienced weak currents overall during the monitoring period with average current speeds of  $0.06 \text{ m s}^{-1}$ , which are too slow to transport sediment, unless wave induced currents caused by large swell events combine with tidal currents. Wave heights were insignificant at the wharf site and the Buffalo Bay site experienced average wave heights of 0.3 metres, predominantly from the east during the monitoring period.

Sediment trap data collected at four sites indicated Buffalo Bay and the entrance sites trapped the most sediment and possessed similar textural characteristics. Average grain sizes obtained in the traps at the Buffalo Bay, entrance and river sites were  $\sim 0.14\text{-}0.15 \text{ mm}$ . Sediment in the entrance trap most likely originated from the estuary whereas sediment in the Buffalo Bay site trap is likely to represent sediment reworked by waves.

### **7.4 Model Results**

A key finding of this study is the importance of the ebb tidal jet discharge influencing Buffalo Bay hydrodynamics and sediment transport. The discharging jet results in two eddy systems, one landward and one seaward of the discharge. The landward eddy flows in an anti clockwise direction returning flow towards the inlet, and the seaward eddy flows clockwise into Maramaratotara Bay then gradually moves out into Mercury Bay. The ebb and flood tidal currents are slow within northern Buffalo Bay, and the current direction was hard to calibrate. This is likely to be due to

seiching that was identified in modelling outputs on the flood tide within Buffalo Bay, and the fact this site was sheltered from the main tidal flows. The flood tide pulls water along Buffalo Beach towards the inlet, creating a current to the south along Buffalo Beach. Residual velocity vector patterns within Buffalo Bay suggest zones of deposition northeast of the inlet entrance and also in the vicinity of the ebb delta. Scour could be expected offshore in northern Buffalo Bay and along southern Ohuka Beach.

#### *7.4.1 Wave behaviour*

Waves within Mercury Bay are significantly influenced by the 'box-on-box' shape of Buffalo Bay in Mercury Bay. The wave modelling demonstrates that along Buffalo Beach wave energy converges on the southern section from most approach directions. There is significant refraction of swell waves around the Whakapenui Point so the inlet may experience moderate energy waves, but the ebb delta protects the southern tip of Buffalo Beach. Swell approaching the entrance to Mercury Bay from 50-90° (northeast to east) brings the highest energy into Buffalo Bay, with waves from 70° (east northeast) resulting in the largest wave heights. This direction is a common swell approach direction and results in high wave energy converging on mid and southern sections of Buffalo Beach. Northern Buffalo Beach (Ohuka) experiences minimal wave energy under all swell directions due to the shelter provided by the headland separating Buffalo and Wharekaho Beaches. Longer period waves are more able to bend but 11 second period waves still did not impinge on northern Ohuka Beach. The variation in wave heights along Buffalo Beach is suggestive of localised zones of littoral drift but not continuous, unidirectional flow along Buffalo Beach.

#### *7.4.2 Boat ramp location*

As part of the wave investigation, this study included an initial assessment for a potential boat loading ramp. The ideal location for a new boat loading ramp along Buffalo Beach is in the northern section of Ohuka where wave activity is minimal due to the sheltering effect of the adjacent headland. A breakwater would provide further protection from locally generated sea waves. A straight breakwater structure perpendicular to Buffalo Beach would provide the best shelter and cause the least interference with wave behaviour in Buffalo Bay and along the adjacent Buffalo Beach.

### *7.4.3 Sediment transport*

From the sediment transport modelling, the sediment transport within Buffalo Bay can be divided into three zones, Buffalo Beach, Buffalo Bay, and the Whitianga inlet. Sediment transport along the northern half of Buffalo Beach is limited to ~200 m of the beach. Ohuka Beach in particular has little interaction with the rest of Buffalo Beach or Buffalo Bay, with no apparent sediment in- or out-flow. Sediment transport on the southern half of Buffalo Beach is southwards directed, along the beach towards the inlet. This appears to be driven primarily as a result of the return flow from the ebb jet landward eddy system, and the flood tidal currents. Suspended sediment in this southward current is deposited on the southern tip of Buffalo Beach and the ebb delta. It is likely the ebb delta traps sediment on both ebb and flood tides, which accounts for its rapid growth.

Within Buffalo Bay sediment transport primarily occurs within the two eddy systems. Sediment from the inlet gorge and ebb delta is carried out into Buffalo Bay and then deposited either offshore from Maramaratotara Bay by the seaward eddy, taken out into northern Mercury Bay by the ebb tidal discharge, or moved back around towards the inlet and deposited on the southern tip of Buffalo Beach by the landward eddy and flood tidal currents.

Sediment transport within the inlet is controlled by the velocity distribution and ebb and flood channels. In terms of sediment transport the inlet is flood dominated so available sediment tends to move into the estuary from Buffalo Bay and enter the inlet from the estuary with the ebb tide. Sediment in sheltered areas remains relatively stationary. Sediment caught in the ebb tidal flows is transported into Buffalo Bay by ebb currents. Sandwaves may be present within the inlet gorge and represent a possible bed load transport mechanism.

### *7.4.4 Isolated shallow zone*

Results from the modelling suggest the cause of this shallow zone north east of Whakapenui Point near Pandora Rock, is the transient seaward eddy system circulating in this area with the ebb tide. It is likely the shallow zone has extended out from Maramaratotara Bay which is where the seaward eddy originally resided in

1938 (according to modelling results). The shallow zone would most likely be orientated northeast-southwest, mimicking the migrating path of the seaward eddy with the ebb tide and is likely to continue to accumulate sediment. One solution to this problem may be to periodically dredge sediment from the shallow zone.

#### ***7.4.5 Renourishment***

Renourishment has occurred along Buffalo Beach in two positions, at Taputapuatea Stream and at Ohuka Beach. If sediment were to be placed on the active beach face or offshore at or south of the Taputapuatea Stream it would be carried south along Buffalo Beach and deposited on the ebb delta or southern tip of Buffalo Beach. The best location to place material for renourishment is in the northern section of Buffalo Beach (Ohuka). Results from the modelling in this study suggest particles here move less than 200 m from their source after 10 days, remaining in the nearshore zone. Results obtained from Chapters 3 and 4 suggest sediment transport in northern Buffalo Bay is minimal, but scour, induced by wave and wind activity and littoral drift, is exaggerated due to the lack of sediment input. This provides a positive outcome as dredged material from the canal development in the Whitianga estuary can be adequately disposed of without significantly altering the Buffalo Bay hydrodynamics or adding to the rapid sedimentation in southern Buffalo Bay, and Ohuka beach receives much some needed sediment input. Potential sites for further renourishment borrow material if needed, are the ebb tidal delta and the isolated shallow zone in Buffalo Bay.

#### ***7.5 Future Morphology***

Comparing bathymetries between 1938 and 1995 and aerial photos between 1944 and 2002, illustrates the natural evolution of the inlet and Buffalo Bay. If left to naturally evolve, the growth of the ebb delta would result in the widening of the southern section of Buffalo Bay and the narrowing of the inlet channel. Combined with deposition in the centre of the landward eddy, this would make southern Buffalo Bay very shallow and force the ebb jet north east. The isolated sandbar north of Whakapenui Point would continue to shallow as a result of the seaward eddy system, leaving only a narrow opening for boats to exit Buffalo Bay at the northern end and eventually transforming Buffalo Beach into a harbour beach. Sediment yield from the Whitianga catchment is unlikely to decrease so in order to counteract the

natural evolution of the inlet, the use of dredging or hard structures will likely be needed in the future to maintain a navigable inlet.

### **7.6 Suggestions for Future Research**

A necessary tool for accurate management of the Whitianga inlet is detailed and up-to-date depth soundings. This would define the orientation, shape and size of the shallow zone around Pandora Rock, and the ebb delta and also determine the extent the hydrodynamic conditions have changed between surveys. The detailed bathymetry would also provide data needed for dredging of the shallow zone and ebb delta. Similarly, bed type mapping from a side-scan sonar survey and surficial sediment sampling is needed in order to construct a map of 2D friction and grain size distribution within the inlet, which will result in more realistic hydrodynamic and sediment transport modelling.

This study has addressed the sediment transport pathways within Buffalo Bay based upon water levels and current data collected within the Whitianga inlet and northern Buffalo Bay. A more detailed study with up-to-date bathymetry could include the collection of high quality current, water level and suspended sediment data to further calibrate the model. Data relating to the following should specifically be collected:

- Wave refraction behaviour within Mercury Bay, of which the output can then be incorporated in sediment transport modelling in order to determine the role of waves in suspending and transporting sediment in Buffalo Bay, particularly the northern section.
- Storm conditions within Mercury Bay, enabling modelling of extreme events that could produce increased erosion or accretion in Buffalo Bay.
- The landward and seaward eddy, in order to quantify their magnitude and influence on sediment transport.

A parallel study could address the sediment quantities and sources within the Whitianga estuary catchment. Sediment cores to establish present sedimentation rates within the Whitianga estuary would be useful for illustrating the effect of changing landuse within the catchment. The sediment study would determine if the sedimentation in the estuary is naturally high or been exacerbated by current landuse.

## **Reference list**

---

- Abrahamson, L., 1987. Aspects of late Quaternary stratigraphy and evolution of some coastal embayments on the east Coromandel Peninsula, New Zealand. M. Sc. Thesis (Earth Sciences) University of Waikato, 164p.
- Aagaard, T., Greenwood, B., 1995. Suspended sediment transport and morphological response on a dissipative beach. *Continental Shelf Research*, 15, 1061–1086.
- Beca Carter Hollings and Ferner, 1976. Omaha foreshore erosion investigation. Prepared for Rodney County Council, 32p.
- Bell, R., Goff, J., Downes, G., Berryman, K., Walters, R., Chague-Goff, C., Barnes, P., Wright, I., 2004. Tsunami Hazard for the Bay of Plenty and Eastern Coromandel Peninsula. Environment Waikato Technical Report 2004/33, 82p.
- Bertin, X., Chaumillon, E., Sottolichio, Pedreros, R., 2005. Tidal inlet response to sediment infilling of the associated bay and possible implications of human activities: the Marennes-Oléron Bay and the Maumusson Inlet, France. *Continental Shelf Research*, 25, 1115–1131.
- Bird, E., 2000. *Coastal Geomorphology: An introduction*. John Wiley and Sons Ltd, England, 317p.
- Black, K. P., Healy, T. R., Hunter, M. G., 1989. Sediment dynamics in the lower section of a mixed sand and shell-lagged tidal estuary, New Zealand. *Journal of Coastal Research*, 5(3), 503–521.
- Boothroyd, J. C., 1985. Tidal inlets and tidal deltas. In R. A. Davies Jr., (ed) *Coastal Sedimentary Environments*, Second revised, expanded edition. Springer-Verlag, New York, pp 445–532.
- Bradshaw, B. E., 1991. Nearshore and Inner Shelf Sedimentation on the East Coromandel Coast, New Zealand. PhD, University of Waikato, Hamilton, 160p.
- Bradshaw, B. E., Healy, T.R., Dell, P. M., 1991. Shelf sedimentation on the East Coromandel Coast New Zealand – Implications for resource management. In *Proceedings of the 10th Australasian Conference on Coastal and Ocean Engineering*, pp 351–356.

- Brun-Cottan, J.C., Guillou, S., Li, Z.H., 2000. Behaviour of a puff of sediment: a conceptual model. *Marine Geology*, 167, 355–373.
- Bruun, P., 1978. *Stability of tidal inlets: Theory and engineering*. Elsevier Scientific Publishing Company, New York, pp 13–463.
- Catano-Lopera, Y. A., Garcia, M. H., 2006. Geometry and migration characteristics of bedforms under waves and currents. Part 1: Sandwave morphodynamics. *Coastal Engineering*, 53, 767–780.
- Cayocca, F., 2001. Long-term morphological modelling of a tidal inlet: the Arcachon Basin, France. *Coastal Engineering*, 42, 115–142.
- Chau, K. W., 2003. Manipulation of numerical coastal flow and water quality models. *Environmental Modelling and Software*, 18, 99-108.
- Committee on Coastal Engineering and Japan Society of Civil Engineers, 1994. *Japanese Coasts and Ports (no.2)*. Japan
- Cooper, G. G., 2003. Coastal hydrodynamics and shoreline change at Buffalo Beach, *Mercury Bay*. M. Sc. Thesis (Earth Sciences) 152p.
- Dames and Moore., 1977. Omaha beach stabilisation study. Prepared for Broadlands Properties Ltd, 11p.
- Davies-Colley, R. J., Healy, T. R., 1978. Sediment and hydrodynamics of the Tauranga entrance to Tauranga harbour. *New Zealand Journal of Marine and Freshwater Research*, 12(3), 225-236
- Department of Conservation, 1990. Cathedral Cove: An application for a marine reserve. Department of Conservation, Waikato Conservancy, Hamilton, 14p.
- de Vriend, H. J, Zyserman, J., Nicholson, J., Roelvink, J. A., Pechon, P., Southgate, H. N., 1993. Medium-term 2DH coastal area modelling. *Coastal Engineering*, 21, 193–224.
- DHI, 2004. MIKE 21 flow model, hydrodynamic module user guide. Danish Hydraulics Institute, 88p.
- Dyer, K. R., 1986. *Coastal and estuarine sediment dynamics*. John Wiley and Sons, 342p.

- Elias, E. P. L., van der Spek, A. J. F., 2006. Long-term morphodynamics evolution of Texel Inlet and its ebb tidal delta (The Netherlands). *Marine Geology*, 225, 5–21.
- Environment Waikato, 2006. Latest Rainfall Reading for Tairua. 17 April 2006. [www.ew.govt.nz](http://www.ew.govt.nz)
- FitzGerald, D. M., 1988. Shoreline erosional-depositional processes associated with tidal inlets. In Aubrey, D. G, Weishar, W., (Eds), *Hydrodynamics and Sediment Dynamics of Tidal Inlets*, Springer-Verlag, New York, pp 187–225.
- FitzGerald, D. M., Buyenvich, I. V., Fenster, M. S., Kelley, J. T., Belknap, D. F., 2005. Chapter 10: Coarse grained sediment transport in northern New England estuaries: A synthesis. In Fitzgerald, D. M., and Knight, J., (Eds), *High Resolution Morphodynamics and Sediment Evolution of Estuaries*. Springer, The Netherlands, pp 195–214.
- Flint, S., B., 1998. Sediment Trapping in the Nearshore Coastal Environment. University of Waikato M. Sc. Thesis (Earth Sciences) pp 196p.
- Franco, L., Marconi, R., Neroni, G., 1988. Mathematical modelling of sedimentation in a shallow harbour channel. In Schrefler, B. A., Zienkiwicz, O. C (eds), *Computer Modelling in ocean engineering*, A. A. Balkema, Rotterdam pp 341–348.
- Fredsoe, J., 1993 Modelling of non-cohesive sediment transport processes in the marine environment. *Coastal Engineering*, 21, 71–104.
- Fredsoe, J., and Deigaard, R., 1992. *Mechanics of Coastal Sediment Transport*. Advanced Series on Ocean Engineering – Volume 3 World Scientific, London 356p.
- Galoway, D., Wolanski, E., King, B., 1996. Modelling eddy formation in coastal waters: a comparison between model capabilities. In Spaulding, L., Cheng, R. T (eds), *Estuarine and Coastal Modelling, Proceedings of the 4<sup>th</sup> international conference*, American Society of Civil Engineers, New York, pp 13–25.
- Goring, D., 1997. Tides around NZ, a pictorial essay. *Water and Atmosphere*, 5(1), 13-16.

- Goring, D., 1999. Whitianga sea-level recorder: preliminary analysis. NIWA client report CHC99/87.
- Goring, D., 2003. MSL for Eastern Coromandel Peninsula. Prepared for Environment Waikato. NIWA Client Report: CHC2003-068.
- Grant, D., Black, K., Osbourne, P., Gorman, R., Bryan, K., Villard, P., Douglass, S., Radford, J., Flint, S., Watkins, N., 1998. Surf Zone experiments at Cooks Beach and Tairua North, Coromandel, New Zealand. NIWA internal report 98/03 pp 29–34.
- Green, M. O., Black, K. P., Amos, C.L., 1997. Control of estuarine sediment dynamics by interactions between currents and waves at several scales. *Marine Geology*, 144 (1-3), pp 97–116.
- Hancock, N, 2003. The Effect of Wave Period on the Amplitude Response of Pressure Sensors Under Simulated Wave Conditions. University of Waikato M. Sc. Thesis (Earth Sciences), 93p.
- Harris, T. F. W., 1985. *North Cape to east cape: Aspects of physical oceanography*. University of Auckland, department of Physics and Marine Laboratory, Leigh, 178p
- Harris, T. F. W., Hughes, T. S. Valentine, E. M., 1983. Deep waves off Hicks Bay and the north-east coast, North Island. Water and Soils Miscellaneous publications, No. 56, 83p
- Hayes, M. O., 1973. Morphology of sand accumulation in estuaries: An introduction to the symposium. In Cronin L. E. (ed), *Estuarine Research Volume 2, Geology and Engineering*, Academic Press, New York pp 3–22.
- Hayes, M. O., 1980. General morphology and sediment patterns in tidal inlets. *Sedimentary Geology*, 26,139–156.
- Hayes, M. O., Owens, E. H., Hubbard, D. K., Abele, R. W., 1972. The investigation of form and process in the coastal zone. In D.R. Coates (Ed), *Coastal Geomorphology*, University of New York, New York, pp 11–42.
- Headland, J., Smith, W. G., Kotulak, P., and S. Alfageme 2000. Coastal Protection Methods. In Herbich, J. B (ed), *Handbook of coastal engineering*, McGraw-Hill, pp 8.1-8.66.

- 
- Healy, T. R., 2003. Erosion remediation for Ohuka Beach, Mercury Bay. Report for Whitianga Community Council, 24p.
- Healy, T. R., Dell, P. M., Willoughby, A.J., 1981. Coromandel Coastal Survey: Volume 1 Basic Survey Data. Hauraki Catchment Board Report number 114, pp 1–127.
- Healy, T. R., Dell, P. M., 1982. Coromandel Coastal Survey: Volume 2 Beach Sediment Textural and Mineralogical Data. Hauraki Catchment Board Report number 115, pp 8–25.
- Healy, T., Dell, T., 1987. Baseline data beach surveys for management of an embayed Coastline, East Coromandel New Zealand. *Journal of Shoreline Management*, 3, 129–157.
- Heath, R. A., 1975. Stability of Some New Zealand Coastal Inlets. *New Zealand Journal of Marine and Freshwater Research*, 9(4), 449–457.
- Hicks, D.M., Hume, T. M., 1991. Sand Storage in New Zealand Inlets. In: *Proceedings 10th Australasian Conference on Coastal and Ocean Engineering*, pp 213–219.
- Hicks, D.M., Hume, T. M., 1996. Morphology and size of ebb tidal deltas at natural inlets on open-sea and pocket-bay coasts, North Island, New Zealand. *Journal of Coastal Research*, 12(1), 47–63.
- Hicks, D. M., Hume, T. M., 1997. Determining sand volumes and bathymetric change on an ebb-tidal delta. *Journal of Coastal Research*, 13(2), 407–416.
- Holland, W. R., Capotondi, A., 1996. Recent developments in prognostic ocean modelling. In Malanotte-Rizzoli, P (ed), *Modern approaches to data assimilation ocean modelling*, Elsevier Oceanography Series, pp 21–56.
- Hoyal, D. C. J. D., van Wagoner, J. C., Adair, N. L., Deffenbaugh, M., Li, D., Sun, T., Huh, C., Giffin, D. E., 2003. Sedimentation from Jets: A depositional model for clastic deposits of all scales and environments. Adapted from extended abstract of poster session presentation at AAPG Annual Meeting May 14, 2003, Salt Lake City, Utah, 10p.
- Hume, T. M., 2003. Estuaries and tidal inlets. In Goff, J. R., Nichol, S. L., Rouse, H. L., (Eds), *The New Zealand Coast; Te tai O Aotearoa*. Dunmore Press, Palmerston North NZ, pp 191–214.

- 
- Hume, T. M., Bell, R. G., de Lange, W. P., Healy, T. R., Hicks, D. M., Kirk, R. M., 1992. Coastal oceanography and sedimentology in New Zealand, 1967-91. *New Zealand Journal of Marine and Freshwater Research*, 26(1), 1–36.
- Hume, T. M., Dahm J., 1991. An investigation of the effects of Polynesian and European land use on sedimentation in Coromandel Estuaries, Water Quality Centre, DSIR Hamilton. Consultancy Report No. 7106, pp1–16.
- Hume, T. M., Gibb, J. G., 1987. The “Wooden-Floor” Marker Bed – A new method of determining historical sedimentation rates in some New Zealand estuaries. *Journal of the Royal Society of New Zealand*, 17(1), 1–7.
- Hume, T. M., Herdendorf, C. E., 1985. Tidal Inlet Stability: Proceedings of a Workshop, Christchurch 4 December 1985. *Water and Soil Miscellaneous Publication*, 108, pp 7–40.
- Hume, T. M., Herdendorf, C. E., 1988a. The ‘Furket-Heath’ relationship for tidal inlet stability reviewed. *New Zealand Journal of Marine and Freshwater Research*, 22(1), 129–134.
- Hume, T. M., Herdendorf, C. E., 1988b. A geomorphic classification of estuaries and its application to coastal resource management - A New Zealand example. *Journal of Ocean and Shoreline Management*, 11, 249–274.
- Hume, T. M., Herdendorf, C. E., 1992. Factors controlling tidal inlet characteristics on low drift coasts. *Journal of Coastal Research*, 8(2), 55–375.
- Hume, T. M., Herdendorf, C. E., 1993. On the use of empirical stability relationships for characterising estuaries. *Journal of Coastal Research*, 9(2), 413–422.
- Hume, T., Swales, A., 2003. How estuaries grow old. *Water and Atmosphere*, 11(1), pp 14–15.
- Hume, T., Vennel, R., Black, K., 1997. Sounding out the currents: acoustic mapping of current structure at a coastal headland. *Water and Atmosphere*, 5(2), 19–21
- Imasato, N., 1983. What is a tide-induced current? *Journal of Physical Oceanography*, 13(7), 1307–1317.

- 
- Interocean, 2006. Description, Application and Theory of S4 Family. Retrieved from the World Wide Web:<http://www.interoceansystems.com/s4theory.htm>
- Jimenez, J. A., Sanchez-Arcilla, A., Valdemoro, H. I., Gracia, V., Nieto, F., 1997. Processes reshaping the Ebro delta. *Marine Geology*, 144(1-3), 59–79.
- Kerper, D. R., Broker, I., Christensen, E. D., Zyserman, J. A., 2002. Application of coastal modelling systems in support of integrated coastal zone management. *Proceedings of Solutions to Coastal Disasters Conference*, San Diego, 2002 pp 28–42.
- Komar, P.D., Miller, M.C., 1975. On the comparison between the threshold of sediment motion under waves and unidirectional currents with a discussion of the practical evaluation of threshold. *Journal of Sedimentary Petrology*, 45, 362–367
- Kruger, J., C., Healy, T. R., 2006. Mapping the morphology of a dredged ebb tidal Delta Tauranga Harbour, New Zealand. *Journal of Coastal Research*, 22(3), 720–727.
- Lakhan, V.C., 1989. Chapter 2, Modelling and simulation of the coastal system. In Lakhan, V. C., and Trenhaile, A. S., (eds), *Applications in coastal modelling*. Elsevier Oceanography Series 49, Amsterdam pp 17–42.
- Lakhan, V. C., Trenhaile, A. S., Chapter 1, Models and the coastal system. In Lakhan, V. C., and Trenhaile, A. S., (eds), *Applications in coastal modelling*. Elsevier Oceanography Series 49, Amsterdam, pp 1–16.
- LINZ, 2005a. Great Mercury Island/Ahuahu to Otara Bay. Land Information New Zealand. Scale 1: 50000 NZMS 5318.
- LIINZ, 2005b. New Zealand Notice to Mariners, Edition 18. Land Information New Zealand, Issued 2 September 2005, 1p.
- Loomb, C., 2006. Managing the Impacts of Living on the Coast through Triple Bottom Line Assessments. In: *Coastal News*, 31, 4–5.
- Marino, J. M., Mehta, A. J., 1988. Sediment trapping at Florida's east coast inlets. In Aubrey, D. G., Weishar, W. (Eds), *Hydrodynamics and Sediment Dynamics of Tidal Inlets*, pp 284–296.
- Maunder, W. J., 1974. Climate and Climatic Resources of the Waikato Coromandel King Country region. *New Zealand Meteorological Service Miscellaneous Publication*, 115(7), pp 1–15.

- McGlone, M.S., 1988. Report on the pollen analysis of estuarine cores from Whangapoua and Whitianga harbours, Coromandel Peninsula. DSIR Botany Division Vegetation Report 648, pp 1–21.
- McLay, C.L., 1976. An inventory of the status and origin of New Zealand estuarine systems. *Proceedings of the New Zealand Ecological Society*, 23, 8–26.
- Mead, S., Moores, A., 2004. Estuary Sedimentation: a Review of Estuarine Sedimentation in the Waikato Region. Environment Waikato Technical Report 2004/13, pp 1–15.
- Michel, D., Howa, H. L., 1997. Morphodynamic behaviour of a tidal inlet system in a mixed energy environment. *Physics, Chemistry and Earth*, 22(3-4), 339–343.
- Miller, M. C., McCave, I. N., Komar, P. D., 1977. Threshold of Sediment motion under unidirectional currents. *Sedimentology*, 24, 507–527.
- Neumann, D.R., Orams, M. B., 2005. Behaviour and ecology of common dolphins (*Delphinus delphis*) and the impact of tourism in Mercury Bay, North Island, New Zealand. Department of Conservation, Science for Conservation Report 254, pp 29–30.
- Nicholson, J., Broker, I., Roelvink, J. A., Price, D., Tanguy, J. M., Moreno, L., 1997. Intercomparison of coastal area morphodynamic models. *Coastal Engineering*, 31, 97-123.
- NIWA, 2001. *DOBIE Wave Gauge; Operators Manual Version 4.1*. NIWA, Christchurch New Zealand, 49p.
- NIWA, 2006. Climate Update 44, February 2003. 17 April, 2006. <http://www.niwascience.co.nz/ncc/cu/2003-02/month>.
- Park, M-J., Wang, D-P., 2000. Tidal vorticity around a coastal promontory. *Journal of Oceanography*, 56, 261–273.
- Paton. L., 1993. Hydrodynamics and Morphodynamics of Selected Cuspated Beaches on the Eastern Coromandel Peninsula. University of Waikato M. Sc. Thesis (Earth Sciences), 148p.

- Pechon, P., Rivero, F., Johnson, H., Chester, T., O'Connor, B., Tanguy, J-M., Karambas, T., Mory, M., Hamm, L., 1997. Intercomparison of wave-driven current models. *Coastal Engineering*, 31, 199-215.
- Pickrell, R.A., Mitchell, J.S., 1979. Ocean Wave Characteristics. *New Zealand Journal of Marine and Freshwater Research*, 13 4), 501–520 .
- Pingree, R. D., Maddock, L., 1979. The tidal physics of headland flows and offshore tidal bank formation. *Marine Geology*, 32, 269–289.
- Pingree, R. D., Maddock, L., 1978. Numerical simulation of the Portland tidal eddies. *Estuarine and Coastal Marine Science*, 6, 353–363.
- Ponce, V. M., Yabusaki, S. B., 1981. Modelling circulation in depth-averaged flow. *Journal of the Hydraulics Division*, 107, 1501–1518.
- Priestly, S., 2006. Kohimaramara Beach Replenishment Project Earns Award. *Coastal News* 33, November 2006, pp 1-2.
- Ramming, H-G., Kowalik, Z., 1980. *Numerical Modelling of Marine Hydrodynamics: Applications to Dynamic Physical processes*. Elsevier Oceanography Series, 26. Elsevier Scientific Publishing Co., The Netherlands, 368p.
- Raudkivi, A. J., 1981. Preliminary Report on Coastal Stability and Sediment Movement in the Vicinity of Whitianga Wharf. Hauraki Catchment Board, pp 1–7.
- Sale, E. V., 1978. *Quest for the Kauri: Forest Giants and where to find them*. A. H and A. W Reed, Wellington, pp 157–182.
- Saunders, H. A., 1999. Coastal processes influencing beach erosion at West End Ohope. University of Waikato M. Sc. Thesis (Earth Sciences) 229p.
- Schofield, J. C., 1967. Geological Map of New Zealand 1:250,000. DSIR, Wellington.
- Sheffield., A. T., 1991. *The sedimentation and Hydrodynamics of Whangamata Harbour*. University of Waikato M. Sc. Thesis (Earth Sciences), 190p.

- Sheffield, A. T., Healy, T. R., de Lange, W. P., 1991. Aspects of tidal stability of Whangamata Harbour New Zealand. In *Proceedings 10th Australasian Conference on Coastal and Ocean Engineering*, pp 227–231.
- Sheffield, A. T., Healy, T.R., McGlone, M. S., 1995. Infilling rates of a steepland catchment estuary, Whangamata, New Zealand. *Journal of Coastal Research*, 11(4), 1294–1308.
- Siegle, E., Huntley, D. A., Davidson, M. A., 2002. Modelling water surface topography at a complex inlet system – Teignmouth, UK. International Coastal Symposium 2002, *Journal of Coastal Research* Special Issue No. 36, pp. 675–685
- Siegle, E., Huntley, D. A., Davidson, M. A., 2007. Coupling video imaging and numerical modeling for the study of inlet morphodynamics. *Marine Geology*, 236, 146–163.
- Signell, R. P., Geyer, W. R., 1991. Transient eddy formation around headlands. *Journal of Geophysical research*, 96 (C2), 2561–2575.
- Skinner, D. N. B., 1986. Neogene Volcanism of the Hauraki Volcanic Region. In Smith, I.E.M. (Ed.), Late Cenozoic Volcanism in New Zealand, *The Royal Society of New Zealand Bulletin*, 23, pp 371.
- Skinner, D. N. B., 1995. Geology of the Mercury Bay Area, scale 1: 50 000. Institute of Geological and Nuclear Sciences Geological Map 17. 1 sheet +56 pages. Lower Hutt, New Zealand: Institute of Geological and Nuclear Sciences Limited.
- Smith, D B., 1980. *Sea level oscillations, hydrology and sedimentology of Mercury Bay*. University of Waikato M. Sc. Thesis (Earth Sciences), 144p.
- Somes, N. L. G., Bishop W. A., Wong T. H. F., 1999. Numerical simulation of wetland hydrodynamics. *Environment International*, 25(6-7), 773–779.
- Stauble, D. K., 1993. An overview of Southeast Florida inlet morphodynamics. *Journal of Coastal Research*, Special Issue No. 18, 1–28.
- Stoschek, O., Matheja, A., 2000. Sensitivity analysis of numerical solving techniques for modelling sediment transport under tidal conditions. In Proceedings of 4th International conference on Hydroinformatics, pp 23–27.

- Sutherland, J., Peet, A. H., Soulsby, R. L., 2004. Evaluating the performance of morphological models. *Coastal Engineering*, 51, 917–939.
- Thompson, B. N., 1966. Geology of the Coromandel Region. New Zealand Geological Survey, Department of Scientific and Industrial Research New Zealand. Report NZGS 14.
- White, B., 1998. Spinnaker Strand and Waimanu Bay Reserve. Te Atatu Peninsula Waitakare City: Coastal Protection, Technical Report. Prepared for Wood and Partners Consultants Limited, pp 6-15.
- Wolanski, E., Imberger, J., and Heron, M. L., 1984. Island wakes in shallow coastal waters. *Journal of Geophysical research*, 89 (C6), 10,553–10,569.
- Zimmerman, J. T. F., 1981. Dynamics, diffusion and geomorphological significance of tidal residual eddies. *Nature*, 290, 549–555.

## ***Appendices***

---

Appendix 1 – Notice to Mariners and photo of navigation warning

Appendix 2 – Sediment Sample analysis sheets for RSA and Malvern laser sizer.

Appendix 3 –Model outputs

1. Mercury Bay wave snapshots



**NZ 173(T)/05      NEW ZEALAND – North Island – East Coast – Mercury Bay – Approaches to  
Whitianga – Sandbar.**

1. A sandbar has developed in the approaches to Whitianga extending from Pandora Rock (36° 49'.5S., 175° 43'.3E.) to a position one mile northwards.
2. Depths as shallow as one metre have been recorded in position 36° 49'.27S., 175° 43'.14E.
3. Vessels may encounter steep, breaking waves when onshore swell opposes the outgoing tide.
4. Mariners are cautioned to exercise care when navigating in the vicinity.

**Charts temporarily affected – NZ 53 – NZ 54 – NZ 531 – NZ 534 – NZ 5318**

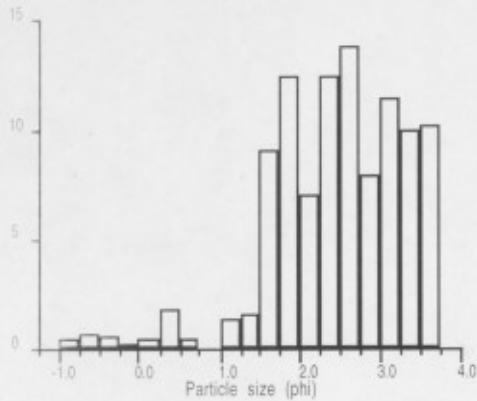
Whitianga Harbourmaster.  
NI 154/2005

# PARTICLE SIZE ANALYSIS

## Earth Sciences - University of Waikato

Sample: 2ND ENTRANCE

### Size distribution histogram



### Results summary

#### Textural size classes

Gravel= 0.00% Sand= 100.00% Silt= 0.00% Clay= 0.00%

Gravel free detrital sediment

Sand

#### Moment method parameters (phi)

Mean= 2.51 Sorting= 0.87 Skewness= -1.19 Kurtosis= 4.94

#### Graphical method parameters (phi)

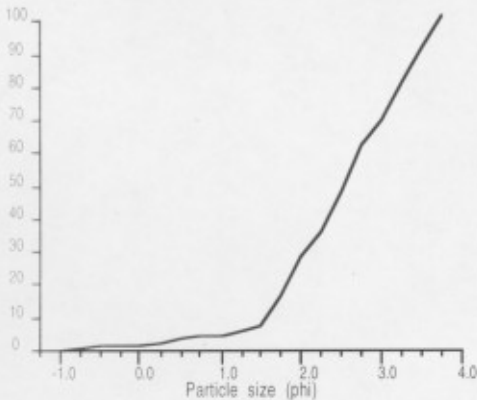
Mean= 2.52 Sorting= 0.78 Skewness= -0.09 Kurtosis= 0.88

Median= 2.53 C= -0.55 D35= 2.21 D65= 2.84

Textural description:

Moderately sorted, Near symmetrical, Platykurtic

### Cumulative frequency

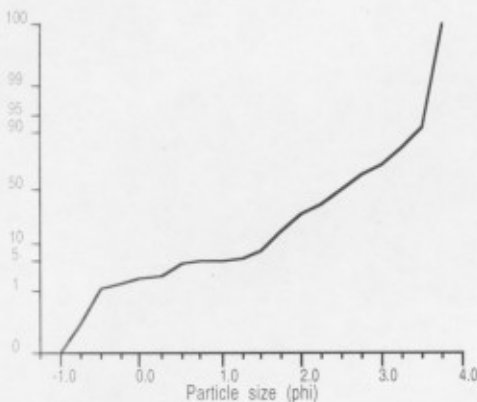


### Raw data summary

Size (phi)	Size (mm)	Cumulative weight (g)	Interval frequency (%)	Cumulative frequency (%)
-1.00	2.0000	0.00	0.00	0.00
-0.75	1.6818	0.03	0.43	0.43
-0.50	1.4142	0.08	0.72	1.16
-0.25	1.1892	0.12	0.58	1.74
0.00	1.0000	0.14	0.29	2.03
0.25	0.8409	0.17	0.43	2.46
0.50	0.7071	0.30	1.88	4.34
0.75	0.5946	0.33	0.43	4.78
1.00	0.5000	0.33	0.00	4.78
1.25	0.4204	0.42	1.30	6.08
1.50	0.3536	0.53	1.59	7.67
1.75	0.2973	1.15	8.97	16.64
2.00	0.2500	2.01	12.45	29.09
2.25	0.2102	2.49	6.95	36.03
2.50	0.1768	3.35	12.45	48.48
2.75	0.1487	4.30	13.75	62.23
3.00	0.1250	4.85	7.96	70.19
3.25	0.1051	5.64	11.43	81.62
3.50	0.0884	6.33	9.99	91.61
3.75	0.0743	7.03	10.13	101.74

Total weight = 6.91 g

### Cumulative frequency

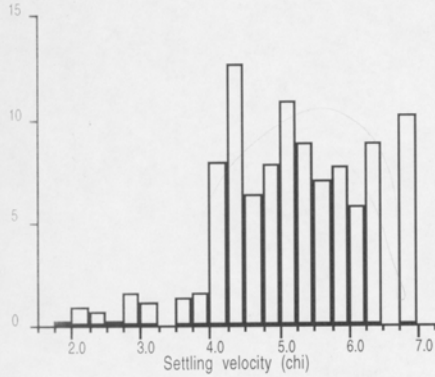


# SETTLING VELOCITY ANALYSIS

Earth Sciences - University of Waikato

Sample: 2ND ENTRANCE

## Size distribution histogram

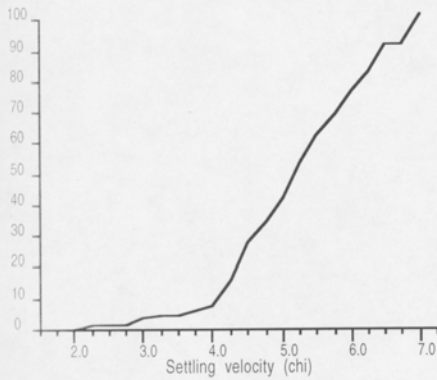


## Results summary

Moment method parameters (chi)

Mean= 5.29 Sorting= 1.04 Skewness= -0.60 Kurtosis= 3.09

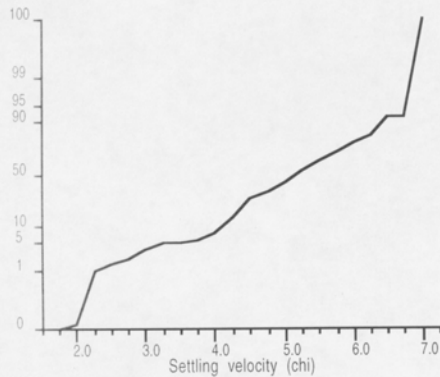
## Cumulative frequency



## Raw data summary

Velocity (chi)	Velocity (m/s)	Cumulative weight (g)	Interval frequency (%)	Cumulative frequency (%)
1.75	0.2973	-0.01	-0.14	-0.14
2.00	0.2500	0.01	0.29	0.14
2.25	0.2102	0.07	0.87	1.01
2.50	0.1768	0.12	0.72	1.74
2.75	0.1487	0.14	0.29	2.03
3.00	0.1250	0.25	1.59	3.62
3.25	0.1051	0.33	1.16	4.78
3.50	0.0884	0.33	0.00	4.78
3.75	0.0743	0.42	1.30	6.08
4.00	0.0625	0.53	1.59	7.67
4.25	0.0526	1.08	7.96	15.63
4.50	0.0442	1.96	12.74	28.36
4.75	0.0372	2.40	6.37	34.73
5.00	0.0312	2.94	7.81	42.55
5.25	0.0263	3.69	10.85	53.40
5.50	0.0221	4.30	8.83	62.23
5.75	0.0186	4.79	7.09	69.32
6.00	0.0156	5.32	7.67	76.99
6.25	0.0131	5.72	5.79	82.78
6.50	0.0110	6.33	8.83	91.61
6.75	0.0093	6.33	0.00	91.61
7.00	0.0078	7.03	10.13	101.74

## Cumulative frequency



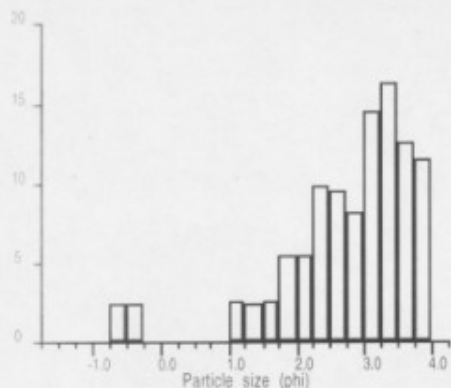
Total weight = 6.91 g

# PARTICLE SIZE ANALYSIS

## Earth Sciences - University of Waikato

Sample: 1STBB

### Size distribution histogram



### Results summary

#### Textural size classes

Gravel= 0.00% Sand= 100.00% Silt= 0.00% Clay= 0.00%

Gravel free detrital sediment

Sand

#### Moment method parameters (phi)

Mean= 2.91 Sorting= 1.03 Skewness= -1.91 Kurtosis= 6.27

#### Graphical method parameters (phi)

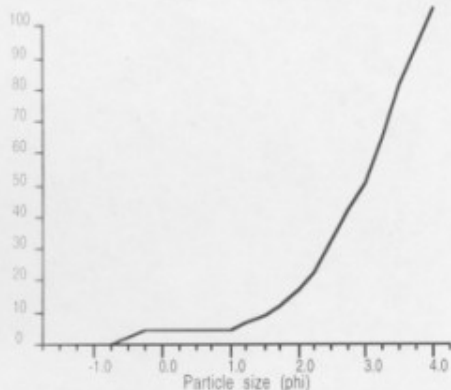
Mean= 2.83 Sorting= 0.82 Skewness= -0.36 Kurtosis= 1.02

Median= 2.99 C= -0.64 D35= 2.56 D65= 3.25

Textural description:

Moderately sorted, Strongly Coarse skewed, Mesokurtic

### Cumulative frequency

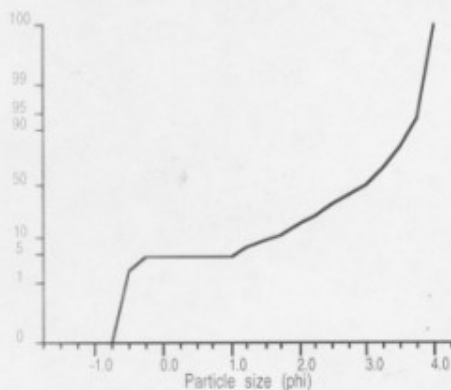


### Raw data summary

Size (phi)	Size (mm)	Cumulative weight (g)	Interval frequency (%)	Cumulative frequency (%)
-1.50	2.8284	0.00	0.00	0.00
-1.25	2.3784	0.00	0.00	0.00
-1.00	2.0000	0.00	0.00	0.00
-0.75	1.6818	0.00	0.00	0.00
-0.50	1.4142	0.10	2.33	2.33
-0.25	1.1892	0.20	2.33	4.66
0.00	1.0000	0.20	0.00	4.66
0.25	0.8409	0.20	0.00	4.66
0.50	0.7071	0.20	0.00	4.66
0.75	0.5946	0.20	0.00	4.66
1.00	0.5000	0.20	0.00	4.66
1.25	0.4204	0.31	2.56	7.23
1.50	0.3536	0.41	2.33	9.56
1.75	0.2973	0.52	2.56	12.12
2.00	0.2500	0.75	5.36	17.48
2.25	0.2102	0.98	5.36	22.84
2.50	0.1768	1.40	9.79	32.63
2.75	0.1487	1.81	9.56	42.19
3.00	0.1250	2.16	8.16	50.35
3.25	0.1051	2.78	14.45	64.80
3.50	0.0884	3.48	16.32	81.12
3.75	0.0743	4.02	12.59	93.71
4.00	0.0625	4.51	11.42	105.13

Total weight = 4.29 g

### Cumulative frequency

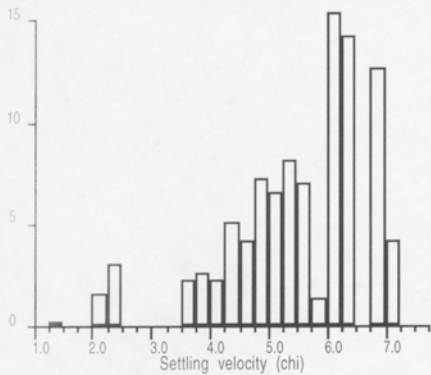


# SETTLING VELOCITY ANALYSIS

Earth Sciences - University of Waikato

Sample: 1STBB

## Size distribution histogram

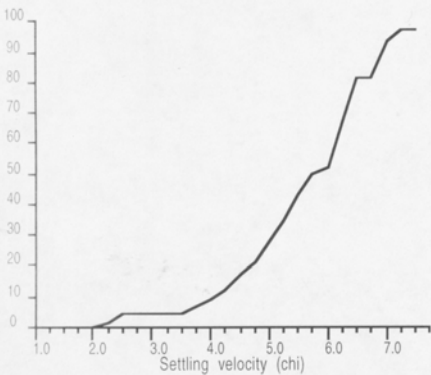


## Results summary

### Moment method parameters (chi)

Mean= 5.42 Sorting= 1.16 Skewness= -0.65 Kurtosis= 3.33

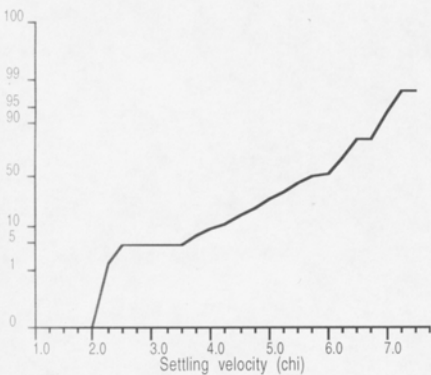
## Cumulative frequency



## Raw data summary

Velocity (chi)	Velocity (m/s)	Cumulative weight (g)	Interval frequency (%)	Cumulative frequency (%)
1.25	0.4204	-0.01	-0.23	-0.23
1.50	0.3536	0.00	0.23	0.00
1.75	0.2973	0.00	0.00	0.00
2.00	0.2500	0.00	0.00	0.00
2.25	0.2102	0.07	1.63	1.63
2.50	0.1768	0.20	3.03	4.66
2.75	0.1487	0.20	0.00	4.66
3.00	0.1250	0.20	0.00	4.66
3.25	0.1051	0.20	0.00	4.66
3.50	0.0884	0.20	0.00	4.66
3.75	0.0743	0.30	2.33	6.99
4.00	0.0625	0.41	2.56	9.56
4.25	0.0526	0.51	2.33	11.89
4.50	0.0442	0.73	5.13	17.02
4.75	0.0372	0.91	4.20	21.21
5.00	0.0312	1.22	7.23	28.44
5.25	0.0263	1.50	6.53	34.97
5.50	0.0221	1.85	8.16	43.12
5.75	0.0186	2.15	6.99	50.12
6.00	0.0156	2.21	1.40	51.52
6.25	0.0131	2.87	15.38	66.90
6.50	0.0110	3.48	14.22	81.12
6.75	0.0093	3.48	0.00	81.12
7.00	0.0078	4.02	12.59	93.71
7.25	0.0066	4.20	4.20	97.90
7.50	0.0055	4.20	0.00	97.90

## Cumulative frequency



Total weight = 4.29 g

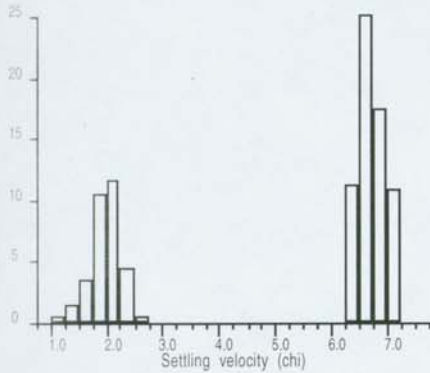
University of Waikato  
Rapid Sediment Analyser  
Operating System Version 7.1

# SETTLING VELOCITY ANALYSIS

Earth Sciences - University of Waikato

Sample: 2NDBB

## Size distribution histogram

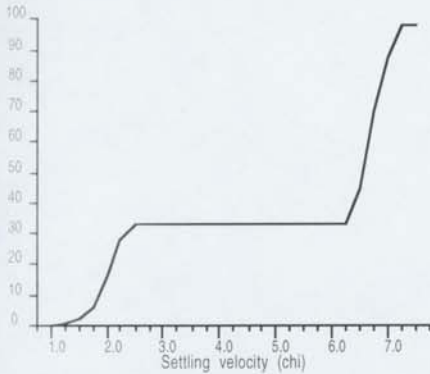


## Results summary

Moment method parameters (chi)

Mean= 5.03 Sorting= 2.25 Skewness= -0.56 Kurtosis= 1.44

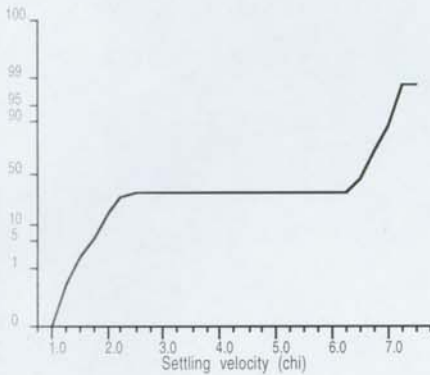
## Cumulative frequency



## Raw data summary

Velocity (chi)	Velocity (m/s)	Cumulative weight (g)	Interval frequency (%)	Cumulative frequency (%)
1.00	0.5000	0.00	0.00	0.00
1.25	0.4204	0.03	0.65	0.65
1.50	0.3536	0.10	1.52	2.16
1.75	0.2973	0.27	3.68	5.84
2.00	0.2500	0.76	10.61	16.45
2.25	0.2102	1.30	11.69	28.14
2.50	0.1768	1.51	4.55	32.68
2.75	0.1487	1.54	0.65	33.33
3.00	0.1250	1.54	0.00	33.33
3.25	0.1051	1.54	0.00	33.33
3.50	0.0884	1.54	0.00	33.33
3.75	0.0743	1.54	0.00	33.33
4.00	0.0625	1.54	0.00	33.33
4.25	0.0526	1.54	0.00	33.33
4.50	0.0442	1.54	0.00	33.33
4.75	0.0372	1.54	0.00	33.33
5.00	0.0312	1.54	0.00	33.33
5.25	0.0263	1.54	0.00	33.33
5.50	0.0221	1.54	0.00	33.33
5.75	0.0186	1.54	0.00	33.33
6.00	0.0156	1.54	0.00	33.33
6.25	0.0131	1.54	0.00	33.33
6.50	0.0110	2.06	11.26	44.59
6.75	0.0093	3.23	25.32	69.91
7.00	0.0078	4.04	17.53	87.45
7.25	0.0066	4.54	10.82	98.27
7.50	0.0055	4.54	0.00	98.27

## Cumulative frequency



University of Waikato  
Rapid Sediment Analyser  
Operating System Version 7.1

Total weight = 4.62 g

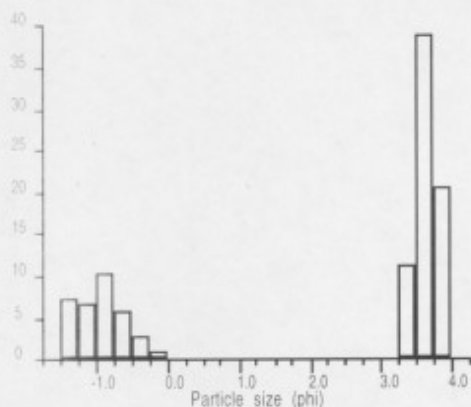
Handwritten notes: 2.00, 2.25

# PARTICLE SIZE ANALYSIS

## Earth Sciences - University of Waikato

Sample: 2NDBB

### Size distribution histogram



### Results summary

#### Textural size classes

Gravel= 13.85% Sand= 90.26% Silt= 0.00% Clay= 0.00%

Gravel bearing detrital sediment

Slightly Gravelly Sand

#### Moment method parameters (phi)

Mean= 2.28 Sorting= 2.20 Skewness= -0.89 Kurtosis= 1.73

#### Graphical method parameters (phi)

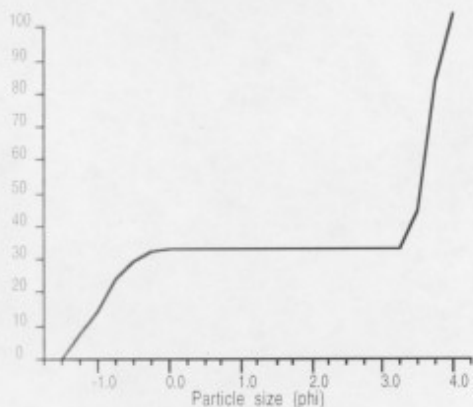
Mean= 2.11 Sorting= 1.97 Skewness= -0.89 Kurtosis= 0.49

Median= 3.53 C= -1.47 D35= 3.29 D65= 3.63

Textural description:

Poorly sorted, Strongly Coarse skewed, Very platykurtic

### Cumulative frequency

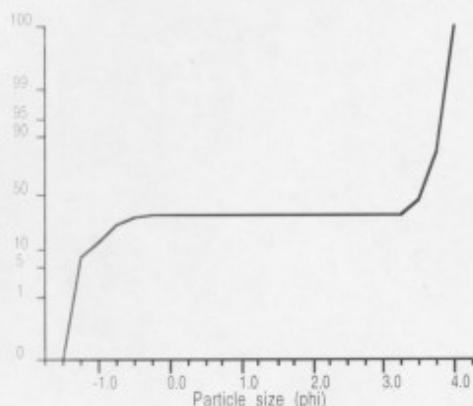


### Raw data summary

Size (phi)	Size (mm)	Cumulative weight (g)	Interval frequency (%)	Cumulative frequency (%)
-1.50	2.8284	0.00	0.00	0.00
-1.25	2.3784	0.34	7.36	7.36
-1.00	2.0000	0.64	6.49	13.85
-0.75	1.6818	1.11	10.17	24.03
-0.50	1.4142	1.37	5.63	29.65
-0.25	1.1892	1.50	2.81	32.47
0.00	1.0000	1.54	0.87	33.33
0.25	0.8409	1.54	0.00	33.33
0.50	0.7071	1.54	0.00	33.33
0.75	0.5946	1.54	0.00	33.33
1.00	0.5000	1.54	0.00	33.33
1.25	0.4204	1.54	0.00	33.33
1.50	0.3536	1.54	0.00	33.33
1.75	0.2973	1.54	0.00	33.33
2.00	0.2500	1.54	0.00	33.33
2.25	0.2102	1.54	0.00	33.33
2.50	0.1768	1.54	0.00	33.33
2.75	0.1487	1.54	0.00	33.33
3.00	0.1250	1.54	0.00	33.33
3.25	0.1051	1.54	0.00	33.33
3.50	0.0884	2.06	11.26	44.59
3.75	0.0743	3.86	38.96	83.55
4.00	0.0625	4.81	20.56	104.11

Total weight = 4.62 g

### Cumulative frequency



## Result Analysis Report

**Sample Name:**  
2nd Buffalo

**SOP Name:**  
Marine Sediment

**Measured:**  
Monday, 4 December 2006 11:01:53 a.m.

**Sample Source & type:**  
Whitianga

**Measured by:**  
jacinta

**Analysed:**  
Monday, 4 December 2006 11:01:54 a.m.

**Sample bulk lot ref:**  
2

**Result Source:**  
Measurement

**Particle Name:**  
Marine Sediment

**Accessory Name:**  
Hydro 2000G (A)

**Analysis model:**  
General purpose

**Sensitivity:**  
Enhanced

**Particle RI:**  
1.500

**Absorption:**  
0

**Size range:**  
0.020 to 2000.000  $\mu\text{m}$

**Obscuration:**  
14.03 %

**Dispersant Name:**  
Water

**Dispersant RI:**  
1.330

**Weighted Residual:**  
0.703 %

**Result Emulation:**  
Off

**Concentration:**  
0.1312 %Vol

**Span :**  
3.501

**Uniformity:**  
1.01

**Result units:**  
Volume

**Specific Surface Area:**  
0.0888  $\text{m}^2/\text{g}$

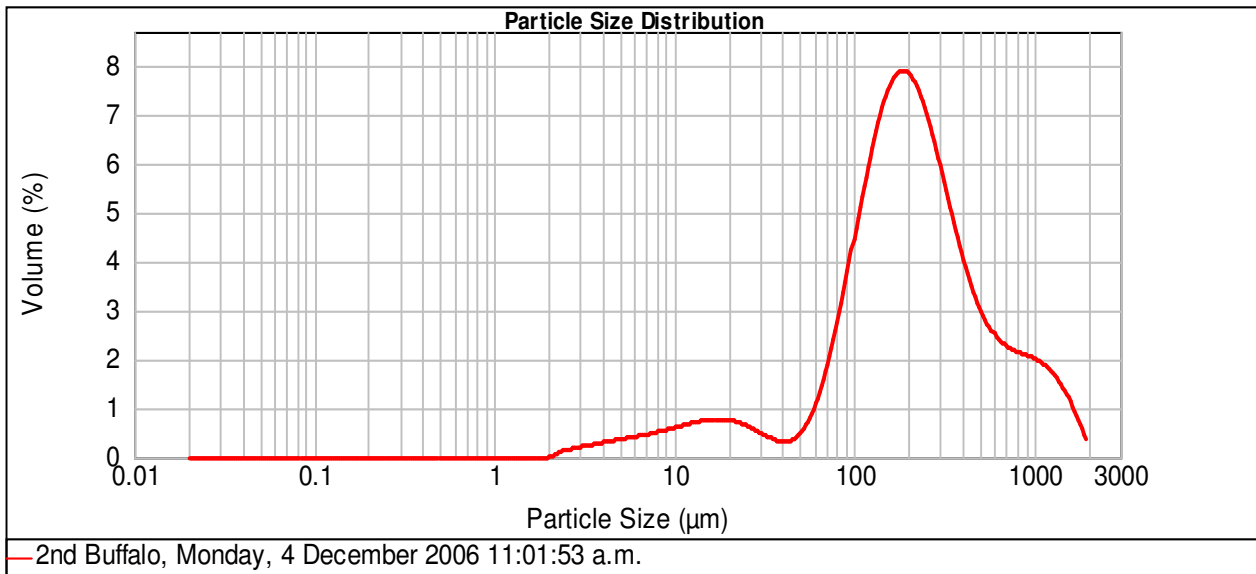
**Surface Weighted Mean D[3,2]:**  
67.588  $\mu\text{m}$

**Vol. Weighted Mean D[4,3]:**  
314.265  $\mu\text{m}$

**d(0.1): 54.302  $\mu\text{m}$**

**d(0.5): 200.964  $\mu\text{m}$**

**d(0.9): 757.777  $\mu\text{m}$**



Size ( $\mu\text{m}$ )	Volume In %	Size ( $\mu\text{m}$ )	Volume In %	Size ( $\mu\text{m}$ )	Volume In %	Size ( $\mu\text{m}$ )	Volume In %	Size ( $\mu\text{m}$ )	Volume In %	Size ( $\mu\text{m}$ )	Volume In %
0.050	0.00	0.980	0.00	37.000	0.37	105.000	6.43	300.000	5.52	840.000	2.36
0.060	0.00	2.000	0.75	44.000	0.52	125.000	7.92	350.000	5.23	1000.000	6.19
0.120	0.00	3.900	1.80	53.000	0.96	149.000	8.65	420.000	3.90	2000.000	
0.240	0.00	7.800	2.90	63.000	1.70	177.000	8.79	500.000	2.99		
0.490	0.00	15.600	3.10	74.000	3.09	210.000	8.49	590.000	2.87		
0.700	0.00	31.000	0.47	88.000	4.80	250.000	7.81	710.000	2.39		
0.980	0.00	37.000		105.000		300.000		840.000			

**Operator notes:**

## Result Analysis Report

**Sample Name:**  
2nd river

**SOP Name:**  
Marine Sediment

**Measured:**  
Monday, 4 December 2006 10:49:55 a.m.

**Sample Source & type:**  
Whitianga

**Measured by:**  
jacinta

**Analysed:**  
Monday, 4 December 2006 10:49:56 a.m.

**Sample bulk lot ref:**  
1

**Result Source:**  
Measurement

**Particle Name:**  
Marine Sediment

**Accessory Name:**  
Hydro 2000G (A)

**Analysis model:**  
General purpose

**Sensitivity:**  
Enhanced

**Particle RI:**  
1.500

**Absorption:**  
0

**Size range:**  
0.020 to 2000.000  $\mu\text{m}$

**Obscuration:**  
14.14 %

**Dispersant Name:**  
Water

**Dispersant RI:**  
1.330

**Weighted Residual:**  
0.667 %

**Result Emulation:**  
Off

**Concentration:**  
0.0581 %Vol

**Span :**  
2.020

**Uniformity:**  
0.608

**Result units:**  
Volume

**Specific Surface Area:**  
0.191  $\text{m}^2/\text{g}$

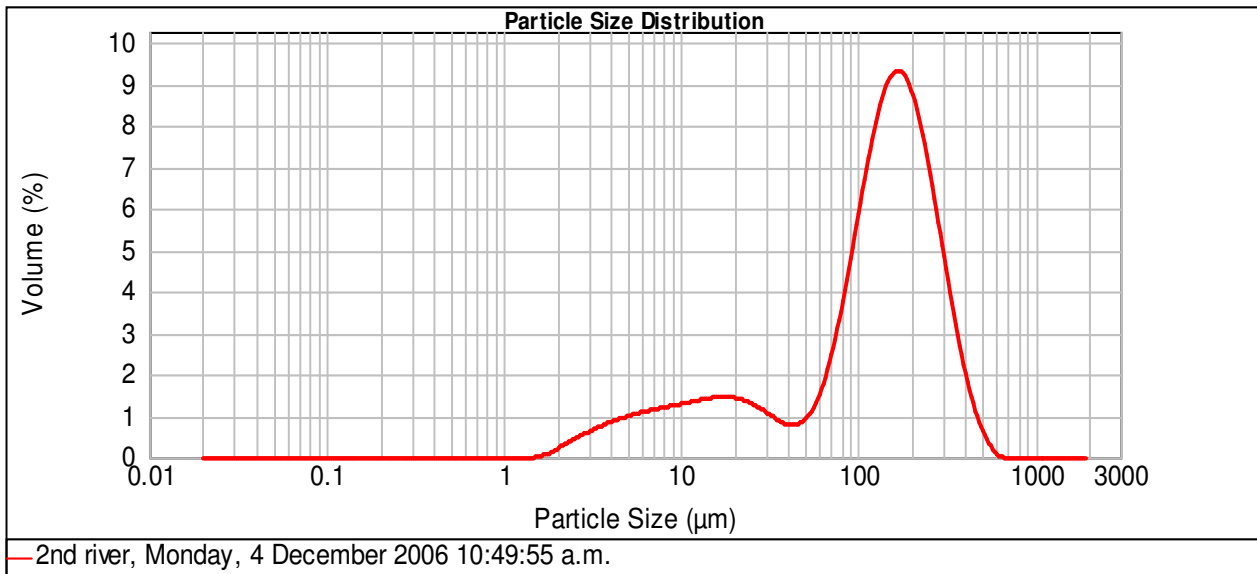
**Surface Weighted Mean D[3,2]:**  
31.360  $\mu\text{m}$

**Vol. Weighted Mean D[4,3]:**  
145.904  $\mu\text{m}$

**d(0.1): 10.929  $\mu\text{m}$**

**d(0.5): 136.211  $\mu\text{m}$**

**d(0.9): 286.056  $\mu\text{m}$**



Size ( $\mu\text{m}$ )	Volume In %	Size ( $\mu\text{m}$ )	Volume In %	Size ( $\mu\text{m}$ )	Volume In %	Size ( $\mu\text{m}$ )	Volume In %	Size ( $\mu\text{m}$ )	Volume In %	Size ( $\mu\text{m}$ )	Volume In %
0.050	0.00	0.980	0.15	37.000	0.89	105.000	8.37	300.000	4.06	840.000	0.00
0.060	0.00	2.000	2.38	44.000	1.06	125.000	10.01	350.000	2.81	1000.000	0.00
0.120	0.00	3.900	4.69	53.000	1.54	149.000	10.48	420.000	1.19	2000.000	0.00
0.240	0.00	7.800	6.02	63.000	2.43	177.000	10.00	500.000	0.34		
0.490	0.00	15.600	6.03	74.000	4.22	210.000	8.82	590.000	0.00		
0.700	0.00	31.000	1.08	88.000	6.39	250.000	7.04	710.000	0.00		
0.980	0.00	37.000		105.000		300.000		840.000	0.00		

**Operator notes:**

## Result Analysis Report

**Sample Name:**  
2nd entrance

**SOP Name:**  
Marine Sediment

**Measured:**  
Monday, 4 December 2006 11:13:48 a.m.

**Sample Source & type:**  
Whitianga

**Measured by:**  
jacinta

**Analysed:**  
Monday, 4 December 2006 11:13:49 a.m.

**Sample bulk lot ref:**  
3

**Result Source:**  
Measurement

**Particle Name:**  
Marine Sediment

**Accessory Name:**  
Hydro 2000G (A)

**Analysis model:**  
General purpose

**Sensitivity:**  
Enhanced

**Particle RI:**  
1.500

**Absorption:**  
0

**Size range:**  
0.020 to 2000.000  $\mu\text{m}$

**Obscuration:**  
12.85 %

**Dispersant Name:**  
Water

**Dispersant RI:**  
1.330

**Weighted Residual:**  
1.010 %

**Result Emulation:**  
Off

**Concentration:**  
0.2745 %Vol

**Span :**  
1.920

**Uniformity:**  
0.653

**Result units:**  
Volume

**Specific Surface Area:**  
0.0415  $\text{m}^2/\text{g}$

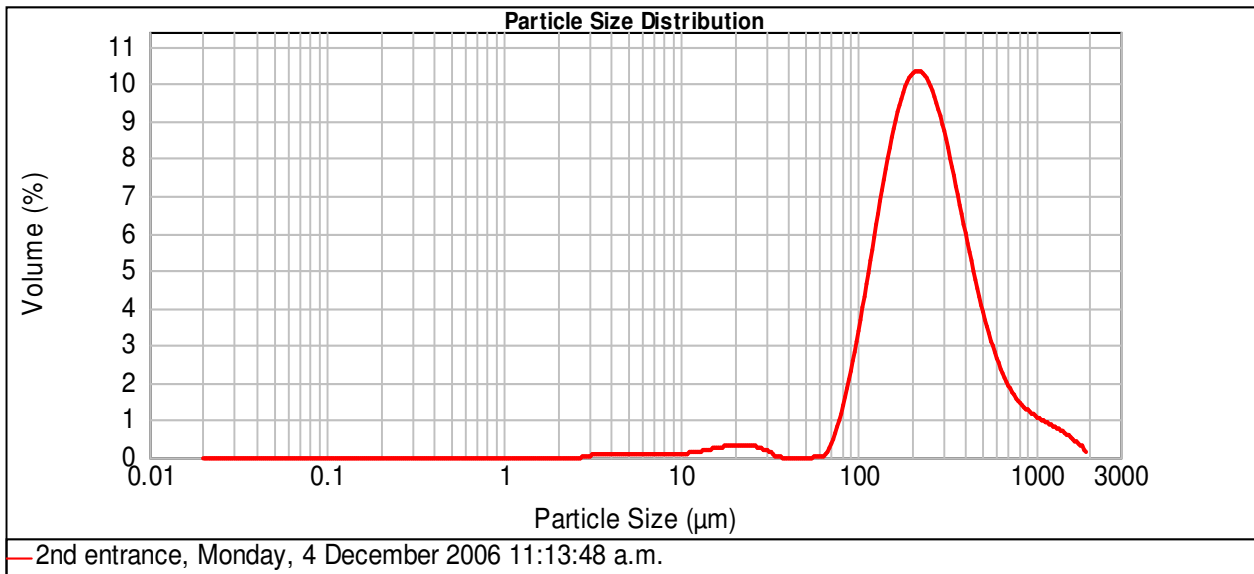
**Surface Weighted Mean D[3,2]:**  
144.618  $\mu\text{m}$

**Vol. Weighted Mean D[4,3]:**  
302.483  $\mu\text{m}$

**d(0.1): 113.024  $\mu\text{m}$**

**d(0.5): 230.537  $\mu\text{m}$**

**d(0.9): 555.612  $\mu\text{m}$**

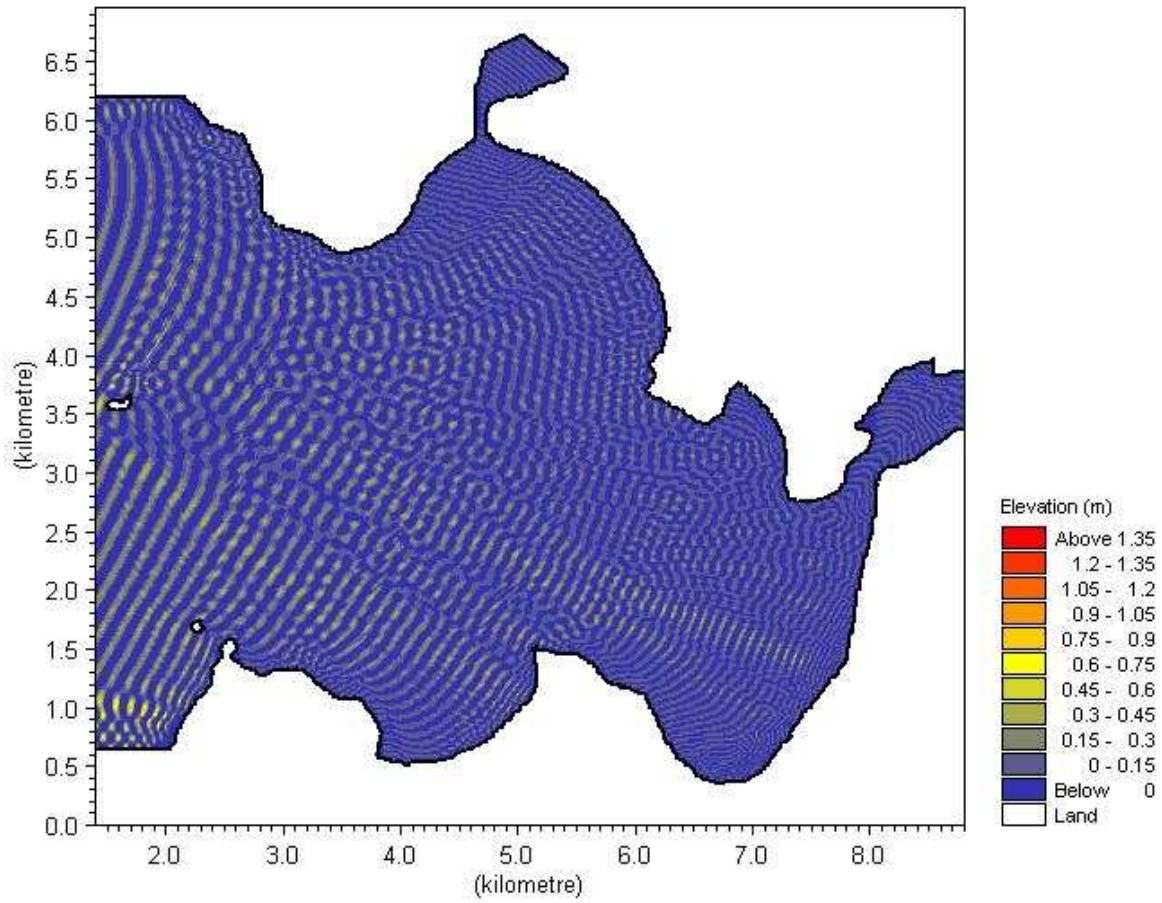


Size ( $\mu\text{m}$ )	Volume In %	Size ( $\mu\text{m}$ )	Volume In %	Size ( $\mu\text{m}$ )	Volume In %	Size ( $\mu\text{m}$ )	Volume In %	Size ( $\mu\text{m}$ )	Volume In %	Size ( $\mu\text{m}$ )	Volume In %
0.050	0.00	0.980	0.00	37.000	0.00	105.000	5.86	300.000	8.11	840.000	1.38
0.060	0.00	2.000	0.14	44.000	0.00	125.000	8.40	350.000	7.59	1000.000	3.07
0.120	0.00	3.900	0.40	53.000	0.00	149.000	10.25	420.000	5.27	2000.000	
0.240	0.00	7.800	0.60	63.000	0.28	177.000	11.34	500.000	3.51		
0.490	0.00	15.600	1.32	74.000	1.53	210.000	11.70	590.000	2.69		
0.700	0.00	31.000	0.06	88.000	3.50	250.000	11.26	710.000	1.72		
0.980	0.00	37.000		105.000		300.000		840.000			

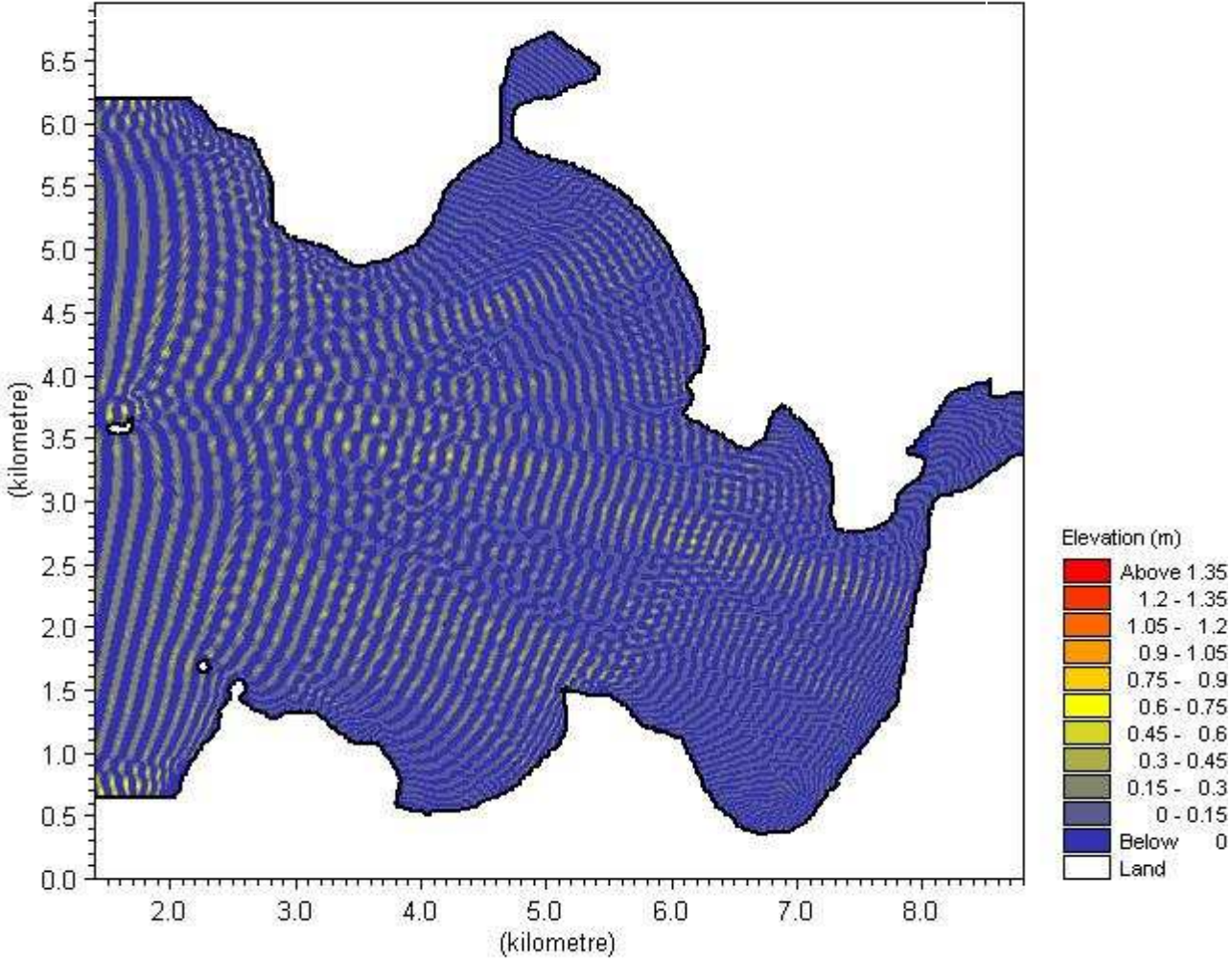
**Operator notes:**

# 0.6 m, 13s wave at open boundary

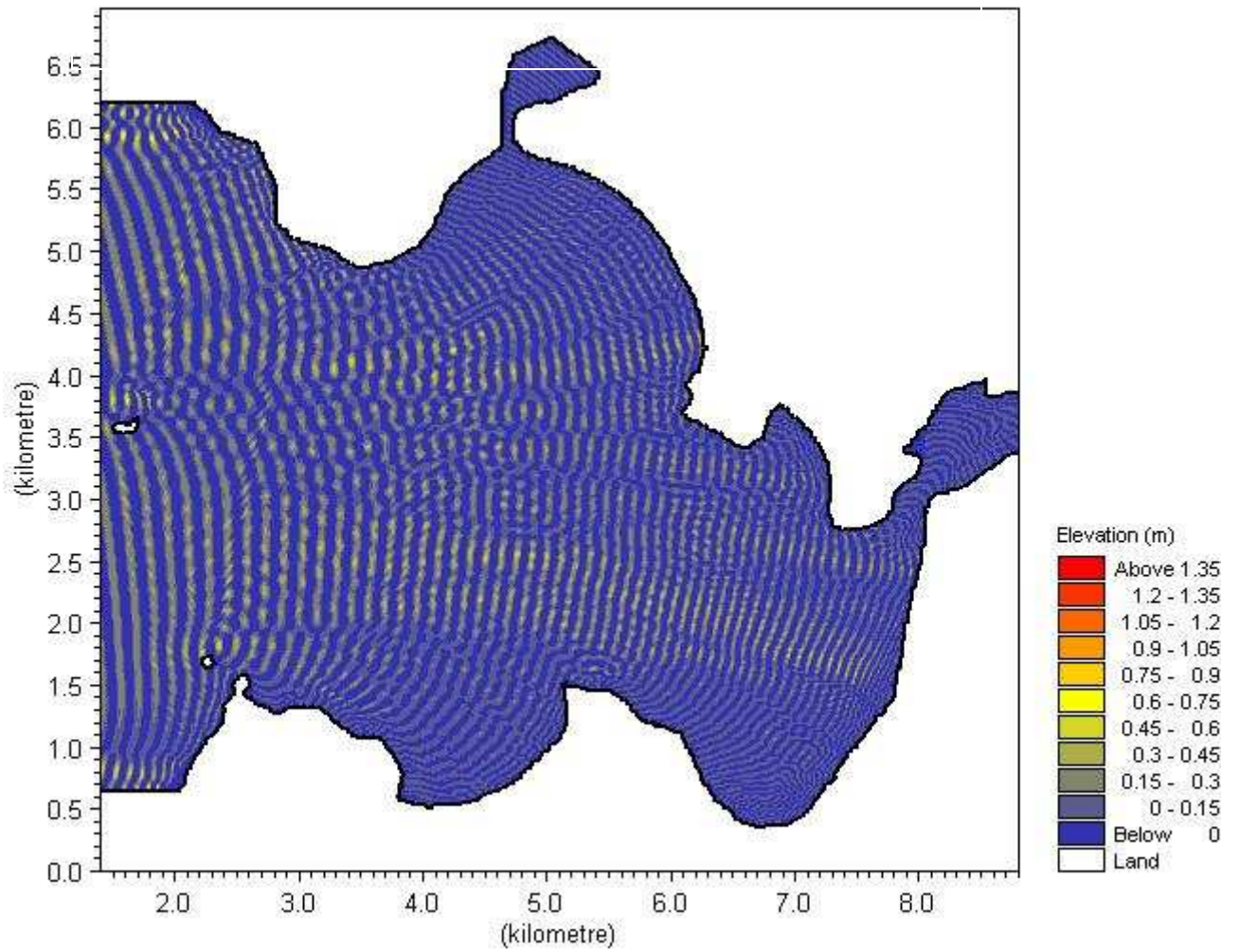
## Wave approach from 90 Degrees



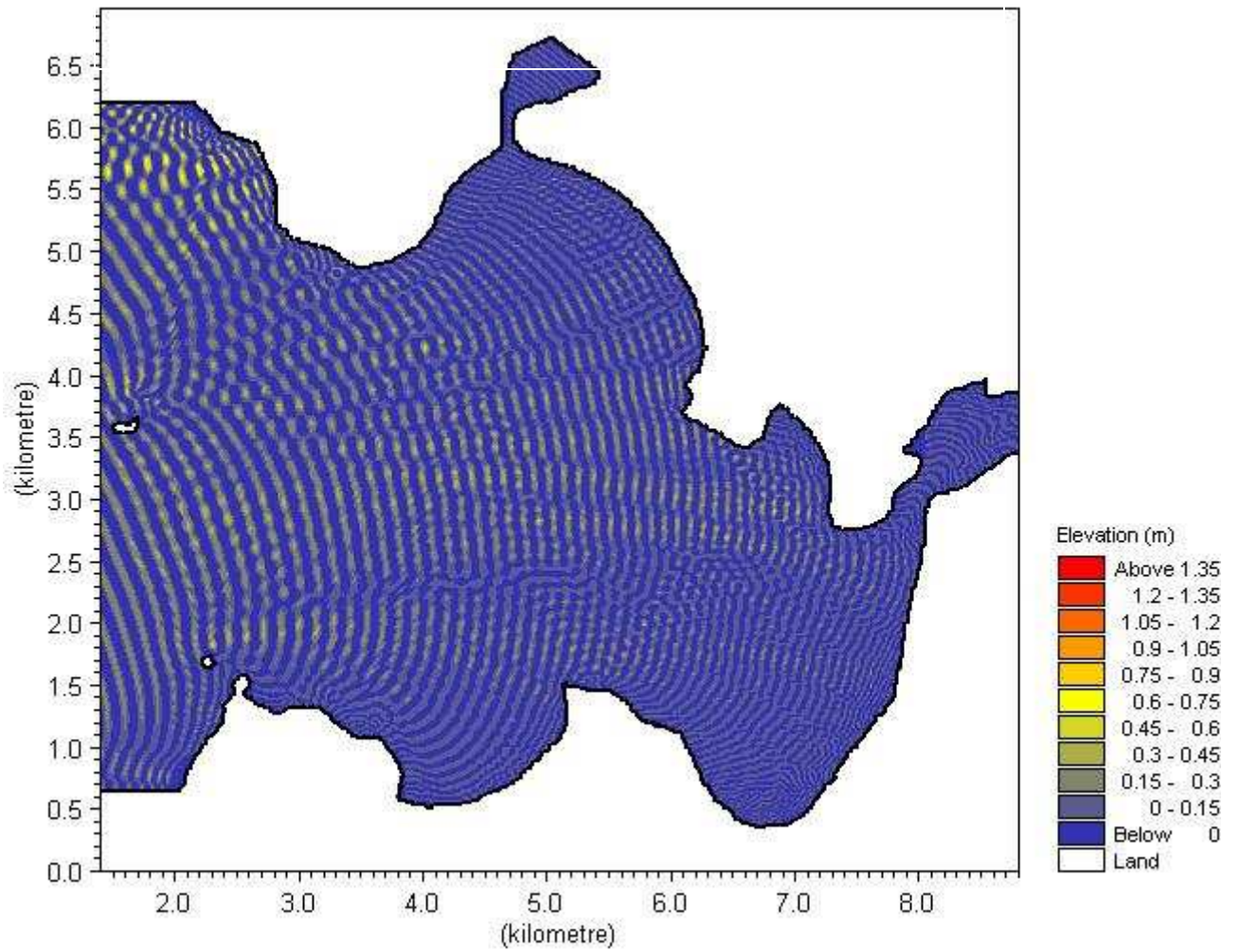
# Wave approach from 70 Degrees



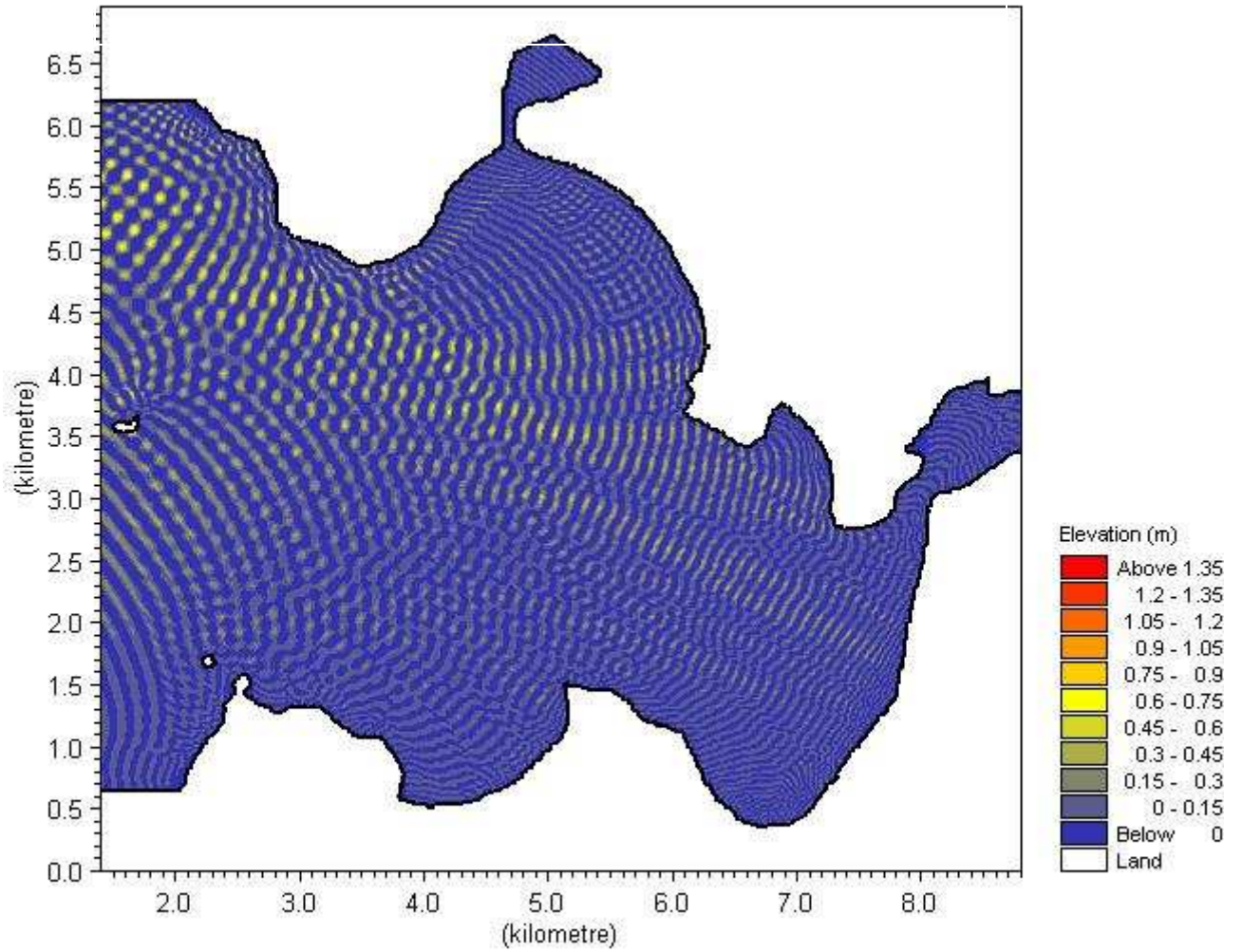
# Wave approach from 50 Degrees



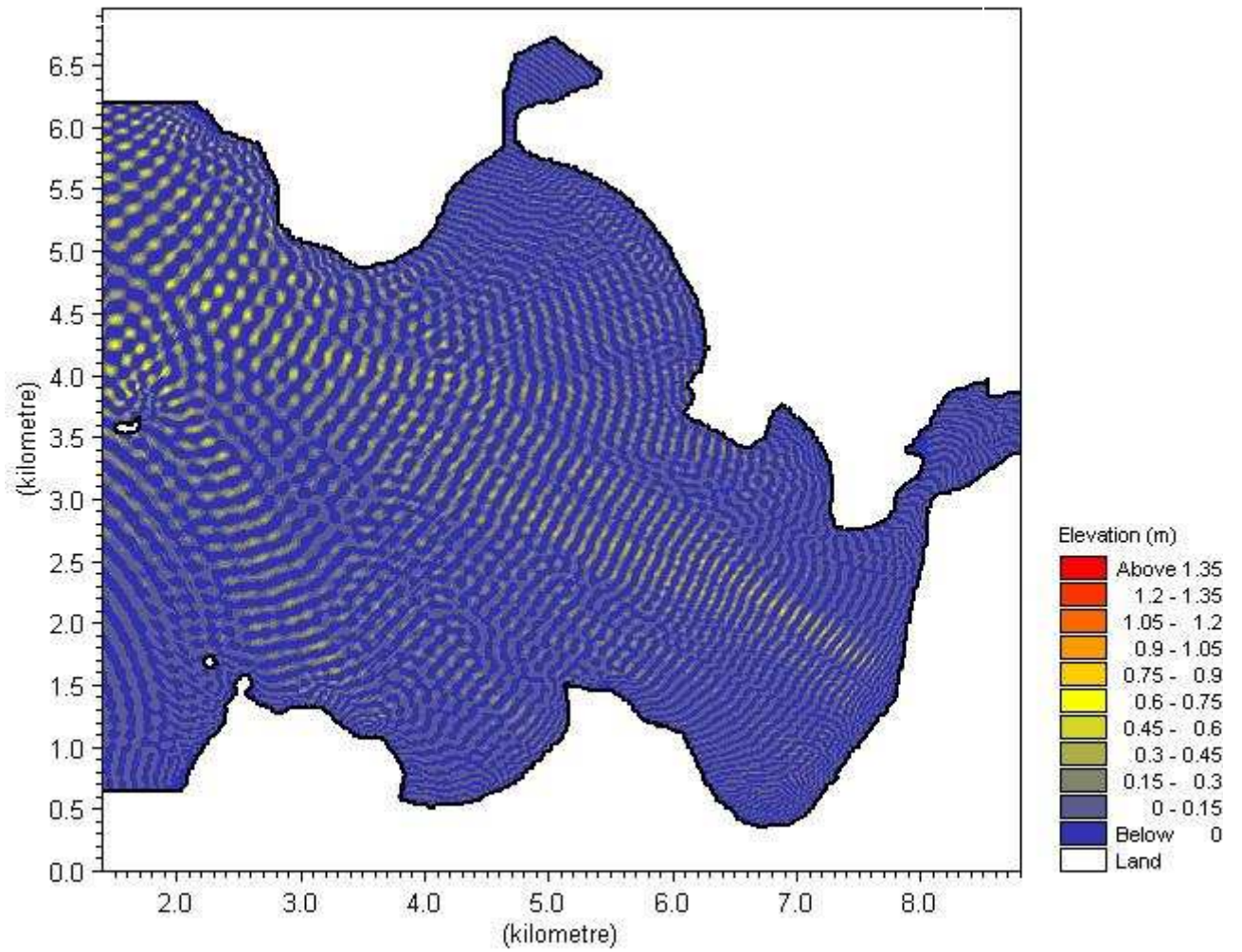
# Wave approach from 30 Degrees



# Wave approach from 10 Degrees

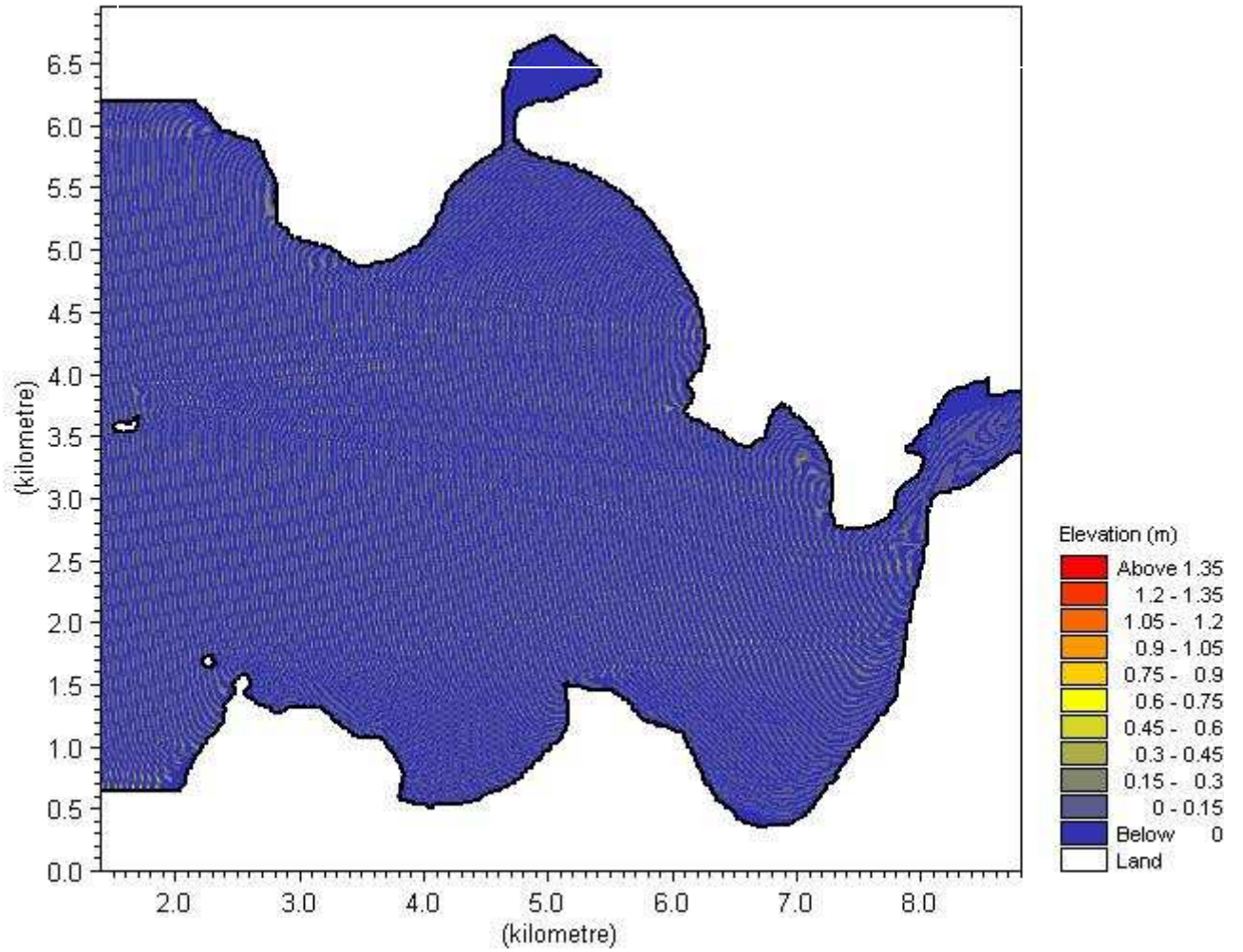


# Wave approach from 0 Degrees

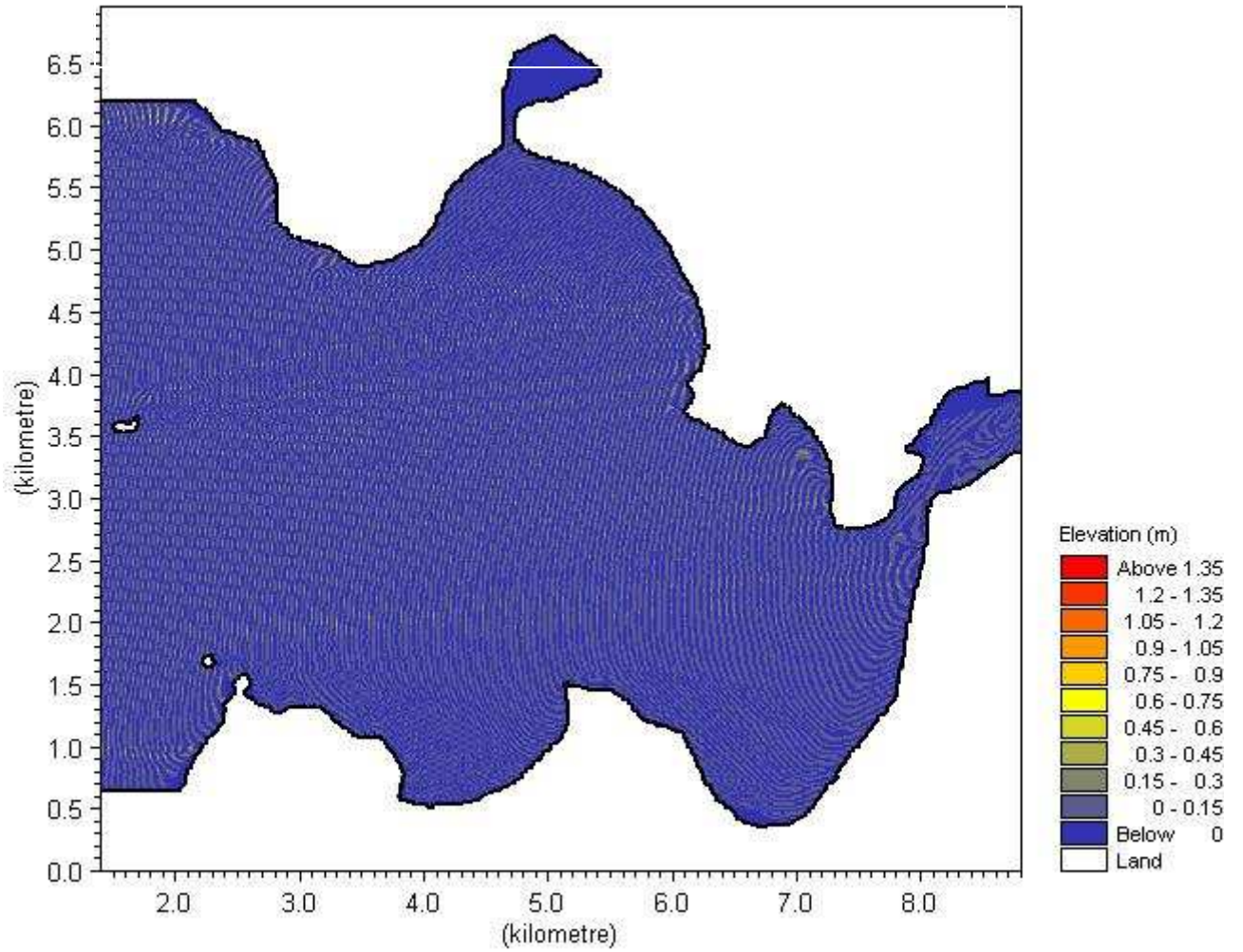


# 0.6 m, 5s wave at open boundary

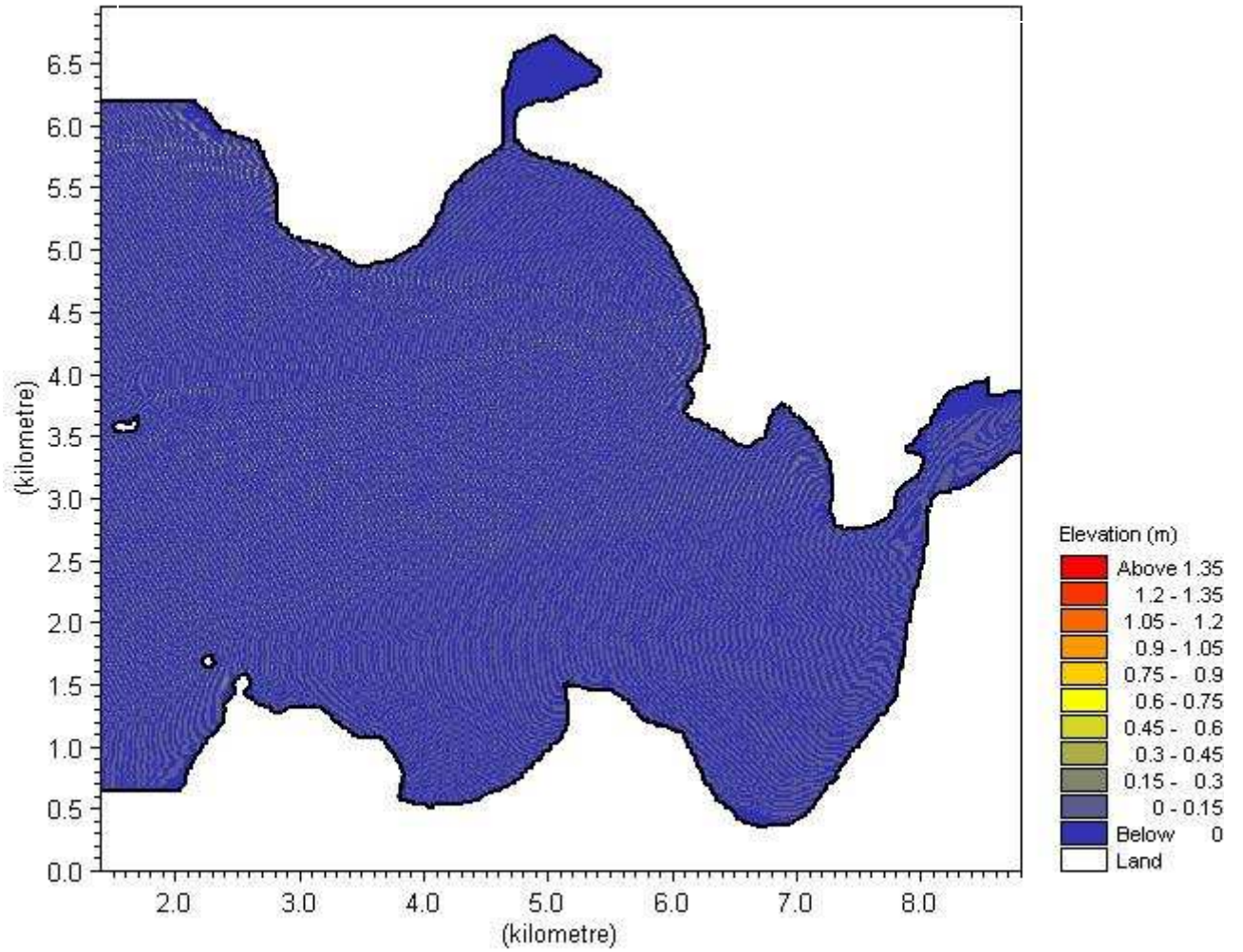
## Wave approach from 0 Degrees



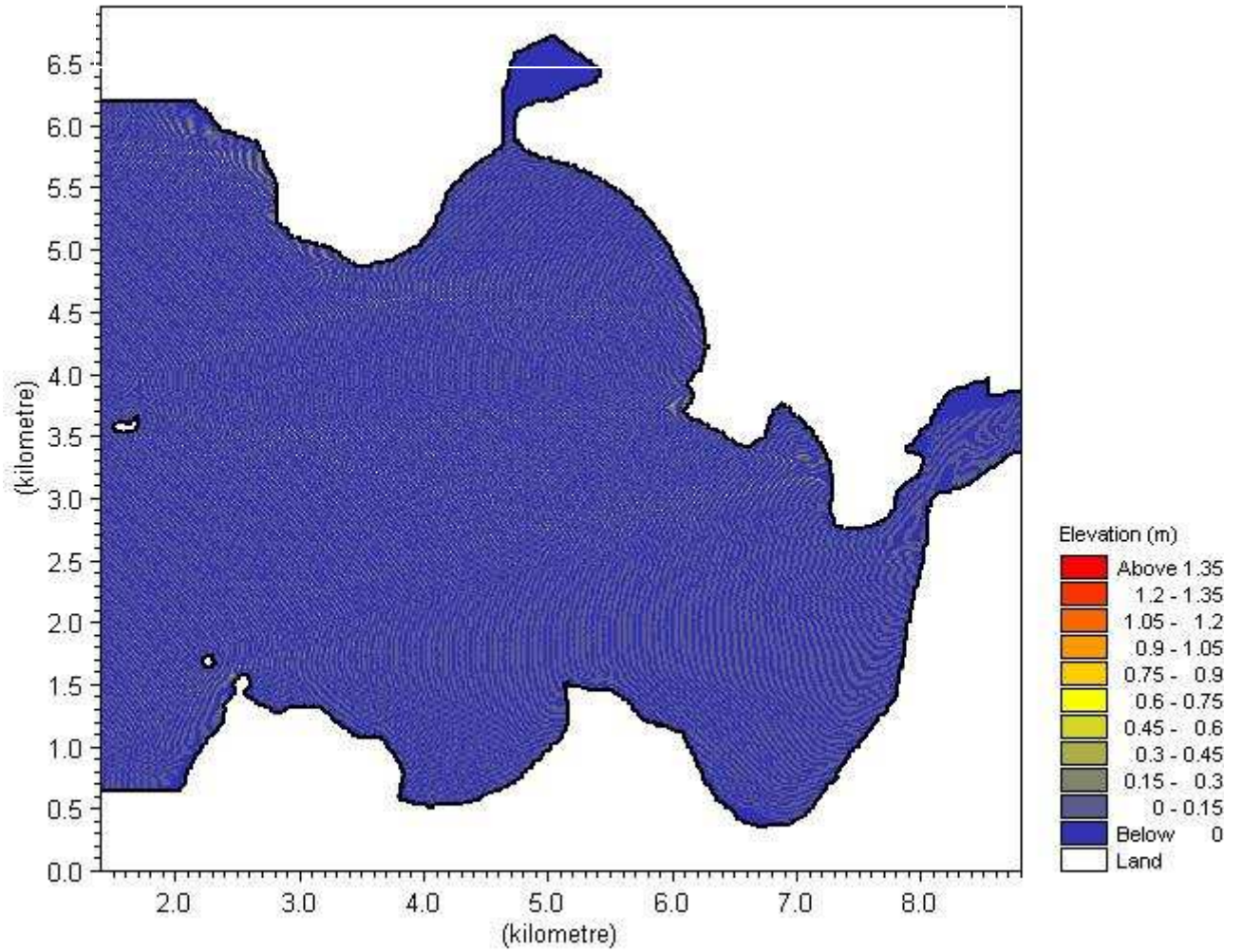
# Wave approach from 10 Degrees



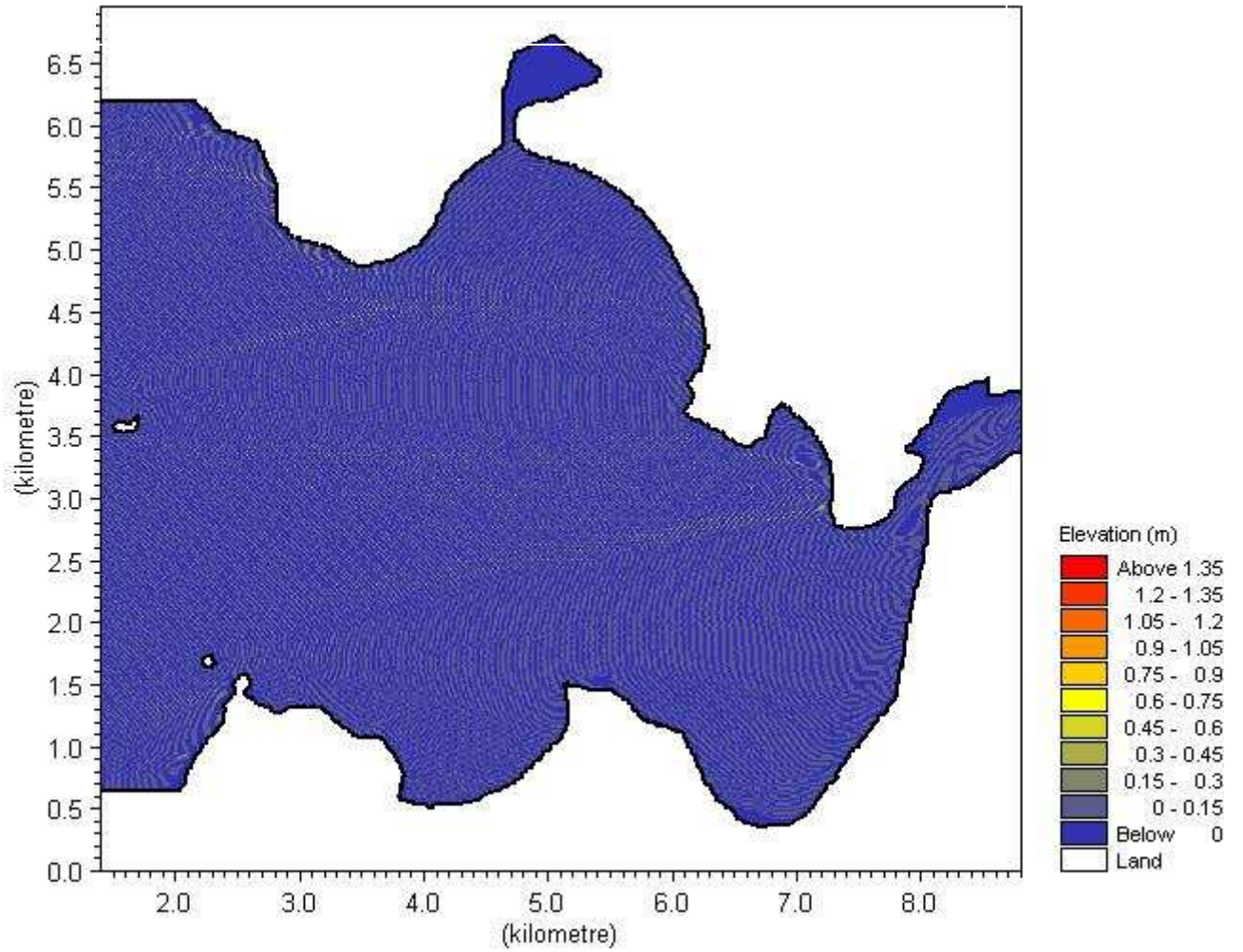
# Wave approach from 30 Degrees



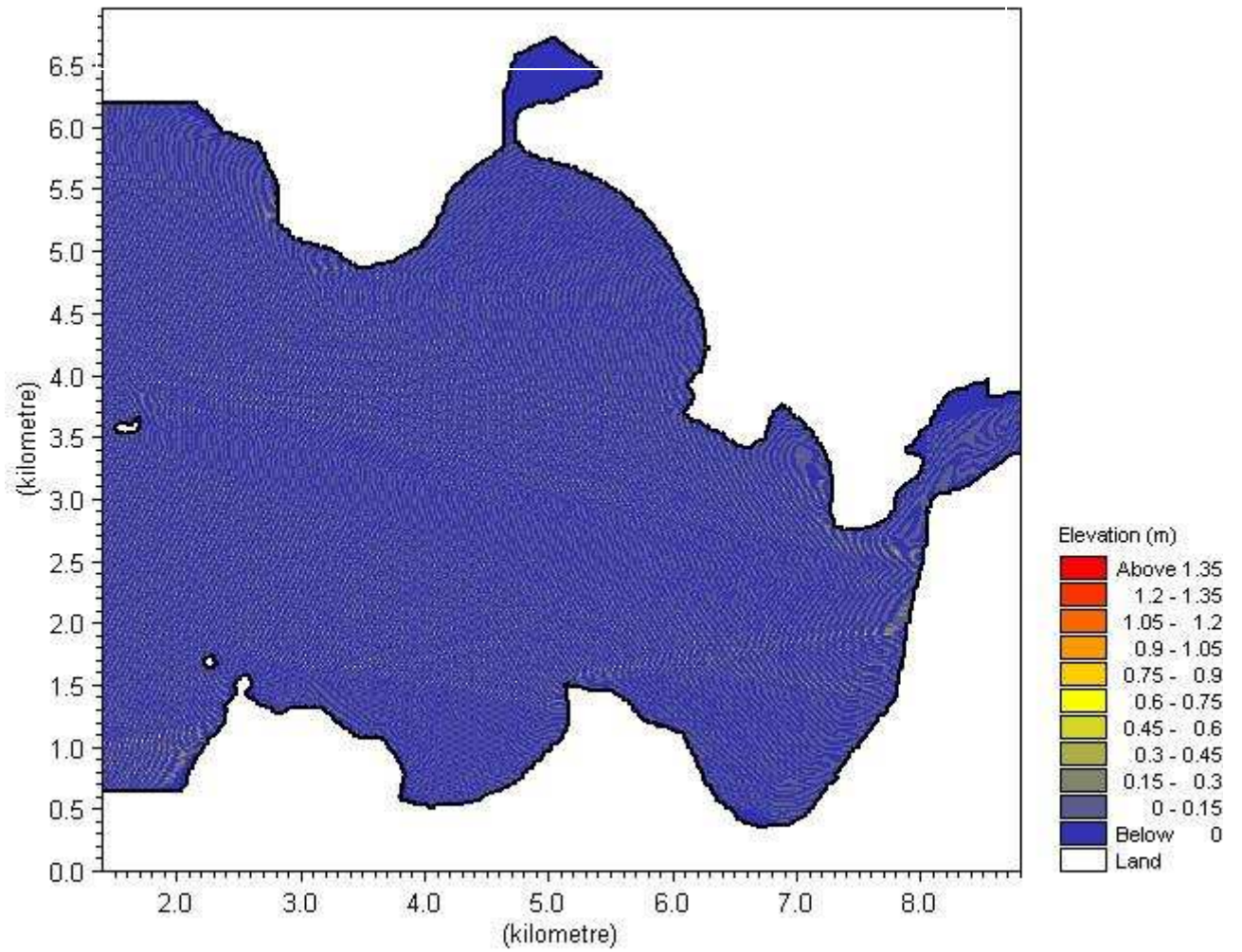
# Wave approach from 50 Degrees



# Wave approach from 70 Degrees

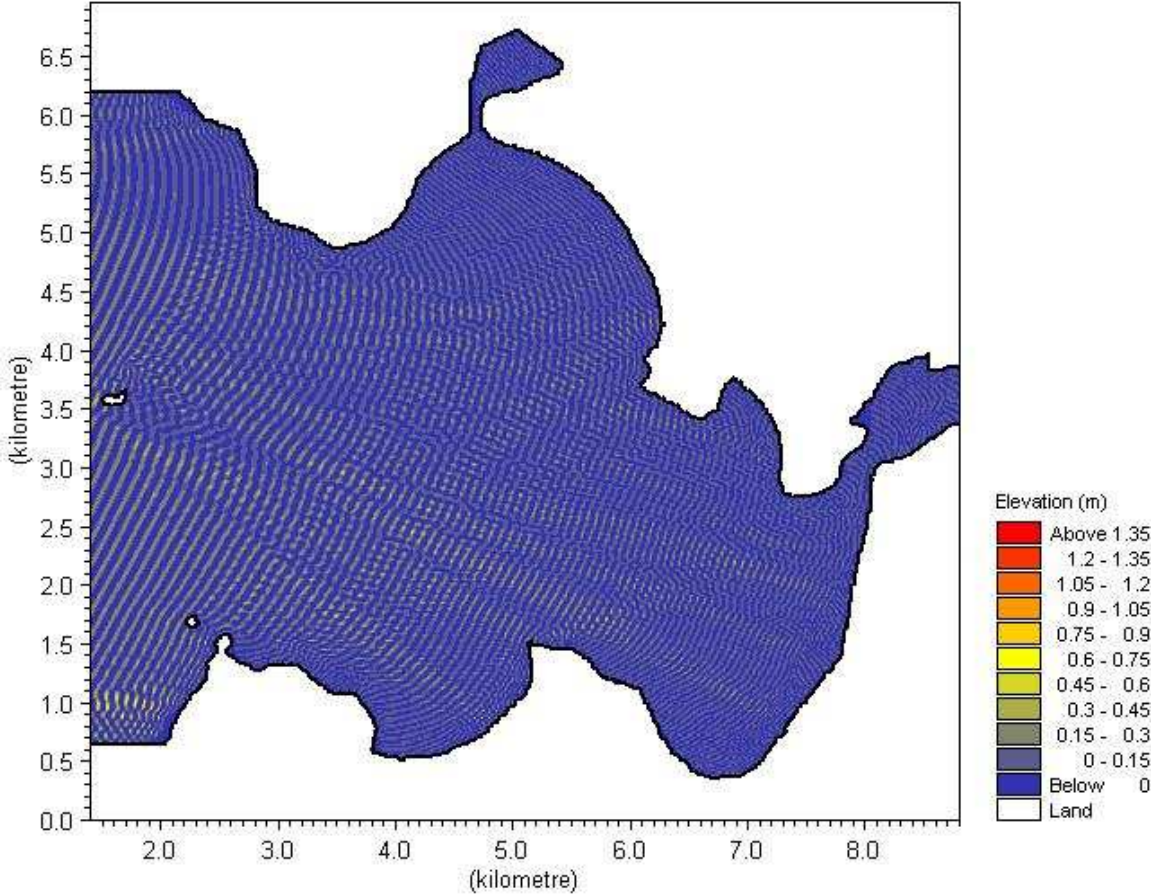


# Wave approach from 90 Degrees

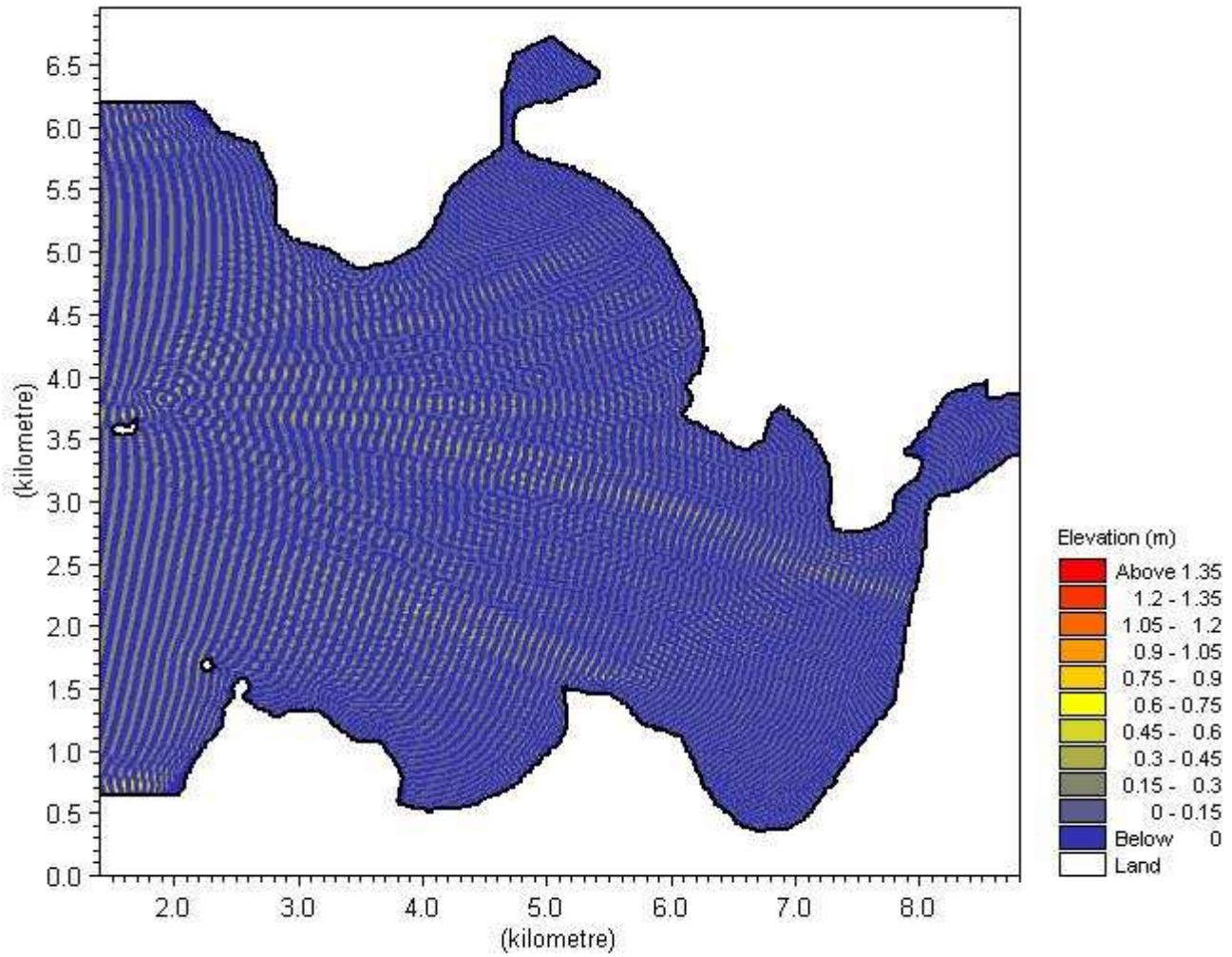


# 0.6 m, 9s wave at open boundary

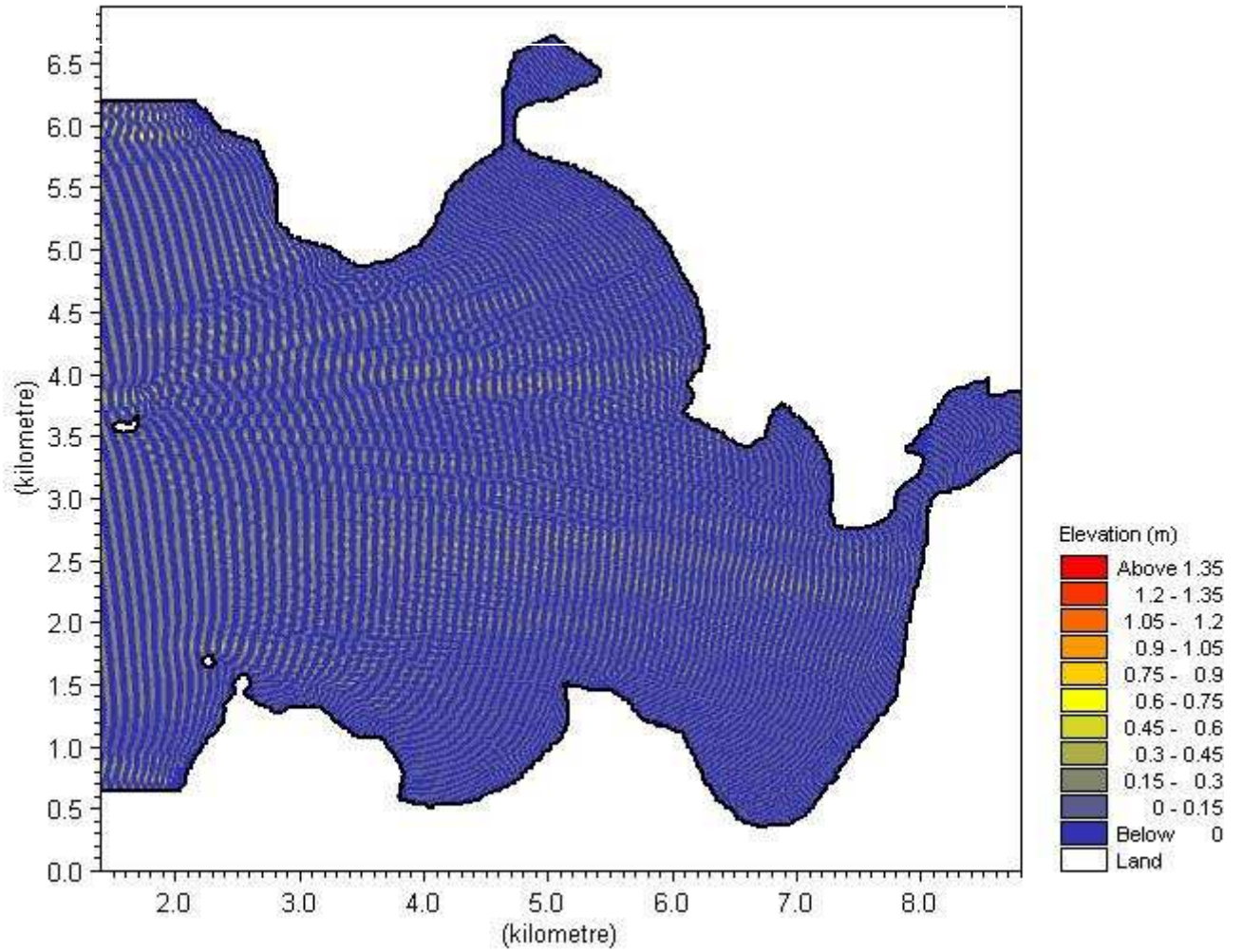
## Wave approach from 90 Degrees



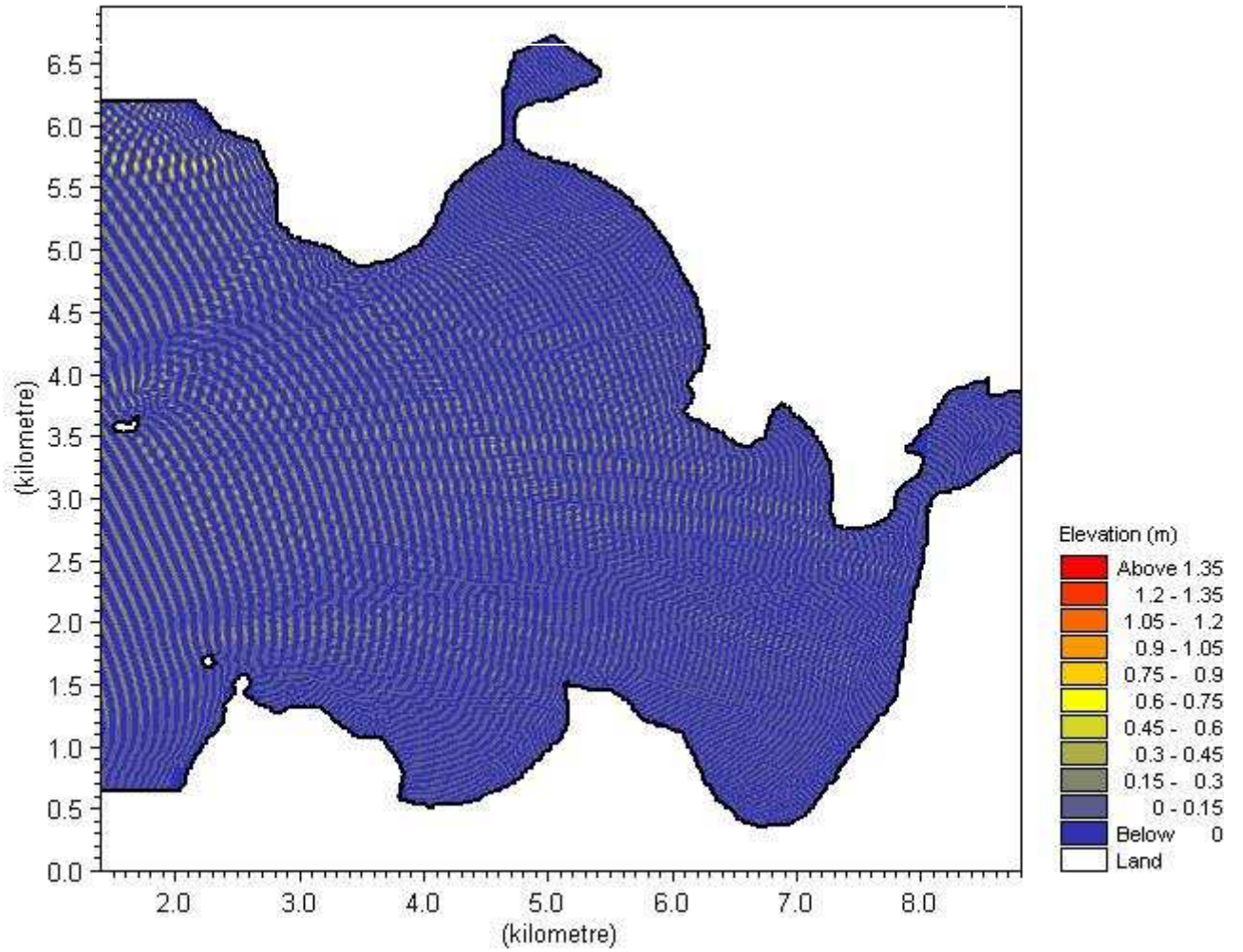
# Wave approach from 70 Degrees



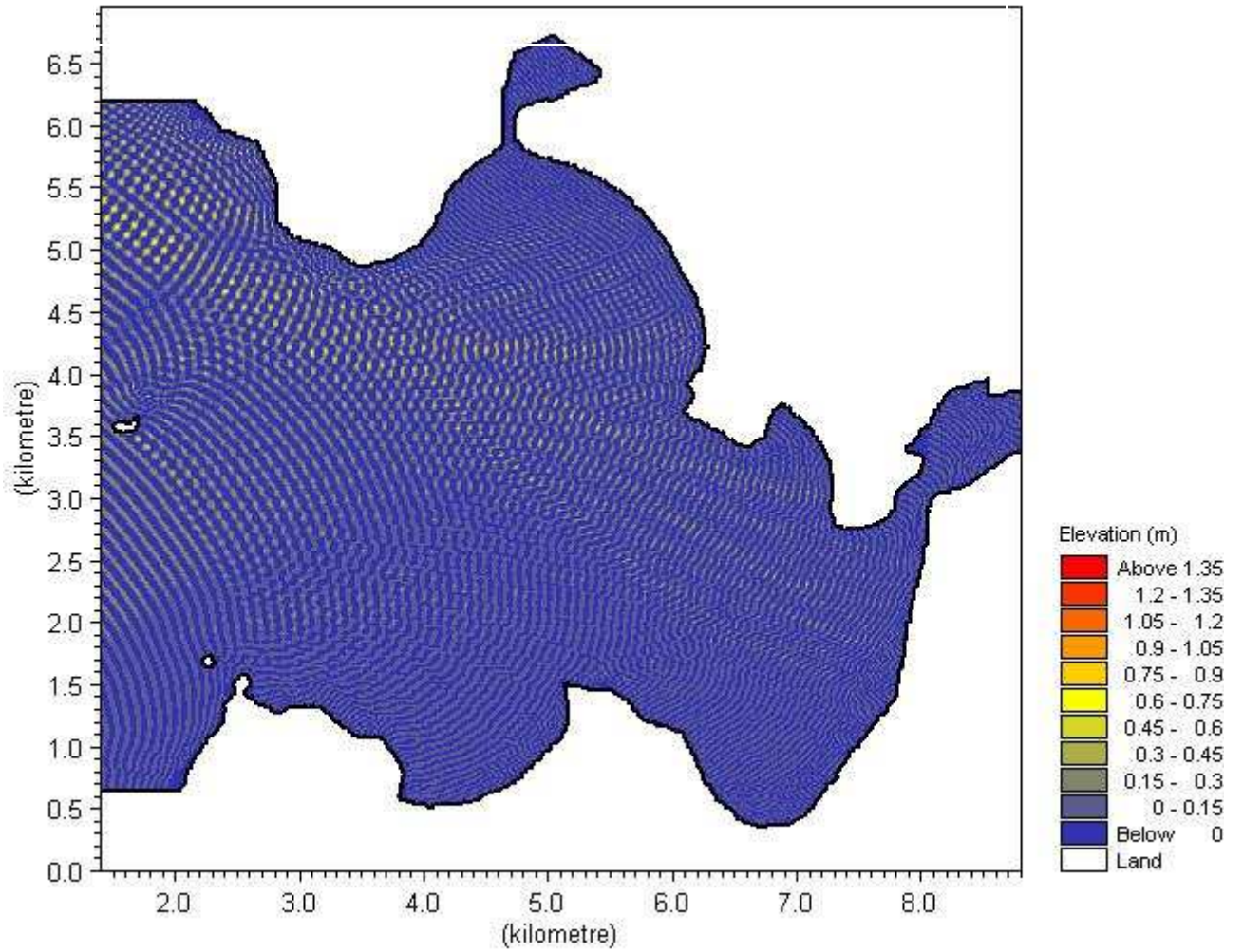
# Wave approach from 50 Degrees



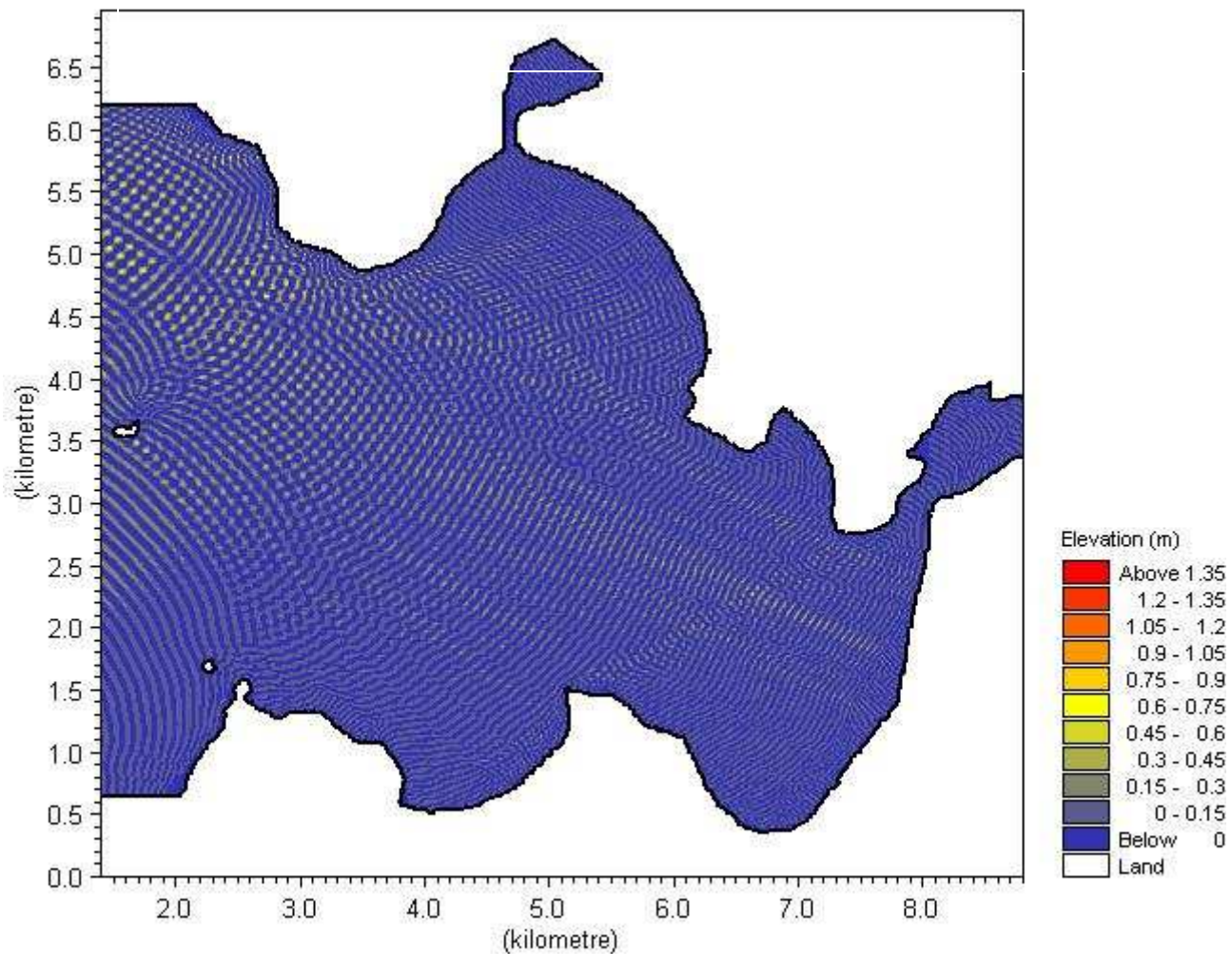
# Wave approach from 30 Degrees



# Wave approach from 10 Degrees

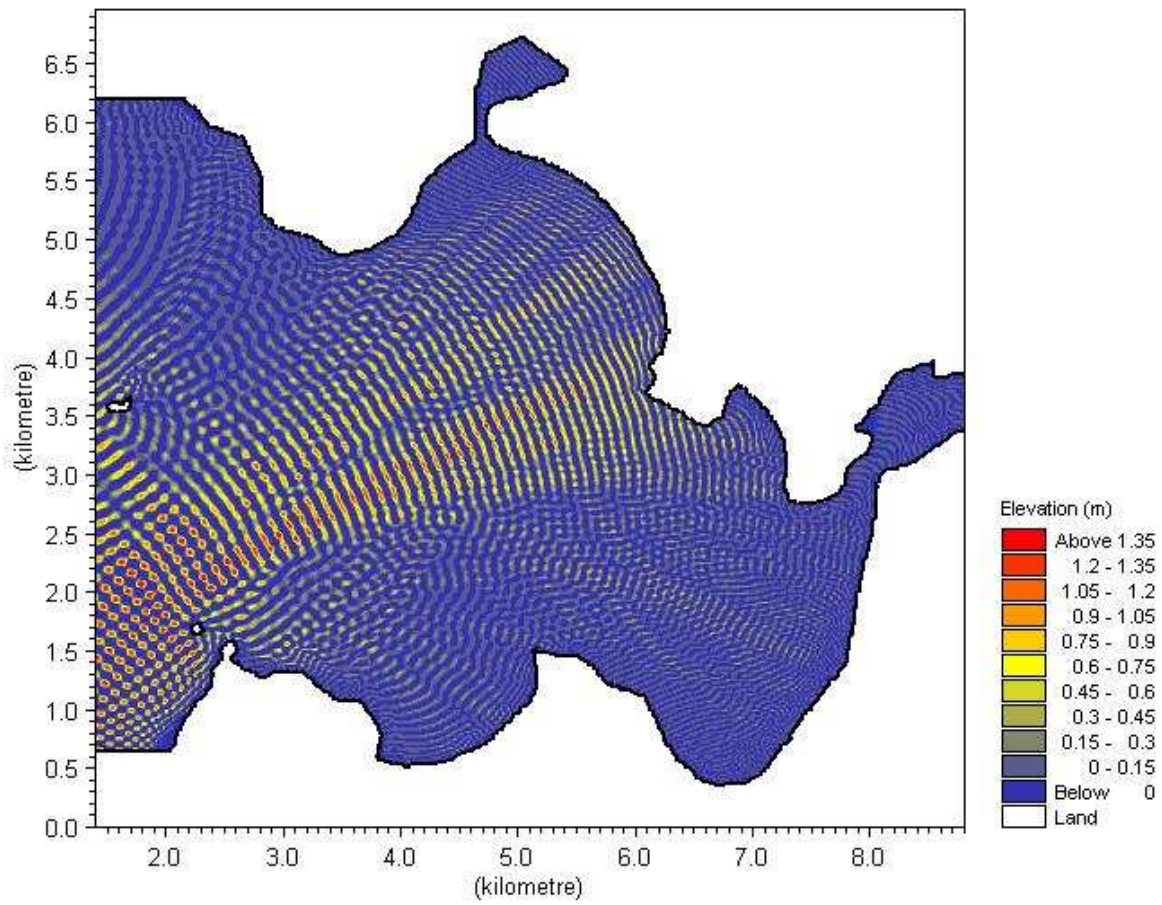


# Wave approach from 0 Degrees

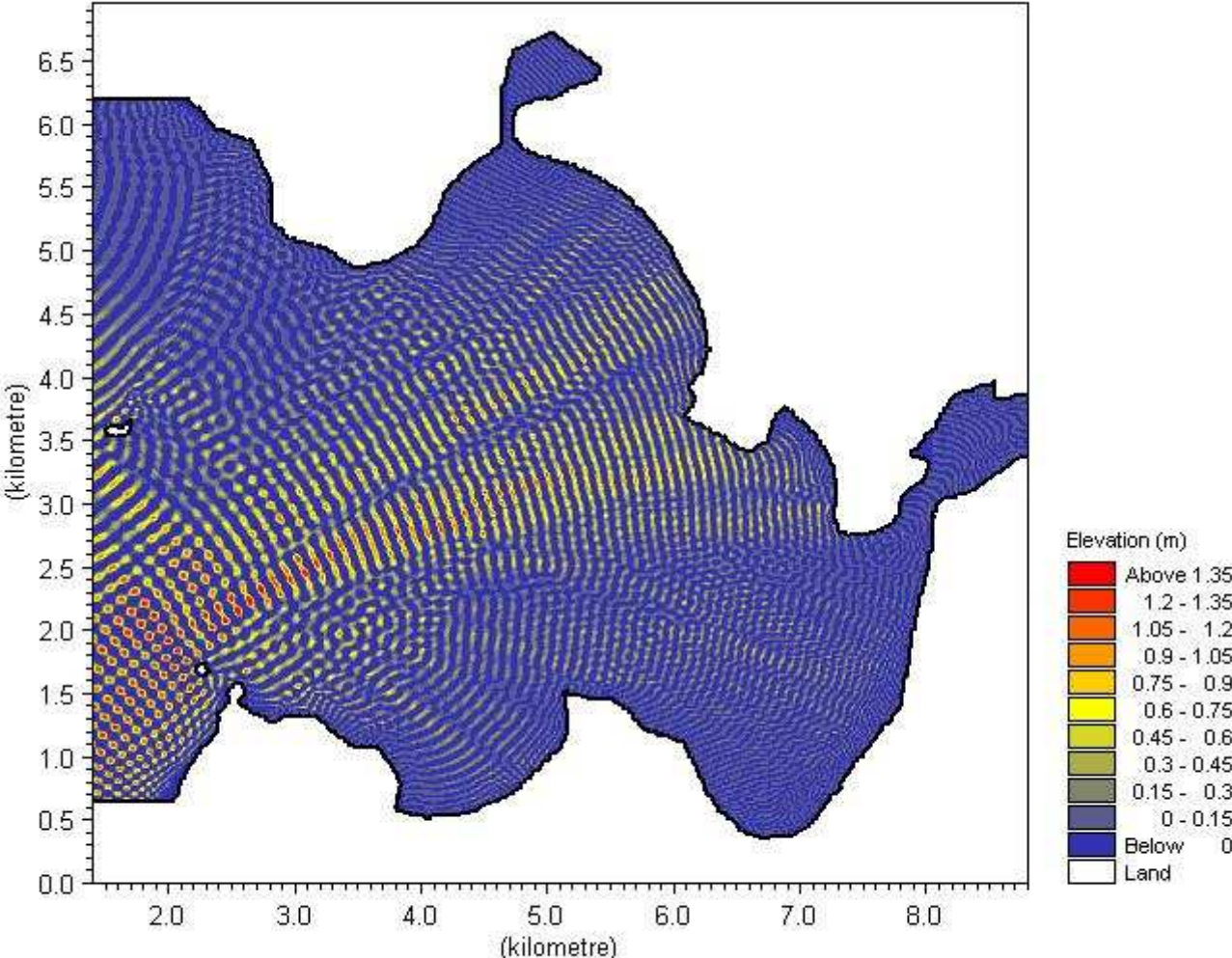


# 1.5 m, 11s wave at open boundary

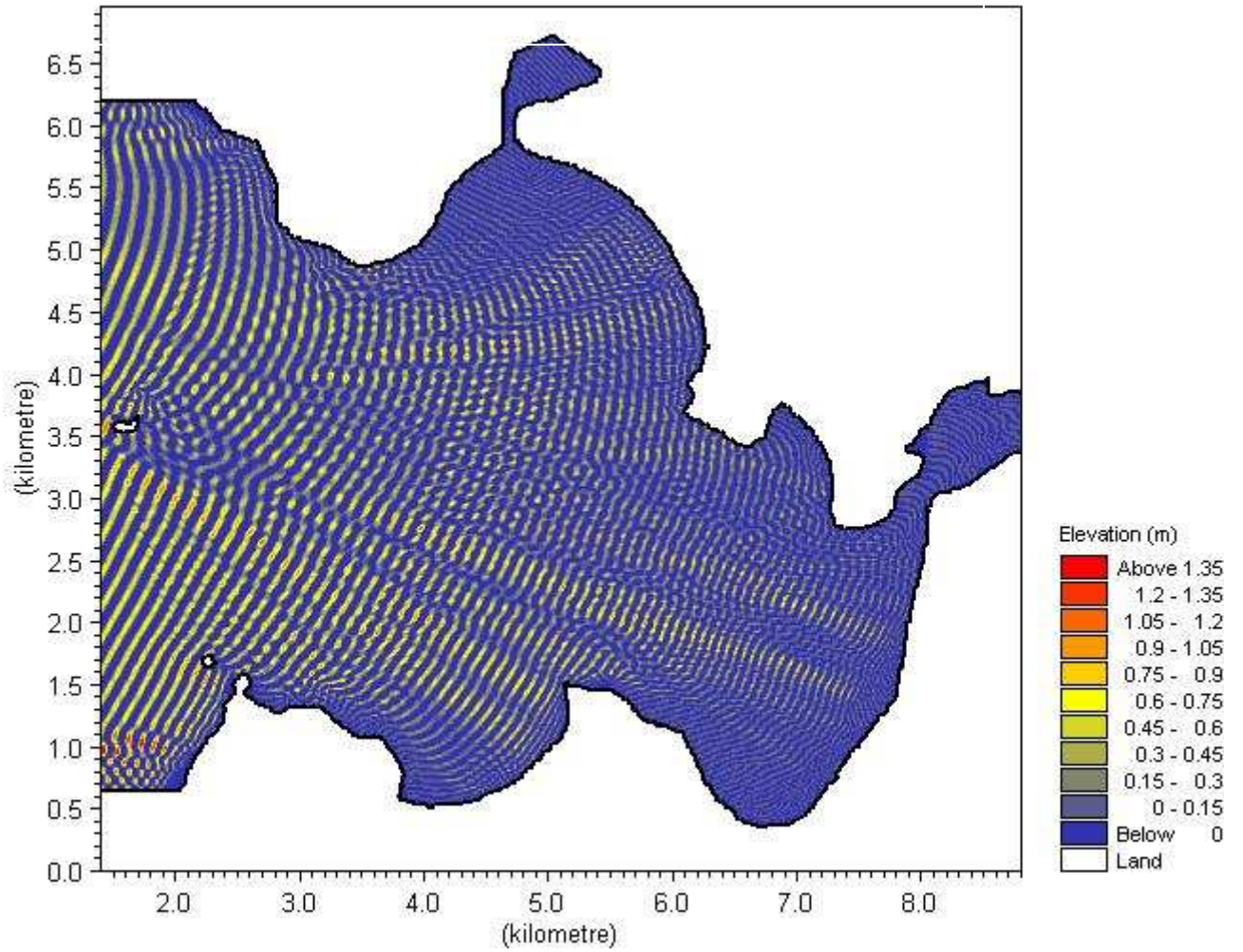
## Wave approach from 170 Degrees



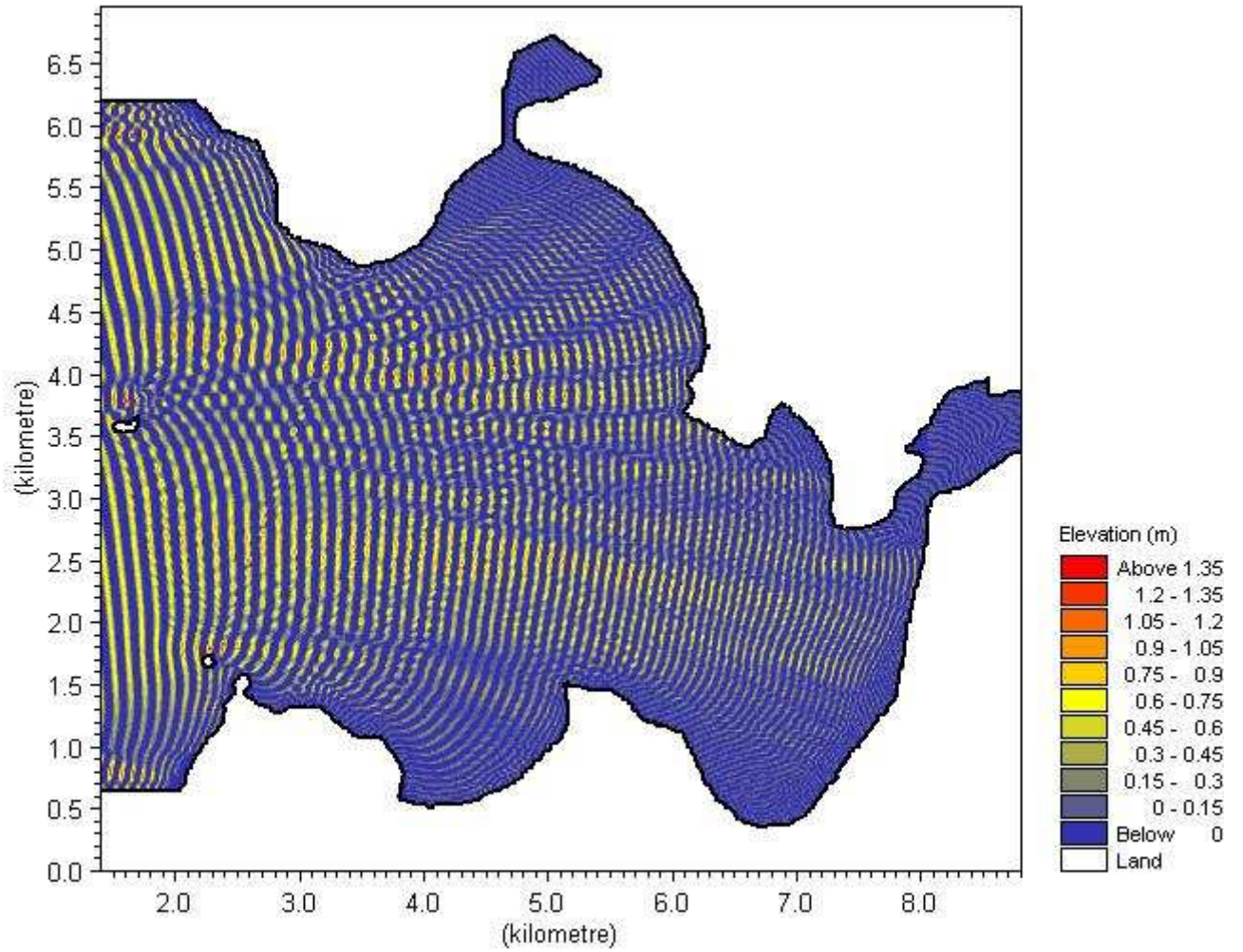
# Wave approach from 130 Degrees



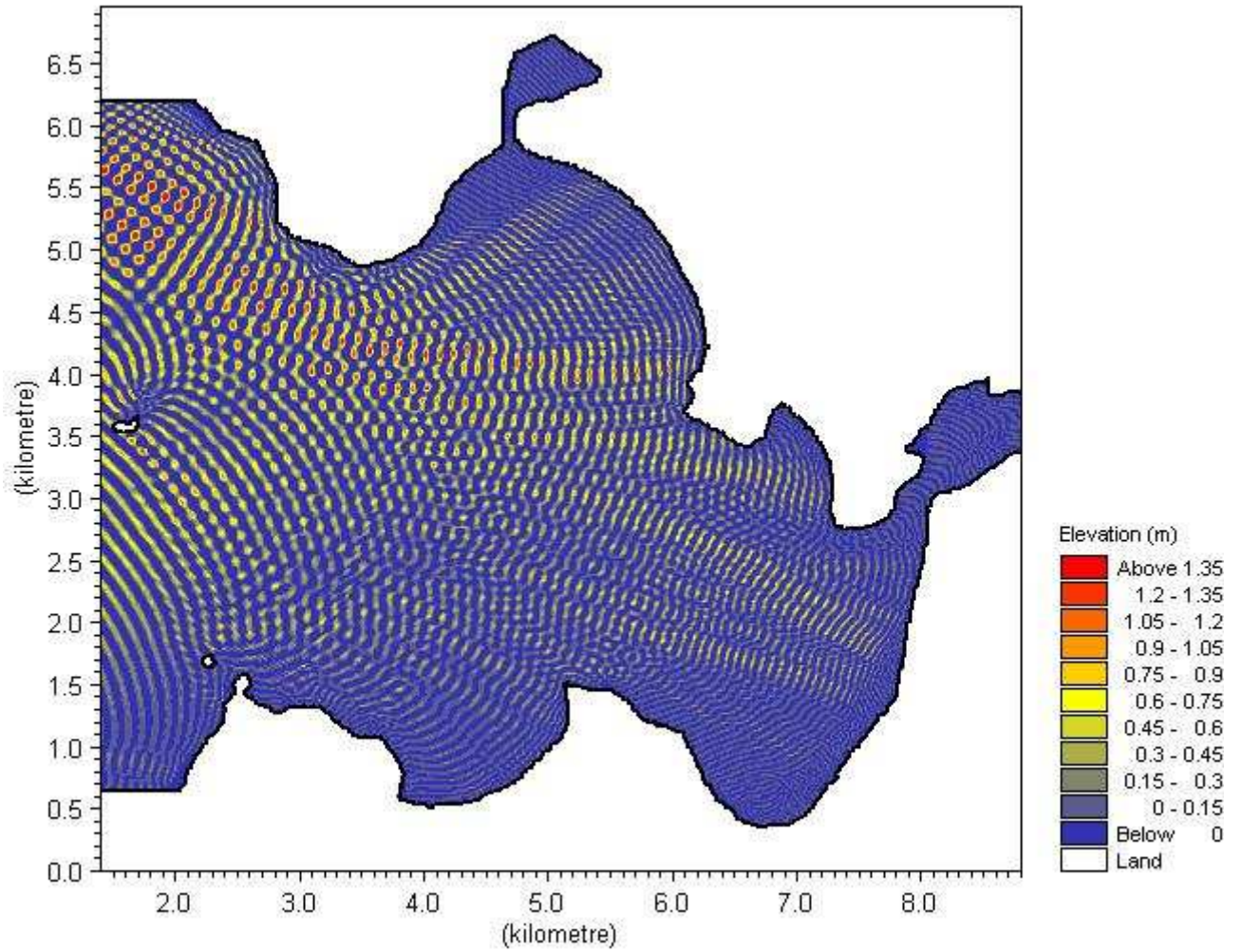
# Wave approach from 90 Degrees



# Wave approach from 50 Degrees

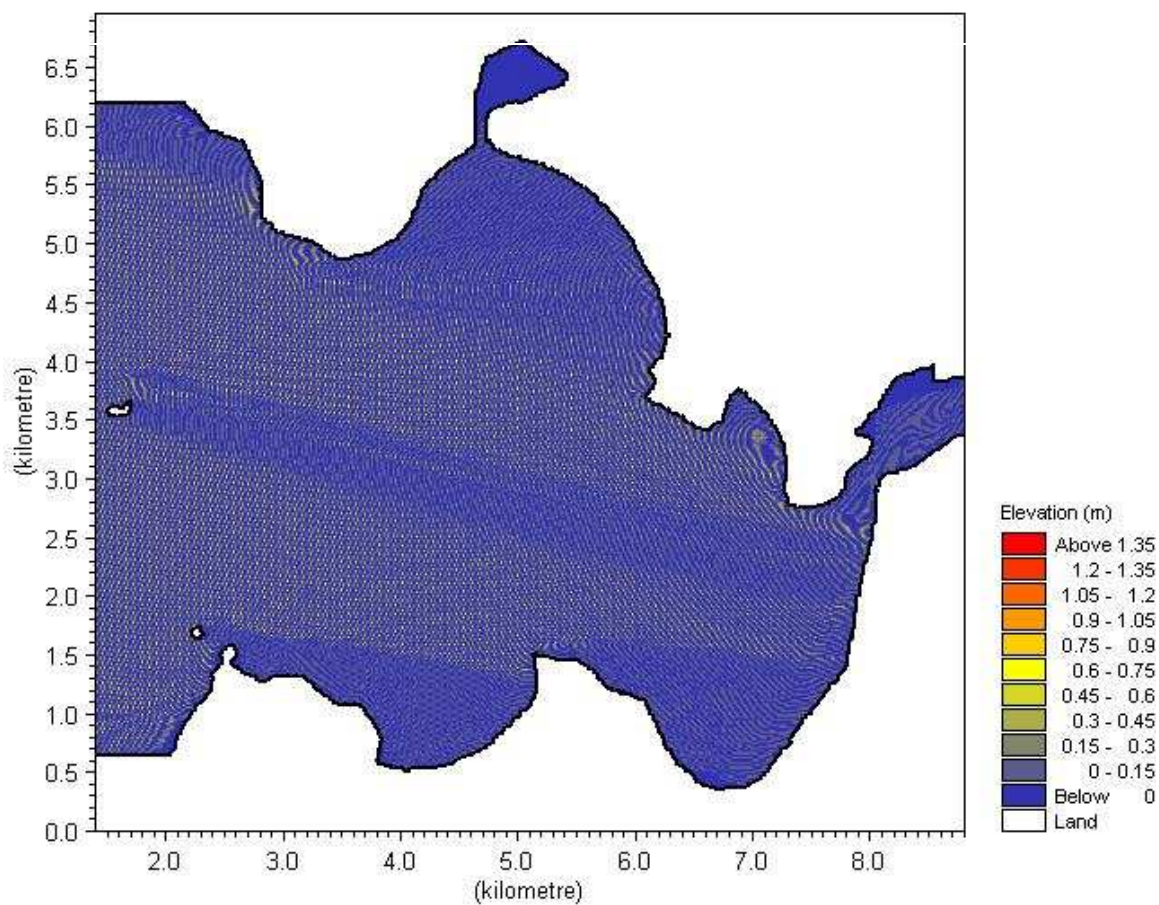


# Wave approach from 10 Degrees

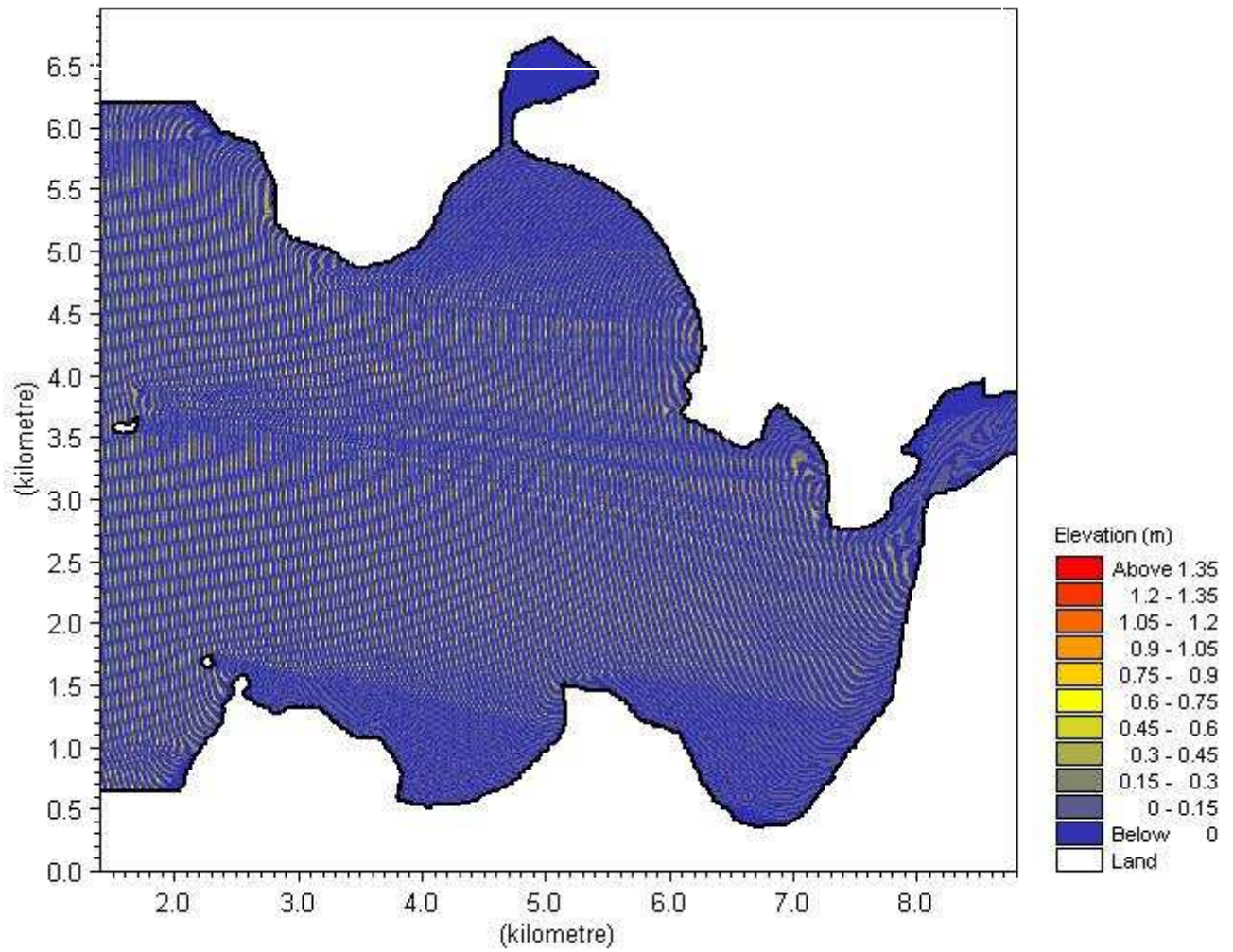


# 1.5 m, 5s wave at open boundary

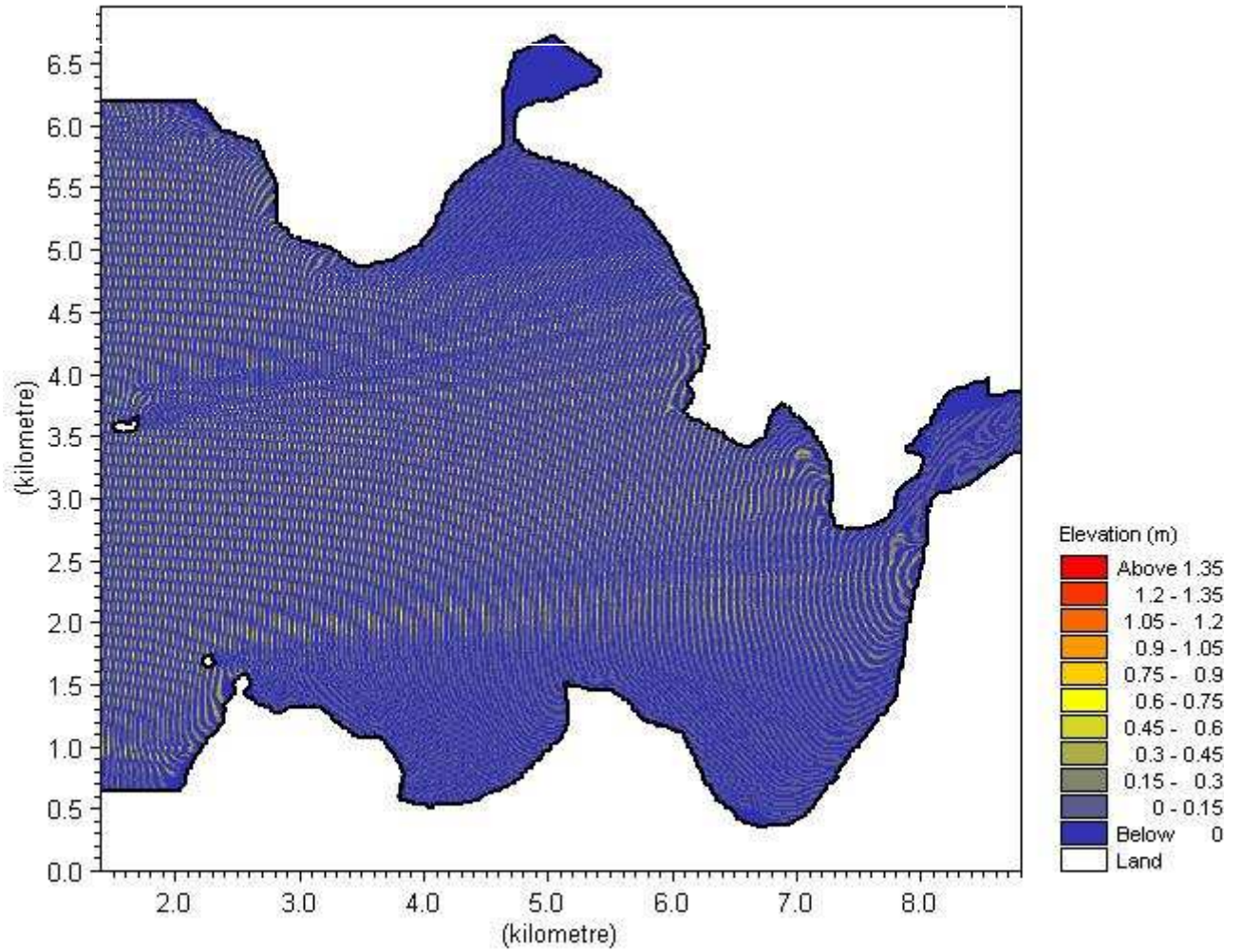
## Wave approach from 90 Degrees



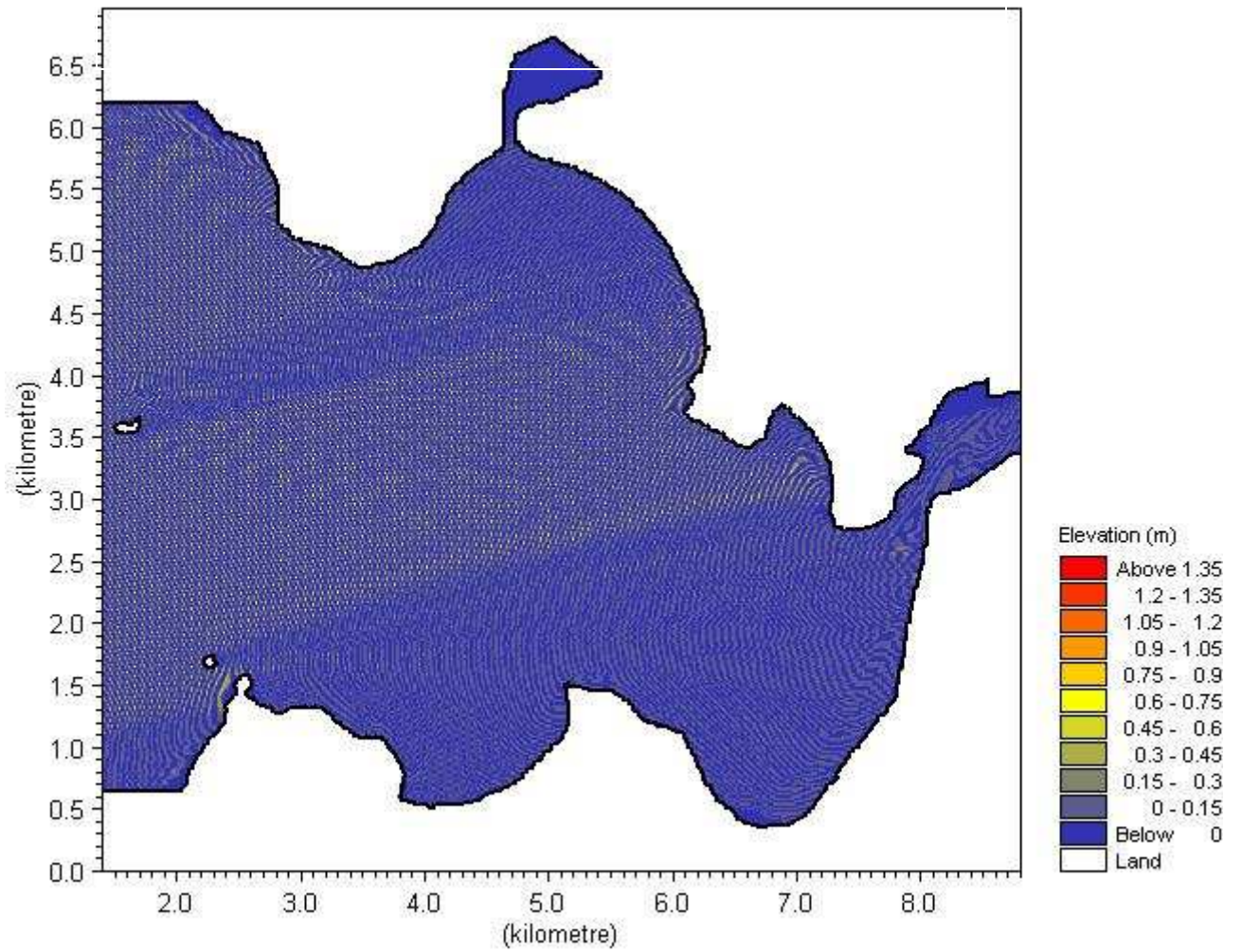
# Wave approach from 70 Degrees



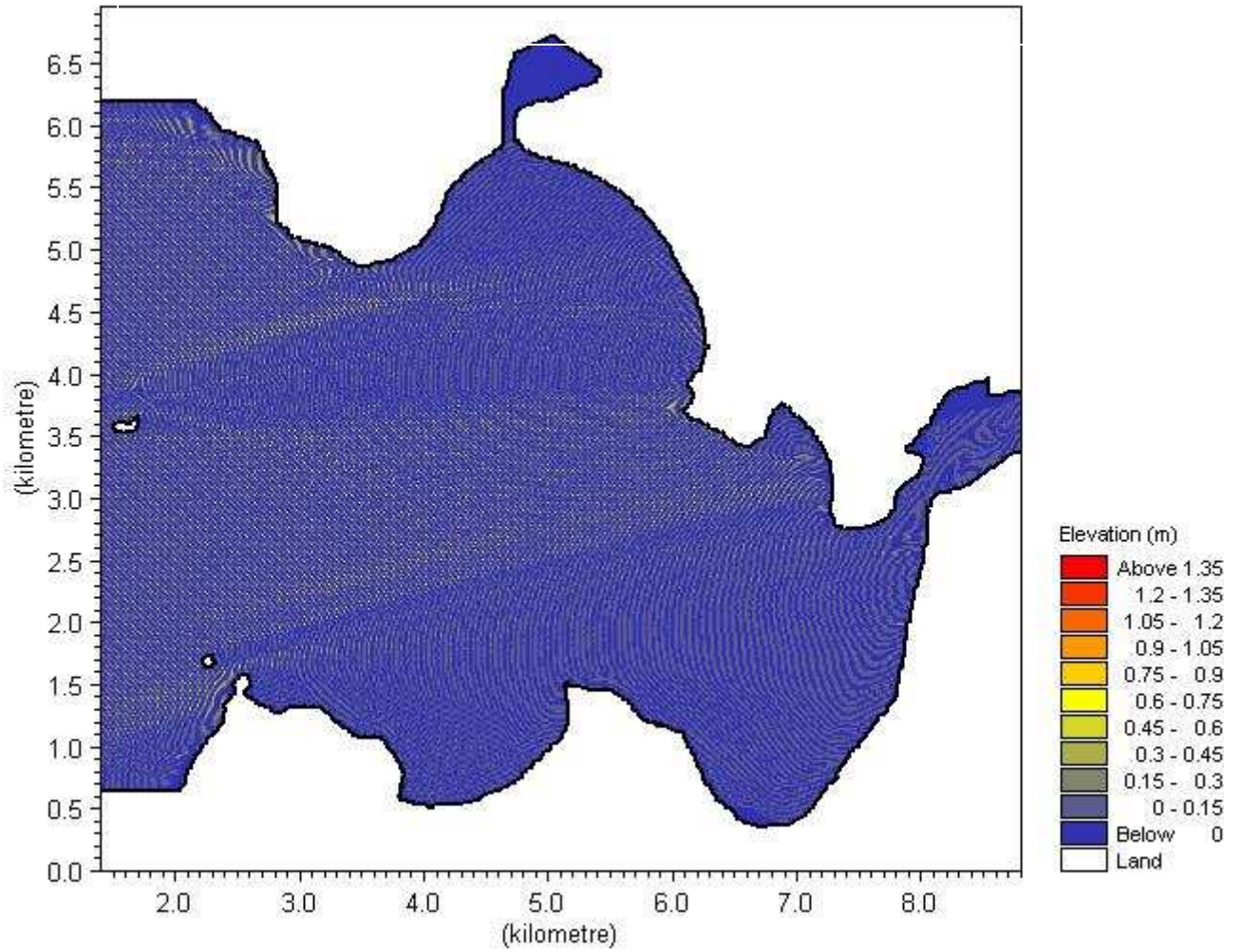
# Wave approach from 50 Degrees



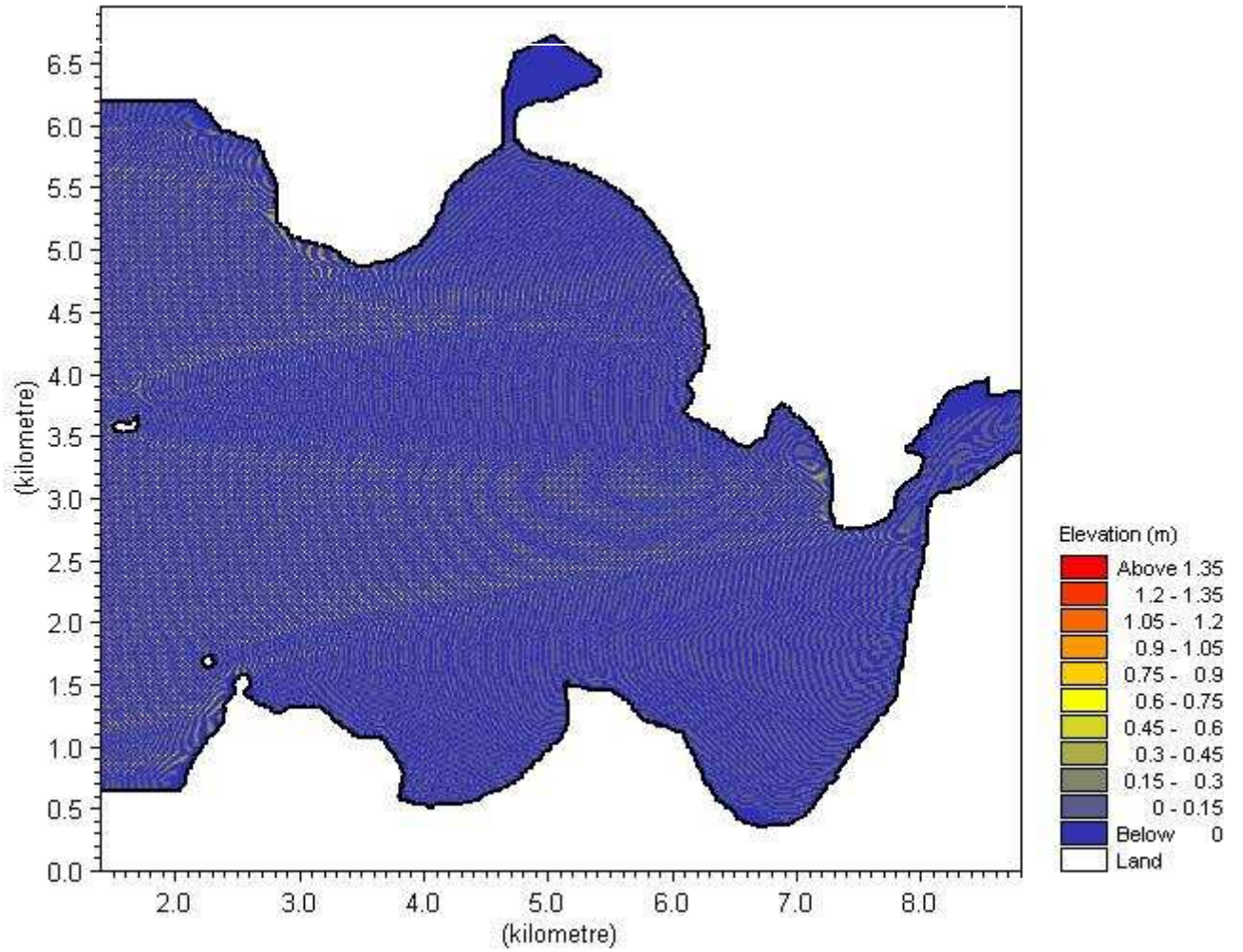
# Wave approach from 30 Degrees



# Wave approach from 10 Degrees

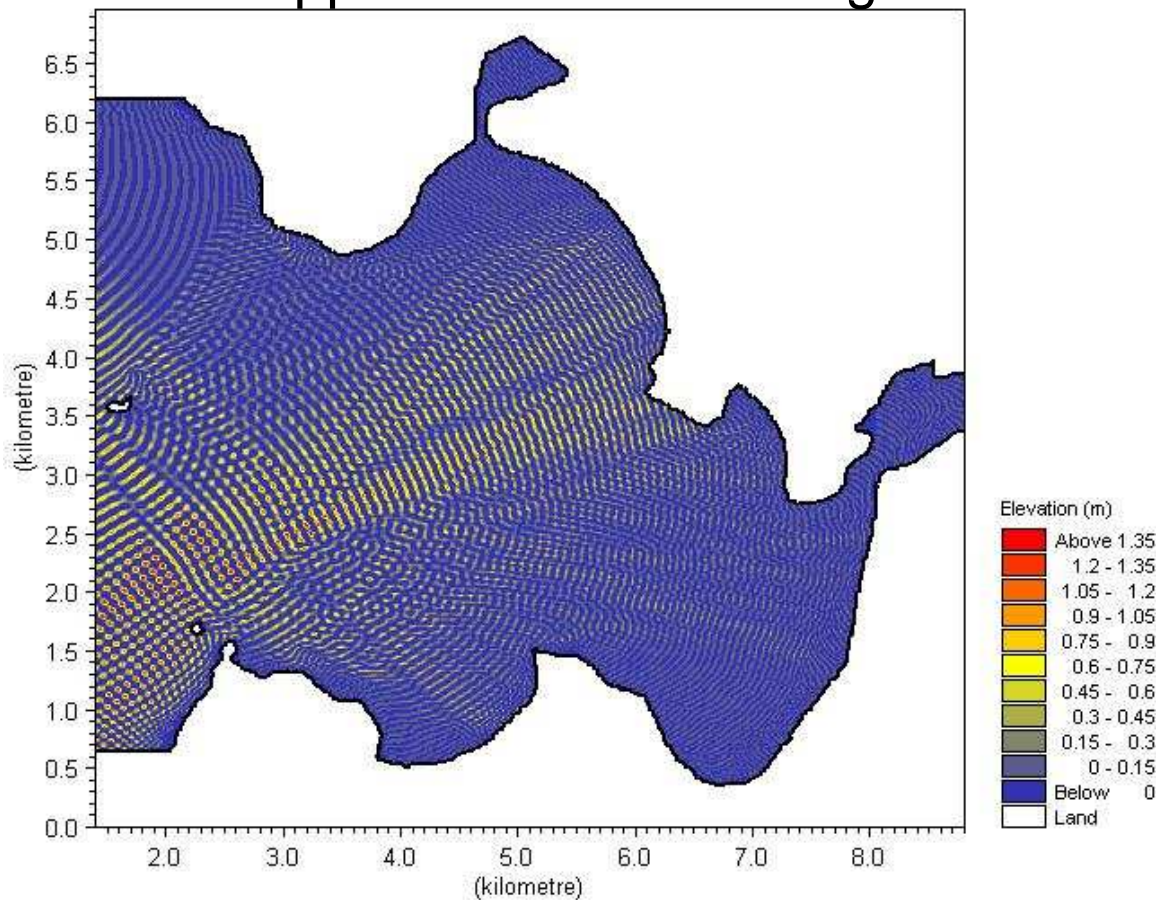


# Wave approach from 0 Degrees

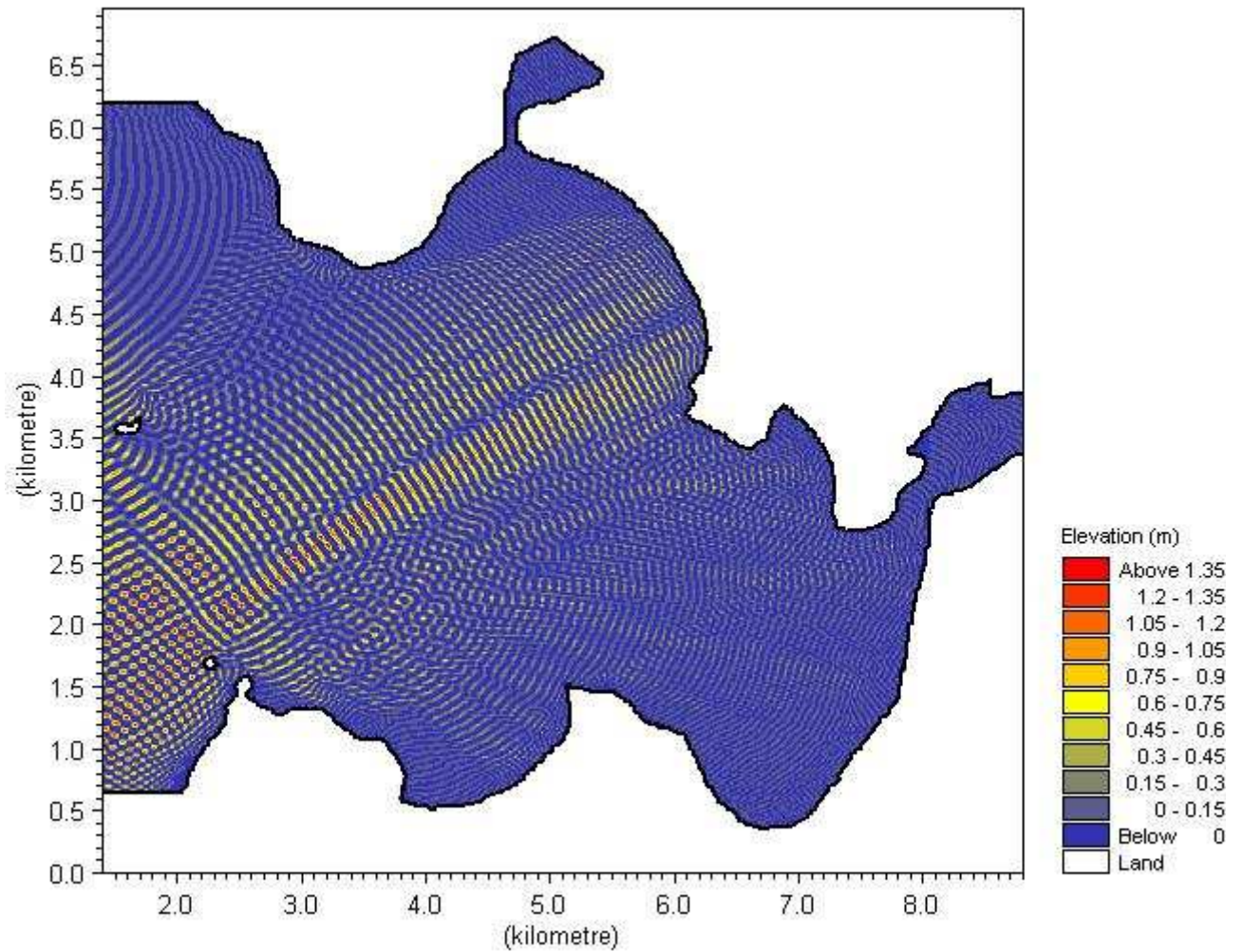


# 1.5 m, 9s wave at open boundary

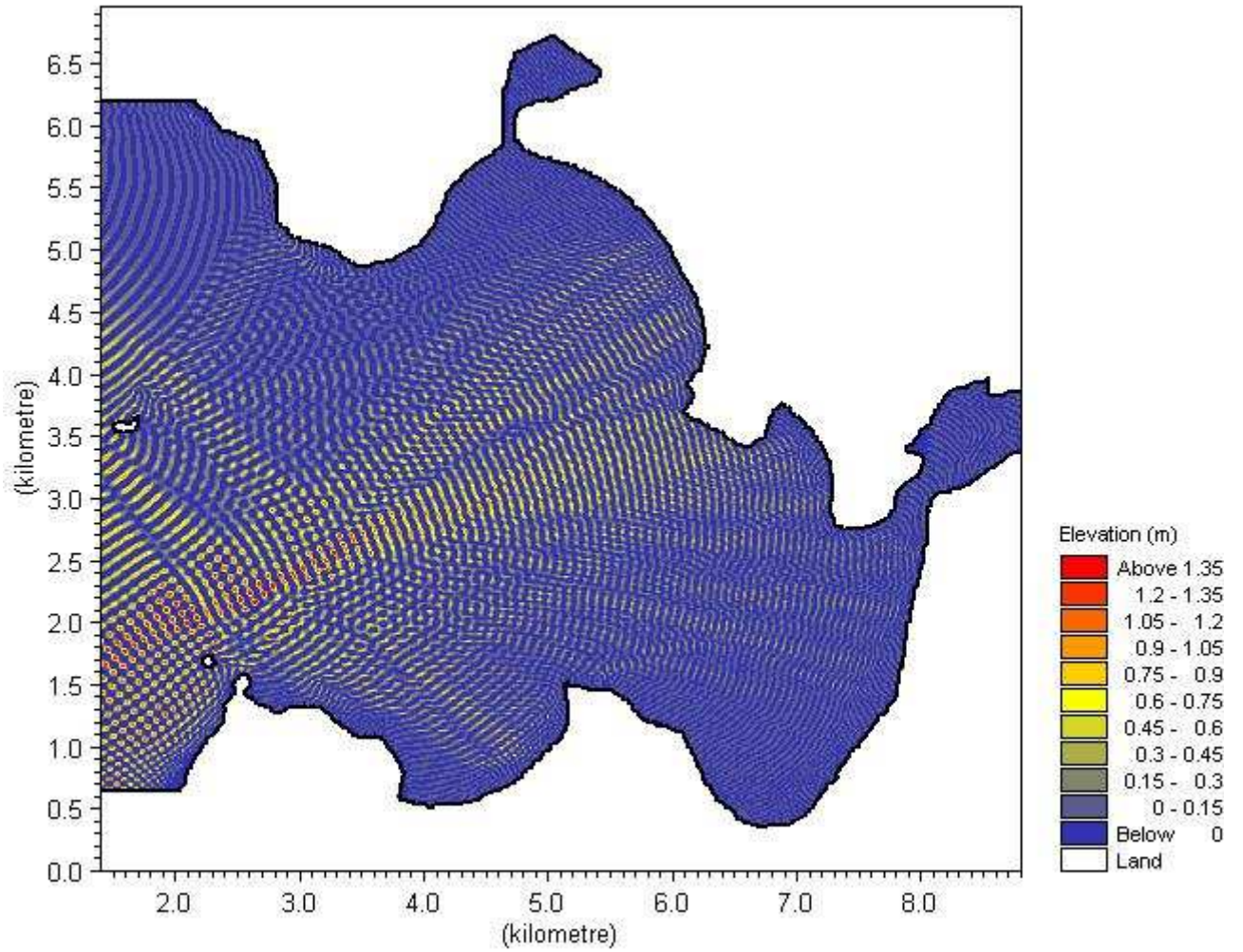
## Wave approach from 170 Degrees



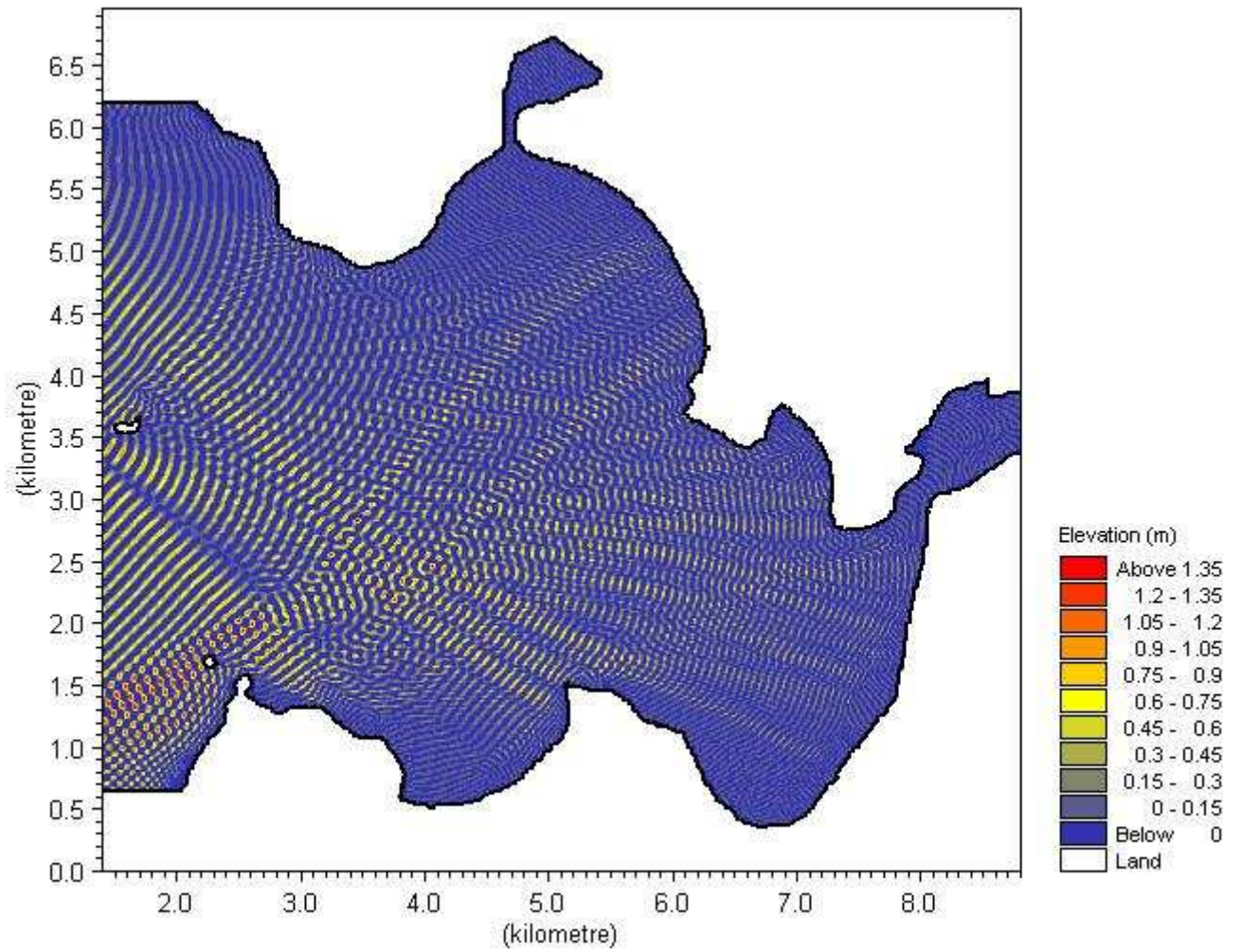
# Wave approach from 150 Degrees



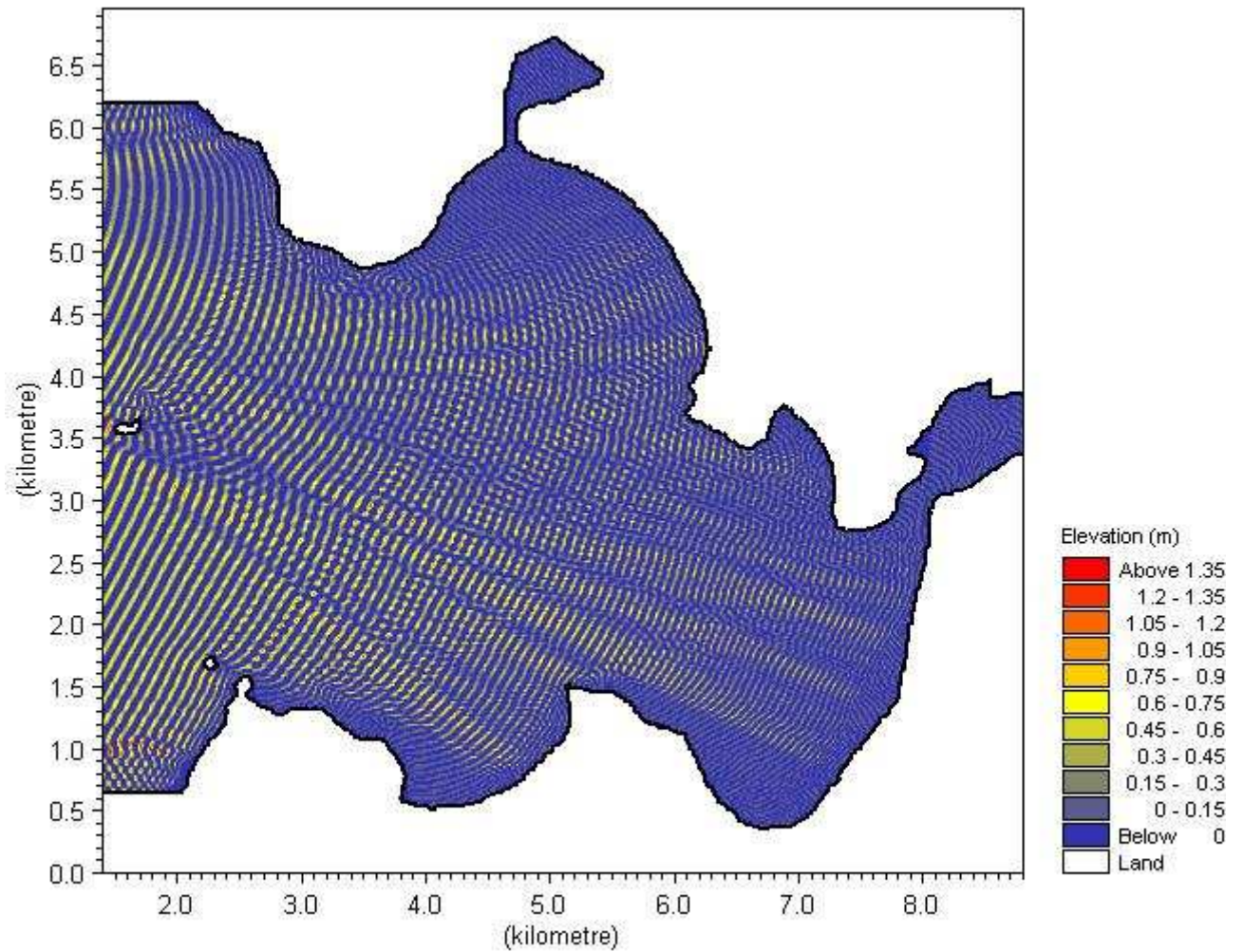
# Wave approach from 130 Degrees



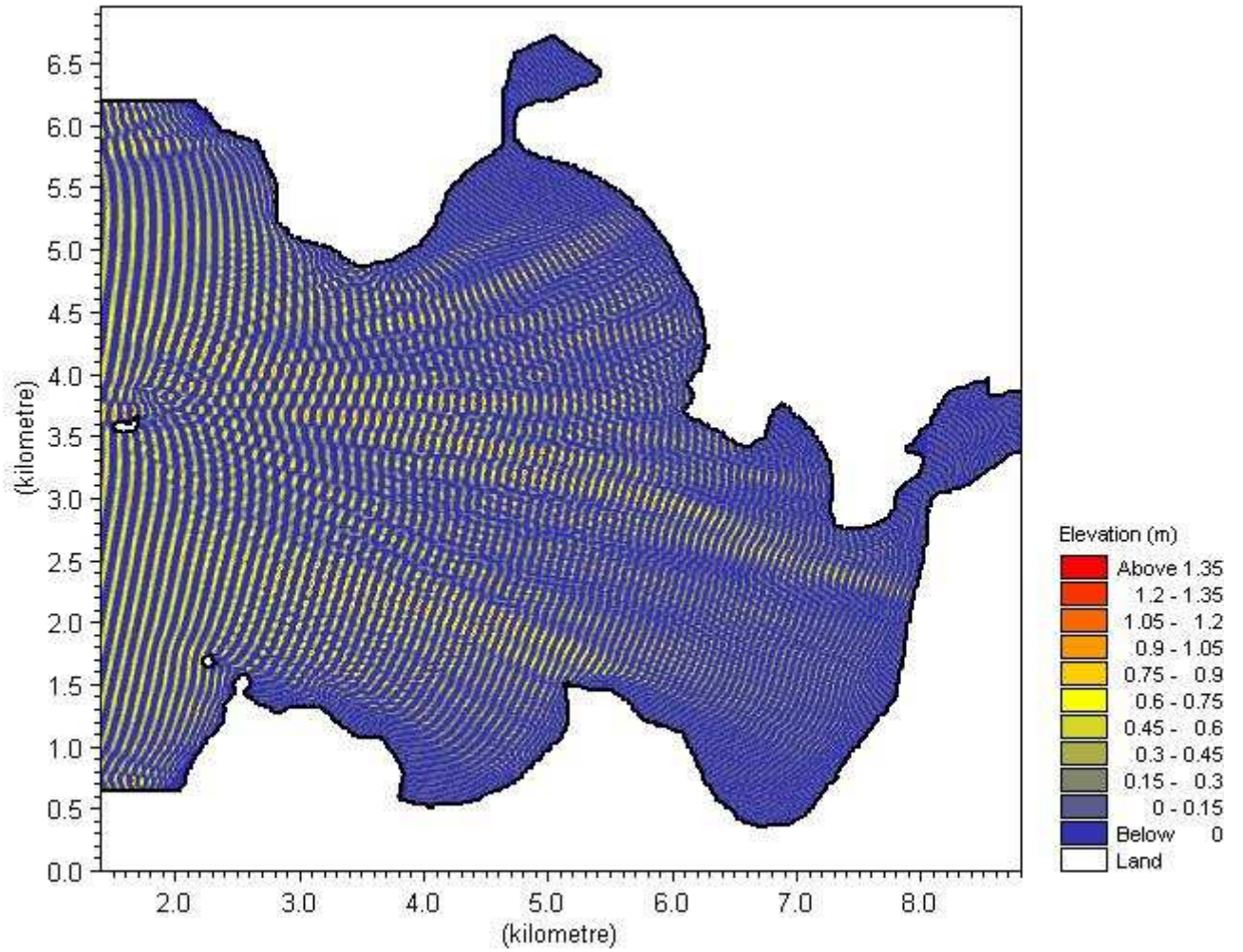
# Wave approach from 110 Degrees



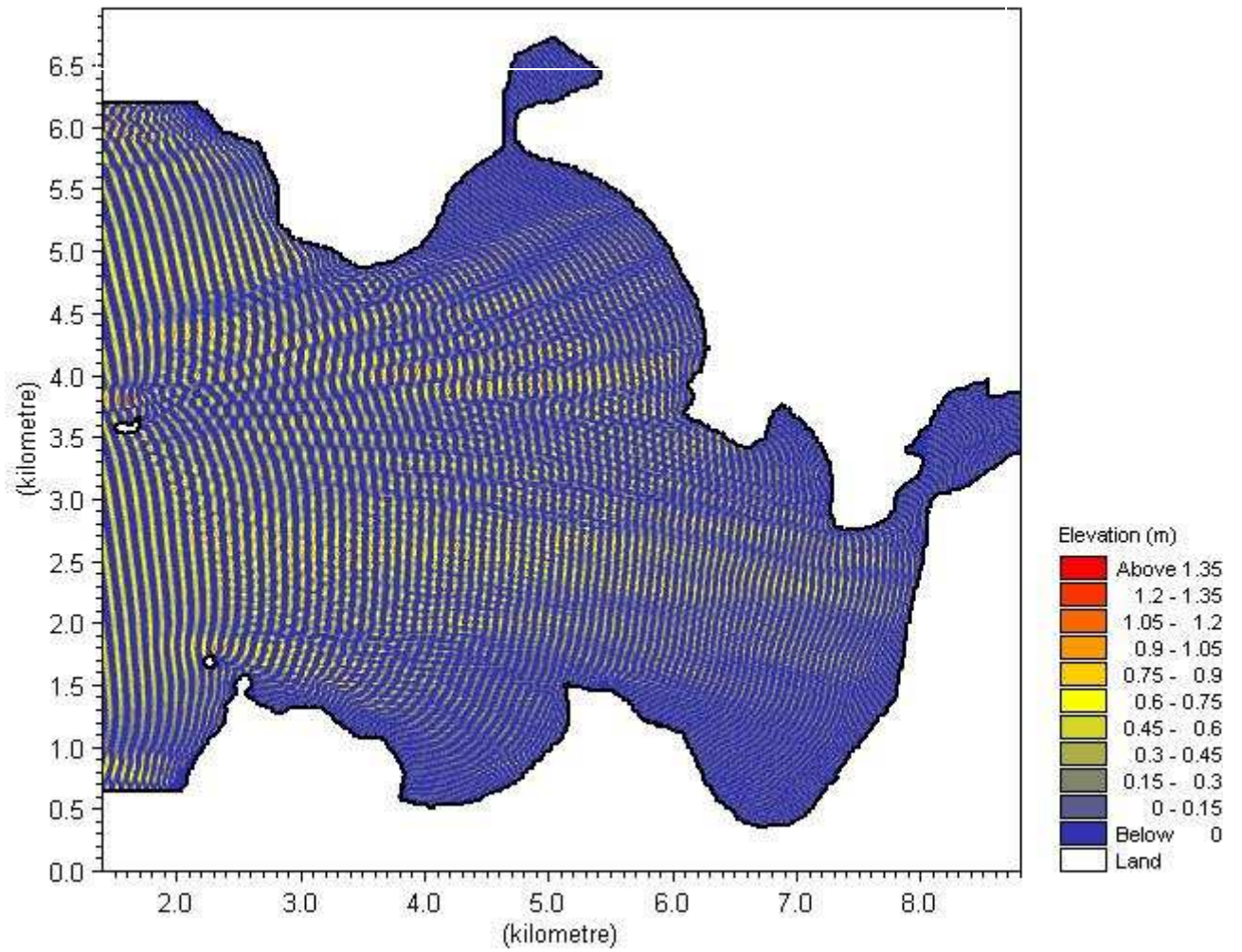
# Wave approach from 90 Degrees



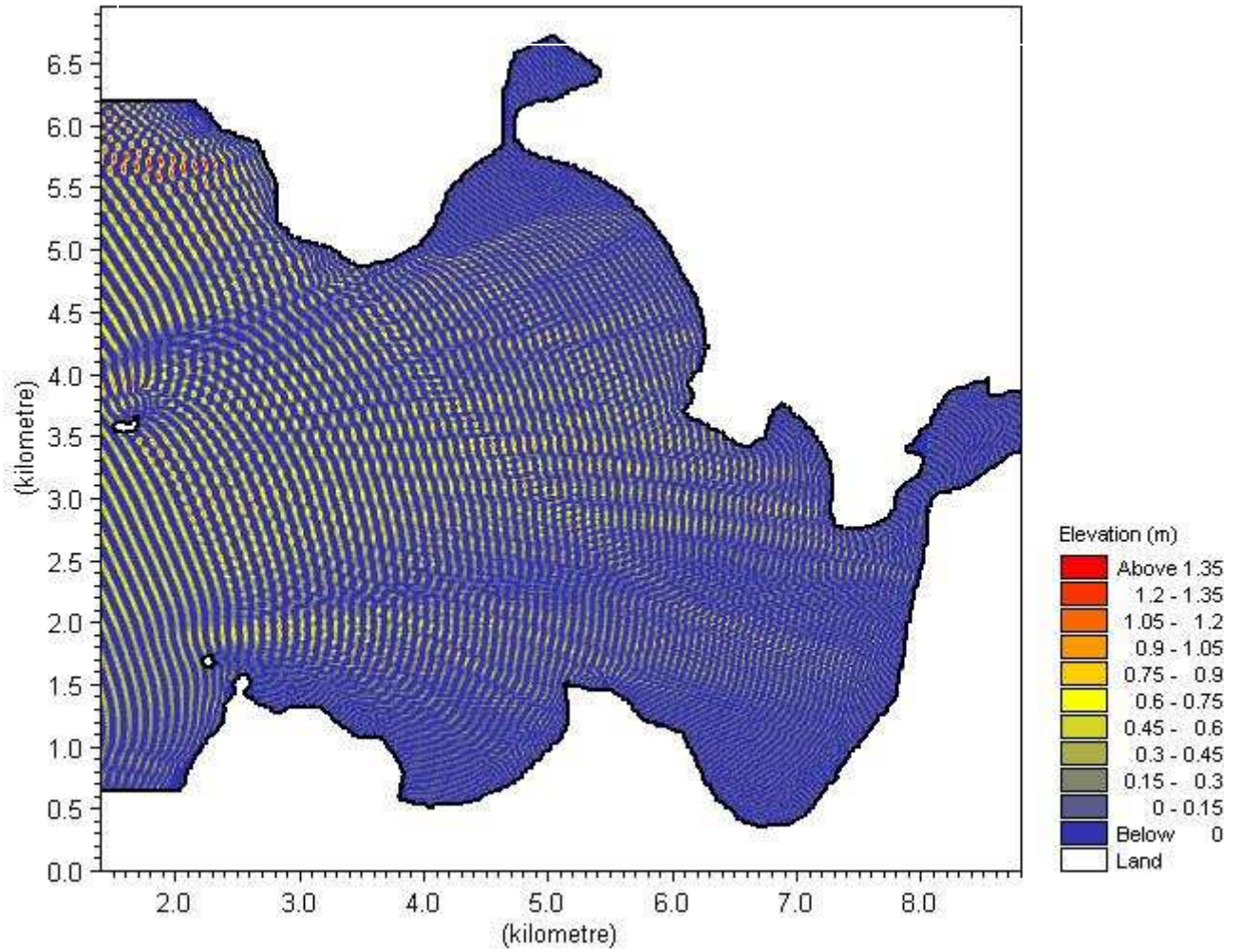
# Wave approach from 70 Degrees



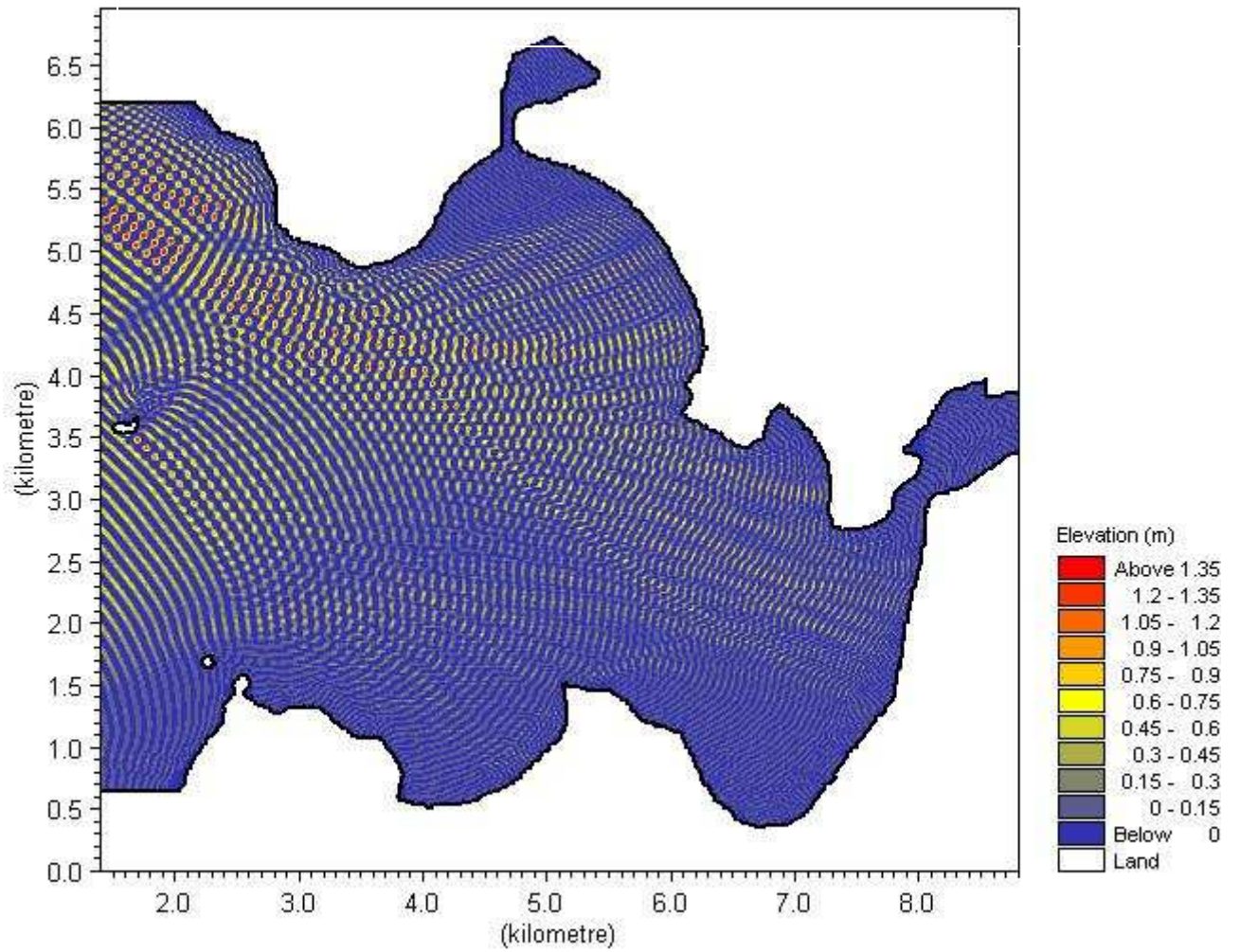
# Wave approach from 50 Degrees



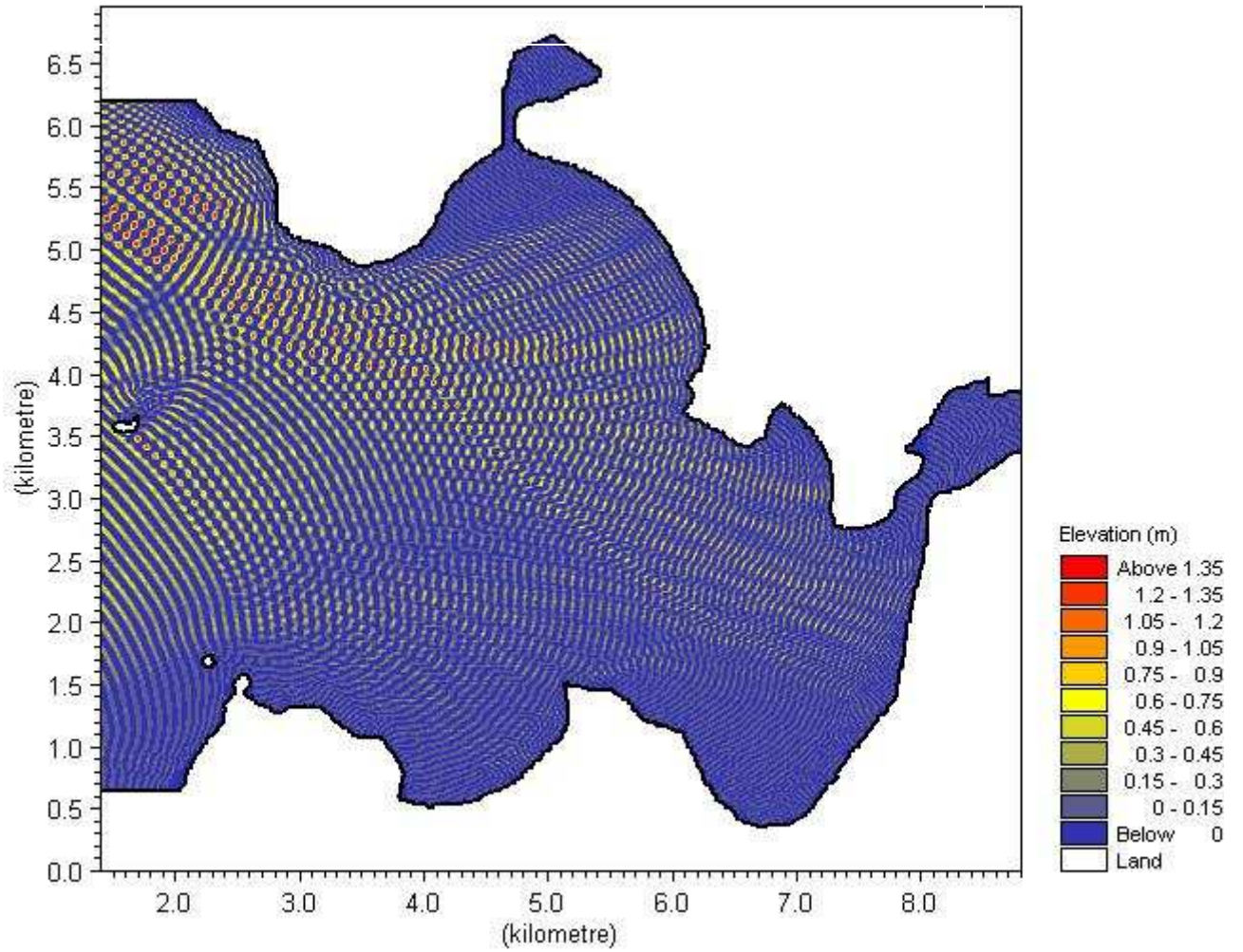
# Wave approach from 30 Degrees



# Wave approach from 10 Degrees

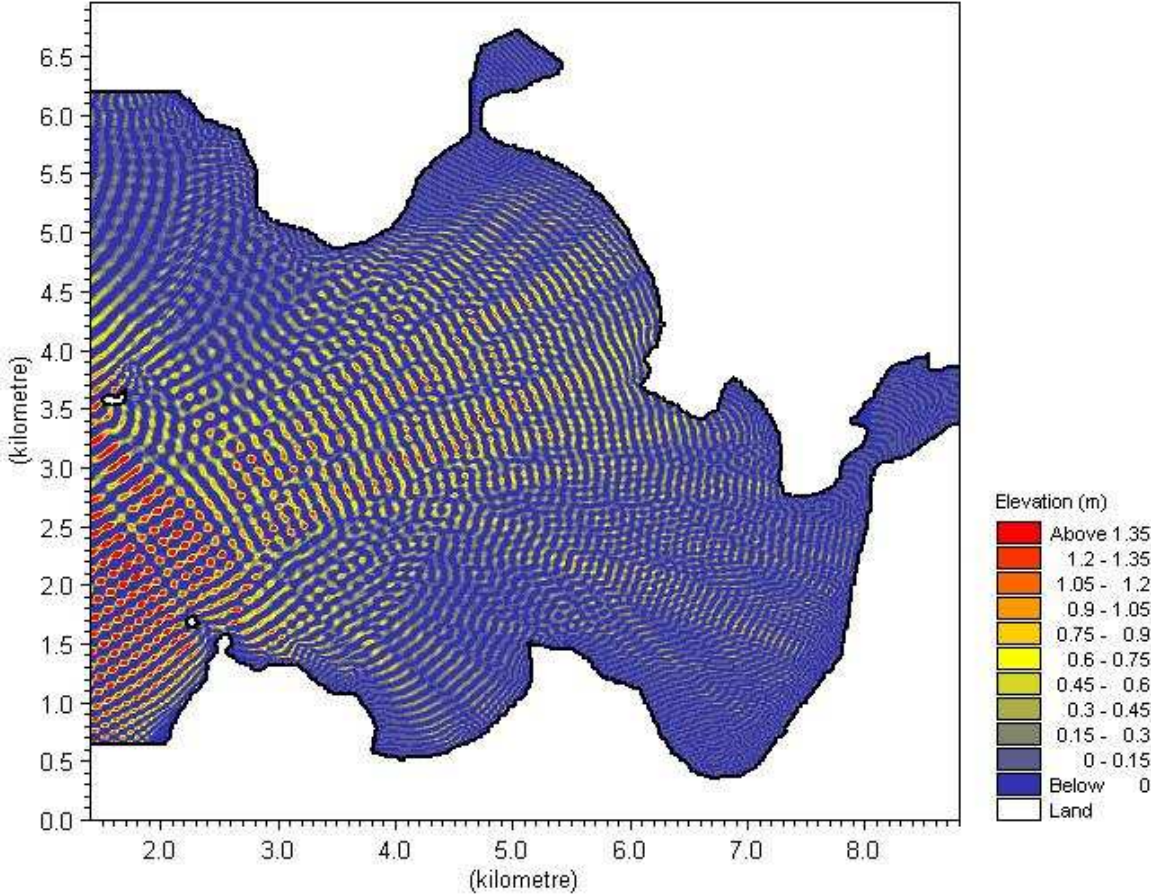


# Wave approach from 0 Degrees

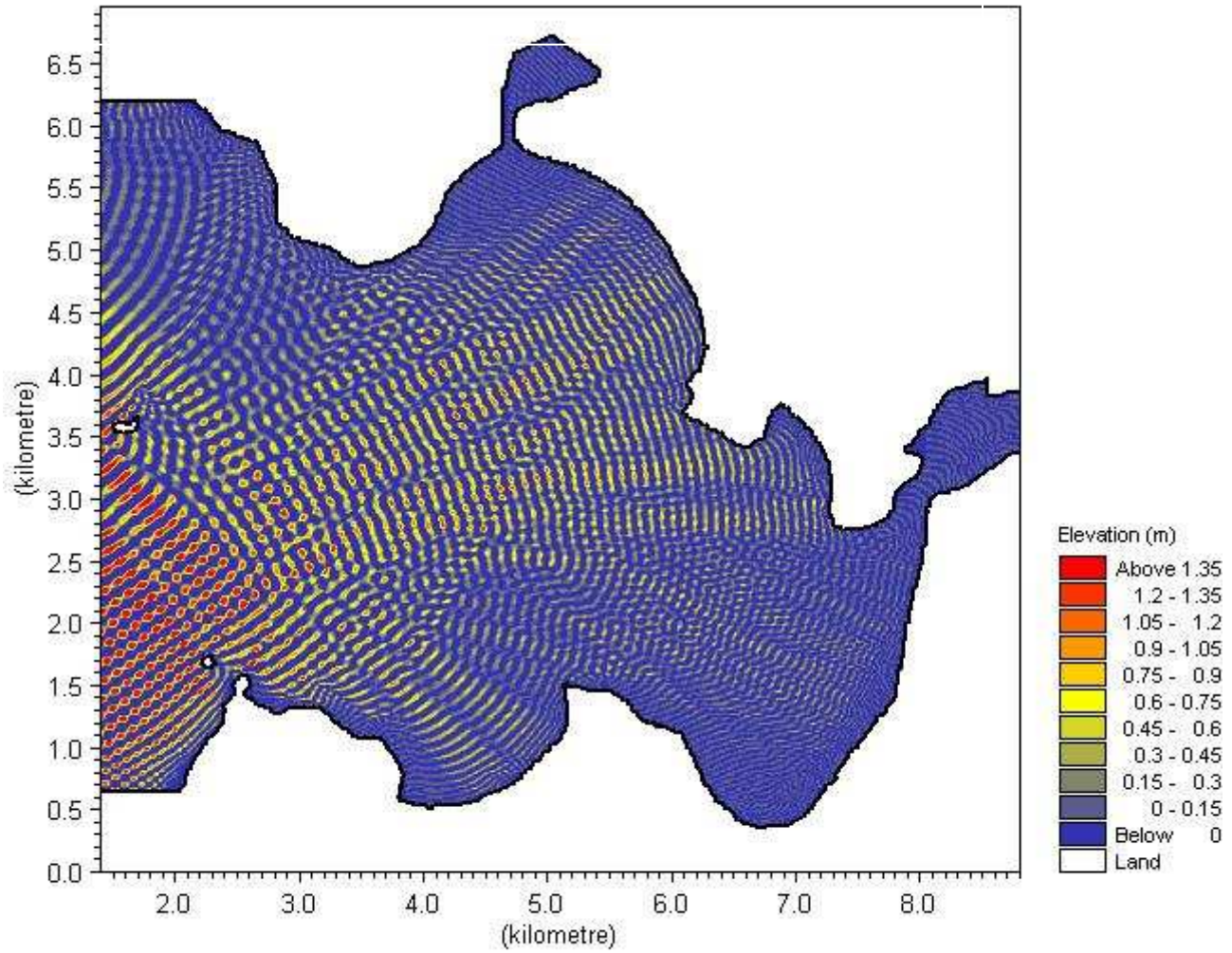


# 3 m, 11s wave at open boundary

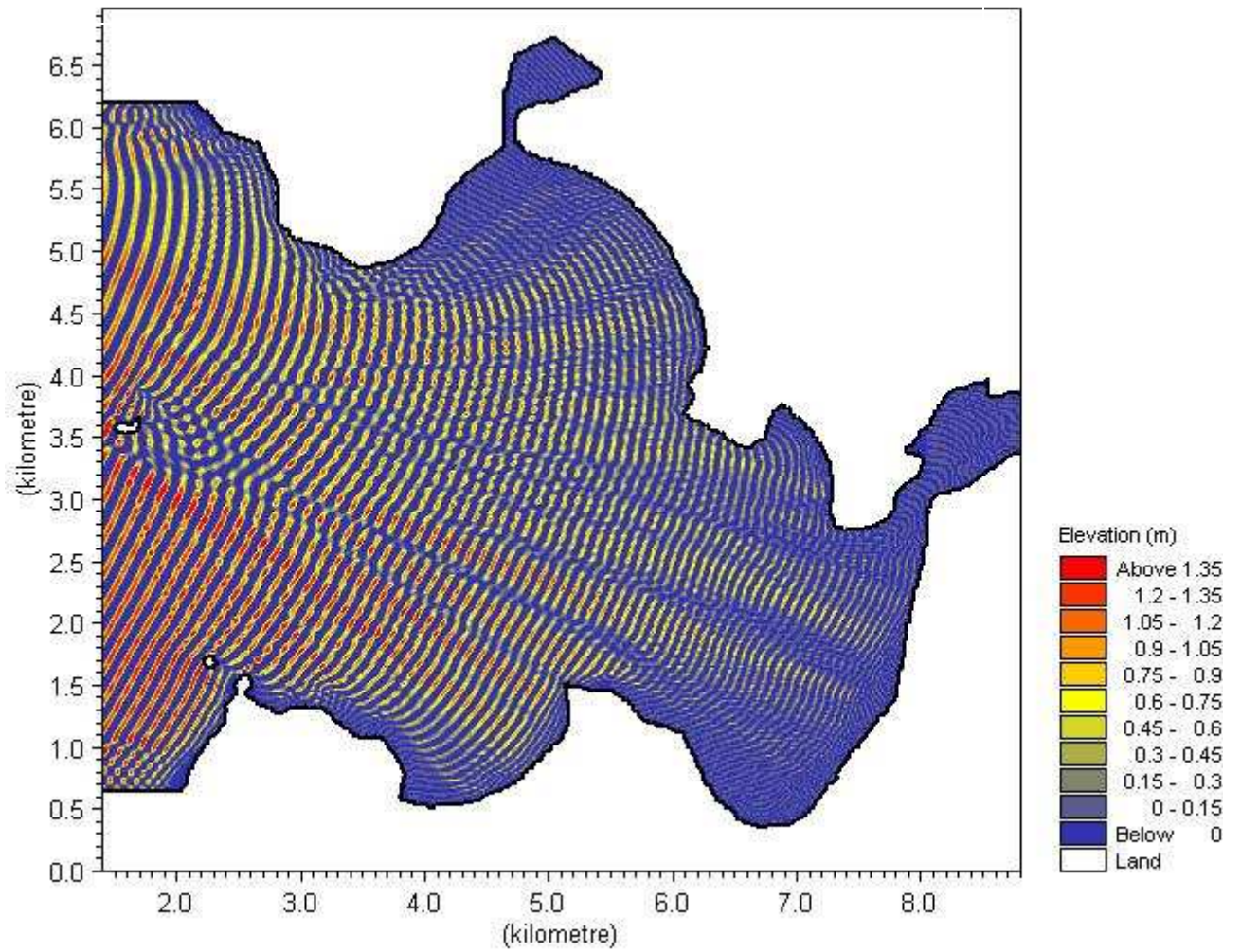
## Wave approach from 170 Degrees



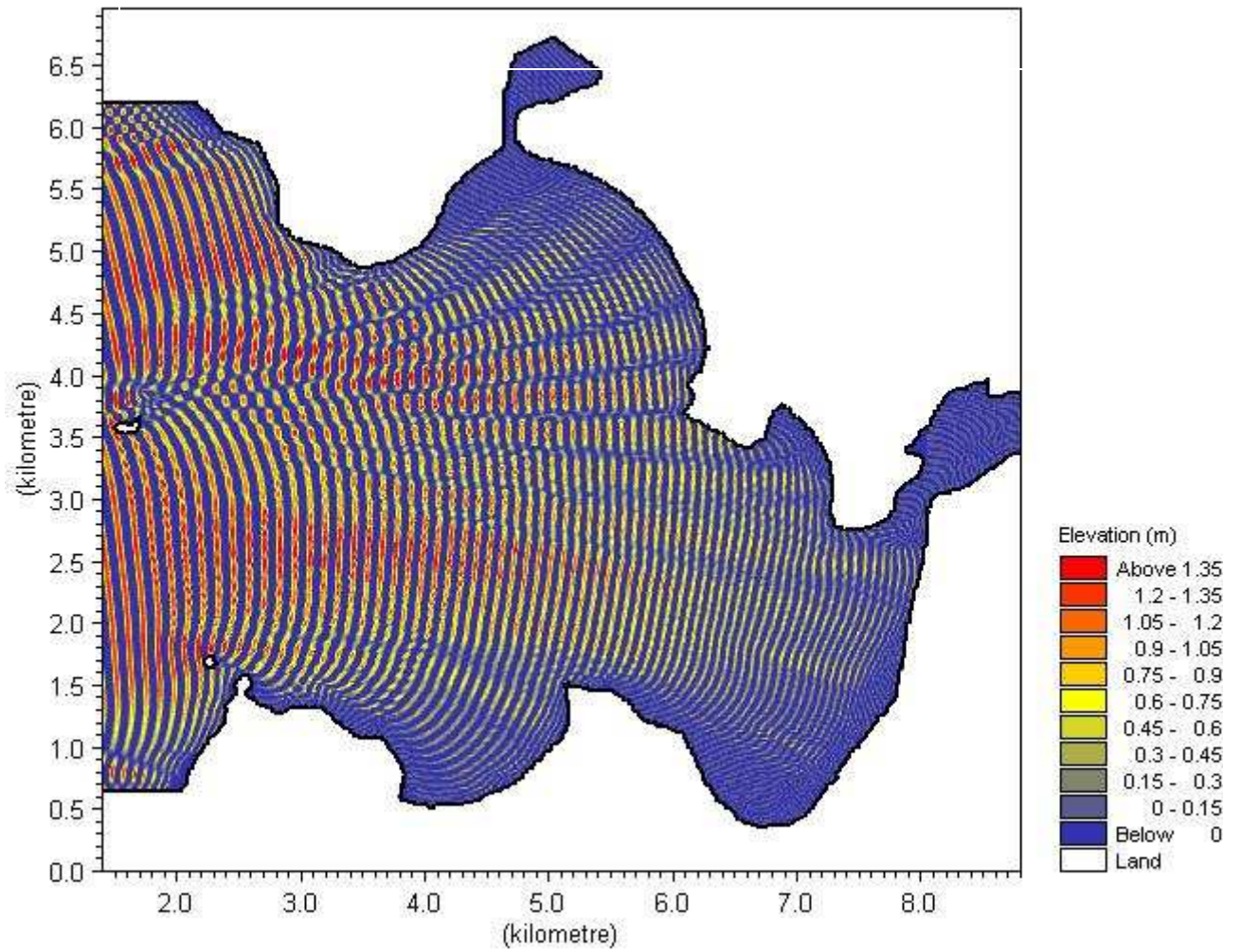
# Wave approach from 130 Degrees



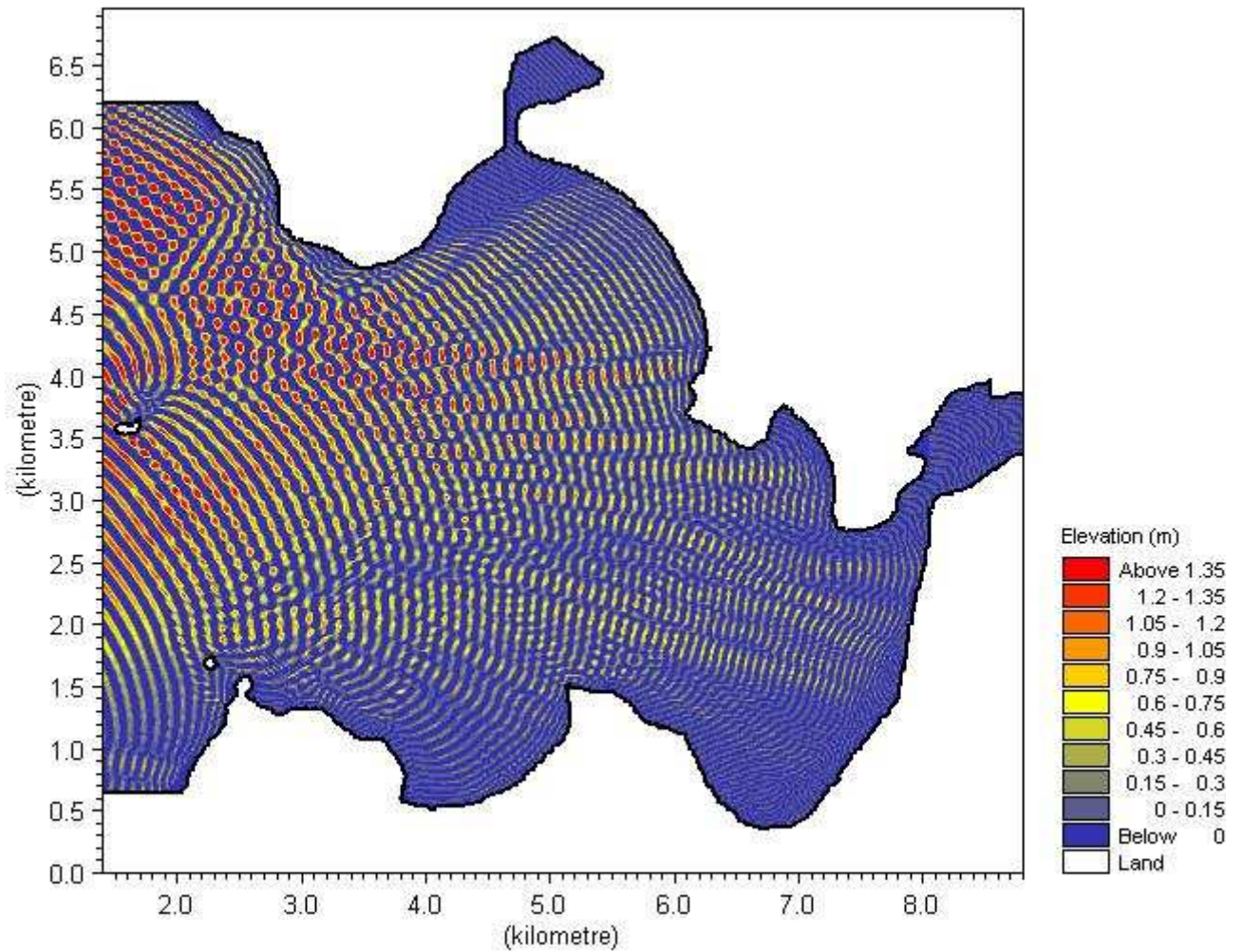
# Wave approach from 90 Degrees



# Wave approach from 50 Degrees

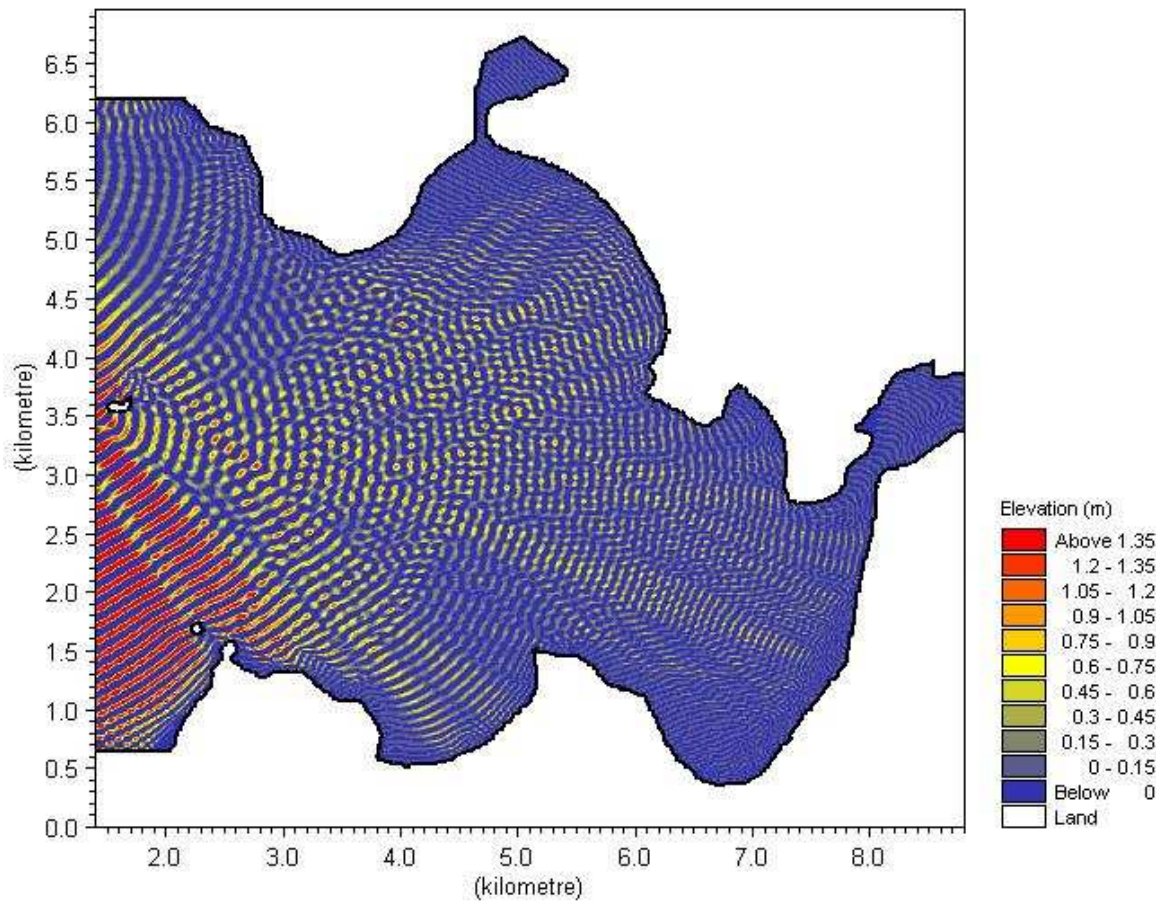


# Wave approach from 10 Degrees

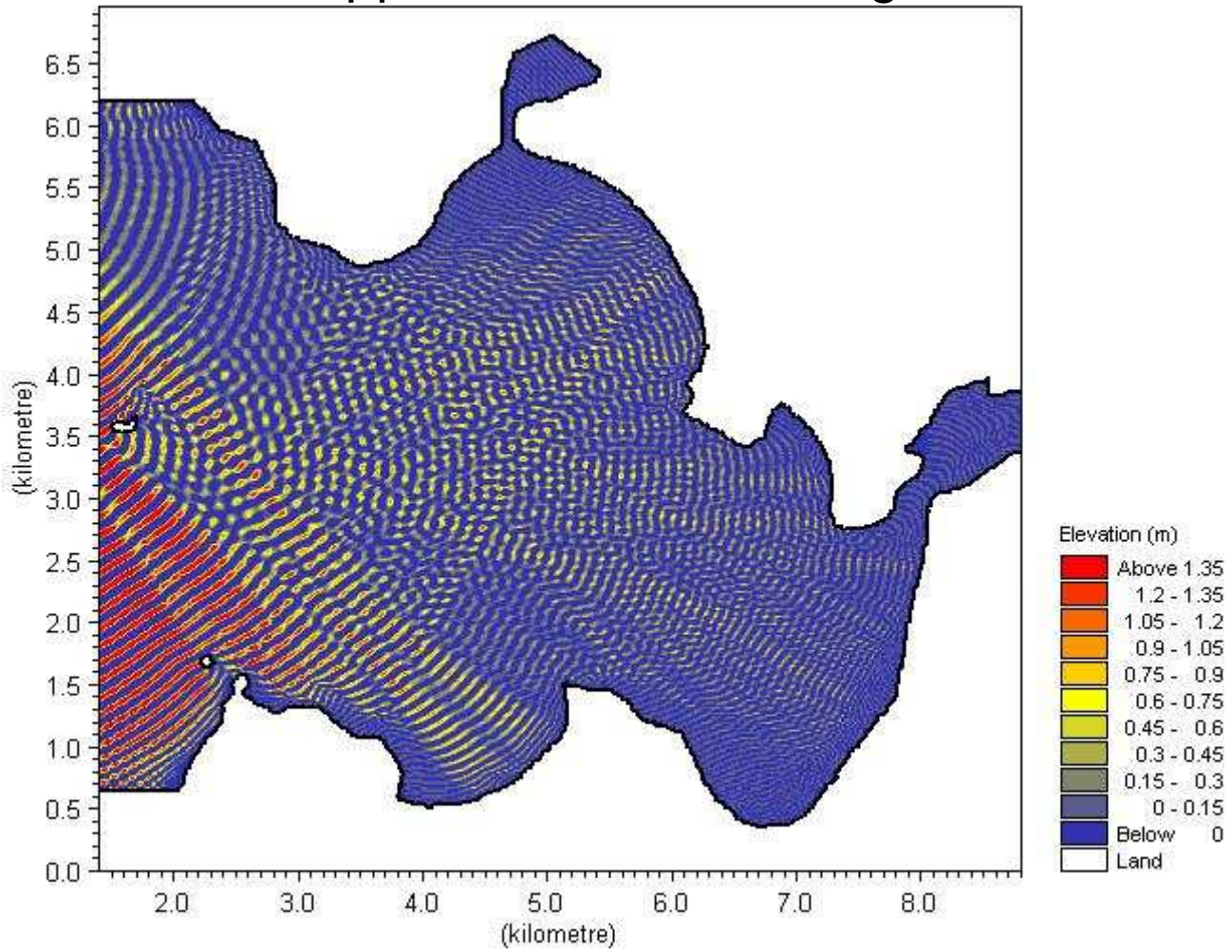


# 5m, 11s wave at open boundary

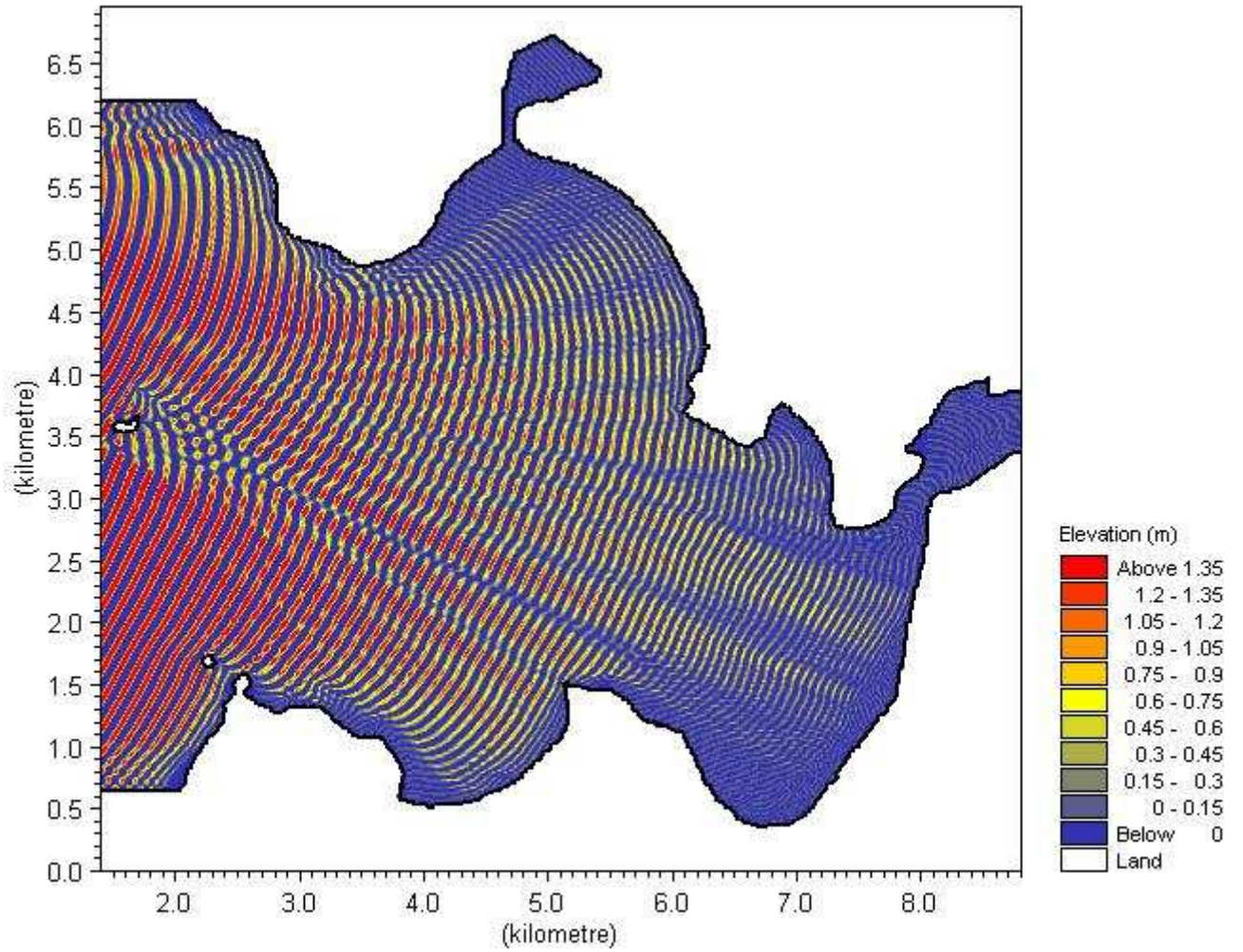
## Wave approach from 170 Degrees



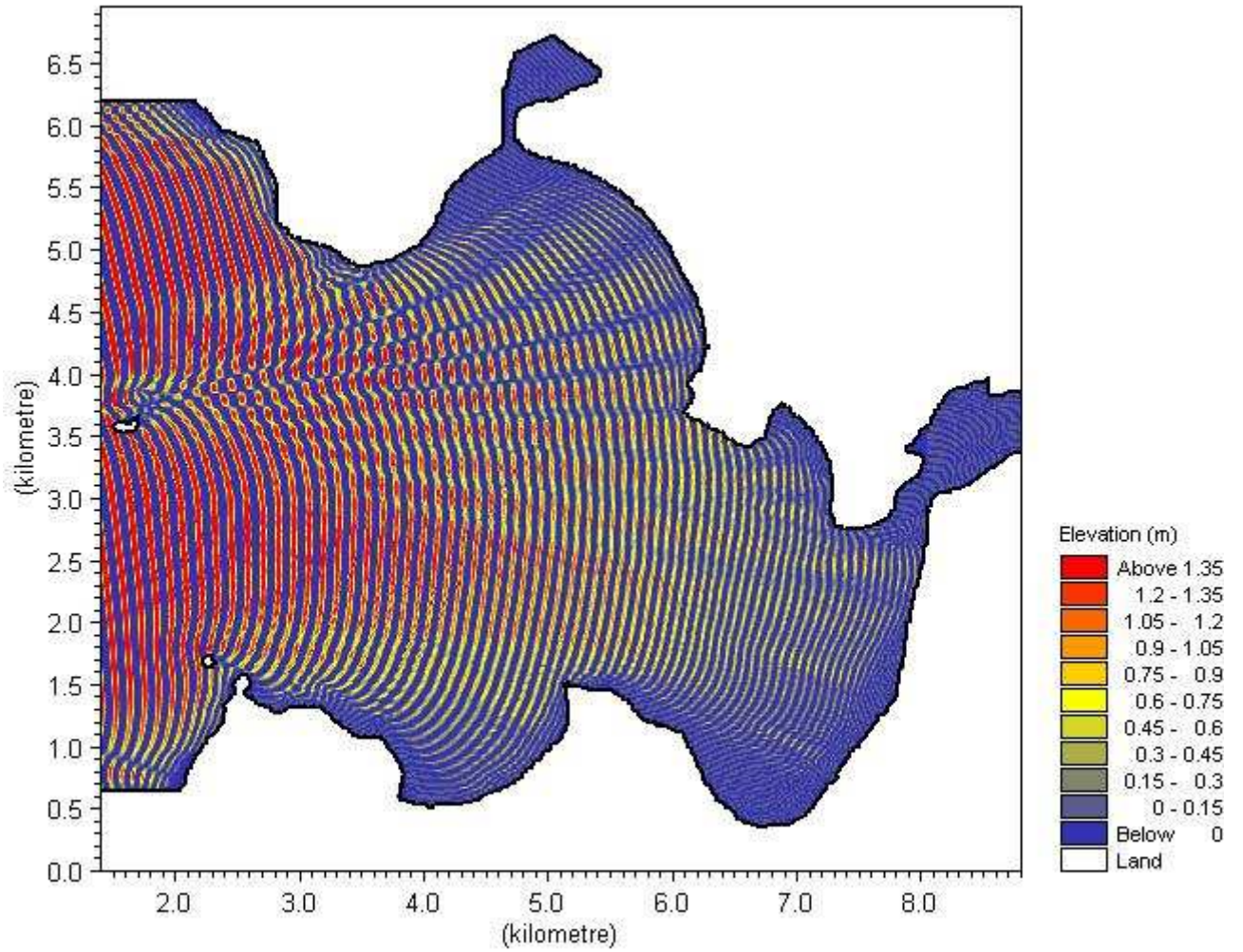
# Wave approach from 130 Degrees



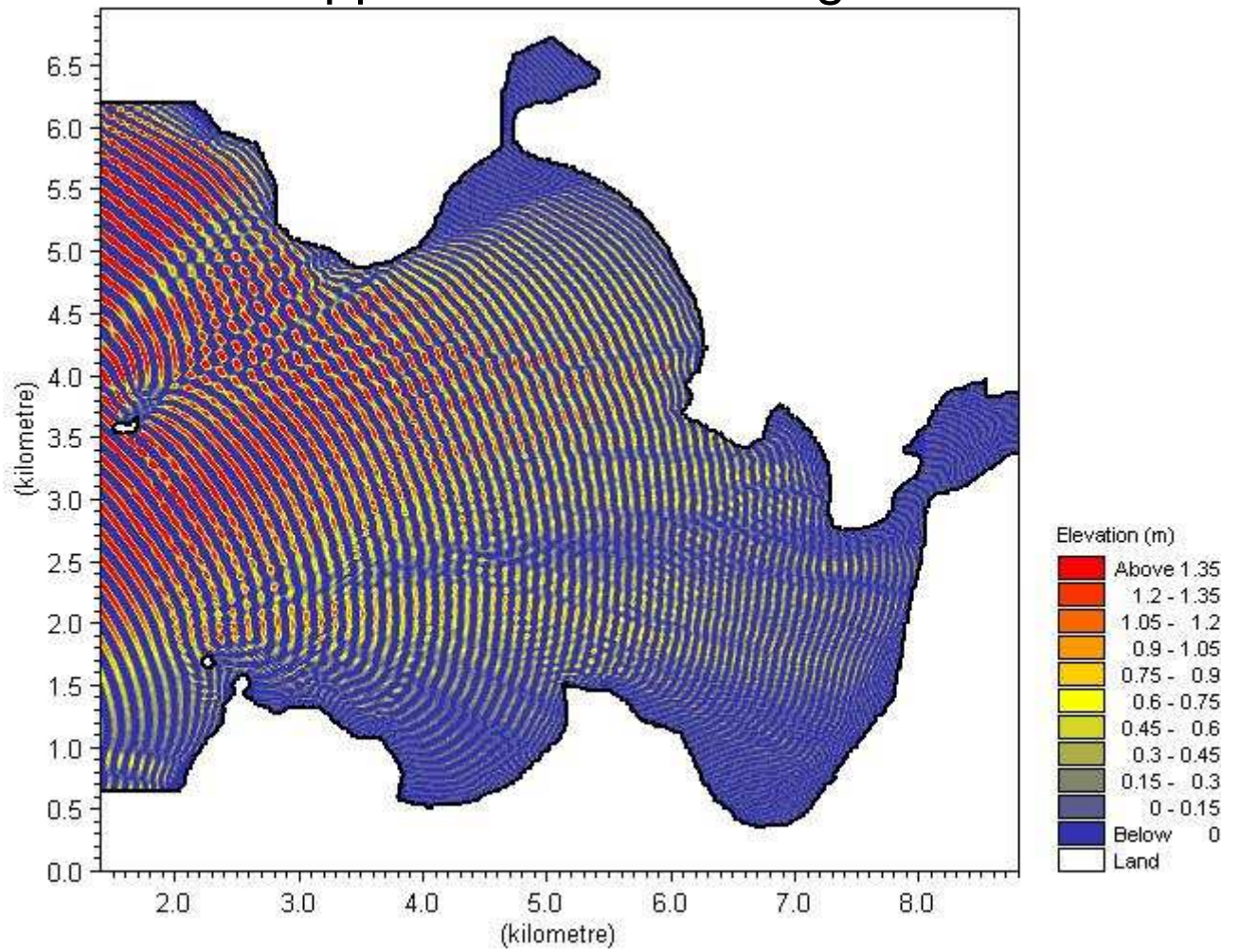
# Wave approach from 90 Degrees



# Wave approach from 50 Degrees

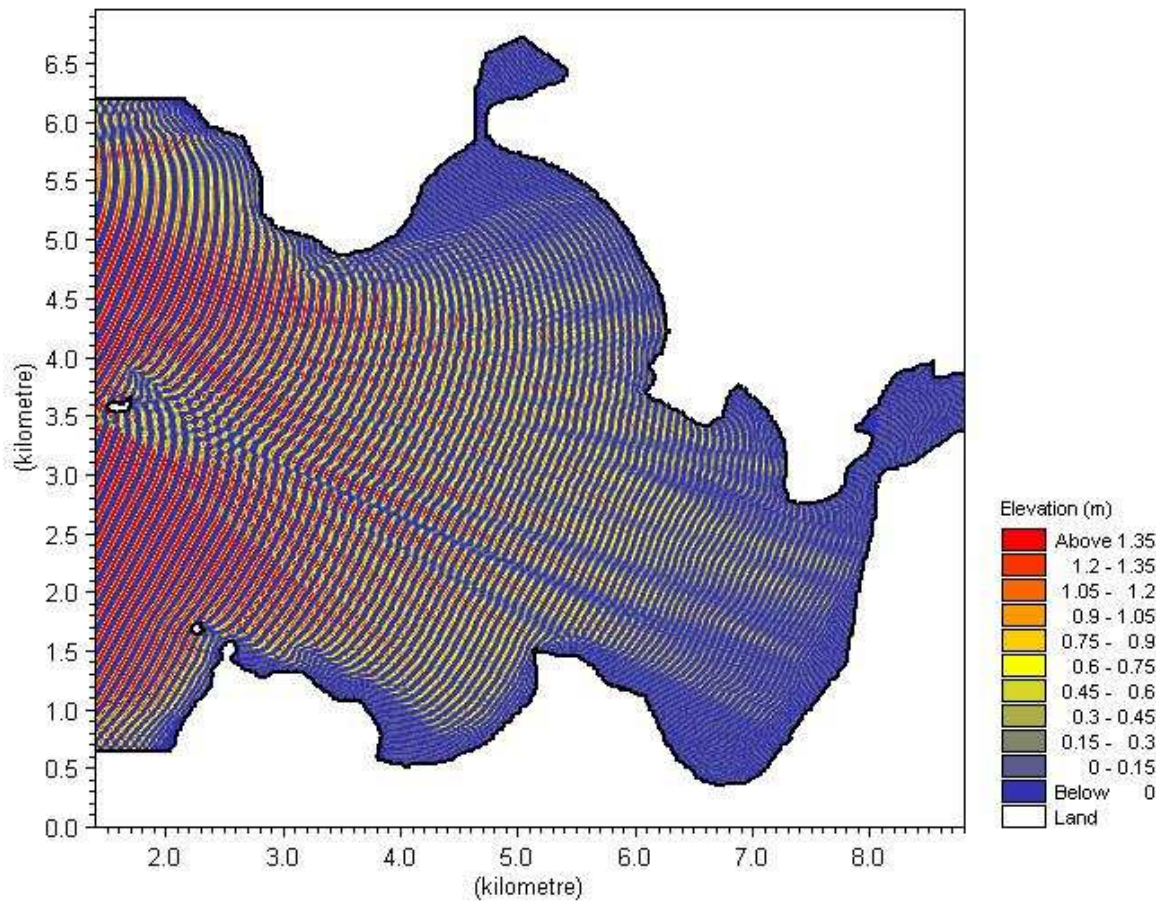


# Wave approach from 10 Degrees

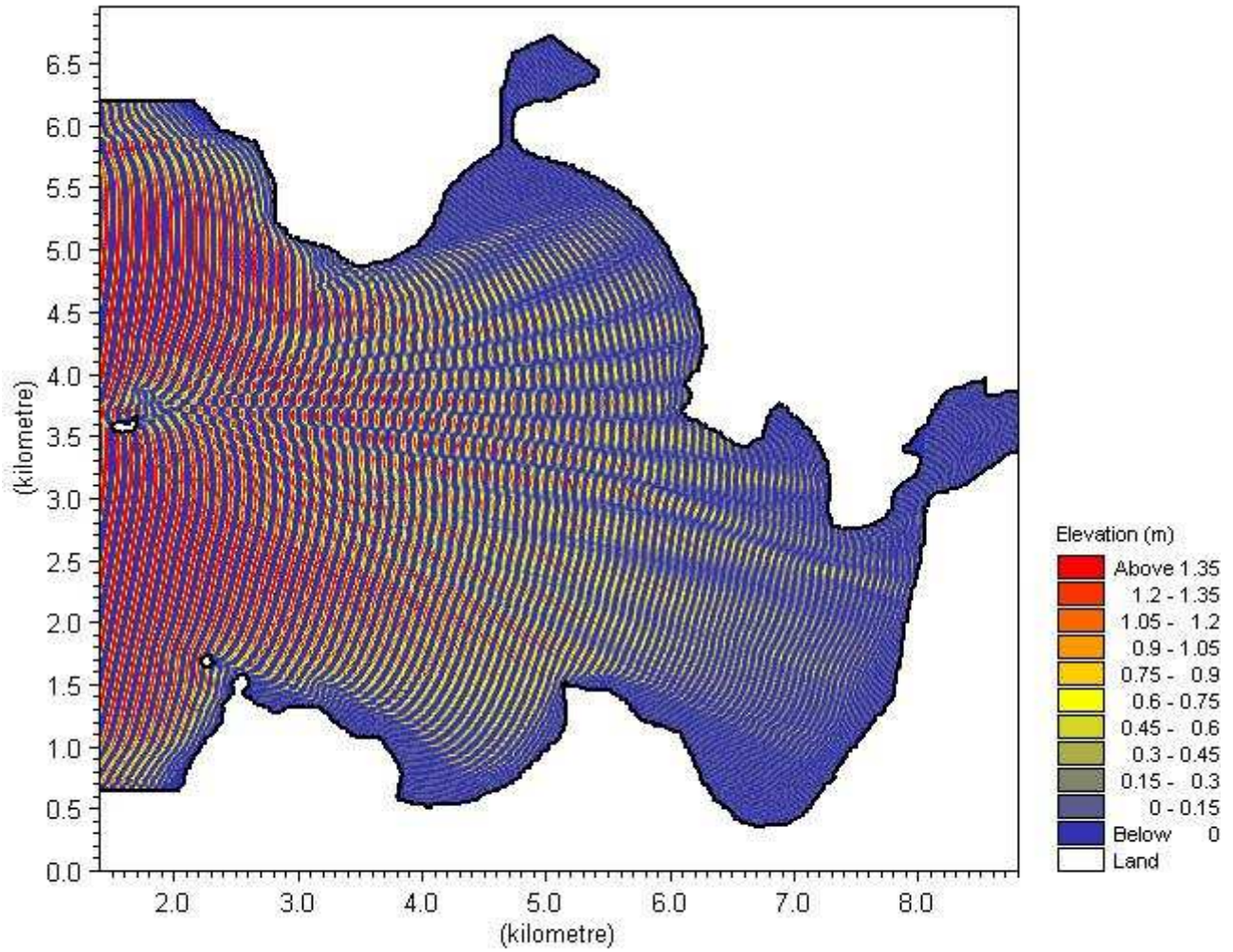


# 5 m, 9s wave at open boundary

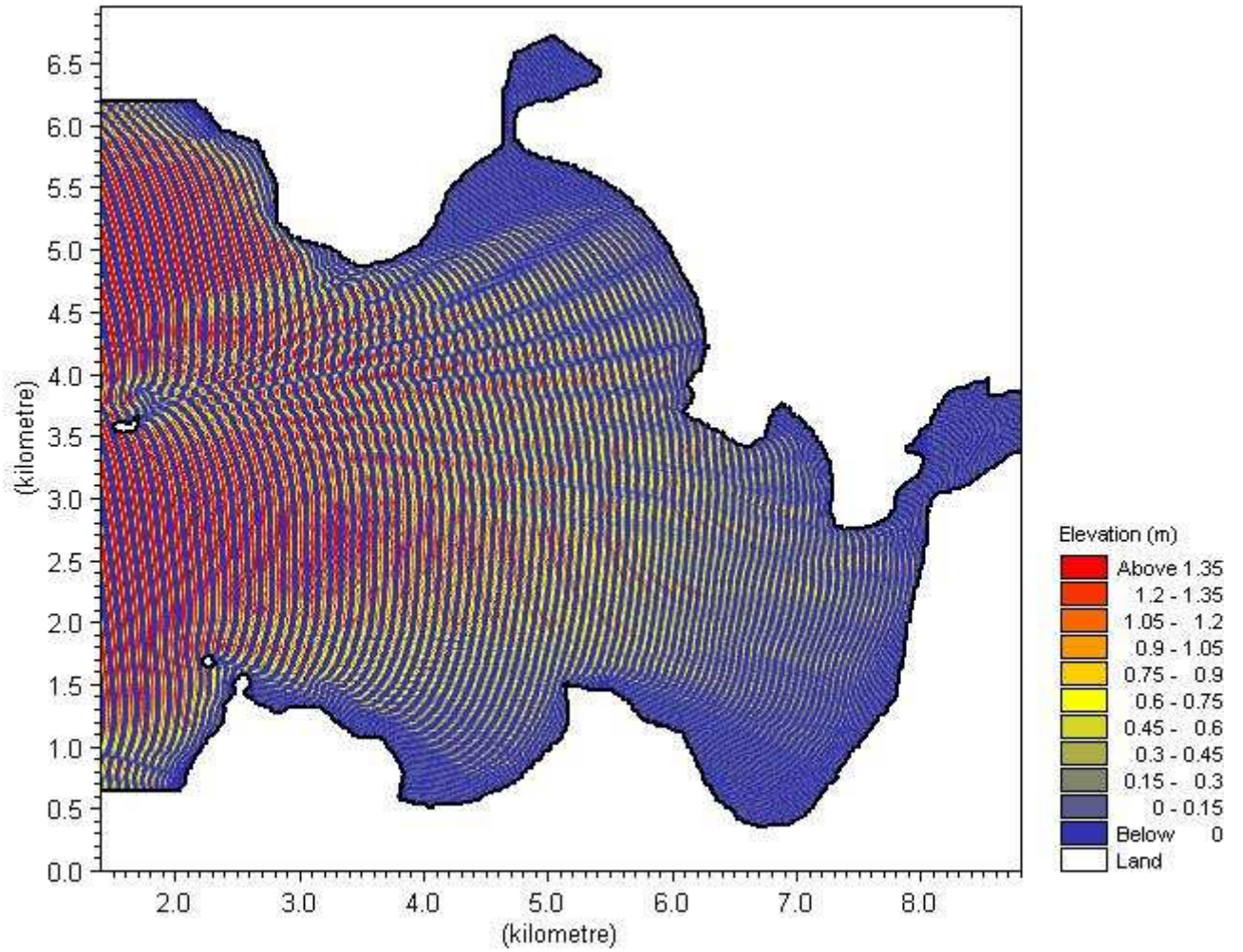
## Wave approach from 90 Degrees



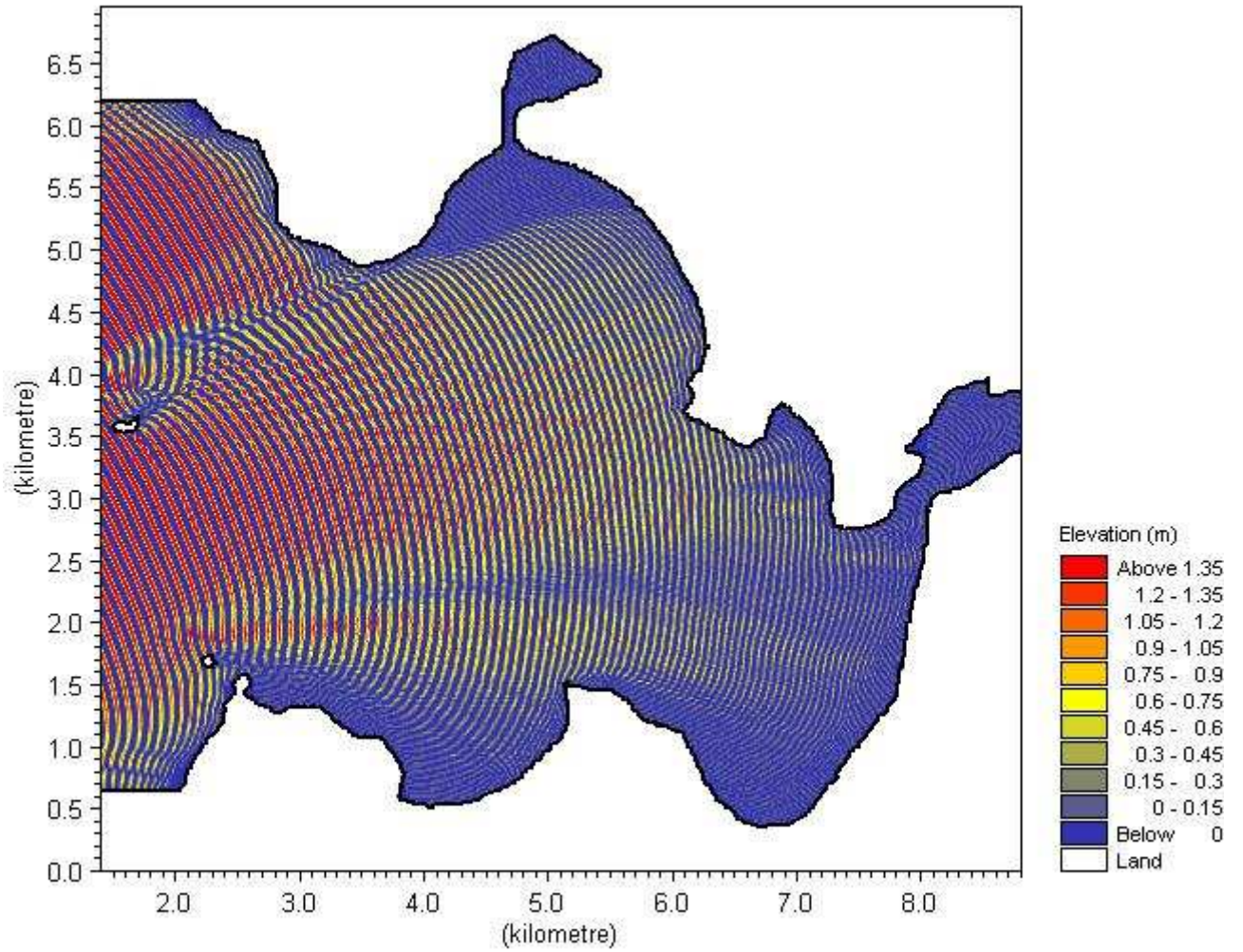
# Wave approach from 70 Degrees



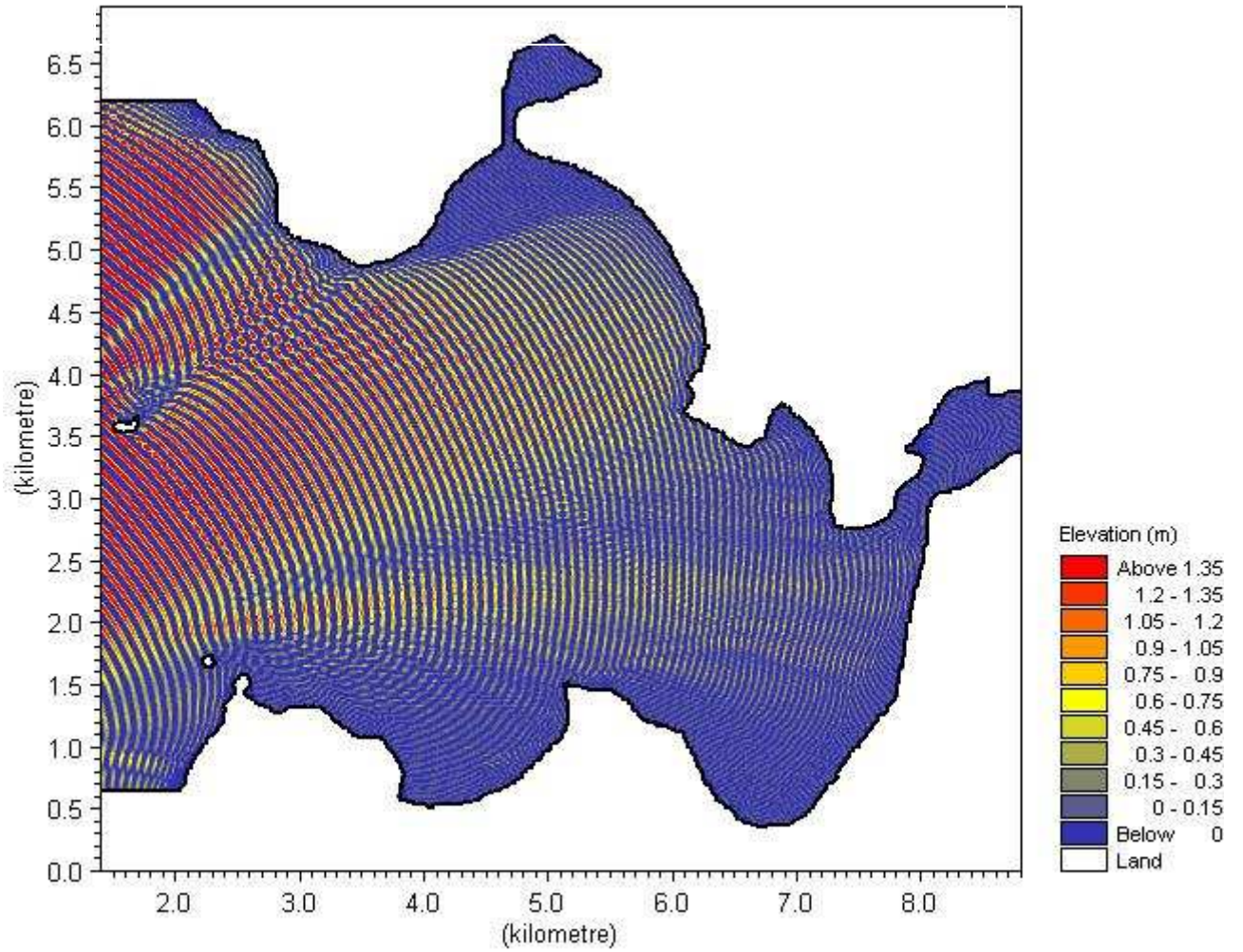
# Wave approach from 50 Degrees



# Wave approach from 30 Degrees



# Wave approach from 10 Degrees



# Wave approach from 0 Degrees

